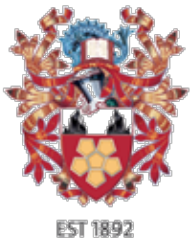

Heat Transfer Performance of Radiator Heating System with Alternative Heat Transfer Fluids

Prepared by

Shatha Fadel Haddowe

M.Sc.

A thesis submitted in partial fulfilment of the requirements of the

London South Bank University

for the degree of Doctor of Philosophy

May 2020

ABSTRACT

Heat transfer fluids (HTFs) are an essential heat transport medium in many wet heating and cooling systems. They carry Heat from the generation source to the place where it is being used. Therefore, HTFs should have the capability of carrying Heat efficiently. The ability of HTFs to carry out the maximum amount of Heat with minimum loss is dependent on the characteristics and properties of the fluids; better heat transfer will result in better heating system performance. The majority of conventional heat transfer systems, within the built environment, currently use water as the heat transfer medium between the source and the point of use. This is mainly due to the availability, low price and acceptable thermal properties of water. However, water has its limitations in terms of heat transfer rates in intense energy systems due to aeration, oxidation and fouling. In addition, it has a high freezing point (0°C) which affect its use in a cold climate. Therefore, using alternative heat transfer fluids is considered as a choice to overcome the limitations that are associated with water as a HTF.

The conducted literature review has demonstrated a lack of knowledge in the use of alternative heat transfer fluids, especially nanofluids in hydronic radiator heating systems (HRHS) and the effect of these fluids on the overall system energy performance. Therefore, this research was designed to experimentally investigate and compare the energy performance of a radiator heating system with alternative heat transfer fluids compared to water. For this research project, a commercially available nano-based heat transfer fluid (50%HX/W) was researched and compared using energy performance tests to potable water, 30% ethylene glycol/water (30%EG/W) and 50% ethylene glycol/water (50%EG/W) mixtures. To achieve the target of this research a bespoke test facility (simulating a residential heating system) was designed, constructed and fully instrumented to investigate the performance of the hydronic heating system with the different options of heat transfer fluids under similar and repeatable controlled conditions.

Test methods were developed for both steady state and thermostat tests and two independent scenarios; Drop-in scenario and optimised scenario. The drop-in-scenario replicates a situation where the alternative fluids are charged into the system without changing the system settings (flow rate and temperatures settings). The optimised scenario replicates a situation where the alternative fluids are charged into the system and adjustment are made to the settings, including the mass flow rate and temperature difference (ΔT) across the radiator. These scenarios were designed to test the radiator heating system performance with the alternative heat transfer fluids (AHTFs) under investigation to obtain the required results. System energy data, air and system temperatures data, as well as heat output from the radiator, were considered for the evaluation and comparing of the system performance with all examined fluids.

In order to evaluate the heat output from the radiator heating system working with the examined AHTFs, an energy balance approach was developed during this project. This approach allows evaluation of the heat output from the radiator of the considered heating system to the air-side during steady-state and transient conditions without considering the dynamic changes in the thermal properties of the working fluid at different temperatures.

The results obtained show that the properties of the examined fluids have an impact on system operational behaviour and performance. For the drop-in scenario, test results revealed that the system flow rate was related to the density and viscosity of the working fluids. The flow rate in the system was lower (compared to water) when 30% and 50% EG/W and 50% HX/W were used in the system as follow, 9%, 32% and 46% respectively. The internal booth temperature (IBT) and energy consumption obtained from 30% EG/W test were very close to the results obtained from the water test. While lower IBT (by 1.4K – 2.5K) was obtained when 50% EG/W and 50% HX/W used as a working fluid in the radiator compared to the base case (water test) value. Comparison data of energy consumption showed that less energy was consumed when 50% EG/W and 50% HX/W

used in the heating system, and this reduction was 1.7 kWh and 2.6 kWh respectively, during the duration of the test. The test results of the optimised scenario revealed that the adoption of the radiator design mass flow rate with 50% EG/W and 50% HX/W tests resulted in a lower volumetric flow rate. This resulted in a bigger ΔT across the radiator (by 18%), better temperature uniformity on the radiator surface and lower return temperature (by 2K) compared to the water test. Considering the 50% EG/W and 50% HX/W as a working fluid in the radiator heating system with the option of design ΔT across the radiator (10K) resulted in a higher mass flow rate in the system (by 17%) compared to water test. For all optimised tests, it was noted that using 30% EG/W as working fluids in the heating system resulted in similar behaviour to the base case.

This research has contributed to knowledge through the followings:

- A bespoke test facility and methodology for conducting repeatable tests to evaluate the performance of a HRHS when using different heat transfer fluids under the same environmental conditions.
- An innovative approach (based on the energy balance principle) to evaluating the heat output from a radiator when operating with AHTFs. This approach allows assessing the heat output during steady state and transient conditions, as well as during the period when the heating system is 'off'. Also, it helps to overcome the limitations of the BS EN 442-2 model, which is only applicable to radiators that operate with water or steam.
- A better understanding of the performance of radiator heating systems when using alternative fluids in terms of flow, heat transfer and energy.

DECLARATION

The research described in this thesis is the original work of the author except where otherwise specified or acknowledgement is made by reference.

This research project was carried out at the School of Built Environment and Architecture, London South Bank University and under the supervision of Professor Issa Chaer, Dr Metkel Yebiyo and Dr Ye Zhihui.

The work has not been submitted for another degree or award of another academic or professional institution during the research program.

Shatha Fadel Haddowe

ACKNOWLEDGEMENTS

I would like to thank all the people who helped me directly or indirectly in the course of my PhD study and created an enjoyable, peaceful working environment to complete this project. I would like to express warm gratitude for my first supervisor Professor Issa Chaer for his invaluable ideas, suggestions, encouragement and support through my PhD journey. My honest appreciation is to my supervisor Dr Metkel Yebiyo for his help, kindness and motivation. I would like to say thanks to my supervisor Dr Ye Zhihui.

I am also grateful to the Built Environment and Architecture School and its staff for their assistance and special thanks to Dr Alex for his help and support. Biggest thanks are to my colleagues and friends for their encouragements. My special thanks go to my family for their encouragements and support during my study, especially My brother Dr Abas.

I would like to dedicate this thesis to my Father soul, my Mother, my Brother Dr Abas, my sisters Dr Hend and Marah and to my nephews and niece who have always supported and encouraged me to be in this position.

I would like to express my appreciation to the sponsor of this project, their sponsorship gratefully acknowledgement. I am also grateful to my industrial supervisors Mr Peter Stanley and Dr Andrew Eccleston from Energy Solutions Ltd, for their initial support with this PhD.

TABLE OF CONTENTS

LIST OF FIGURES

LIST OF TABLES

NOMENCLATURE

Symbol	Description	Units
A	Area	m^2
$Avg.\,hE$	Average hourly energy	kWh/h
$Avg.\,R.\,S.\,T$	Average radiator surface temperature	^oC
C_p	Specific heat capacity	kJ/kg/K
$C_{p_{eff}}$	Effective specific Heat of nanofluids	kJ/kg/K
C_{p_b}	Specific heat of the base fluid	kJ/kg/K
C_{p_p}	Specific heat of the nanoparticles	kJ/kg/K
DC	Duty cycle	%
ES	percentage of energy saved	%
F_T	Fluid flow temperature	^oC
g	Acceleration of gravity	N/kg
h	Heat transfer coefficient	$W / m^2.K$
I	Current	Ampere
k	Thermal conductivity	W / m. K
k_{eff}	Effective thermal conductivity	W / m. K
m	mass	kg
$\dot{m}$	Mass flow rate	kg/s
ΔT	Temperature difference across the radiator	K
$\Delta T_{\dot{e}}$	Radiator access temperature	K
q	Heat flux	W/m^2
$\dot{Q}_{Convection}$	Convection heat transfer	kW
$\dot{Q}_{Radiation}$	Radiation heat transfer	kW
$\dot{Q}_{output}$	Heat output from the radiator	kW
$\dot{Q}_{50}$	Nominal heat output of the radiator	kW
$\dot{Q}_{loss}$	Heat loss	kW
$\dot{Q}_{(sen)air}$	Sensible heat in the air	kW
$\dot{Q}_{(sen)B,walls}$	Sensible heat in the Booth's walls	kW
$\dot{Q}_T$	Total heat entering the radiator	kW
R_T	Return temperature	^oC
T_s	Absolute surface temperature	^oC
t	Time	second

V	Voltage	Volts
v	Velocity	m/s
$\dot{V}$	Volumetric flow rate	m^3/s
U	Thermal transmittance of the booth's wall	W/m^2K
F_r	A radiation exchange factor for two surfaces	/
u_{Random}	Precision error	/
u_{sys}	Bias error	/
u_{tot}	Total uncertainty	

GREEK SYMBOLS

Symbol	Description	Units
ρ_p	Density of practical	kg/m^3
ρ_b	Density of base fluid	kg/m^3
μ	Dynamic viscosity	Pa. s
ρ_{eff}	Effective density of nanofluid	kg/m^3
φ	Partials volume fraction in the base fluid	%
ζ	Pressure loss factor	/
$\overline{\sigma}_s$	Standard deviation	/
δ	Stefan-Boltzmann constant	/

ABBREVIATIONS

Abbreviation	Description
Ag	Silver
Al_2O_3	Aluminum Oxide
AHTFs	Alternative Heat Transfer Fluids
ASP	Assessment Standard Procedure
Au	Gold
CuO	Copper Oxide
Cu	Copper
CUSUM	Cumulative sum difference
EG	Ethylene glycol
EG/W	Ethylene glycol/water mixture
ETC	Environmental test chamber
Fe	Iron
GT	Globe temperature
HRHS	Hydronic radiator heating system
HTFs	Heat Transfer Fluids
HVAC	Heating, ventilation and air conditioning
HX	New nano-based heat transfer fluid
HX/W	Nano-based fluid /water mixture
IBT	Internal booth temperature
kW	kilowatt
kWh	kilo Watt-hour
LSBU	London south bank university
MDF	Medium-density fiberboard
NPL	National physical laboratory
PID	Proportional–Integral–Derivative controller
PT100	Platinum resistance temperature sensors
TiO_2	Titanium oxide
UK	United Kingdom

CHAPTER 1

Introduction

1.1 Overview

The built environment is responsible for a significant amount of energy use, for example, in the UK approximately 80% of domestic energy is used for space heating and the production of domestic hot water as shown in Figure 1.1 [1].

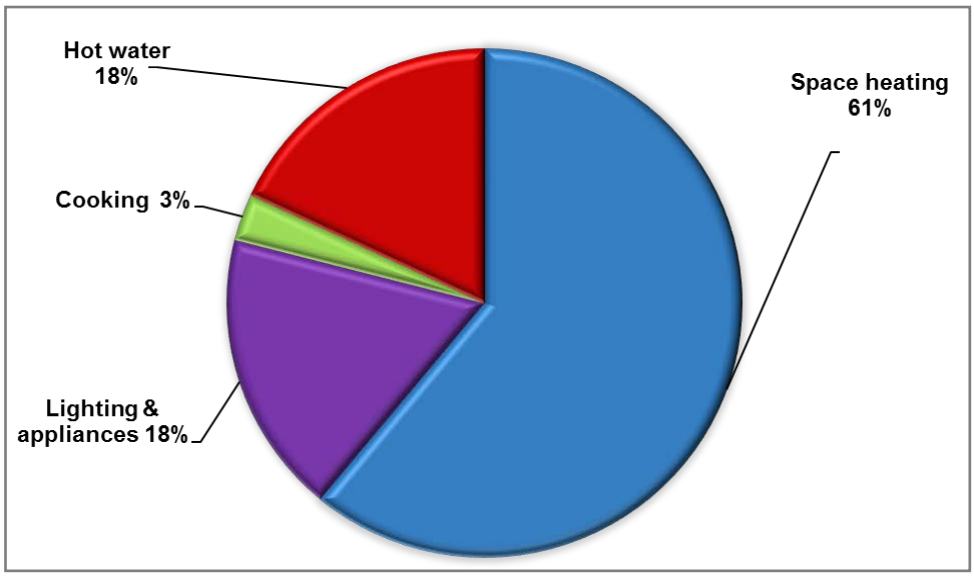

Figure 1.1: Breakdown of Energy Use in UK Dwellings

Furthermore, energy consumption in the domestic sector increased by 3.1% in 2016 compared to that in 2015, and in 2017 was higher by 0.3% compared to 2016. The majority of the increase was gas consumption, which is mainly used for powering heating systems [2&3]. According to the climate change act 2008, the UK government is committed to reducing energy used in buildings by 80% by 2050 [4]. This ambitious target could only be achieved through the integration of; (i) stringent building regulation strategies, (ii) developing innovative low carbon technologies and (iii) through better energy efficiency solutions that deliver better heat transfer and less heat loss. Therefore, given the significance of heat energy produced, energy saving could be achieved with better energy

efficiency solutions that deliver better heat transfer and less heat loss. This is thought to be improved by the integration of products that can enhance heat transfer capability and thus increase energy output and reduce costs. Heat transfer fluids (HTFs) are an essential part of the heating and cooling systems as they are the transfer medium between the heat source and heat sink. Thus, there is a need for the properties of such fluids to be, not just compatible with the systems, but also possess excellent heat transfer characteristics that give a better thermal performance.

Water is one of the most common heat transfer fluids used in heating systems due to its availability, low cost and acceptable thermal and transport properties. However, water has limitations in terms of heat transfer rates in energy-intense systems and reduced effectiveness due to aeration, oxidation and fouling. Furthermore, water has a freezing point of Zero Degree Centigrade (0ºC). This creates a high risk of freezing and bursting pipes in colder climates. Therefore, in colder climates, it is common practice to use ethylene glycol or propylene glycol as aqueous freezing point depressants and heat transfer mediums in Heating, Ventilation and Air Conditioning systems (HVAC) [5].

Based on the above researchers are always trying to develop and find out an alternative heat transfer medium which could enhance the heat transfer and overcome the limitations of water. During the last decade, nanoscience and nanotechnology have produced a new HTFs by introducing nanofluids; these are a mixture of suspended nanoparticles in a base liquid, which if applied correctly could enhance the heat transfer between the heat source and heat sink. A nano-based heat transfer fluid has been introduced as a nanofluid with a base of 50% ethylene glycol /water mixture to apply in heating and cooling systems, (for confidentially the nano-based fluid is identified as HX in this thesis). Published data from on-site tests have shown improvement in some heat transfer characteristics in closed-loop heating systems where the nano-based fluid was used [6]. A preliminary test by LSBU for the nano-based fluid had shown that a faster heat transfer response was achieved with

the nano-based fluid compared to water [7]. However, there is a lack of understanding of the theoretical and practical features of the nano-based fluid, which resulted in these improvements and how this could be transferred/ optimised and applied to different applications. According to the Standard Assessment Procedure (SAP) for Energy Rating of Dwellings [8], no conclusions can be drawn that any modified HTFs could cause a change in the performance of the systems without accurate measurements under controlled laboratory conditions. Therefore, this research was set to experimentally investigate and compare the performance of the hydronic radiator heating system (HRHS) with the new nano-based heat transfer fluid, under controlled test conditions against that with potable water, 30% and 50 % ethylene glycol/water mixtures.

1.2 Aims and Objectives

This project aims to research and experimentally investigate the performance of a hydronic radiator heating system (HRHS) when using various fluids as an alternative to water under controlled conditions. The effects of using the new nano-based fluid (HX) as an alternative heat transfer fluid (AHTF), and also 30% and 50% ethylene glycol/water mixtures are compared to potable water. The main objectives are as follows:

1. To provide a critical literature review of research on heat transfer fluids in the built environment and current research on alternative nanofluids and their applications in the heat transfer field.
2. To understand the thermo-physical properties of the proposed heat transfer fluids and compare these properties with the values available in the literature.
3. To design and construct a bespoke test facility which can be used to carry out the performance tests, using different heat transfer fluids within a HRHS under controlled conditions.

4. To develop a test procedure and performance evaluation approach that enables credible comparison between the proposed alternative fluids and water as a base case HTF under the same controlled conditions.
5. To validate the test facility by conducting base-case experiments using water as a heat transfer fluid.
6. To conduct a range of experiments under controlled conditions to investigate the performance of the HRHS when using the proposed AHTFs, by analysing both the amount of energy consumed and the air temperature inside the booth.

1.4 Outline of the Thesis

This thesis is split into eight chapters, which are outlined as follows:

Chapter 1

The first chapter introduces the subject of the thesis and explains the supporting reasons for carrying out this research. It also presents the aims and objectives of the project.

Chapter 2

This chapter provides a review of current literature on heat transfer fluids used within the built environment, and relevant research focused on the performance and reliability of nanofluids and their application in different fields. The chapter also reviews a range of existing theoretical models that are currently used to evaluate the effective thermophysical properties of nanofluids and explores empirical research into their thermal conductivity. Additionally, it includes information about the new nano-based heat transfer fluid (HX). The chapter delivers background information about hydronic radiator heating systems (HRHS) and summarising the findings from existing research into HRHS, especially in regard to improving the performance of the hydronic radiator.

Chapter 3

This chapter provides an overview of the alternative heat transfer fluids (AHTFs) used in this research project, providing detailed information on the supplier and preparation of each fluid. It explains the process taken to measure the thermophysical properties of the examined fluids, in particular their thermal conductivity, viscosity, specific heat capacity and density. The measurements are then compared with available values in the literature. The chapter also presented the theoretical evaluation of the effective thermal conductivity for the new nano-based fluid (HX) the comparison with the results from experiments carried out with HX samples.

Chapter 4

This chapter outlines the design and develop a bespoke test facility for this research project and describing the data monitoring system used. The chapter includes a detailed explanation of the calibration procedure and confidence analysis conducted on the temperature and flow rate readings. An outline of the experiment is provided, including the different test techniques and scenarios used. Two different scenarios (drop-in and optimised scenarios) are presented in order to get a deep understanding on how the HRHS's performance is affected by the different types of heat transfer fluid, as well as two different methods of testing: steady state and thermostat tests. The steady state tests were designed to ascertain the parameters of the test once it had reached a stable point and was, therefore at a steady state. The thermostat tests were designed to replicate real-life conditions of a heating system, with the air thermostat being used to control the indoor temperature at a certain setpoint.

Chapter 5

This chapter begins with a review of current standards and procedures used to determine the thermal output of radiators fed by heat from a remote energy source and the limitations of the current standards. It then describes the new approach taken in this research to

evaluate the thermal output of radiators using alternative heat transfer fluids and measuring the amount of heat transferred from the radiator into the indoor air. This approach was developed based on the energy balance principle to overcome limitations of the current standard performance evaluation model (BS EN 442-2), as this only applies to radiators that use water or steam as a heat transfer fluid. The advantages of taking this approach to evaluate the heat output from a radiator are identified and discussed.

Chapter 6

In this chapter, the data obtained from the experiments carried out is analysed and interpreted. This includes the results of base case tests using water as a heat transfer fluid, as well as other tests using the alternative heat transfer fluids (AHTFs). The monitored parameters of the base case tests are compared to those with the AHTFs. Most significantly, a comparison of the dynamic heat-up response of the heated zone (booth). This chapter compares the response of the HRHS to the different fluids by monitoring the indoor air temperature in the heated zone (booth) and the amount of energy that was consumed during each test. Results from different test scenarios (drop-in and optimised scenario), as well as different testing methods (steady state and thermostat), are analysed and demonstrated in this chapter.

Chapter 7

This chapter presents the radiator heat output results obtained when using the energy balance approach to assess the performance of the radiator, for the base case (water) tests. Besides, it determines the verification of the considered approach. The chapter also presents an analysis of the radiator heat output results with the AHTFs and concludes with a comparison of the results against base case (water test) outputs.

Chapter 8

The final chapter summarises the findings from the research project and draws various

conclusions, taking into account the literature review, the experiment results and the performance evaluation approach. Highlighting how this project contributes to knowledge, the chapter closes by suggesting future avenues of research which can be carried out using the work presented in this thesis.

CHAPTER 2

Literature Review

2.1 Introduction

This chapter provides a review of relevant literature related to heat transfer fluids (HTFs) in the built environment and advances in nano-based fluids as alternative heat transfer fluids (AHTFs). The chapter highlights different theoretical models for evaluating the effective thermophysical properties of nanofluids as a two-phase material. Also, this chapter outlines the materials that are used to produce the nanofluids, including the base fluid and nanoparticles. As well as, it covers the studies related to the preparation, stability of the nanofluids and applications of nanofluids in different fields. Furthermore, it presents background information about the new nanofluid (HX) as an alternative heat transfer fluid (AHTF). In addition, this chapter gives a detailed review of hydronic radiator heating system (HRHS) and the studies related to enhancing the hydronic radiator performance from different aspects.

2.2 Heat Transfer Fluids

Heat transfer fluids (HTFs) are currently used in most centralised and partially centralised heating and cooling systems. This includes liquids such as water; aqueous brines, glycols, and refrigerant fluids as used in many cooling and heating systems in buildings, data centres, processing plants, vehicles air conditioning and thermal storage systems. Heat transfer fluids are expected to have high thermal conductivity, high volumetric heat capacity, and low viscosity. They also need to be environmentally benign, non-corrosive, safe and cost-effective [9]. According to ENNIS [10], the factors which need to be considered in the selection of a heat transfer fluid are:

- High heat capacity - enables more heat to be carried between the heat source and heat sink.
- High thermal conductivity - provides a higher heat transfer rate across the surfaces in heat exchangers and pipes
- Low viscosity, requires less pumping power which means operating costs are lowered
- Non-toxic and chemically inert, the fluids could be used in a wider range of applications like food processing and refrigeration and eliminates the need for specially designed equipment and piping, which in turn lowers the total cost.
- Availability
- Cost of production
- Low maintenance of the systems
- Thermal stability as well as the freezing and boiling temperatures of the fluids
- Environmentally friendly.

The operating condition of the systems as well as the fluid properties influence the selection of the HTFs and make one better or more efficient than the other.

2.3 Types of Heat Transfer Fluids

Wide ranges of heat transfer fluids are currently used within different sectors. Their use is dependent on the application operating parameters and thermophysical properties of the fluid. For this study, the most common types of HTFs in the built environment, followed by a detailed review of nanofluids are discussed and presented.

2.3.1 Water

Water is one of the most common and cheapest HTF. It is non-toxic with high specific heat, and low viscosity, However, it has a significant disadvantage of operation in extreme conditions due to high freezing point (0°C). As temperatures reach chilling values, the water pipes in home and business are at a higher risk of freezing and bursting [11]. A

record £194 million was paid out to help people deal with burst pipes in the first quarter of 2018 as the freezing weather took its toll, according to insurers [12]. Moreover, water easily loses the neutrality in PH value by picking up contamination, so it causes corrosion hazards and that can cause mineral deposits on the heat transfer surfaces, which reduces its heat transfer capability. These deposits also could cause blockages in the piping systems and affect some of the water properties, thermal performance, system reliability and system maintenance costs [11]. Many alternative fluids have been developed to improve upon the basic characteristics of water and facilitate effective heat transfer.

2.3.2 Steam

Steam is pressurised water vapour and it is widely used as a heat transfer medium to convey heat over distances because it eliminates the need for pumping, as it is flowing in the pipes under its pressure. However, higher pressure and high temperatures introduce higher risk and limit the local proximity and control options. Furthermore, overuse of control devices in such systems could cause the heating system to be filled with air and that would affect the performance of the system. For small commercial buildings and domestic dwelling, normally low pressure (less 200 kPa) steam is used in the heating system. For safety issue, the steam systems require strict monitoring as the leak of the steam could cause series problems to the people and properties [5&11].

2.3.3 Air

Air as a HTF has suitable properties and freely available. Using air as a means of heat transport dates back to Roman times when underfloor air heating systems were in place to heat public baths. The usage of air as the heat transport medium is still used in American offices and homes, though there has been a growing preference for hot-water systems, which have been used in European countries for some time. Air also works in combination with other systems when the primary heated medium is steam or hot water. Air does not

freeze or boil and is non-corrosive. However, it has low specific heat capacity (1.018 kJ/kg. K), and low density (1.2 kg/m^3) at ambient temperature compared to water (4.183 kJ/kg. K and 999.8 kg/m^3), so it carries less heat for shorter distances than hot water or steam does [11].

2.3.4 Glycol/Water Mixtures

Ethylene and propylene glycol are antifreeze fluids that provide freeze protection as long as the proper concentration is maintained. In many applications, ethylene glycol is more commonly used due to lower cost, lower viscosity and better heat transfer properties compared to propylene glycol. Glycol-water mixtures of 50/50, 30/70 or 60/40 are used as a heat transfer media to provide freeze protection for closed-loop heating and cooling systems and other industrial processes. Glycol/water mixtures provide a higher evaporating and boiling point than water on its own. It is common to use ethylene glycol or propylene glycol water mixture as the heat transfer mediums for the heating system in cold regions due to the low freezing temperature [5].

Ethylene glycol has a low freezing point, has a high boiling point compared to water. However, it could degrade into acid over time in the presence of oxygen and that could affect the freezing point. Therefore, it needs regular tests to determine the percentage of the mixture, pH and inhibitor levels. The glycol-water mixtures need to be replaced every 3 to 8 years, depending on the working temperatures [13]. Glycol mixtures have some disadvantages compared to water, for instance; ethylene Glycol is toxic and has a higher viscosity than water, thus increasing the pressure drop and in turn, required pumping power. Glycol as an automotive antifreeze is not suitable for heating and cooling systems and industrial applications due to high levels of silicate inhibitors which can affect the evaporators and pumps [14].

2.3.5 Nanofluids

Nanofluid is defined as a mixture of suspended nanoscale particles of average size less than 100 nm in a base fluid that does not dissolve the nanoparticles. In the last decade, extensive research has been conducted in both fundamental and practical sides to develop nanofluids, which can be used to enhance the heat transfer process in most heat transfer applications. However, research on this topic has some limitations in terms of using the nanofluids and evaluate the heat transfer enhancement in real applications. The theory of nanofluids and relevant research related to their applications are presented in the following subsections.

2.3.5.1 Theory and History of Nanofluids

Fluids play an important role as the heat carrier in many heat transfer applications including power stations, cooling and heating systems, data centres, processing plants, vehicles air conditioning (AC) and thermal storage systems. In all of these applications, the thermal conductivity of the heat transfer fluid has a strong effect on the efficiency of the heat transfer process and overall efficiency of the system. For such reason, researchers have continuously worked on developing advanced heat transfer fluids that have significantly higher thermal conductivity than the conventional fluids. As of most the solids, such as aluminium, diamond and silver have a thermal conductivity higher than conventional fluid (such as water or ethylene glycol) [15]. This fact leads the researchers to study the dispersing of nano-meter-sized particles in conventional fluids to increase the thermal conductivity of the fluids.

Choi [15], is the first researcher who developed the new heat transfer fluids by suspending nanoscale (with an average size of less than 100 nm) of metallic particles in conventional heat transfer fluids and introduced nanofluids. The principles of Choi’s work depended on Maxwell's theoretical model [18], which was introduced over 100 years ago. Maxwell's

model showed that the effective thermal conductivity of fluids that contain circular particles increases with the volume fraction of the solid particles with the ratio of the surface area to volume of the particle. Choi [15] claimed that stably suspended aluminium oxide nanoparticles in the water enhanced thermal conductivity of the nanofluid in comparison to water. Incidentally, this became the first publication to have used the term nanofluids. Furthermore, the useful properties of the nanophase materials come from the relatively high surface area to volume ratio that is due to the high proportion of constituent atoms that exist at the particle boundaries.

The thermal, mechanical, optical, magnetic, and electrical properties of nanophase materials are higher to those of ordinary materials with coarse grain structures [16]. By suspending nanophase particles in heat transfer fluids, the heat transfer performance of the fluid can be significantly improved. The main reasons for that are as reported by [17]:

- The nanoparticles in the base fluid increase the apparent or effective thermal conductivity of the fluid.
- Increase the collision and interaction among particles, fluid and the flow passing surface
- Intensify mixing fluctuation and turbulence of the fluid.

2.3.5.2 Types of Nanofluids

Types of nanofluids depend on the nanoparticle material dispersed in the base fluid. Some of these materials are oxide ceramic (Al_2O_3 and CuO), nitride ceramics (AIN and SiN), carbide ceramics (SiC andTiC), metals (Ag, Au, Cu and Fe), semiconductors (TiO_2), single –double or multi-walled carbon Nanotubes (SWCNT, DWCNTand MWCNT). Also, there is a composite material such as nanoparticles core- polymer shell composites as well. Furthermore, new material and structures are attractive for use in nanofluid where various

molecules influence the particle-liquid interface. Most common nanoparticles and base fluids that have been used to prepare the nanofluids are presented in Figure 2.1.

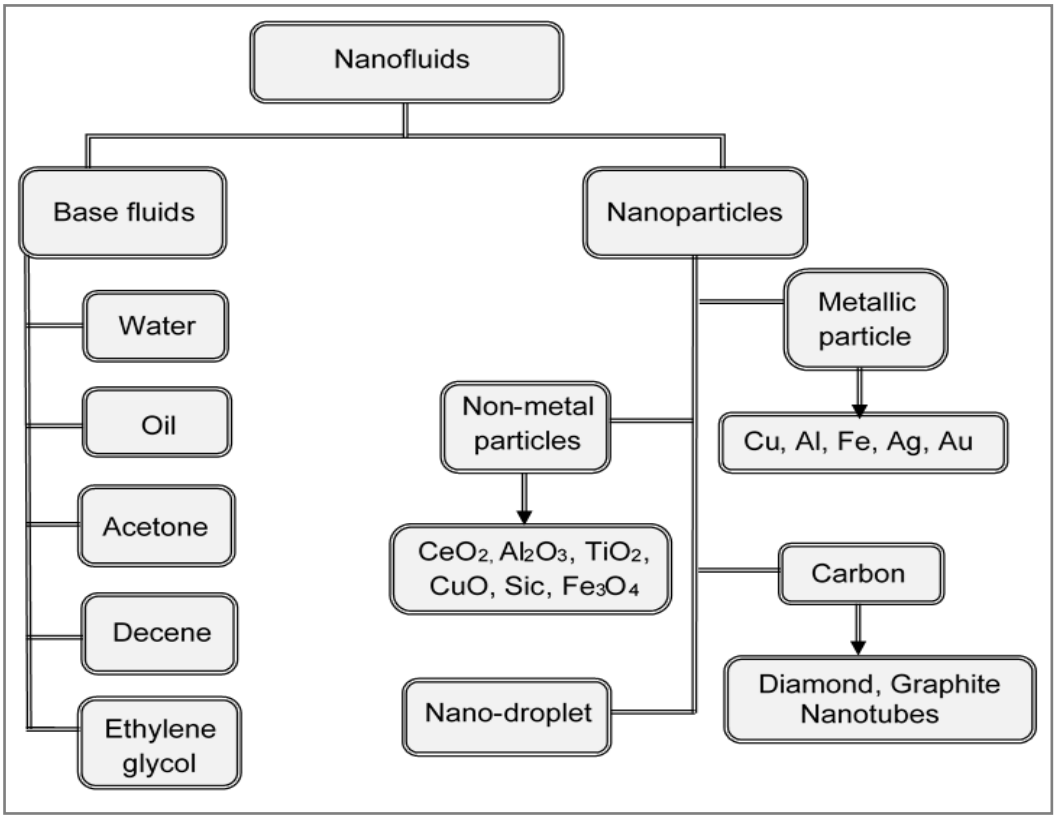

Figure 2.1: Most Common Types of Nanoparticles and Base Fluids [16&17]

Besides the type of nanoparticles and the base fluids, several factors could affect the thermal properties of the nanofluids such as the size, shape, structure and concentration of the nanoparticles in the base fluids.

2.3.5.3 Preparation of Nanofluids

Preparation of nanofluids is the most important stage in the use of nanoparticles or any nanostructured materials to improve the thermal characteristics of conventional HTFs. Better preparation result in better performance and improved thermal transport properties. The prepared nanofluids, with no contamination to medium, good fluidity, high stability, low viscosity and high thermal conductivity would have potential applications as coolants in advanced thermal systems [19]. Preparation of stable nanofluids is the first and essential

step of nanofluid research and applications. The properties and behaviour of the nanofluid depend on some parameters including the properties of the base liquid, the particle concentration, dispersed phases, particle size and morphology, as well as the presence of dispersants and surfactants [20]. There are two main methods, which are used for nanofluid preparation, single-step method and two-step method. In the single-step method, preparing nanoparticles and dispersing them inside a base fluid occurs instantaneously. It is a process combining the preparation of nanoparticles with the synthesis of nanofluids, for which the nanoparticles are directly prepared by physical vapour deposition (PVD) technique or liquid chemical method [21]. In this method, the processes of drying, transportation, storage, and dispersion of nanoparticles are avoided, so the cluster of nanoparticles is minimised, and the stability of fluids is increased [22]. The most significant disadvantage of the single-step method is the residual reactants are left in the nanofluids due to incomplete reaction or stabilisation. It is hard to clarify the nanoparticle effect without eliminating this impurity effect [19].

Most nanofluids, including oxide nanoparticles and carbon nanotube, are produced using the two-step method, but for metallic nanoparticles or particles with the high thermal conductivity, one-step method is preferred [23, 24&25]. In the two-step method, nanoparticles are processed and made by other techniques first and then dispersed into a base fluid.

The main advantage of this two-step synthesis method is that it produces nanoparticles under clean conditions, without undesirable surface coatings and other contaminants [26]. Also, the disadvantage of the two-step technique is that the nanoparticles form clusters during the preparation of the nanofluid, which stops the proper dispersion of nanoparticles inside the base fluid. Many nanoparticles aggregate together in forms of clumps, for this reason, preparation of nanofluid using one-step method has received notable attention [24, 26&27].

2.3.5.4 Stability of Nanofluids

The stability of nanofluids depends on different characteristics such as preparation of nanofluids, concentration, size and shape of nanoparticles and the type of base fluid. Based on Ibrahim et al. [28], adding a dispersing agent such as a surfactant can enhance the stability of nanofluids. Surfactants are the chemical compounds added to nanofluids to reduce the surface tension of fluids, increase the immersion of nanoparticles in the base fluids to avoid sedimentation. The most common types of surfactants are listed below [28, 29& 30]:

1- Sodium dodecyl sulfate (SDS)

2- Sodium dodecyl benzoic sulfate (SDBS)

3- Hexadecyltrimethylammonium bromide (CTAB)

4- Polyvinylpyrrolidone (PVP)

5- Dodecyl trimethyl ammonium bromide (DTAB) and sodium octanoate (SOCT)

7- Arabic gum (AG) Natural polysaccharides and glycoproteins complex

Surfactants have some disadvantages; they may produce foams during the heating process. Furthermore, they could increase the thermal resistance between nanoparticles and the base fluid, as the surfactants can attach on the surfaces of the nanoparticles and that may limit the enhancement of the thermal conductivity of the nanofluids [20].

The stability of nanofluids is an important issue that can affect the thermophysical properties of these fluids, as nanofluids can lose their ability to transfer heat if coagulation occurs. However, production of homogeneous nanofluids with high stability is still a challenge, The main factors that can affect the stability of nanofluids are types, diameter and density of the nanoparticles as well as the viscosity and pH value of the base fluid.

[31&32]. Many methods are used to evaluate the stability of the nanofluids [34]; the most common methods are shown in Figure 2.2.

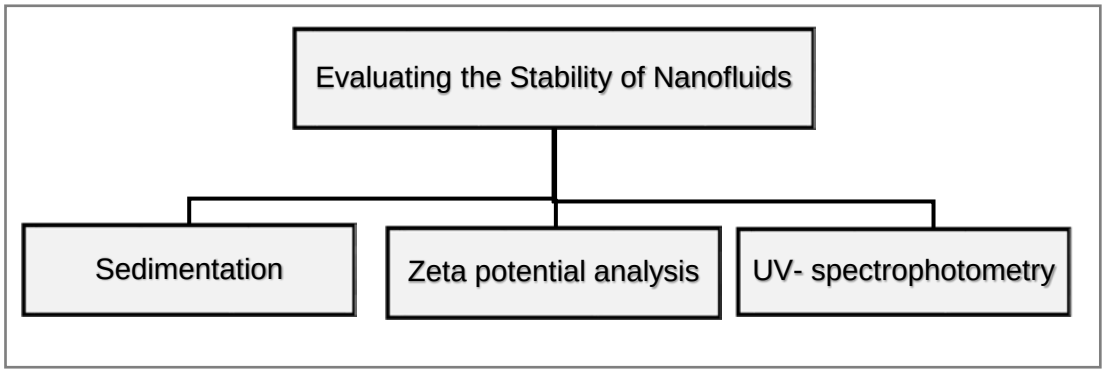

Figure 2.2: Methods of Evaluating the Stability of Nanofluids

The sedimentation method is the simplest and most reliable method to evaluate the stability of nanofluids. However, it is time-consuming as it requires a long period of observation. In this method, after preparation of nanofluids, they could be kept in a stable standing condition in glass tubes, and settlement of nanoparticles should be recorded continuously by capturing photos. For instance, Xian-ju et al. [35], tested nanofluids samples (Al_2O_3 nanofluid - water as a base fluid) to investigate the stability of the nanoparticles. Sedimentation photograph capturing method was implemented; their results showed that the maximum nanoparticles spreading could be obtained at a pH value of 8.0 for the fluid.

Nanofluids can be considered to be stable when the particle size or concentration of particles keeps constant. Sedimentation photograph of nanofluids in test tubes can be taken by a camera to observe the stability of nanofluids [22, 23 and 36]. Another parameter that needs to be considered in getting information on the stability of nanofluid is the Zeta potential. Zeta potential is the electric potential existing between the dispersing liquid and the particle surface at the clipping plane [37]. Spectral analysis using UV-spectrophotometer is another method to evaluate the stability of nanofluids. In the UV–vis spectrophotometer light is passed through the suspension, then a graph of absorbance

against wavelength provides the absorption spectrum of the sample. There is a direct relationship between the intensity of absorbance and the concentration of nanoparticles present in the fluid. This method is applied for the nanofluids with low concentration [24].

2.3.5.5 Thermal Properties of Nanofluids

Heat transfer enhancements can be achieved by improving the thermal properties of HTFs. For instance, glycols are added to water to reduce its freezing point and to increase its boiling point. The heat transfer properties can be improved by adding solid particles to the liquid. The goal of nanofluids is to achieve the highest possible thermal properties at the smallest possible concentrations of nanoparticles in base fluids to accomplish this goal; it is essential to understand how nanoparticles enhance energy transport in liquids. The thermal conductivities of the particle materials are typically higher than those of the base fluids such as water and ethylene glycol. For each specific nanofluid, thermal conductivity, density, specific heat and dynamic viscosity all depend on the nanoparticles' material, concentration and base fluid [37].

Elena et al. [38] stated that there is a complex correlation between nanofluids parameters (nanoparticles and base fluids type) and their properties such as density, thermal conductivity, specific heat capacity and viscosity. Therefore, the development of nanofluid requires a complex approach that considered the changes in all essential thermophysical properties caused by the introduction of nanomaterials to the fluids.

2.3.5.6 Nanofluids Thermal Conductivity

Various theories have been developed, by the researchers to compute the thermal conductivity of two-phase materials based on the thermal conductivity of the solid and liquid considering their relative volume fractions [39]. Over 100 years ago, Maxwell [18] was the first to investigate the thermal conductivity of a colloid solution. This investigation

led to development of a mathematical model which is well known as Maxwell's model. This model applies to homogeneous and low-volume fraction liquid-solid suspension with randomly dispersed, uniformly sized and non-interacting spherical particles. Hamilton and Crosser [40] extended the Maxwell model by considering irregular particle geometries and introducing a shape factor to the Maxwell model. An additional model presented by Davis et al. [41] is applied to spherical suspensions. More models were developed to predict the effective thermal conductivity of nanofluids. Bruggeman [42] developed a model based on Maxwell's model to study the interactions between randomly dispersed spherical particles. This model is applicable for the large volume fraction of spherical particles. For low-volume fractions, the Bruggeman model results were very close to that obtained with Maxwell's model. Khalil & Kambiz [43] developed a model to evaluate the effective thermal conductivity at different temperatures by considering nanoparticles diameter, volume fraction, the dynamic viscosity of (base fluid).

The most common models (found in the literature) that were used to estimate the effective thermal conductivity of nanofluids are presented in Appendix 2.A. On the experimental side, measuring the thermal conductivity of fluids is a challenging task because the fluids do not have an exact shape, size, and cross-sectional area. Fourier's law of heat conduction is exploited for the measurement of the thermal conductivity. In the most straightforward preparation, first needs to establish a steady one-dimensional heat flow by the application of known heat flux (q). Then by measuring the temperatures at two known locations (ΔT_L) along the direction of heat transmission (L), the thermal conductivity (k) can be estimated from equation 2.1.

$$k = q \,/\, (\Delta T_L \,/\, L) \qquad \textbf{(2.1)}$$

For nanofluids, the presence of suspended nanoparticles could cause a problem when measuring the thermal conductivity; as the homogeneity of the medium has to be maintained. The thermal conductivity of fluids can be measured if the time taken for

measurement is minimal so, that the convection current does not build up and affect the results. Also, instead of heating the fluid from below, heat applies from the top, and that facilitate the conduction of heat within the layer in a reasonable manner. The most common techniques for nanofluids thermal conductivity measurements are [44&45]:

- Transient hot-wire (THW) technique
- Thermal constants analyser technique
- Steady-state parallel-plate technique
- Cylindrical cell technique
- Temperature oscillation technique
- Thermal comparator technique
- (3 ω) technique

The Transient hot-wire technique has been introduced as the most popular technique used by scientists and researchers to measure nanofluids thermal conductivity. Figure 2.3 shows the percentages of using different techniques for measuring nanofluids thermal conductivity in the literature (extracted based on data in conductivity measurements).

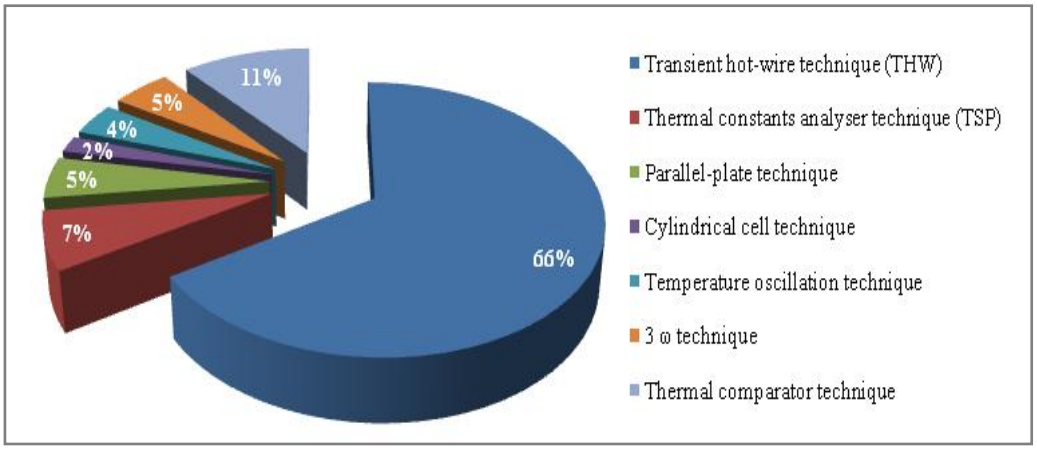

Figure 2.3: Common Methods for Thermal Conductivity Measurement of Nanofluids

From the above figure, it is clear that the Transient hot-wire technique is the most dominant technique used to measure the thermal conductivity of nanofluids. This is mainly due to its low uncertainty which can be attributed to the short measurement time, thus reducing the effect of natural convection on the actual reading. Review of current literature revealed

extensive experimental research on the effect of the base liquid, particle size, shape, material, concentration and temperature on the thermal conductivity of nanofluids. Xie et al. [46] prepared alumina nanofluids with different base fluid (water, ethylene glycol and pump oil) and different particle's size. They used 60.4 and15 nm-sized particles, and they observed enhancement in the thermal conductivity for ethylene glycol as a based fluid with larger nanoparticles.

Choi et al. [47] showed that the addition of a small amount (less than 1% by volume) of nanoparticles increased the thermal conductivity by double. While most researchers worked on increasing the thermal conductivity, others like Han [48] researched other thermal and transport properties such as viscosity and heat capacity. He reported up to 126% and 20% increases in the effective heat capacity were experimentally found with water-in-FC72 (Fluorinert™ Electronic Liquid) nanoemulsions and indium-in-PAO nanofluids, respectively. This was attributed to the large amount of latent heat absorbed in the phase transition from nanoparticles to nanodroplets and released in reverse transition. However, these fluids are low-temperature fluids and their base-fluids have low thermal conductivity; for example, the thermal conductivity of FC72 is only 0.057 W/m.K, that is tenth of the thermal conductivity of water (0.58 W/m.K).

Han [48] also reported an increase in the viscosity of the fluid as a result of the addition of nanoparticles, which can be described by the Einstein-Batchelor model. Due to the enhanced thermal conductivity of the nanofluid he tested, 15% increase in heat transfer coefficient of natural convection was observed with water-in-FC72 nanofluids. He reported that overall nanofluids possess improved thermal transport properties and that nanofluids have potential as the next-generation heat transfer fluids. Most efforts by the researcher were pushed to increase thermal conductivity while other thermal transport properties such as viscosity and heat capacity, have been paid less attention [48].

2.3.5.7 Nanofluids Specific Heat Capacity and Density

The specific heat capacity and density of nanofluids can be enhanced based on the specific heat capacity and density of the nanoparticles. The effective specific heat capacity ($C_{P_{eff}}$) and density (ρ_{eff}) of nanofluids can be evaluated based on the physical principle of the mixture rule as follows [49].

$$C_{P_{eff}} = [(1-\varphi)(\rho C_p)_b] + \frac{\varphi(\rho C_p)_p}{[(1-\varphi)\rho_b + \varphi(\rho_p)]} \quad \textbf{(2.2)}$$

$$\rho_{eff} = \rho_p \varphi + \rho_p(1-\varphi) \quad \textbf{(2.3)}$$

Where, $C_{P_{eff}}$ and ρ_{eff} are the effective specific heat capacity and density, respectively. The C_p and ρ_p are nanoparticle specific heat capacity and density while $(\rho\, C_p)_b$ are specific heat capacity and density for the base fluid. Where φ is the volume frication of the nanoparticle in the base fluid. Nelson et al. [50] reported that the specific heat capacity of polyalphaolefin enhanced by 50% with the addition of 0.6% exfoliated graphite nanoparticles. Shin et al. [51] synthesised molten salt-based silica nanofluid and they observed 14.5% enhancement in the specific heat capacity by adding 1% of the silica to the base fluid. The thermal properties of nanofluids are dependent on the specification of the practical materials, concentration and base fluids. Therefore, each nanofluid has individual and unique thermal properties which need to be investigated, measured and compared with the base fluid properties to evaluate the enhancement in the thermal properties of the nanofluids.

2.4 Applications of Nanofluids

Nanofluids can be used for a wide variety of applications such as transportation, electronics, medical, manufacturing as well as nuclear engineering that can take advantages of nanofluids as an AHTFs due to the enhancement in thermophysical properties of these fluids compared to the conventional fluids. In fact, since the introduction

of the nanofluids, their applications have been discussed in various research papers such as biomedical application, lubrication, surface coating, petroleum industry, cooling of automobile engines and welding equipment. Furthermore, nanotechnology is being considered for use in many applications targeted to provide more efficient energy supplies and cleaner uses. While many of these applications may not affect energy transmission directly, each has the potential to reduce the need for the mains electricity, petroleum distillate fuel, or natural gas [52]. The following sections present research and advances in the applications of nanofluids.

2.4.1 Nanofluids in Automotive

Golakiya et al. [53] experimentally investigated the performances of the heat transfer with Al_2O_3/water nanofluid in an automobile radiator. They observed that by adding 2% by volume fraction of Al_2O_3 to water the heat transfer rate was enhanced by 14% and by adding 4% volume fraction of Al_2O_3 in water resulted in 17% improvement in the heat transfer rate. Leong et al. [54] tested nanofluids as a coolant in automobile engine radiator and they found that the overall heat transfer coefficient increases about 3.8% with the addition of 2% copper particles in a base fluid at the Reynolds number of 6000 and 5000 for air and coolant respectively.

Ramgopal et al. [55] experimentally investigated the heat transfer enhancement with water and coolant base fluids, which have different concentrations of nanoparticles carbon nanotubes (CNTS). They considered a SUZUKI (800CC) - car radiator as a cooling circuit using the nanofluids to replace the conventional engine coolant. They concluded that the improvement in heat transfer of the automobile radiator was around 30% when CNTS and coolant are used as a cooling medium. Some studies have reported that adding nanoparticles to actual fuels resulted in some remarkable advances such as shortening of ignition, higher burning rates and increase in energy densities [56].

2.4.2 Nanofluids in Heating for Buildings

Using ethylene glycol/ water mixture as a heat transfer fluid in the heating systems is a common practice in cold climates regions due to its antifreeze properties. Kulkarni et al. [57] considered the conventional method (duct coils through a bank of tubes with finned surfaces) to heat a building using nanofluids as a heat transfer medium. In their case study; they used different nanofluids (6% Aluminum oxide, 6% Copper oxide, and 6% Silicon dioxide) based on 60% ethylene glycol/water mixture. They indicated that the replacing conventional ethylene glycol/ water mixture in the heating system with the mentioned nanofluids (by controlling the heat transfer rate to be same with all fluids) reduced the volumetric flow rate in the system by 37.22%, 28.95% and 22.18% with the mentioned nanofluids respectively. As a result, the pumping power with the nanofluids (6% Aluminum oxide, 6% Copper oxide, and 6% Silicon dioxide) reduced by 38.26%, 27.57 % and 11.65% respectively compared to the base fluid (60% ethylene glycol/water mixture).

2.4.3 Nanofluids in Solar Thermal

The solar thermal collectors are commonly used to collect thermal energy from the sun. Many researchers applied nanofluids as AHTFs in solar collectors and they studied the improvement in the efficiency of the solar thermal collectors with these fluids. Verma and Kundan [58] experimentally investigated the effect of Al_2O_3 water-based nanofluid as an absorbing medium in a solar collector. They examined the efficiency of the collector with different flow rate (60, 80 and 100 ml/h) and different nanoparticles mass fraction. Their results revealed that the addition of 0.05% Al_2O_3 nanoparticles to the water increased the efficiency of the solar thermal collector by 3% - 5%. They also concluded that higher efficiency of the collector could be obtained by minimising the losses and preventing the settling of the nanoparticles in the base fluid. The size, shape and volume fraction of the nanoparticles in nanofluids can affect the collector efficiency directly.

Mahendran et al. [59] studied the efficiency of the solar collector using 0.3% concentration TiO_2/ water nanofluid. They found that the effectiveness of the collector enhanced by16.7% with TiO_2 /water nanofluid compared to the effectiveness of the collector working with water only (at a fixed flow rate, 2.7 l/min for both fluids). The results obtained from these studies proved that the concentration and type of nanoparticles affect the efficiency of the solar collector, as the application of 0.3% of TiO_2 nanofluid compared to 0.05% Al_2O_3 nanofluid resulted in a better enhancement in the efficiency of the solar collector.

2.4.4 Nanofluids in Refrigeration System

A literature search in this field revealed several research articles relating to nano-lubricants (nanoparticles plus refrigeration oil) beings mixed with pure refrigerant to produce nano-refrigerant as called by Majgaonkar [60]. Reji Kumar et al. [61] performed experimental studies to evaluate the performance parameters of a vapour compression refrigeration system with different lubricants, including nanolubricants. They concluded that the freezing capacity of the refrigeration system was higher with polyol ester (POE) oil and alumina nanoparticles (as nanolubricant) compared to the freezing capacity of the system obtained with POE oil. Also, they observed that the power consumed by the compressor reduced by 11.5% when the nanolubricant applied instead of conventional POE oil. They stated that the coefficient of performance (COP) of the refrigeration system increased by 19.6% when the POE oil was replaced with the nanolubricant.

Haque et al. [62] experimentally investigated the performance of a domestic refrigerator with the addition of nanoparticles into the conventional (POE) oil. They added different sizes of Al_2O_3 and TiO_2 nanoparticles to the POE oil, using two different volume concentrations (0.05 vol.% and 0.1 vol.%) of Al_2O_3 and TiO_2 to produce the nanolubricants for the compressor. They concluded that the nanolubricants enhanced the heat transfer in the evaporator, which resulted in a higher freezing capacity. Also, they highlighted that

using the nanolubricants reduced the energy consumption of the refrigerator by 27.73% and 14.19% respectively. They attributed the reduction in energy consumption to the existing of the nanoparticles, which help to reduce the wear rate and coefficient of friction between moving surfaces in the compressor.

Oluseyi et al. [63] investigated the effect of the Al_2O_3 nanoparticle, adding to the compressor oil (Capella D), on the performance of domestic refrigerator and energy consumption. Their investigation was performed on the domestic refrigerator without any system retrofitting. They concluded that adding the Al_2O_3 nanoparticle to the compressor oil (as nanolubricant) enhanced the performance of the refrigeration process and improved efficiency. They stated that the reason behind the enhancement in the efficiency was the improvement in the thermophysical properties of the nanolubricant, as the thermal conductivity enhanced by 64% by adding the Al_2O_3 nanoparticle to the oil, (Capella D) compared to oil (Capella D) on its own.

Majgaonkar [60] concluded that the use of nanofluids in the refrigeration systems are attractive, but their applications are restricted by many factors such as poor long-term stability, high-pressure drop, high pumping power and high production cost. Therefore, more research is needed to apply the nanofluids in a refrigeration system.

2.4.5 Nanofluids in the Electronic Field

A recent development in electronic and data technologies has shown a significant shift in the need to provide better cooling and heat transfer in this field. Cong et al. [64] experimentally investigated the effect of nanofluids (different concentrations of Al_2O_3 and TiO_2 adding to water) on the heat transfer and flow characteristics in a central processing unit (CPU). They conclude that Al_2O_3 /water and TiO_2 /water nanofluids reduced the temperature of CPU by 23.2% and 14.9% respectively compared to water. However, they

found that the heat transfer performance reduced with higher mass fraction nanoparticle in the base fluid.

Ijam et al. [65] mathematically examined two types of nanoparticles Al_2O_3 and TiO_2 in water as base fluid, with different concentrations. These nanofluids were used in a copper mini-channel heat sink. The maximum improvement in the heat flux was found to be 17.31% by using 0.8% particle volume fraction of Al_2O_3 instead of water, at 0.1 m/s inlet velocity and about 2.95% for the same nanofluid with 4% particle volume fraction at 1.5 m/s. The 16.53% heat flux enhancements were achieved by using 0.8% particle volume fraction of TiO_2 at 0.1 m/s inlet velocity and only 1.88% at 4% particle volume fraction with 1.5 m/s inlet velocity.

2.5 New Nano-based Heat Transfer Fluid

The new nano-based heat transfer fluid (HX) used for this project is a commercially available nano-based mixture made-up of the components listed in Table 2.1. The commercial product has already been introduced into the USA and Europe as an energy-efficient fluid to be used in closed circuit cooling and heating systems as AHTF.

The new nano-based fluid has been certified under the Build-Cert Chemical Inhibitor Approval Scheme to inhibit corrosion inside vital system parts such as pipes and radiators and to prevent scaling on the heating elements, in particular boilers. Also, it has been verified by the Life Cycle Assessment (LCA) and Environmental Product Declaration EPD reports as a green and sustainable solution [6 &66]. The new nano-based heat transfer fluid consists of the components shown in Table 2.1 [66].

Table 2.1: Components of the Nano-based Fluid (HX)

Name of component	Formula	Concentration (%)	Product identifier
Ethanediol or Ethylene glycol	$C_2H_6O_2$	60-90	(CAS No*) 107-21-1
Glycerine	$C_3H_8O_3$	<25	(CAS no)56-81-5
Triethanolamine	$C_6H_{15}NO_3$	<18	(CAS No)102-71-6
Sodium molybdate Dihydrate	$Na_2MoO_4{\cdot}_2H_2O$	<4	CAS No) 10102-40-6
Citric Acid	$C_6H_8O_7$	<3	(CAS No)77-92-9
Tolyltriazole	$C_9H_9N_3$	<2	(CAS No)29385-43-1

Initial products of this nanofluid have been used as a replacement for water in heating systems for some real case study sites, such as Administration and Personnel buildings of the Ministry of Energy in Turkey. The energy data captured from the heating systems of these buildings before (when water was used as a HTF) and after the application of this nanofluid (HX) were analysed using CUSUM technique, which is based on Degree Day weather data. The results demonstrated an enhancement in heat transfer, including the transfer of heat in a shorter amount of time was achieved by using the Nano-fluid and that reflected on energy consumption [68].

2.6 Hydronic Radiator Heating Systems

The heating system is a set of components required to carry the heat generated as a result of utilising energy from a heat source to the emitters. According to Lawrence [69], The essential components of any hydronic heating system are:

- A means of generating heat, i.e. the heat source. This is a point where heat is added to the system. The heat source is a main part of the system.
- A means of distributing the heat, i.e. the distribution medium and pipes network. This distribution system connects all various components of the heating system, and pipes are used as elements that allow transport of working HTF.

- A means of delivering the heat to the space to be heated, i.e. the heat emitters. The hydronic heating emitter is a device that allows heat to emit out of the heating system to space, that required to be heated.

Further components in the system besides the heat generation, distribution and emission contain valves, regulators, vents, expansion tank, etc. The purpose of these components is to provide proper and safe operation of installations. Due to the relatively lower investment cost and easy installation, radiators are widely used as heating devices in dwellings. The size of a radiator, connection type of flow, return pipes, and the location of these pipes can be different in each case. However, radiator dimensions are standard, and the right radiator can be selected from the manufacturers' catalogues according to the heat needed in the space. The manufacturers' radiator specification determined in accordance with the BS EN 442 part 2 [70] standard which is applied only to the heating devices that use water or steam at temperatures below 120ºC as a heat transfer medium. Different supply and return connections types can be used for the radiator, and this can affect the performance of the radiator [71&72]. Introducing the flow at the top-bottom opposite end (TBOE) can improve the temperature distribution within the radiator. However, the most common connection type in the UK is the Bottom, Bottom Opposite End (BBOE) [73].

2.6.1 Theory of Heat Transfer from Hydronic Radiator

Heat transfer is categorised into three modes [74]:

1. Convection
2. Conduction
3. Radiation

Convection results from the fluid moving across a surface at a different temperature. Conduction occurs through solid materials and the heat flows from the warmer to the cooler

side. Radiation is another mode of heat transfer; the heat is transferred as electromagnetic waves, without needs for medium to be present to transfer the heat from one place to another. The convection heat transfer is proportional to the surface area (A), that emitted the heat and the temperature difference between the surface (T_s) and the fluid (T_f) as seen in equation 2.4.

$$\dot{Q}_{Convection}\ \alpha\ A\ (T_s - T_f\ ) \quad \textbf{(2.4)}$$

Newton's law established an algebraic relation between the heat flows by convection, the surface area and the temperature difference between the fluid and solid surface correlated by heat transfer coefficient (h) as expressed in equation 2.5.

$$\dot{Q}_{Convection} = h\ A\ (T_S - T_f) \quad \textbf{(2.5)}$$

The heat transfer coefficient depends on many factors such as the type of flow (laminar or turbulent), the viscosity, specific heat capacity, density, thermal conductivity of the fluid, velocity over the surface and the geometry of the surface [75]. The heat transfer coefficient is a function of the Nusselt number, which is a dimensionless parameter that characterises the intensity of convective between the surface and moving fluid [76].

Radiation heat transfer depends on the surface characteristics of the objects; each body emits and absorbs energy by radiation unless both bodies are at absolute zero temperature [77]. A blackbody is defined as a body which absorbs entirely all radiation falling on its surface. A grey body has a surface which absorbs all wavelengths equally but does not absorb all the radiation [78]. The ideal thermal radiator called a blackbody which emits heat ($\dot{Q}_{Radiation}$) at a rate proportional to the fourth power of the absolute temperature (T_s) of the body and it is surface area (A_s), equation 2.6.

$$\dot{Q}_{Radiation} = A_s\ \delta\ T_s^4 \quad \textbf{(2.6)}$$

Equation 2.6 is only applicable to 'Ideal' blackbody objects, which radiates energy

according to the T^4 law, where (δ) is Stefan Boltzmann constant. The net radiant exchange between two surfaces proportional to the difference in absolute temperatures to the power four [78], equation 2.7.

$$\dot{Q}_{Radiation} = \varepsilon\, \delta\, A_s\, \left({T_{s1}}^4 - {T_{s2}}^4\right) \quad \textbf{(2.7)}$$

Where ε is the emissivity of the surface, equal to absorptive power (lies between 0 to 1), T_{s1} and T_{s2} are the temperatures of surface one and two. The thermal output from the hydronic radiator to the air-side is a combination of convection and radiation. Therefore, the heat output from the radiator to the air-side can be written, as follows:

$$\dot{Q}_{output} = \dot{Q}_{Convection} + \dot{Q}_{Radiation} \quad \textbf{(2.8)}$$

The transmission of heat due to the movement of the heat transfer fluid inside the radiator can be evaluated from equation 2.9 [76].

$$\dot{Q_T} = \dot{m}\, C_p\, \Delta T \quad \textbf{(2.9)}$$

Where $\dot{m}$ are the fluid mass flow rate, C_p fluid specific heat capacity and ΔT is the temperature differences across the radiator (the difference between the flow and return temperatures of the fluid). The first law of thermodynamics states that in steady state heat flow, all of the energy put into a system must come out again. Therefore, the heat output from the radiator at steady state condition can be written, as follows:

$$\dot{m}\, C_p\, \Delta T = \dot{Q}_{Convection} + \dot{Q}_{Radiation} \quad \textbf{(2.10)}$$

2.6.2 Hydronic Radiator Heating System Performance

Hydronic radiators in heating systems have been a primary source of domestic heating in the UK and cold weather countries for several years. The heating system is responsible for a large amount of energy consumption. Therefore, several studies have been carried out to achieve an efficient heating system that helps reduce energy without affecting the comfort of the occupants. The heating process can be improved using passive techniques

include methods to modify the heat transfer fluids, components of the systems, surface roughness and shape to increase the surface area. The performance of the hydronic radiator heating systems (HRHS) was investigated by many researchers from different aspects such as:

- Optimise the location of the radiators within the heated space. The results revealed that the radiator position has a significant effect on both forced and free convection heat transfer rate [79],
- Enhance the thermal output from the radiator using pulsation flow; the results showed that using pulsation flow in hydronic radiator heating systems reduces the energy consumption without compromising thermal comfort [80].
- Enhance the thermal output from radiators by using either one or two high emissivity sheets placed between the interior surfaces of a double radiator [81].

Although the HTFs play an essential role in the radiator heating system, as a distributing medium for the heat from the heat source to the point that providing heat. However, there is no investigation has been carried out to assess the effect of different HTFs on hydronic radiator heating system performance.

2.7 Summary

According to the literature, water is one of the most common heat transfer fluids used in wet heating systems due to its availability and low price. However, water has some limitations that can affect its application, such as:

- High freezing point and that can cause problems during harsh winter periods
- Prone to biological growth, and that can cause an odour problem
- Accelerate corrosion of metal parts in the systems and this can increase leak risks and maintenance cost.

Alternative heat transfer fluids are being proposed continuously by various industries to overcome the limitation of having water as a heat transfer medium. The literature has shown that the nanofluids have been introduced as new heat transfer mediums and they have been investigated by many researchers in different applications of heat transfer field. The reported research work revealed that nanofluids are still under investigation and more studies need to be considered to evaluate the effectiveness of nanofluids in the heat transfer applications. This chapter also provided background information about the hydronic heating system and summarised the studies related to optimised and enhance the performance of the hydronic radiators.

The literature has demonstrated that there are limited research studies available about the measurement of radiators' performance at actual operating conditions. Moreover, no work has been done to study the effect of alternative heat transfer fluids on the performance of hydronic radiator heating systems. In addition, the current BS EN 442-2 standard addressed a model to evaluate the thermal output of the radiators to the air-side, that model is only applicable for hydronic radiators working with water or steam as the heat transfer fluid. Therefore, this research work aims to study the effect of using the proposed alternative heat transfer fluids on the performance of a panel radiator hydronic heating system.

CHAPTER 3

Investigation of the Thermal Properties of the Examined HTFs

3.1 Introduction

This chapter introduces the proposed heat transfer fluids (HTFs) for this research project and provides detailed information about the supplier. Establishing the thermophysical properties of the HTFs is an important first step of researching the behaviours of the fluids. This chapter presents the methods used to measure the thermal conductivity, viscosity, specific heat capacity and density for the proposed HTFs in order to validate the measured data. The chapter also presents a comparison of the measured output with available information in the literature.

3.2 Proposed Heat Transfer Fluids

The proposed heat transfer fluids for this research work are as follows:

1- Potable water (water)
2- 50 % Nano-based fluid (HX) /Water (v/v) mixture (50 % HX/W)
3- 50 % Ethylene glycol /Water (v/v) mixture (50% EG/W)
4- 30 % Ethylene glycol /Water (v/v) mixture (30% EG/W)

Full concentration pigmented nanofluid (100% HX) was supplied by the International partner with recommendations on how to mix the fluid with potable water to get the 50% HX/W mixture. The Ethylene glycol (100% EG) was obtained from Darrant Chemicals company (UK), it was mixed with potable water to prepare the 50% EG/W and 30% EG/W mixtures. The mixture of these fluids was prepared, using the volume/volume (v/v) ratio; the concentration of these mixtures was measured using (RHA 503ATC) portable refractometer. This is an optical device that measures the light passing through a sample

to determine its concentration. Figure 3.1 shows a real reading from the refractometer.

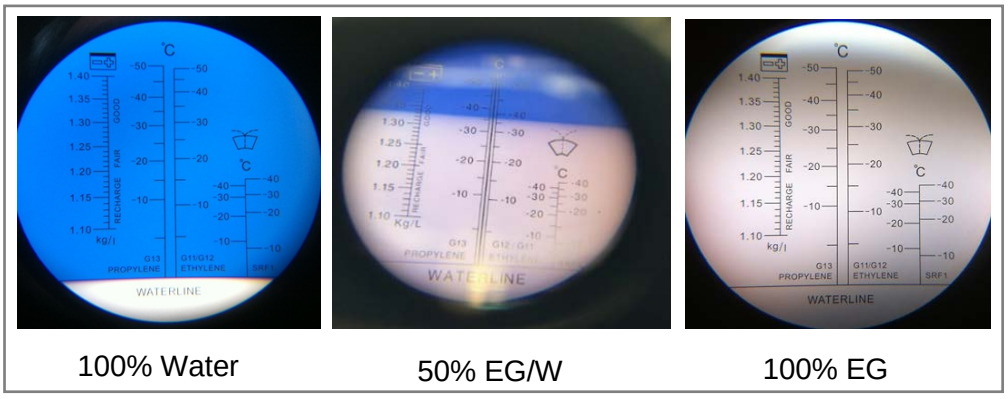

Figure 3.1: Fluid Concentration Reading Using Portable Reflectometer

As could be seen from the above figure, the circular field has an index used for a particular type of fluid. For pure water, the circular area appears entirely dark (blue) up to water level line, while with the EG/W mixtures the concentration can be read on the edge of the dark (blue) and light (white) portions meet. The scale in the circular field shows the freezing temperature of the mixture and the concentration (%) of the mixture can be known according to freezing temperature (as instructed in the RHA 503ATC refractometer guide).

3.3 Thermophysical Properties of the Proposed Fluids

Thermophysical properties of any fluid contribute significantly to the heat transfer performance of fluid in operation. For this project, the first step followed in this research was to study and verify the thermophysical properties of the proposed fluids. The following sections present a detailed description of the thermal properties' tests conducted on the fluids before the experimentation.

3.3.1 Thermal Conductivity

Thermal conductivity (k) is a measure of the material ability to conduct heat in the absence of mass transport. For heat transfer fluids, k plays an important role in the inter-molecular heat exchange. k, for the fluids considered in this research, was measured using the KD2 analyser with related software from Decagon Devices, as presented in Figure 3.2.

Figure 3.2: KD2 Analyser with Different Sensors

The KD2 analyser is a portable field and lab thermal properties analyser. It uses the transient line heat source method to measure the thermal conductivity of fluids with conductivity accuracy of ± 5% for a range between 0.2 W/m to 2 W/m. K and ± 0.01 W/m·K for a range between 0.02 W/m·K to 0.2 W/m·K. The analyser consists of a hand-held read-out unit and a single-needle sensor (KS1 probe), which is ideal for measuring the thermal conductivity of fluids.

The KS1 probe is a single sensor made of stainless steel with a 0.06 m length, 0.0127 m diameter; it contains both a heating element and a thermistor, which measures the temperature change while the microprocessor stores the data. The information on the theory of thermal conductivity calculation by KD2 technique is available via LABCELL [82]. The thermal conductivity of the 50% HX/W and 50% EG/W mixtures were measured at a range of temperatures from 15ºC to 45ºC. The temperature was controlled using a water bath. The first step in thermal conductivity measurements was the calibration of the sensors used to measure the thermal conductivity of the distilled water and glycerine at 20ºC as recommended in the KD2 guide. The fluid sample was placed inside a glass test-tube with 0.03 m diameter and 0.08 m length, to ensure 0.015 m of the fluid is parallel to the sensor in all directions as recommended. Then the needle sensor was positioned at the centre of the test sample and both were kept at the constant initial temperature. Calibration checks of the KD2 analyser were conducted using two base calibration

samples; distilled water and glycerine. The reading obtained for the thermal conductivity of the calibration samples were (0.615 and 0.290 W/m.K), respectively. These reading correlated with the specification provided for the samples and values found in the literature of 0.613 and 0.285 W/m. K, respectively [82]. Following this calibration, measurement of thermal conductivity for water was conducted and the results are presented in Figure 3.3.

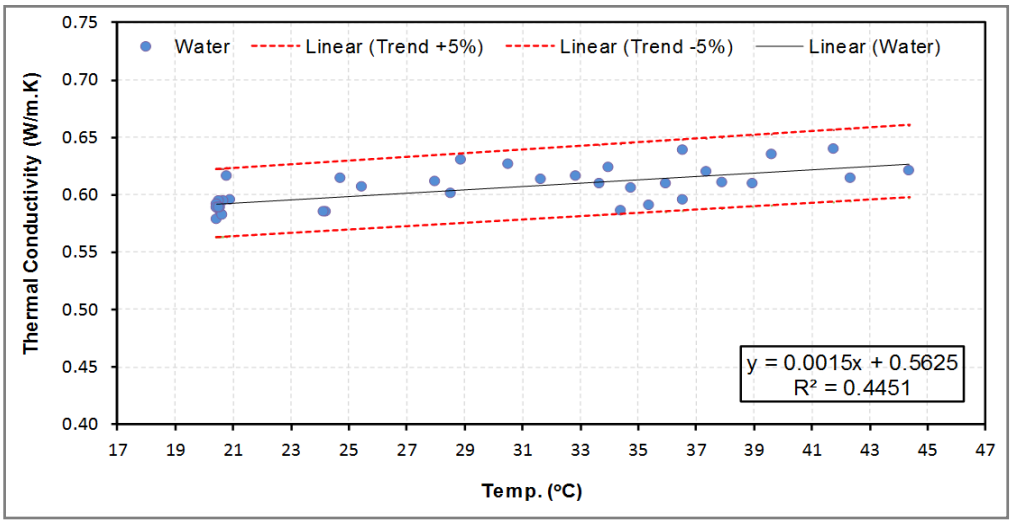

Figure 3.3: Thermal Conductivity Results for Water

Figure 3.3 shows the thermal conductivity for water as a solid line used within the standard error (red lines). It is observed that most of the data points fall within the accuracy range (±5%) of the KD2 analyser. In order to validate the procedure, the results obtained for water were compared and validated against the water thermal conductivity data published in the literature [83&84], (see Table 3.6) as presented in Figure 3.4.

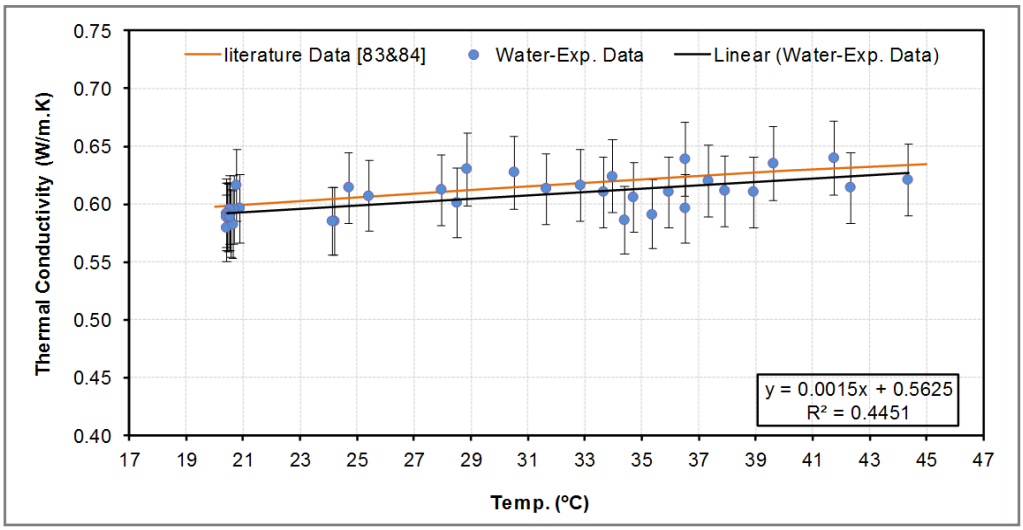

Figure 3.4: Comparison of Water Thermal Conductivity Results with Literature Data

As could be seen from Figure 3.4, the thermal conductivity results obtained with water for a range of temperature of 20ºC to 45ºC correlated well with the literature data [83&84]. This was followed with thermal conductivity tests for all the other fluids (100% HX,100% EG, 50% HX and 50% EG). The measurements (with each fluid) were conducted more than once at each temperature to ensure accurate measurements. The results are presented in Figures 3.5 to 3.8.

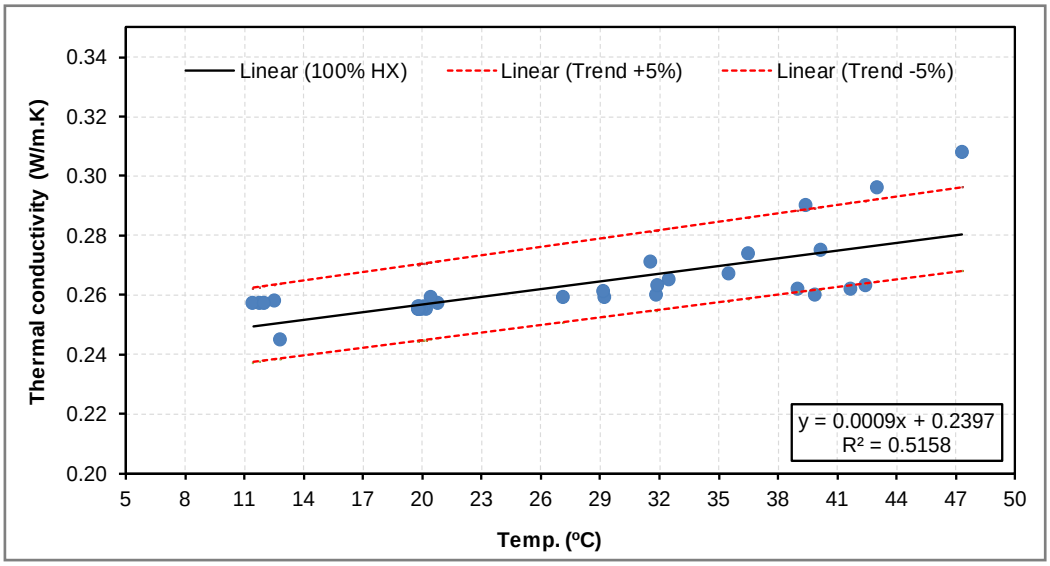

Figure 3.5: Thermal Conductivity Results for 100% HX

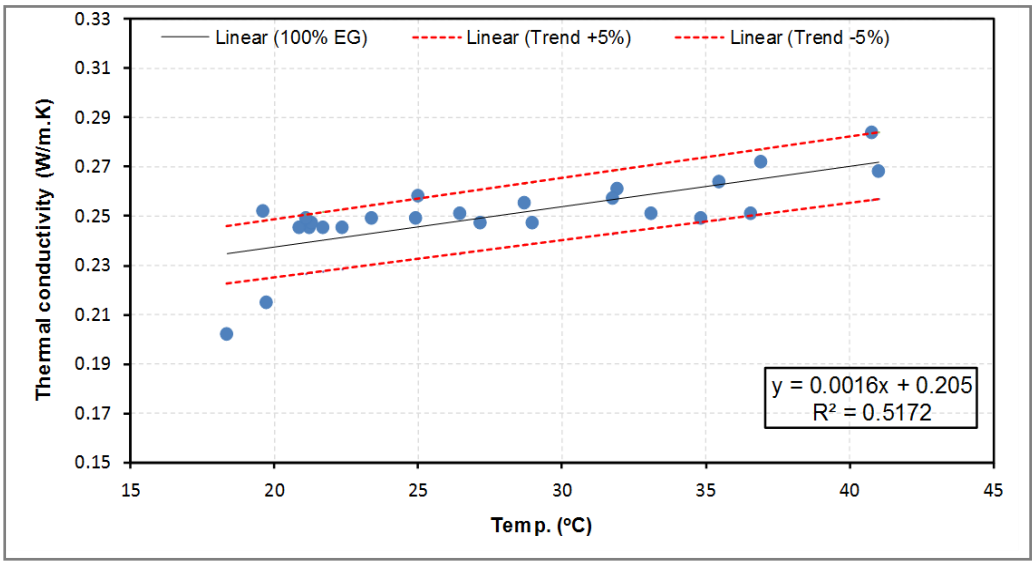

Figure 3.6: Thermal Conductivity Results for 100% EG

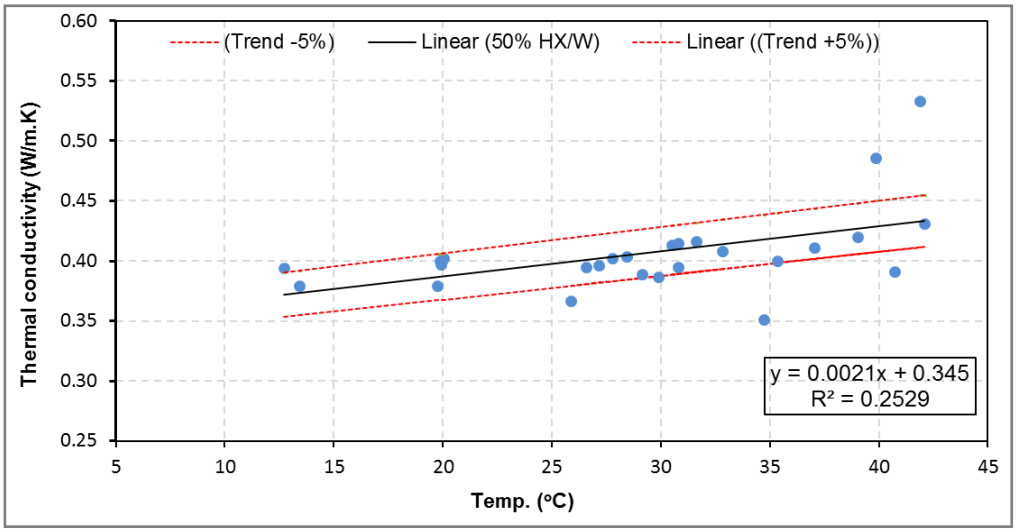

Figure 3.7: Thermal Conductivity Results for 50% HX/W

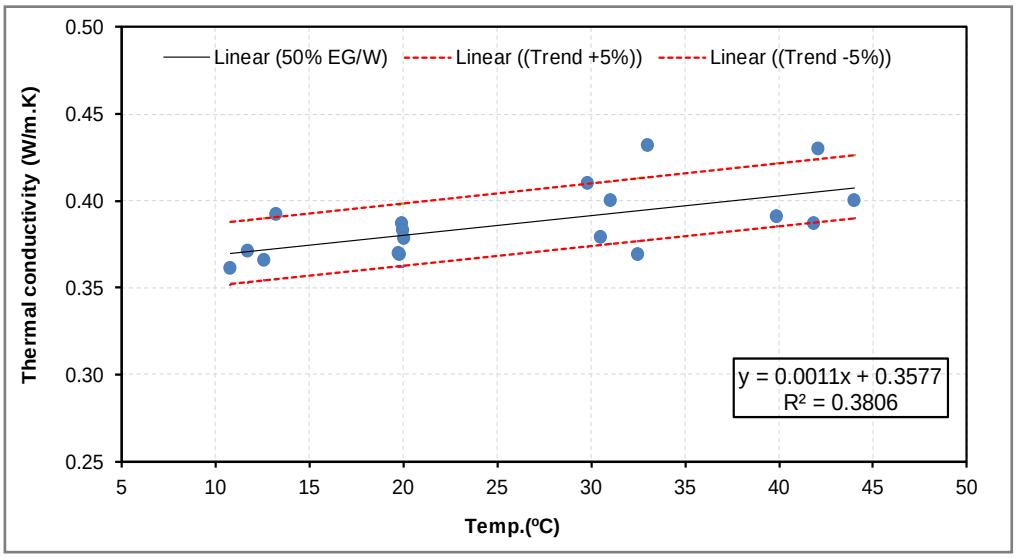

Figure 3.8: Thermal Conductivity Results for 50% EG/W

As could be seen from the above figures (3.5 to 3.8) the trend line of the thermal conductivity of each fluid was obtained as a solid line within the standard error (red lines) and few of data were outlined. The trend line of the results was fitted to the equation of ($k = (A * T) + B$), with a coefficient of determination (R^2). Where k (W/m. K) is the thermal conductivity, T is the temperature, A and B are the gradient of the line and the y-axis intercept respectively. The R^2 is a statistical measure of how close the data are to the fitted line. In general, the higher the R^2, the better the model fits the data. However, in our case, some points were outside the outline range due to short test time and lack of control over

the higher set-temperature. Figure 3.9 and Table 3.1 present the fitted liner curve equations and the results of the thermal conductivity for all the fluids, the percentage of standard deviations of using these equations is less than 2%.

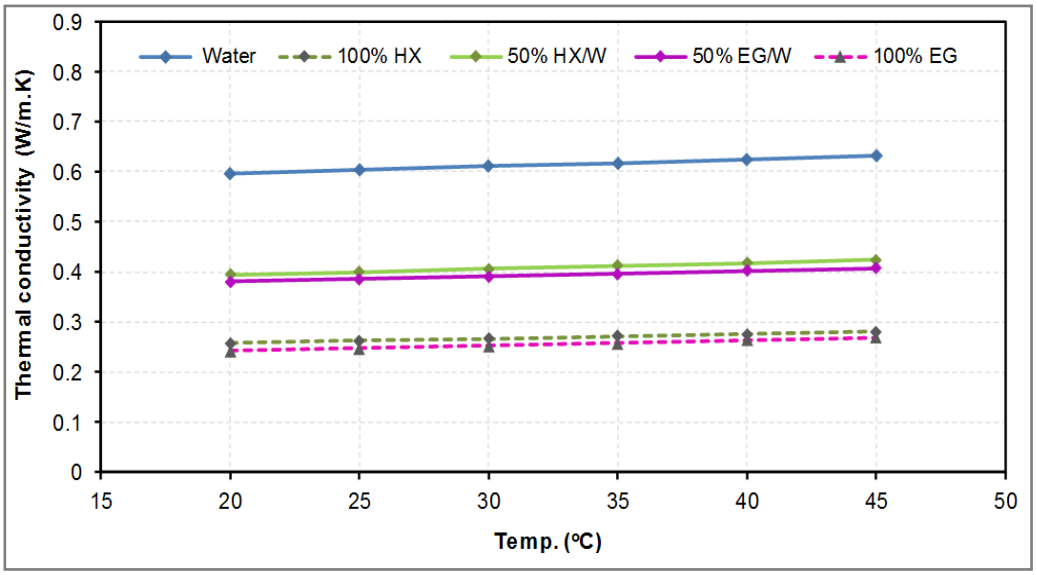

Figure 3.9: Summary of the Thermal Conductivity Results

Table 3.1: Thermal Conductivity Test Results

Temp. °C	Thermal conductivity W/m. K						
	100% Water	100% HX	100% EG	Enhancement (%)	50% HX/W	50% EG/W	Enhancement (%)
20	0.593	0.258	0.237	8.0	0.387	0.380	1.9
25	0.600	0.262	0.245	6.6	0.3975	0.385	3.1
30	0.608	0.267	0.253	5.1	0.408	0.391	4.2
35	0.615	0.271	0.261	3.8	0.4185	0.396	5.3
40	0.623	0.276	0.269	2.4	0.429	0.402	6.4
45	0.630	0.280	0.277	1.1	0.4395	0.407	7.3
Average Enhancement %				4.5			4.7

It is evident from Figure 3.9 and Table 3.1 that the thermal conductivity of 100 % HX and the 50% HX/W mixture is higher than that of 100% EG and 50% EG/W mixtures. The average enhancement in thermal conductivity of 100% HX is 4.5% compared to 100% EG and the average enhancement in thermal conductivity of 50% HX is 4.7% compared to 50% EG/W. The results for all tested fluids (see Figure 3.9) show that the thermal conductivity increased when the temperature increased. The thermal conductivity values

of water, 100% and 50% EG/W mixtures collated with the published values found in the literature [83&84]. Many theoretical models were developed to predict the effective thermal conductivity (k_{eff}) of nanofluids (see Appendix 2.A). Two models (Maxwell and Hamilton & Crosser) [18&40] were considered to develop a calculator based on an Excel spreadsheet to be used to predict the effective thermal conductivity (k_{eff}) for 50% HX/W as a nanofluid (see Appendix 3.A). These models were selected because they are applicable to predict the (k_{eff}) of nanofluid that has a small volume fraction of nanoparticles.

The thermal conductivity of the nanoparticles and the base fluid, as well as the volume fraction of the nanoparticles in the base fluid, were used as input for the effective thermal conductivity (k_{eff}) calculator. The results that were obtained from the calculator compared to the experimental thermal conductivity results, as presented in Figure 3.10.

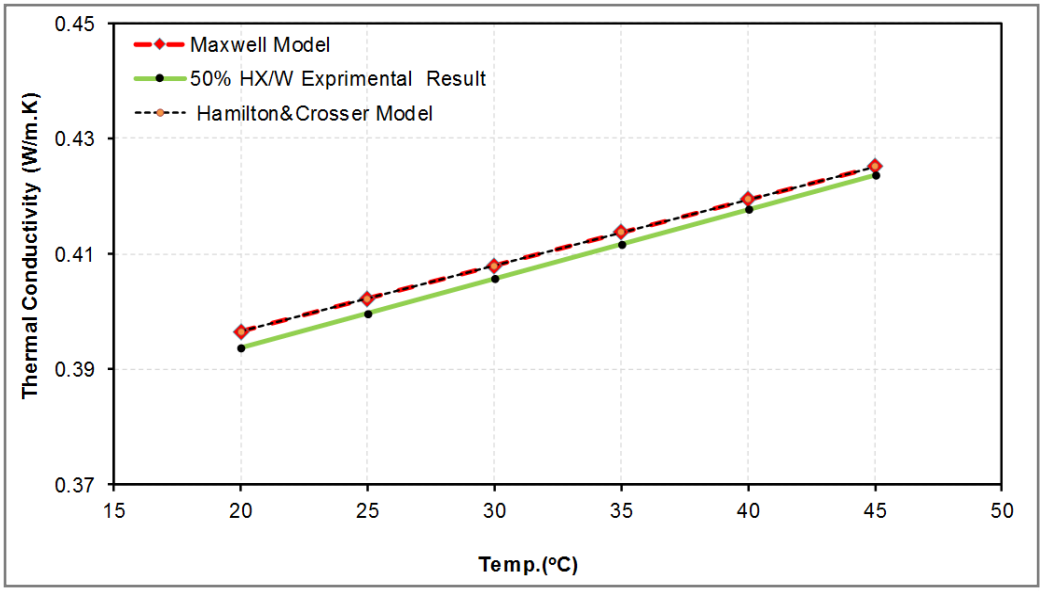

Figure 3.10: Comparison of the Experimental and Theoretical Thermal Conductivity Results for 50% HX/W

Figure 3.10 presents a comparison between the effective thermal conductivity (k_{eff}) and the experimental thermal conductivity results for 50 % HX/W. The comparison illustrated a strong correlation between the experimental and theoretical results of the thermal conductivity for the 50% HX/W as a nanofluid.

3.3.2 Viscosity

Similar to the thermal conductivity, the viscosity of the heat transfer fluids is an important transport property; it describes the fluid's internal resistance to flow. The viscosity tests were performed for water, 50% HX/W and it is base fluid 50% EG/W under the same test conditions. Bohlin Gemini II Rheometer with related software was used to measure the viscosity of the considered fluids. The instrument has a temperature controller to allow measurement of the viscosity of samples at both low and high temperatures. Figure 3.11 shows the Bohlin Gemini II Rheometer and the relevant software that was used to carry out the viscosity test.

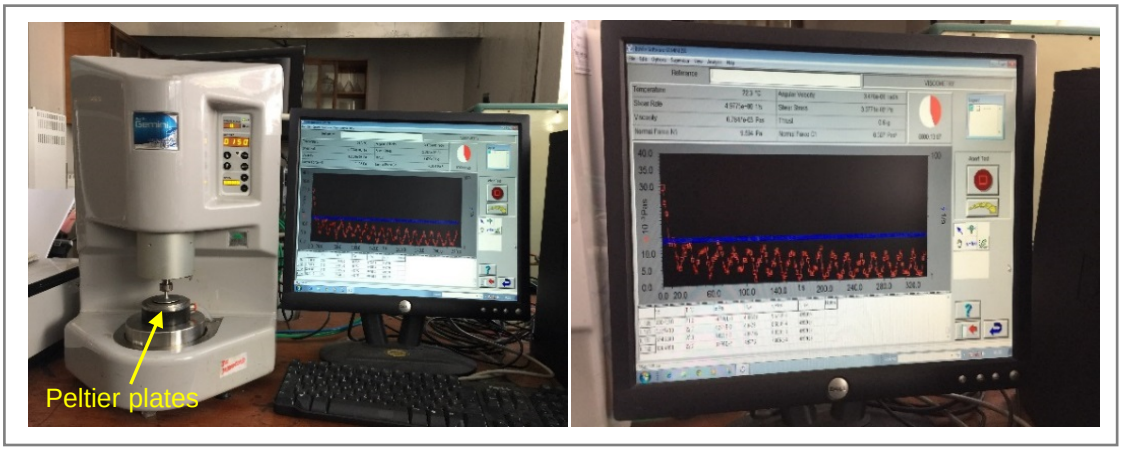

Figure 3.11: Bohlin Gemini II Rheometer and Software Related

The tests were performed for a range of temperatures from 0ºC -75ºC at a rate of 4°C/min and a shear rate of 5 (1/sec) (shear rate is the velocity gradient, which is the rate of change in velocity with distance). The gap between the Peltier plates where the fluids were tested was 1.5 mm, to ensure that the fluids being measured are not held between the Peltier plates by capillary forces alone.

The first step for the viscosity measurement was the calibration of the instrument, which was carried out by measuring the viscosity of water and the results aligned well with the literature values [78]. The actual measurements of the viscosity of water, 50% HX/W and 50% EG/W as a function of the temperature with the best fit logarithmic curve are presented in Figure 3.12.

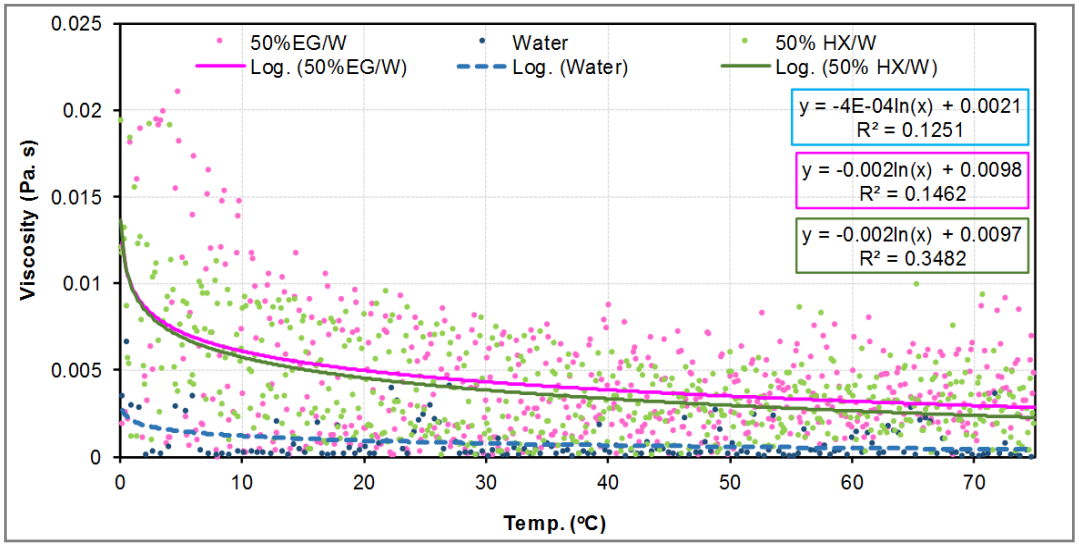

Figure 3.12: Viscosity Results for All Fluids at Different Temperature

It is clear from the above figure that the viscosity values of 50% HX/W and 50% EG/W mixtures are very close and higher than water viscosity. The logarithmic curve fitted equations with R^2 shown in Figure 3.12 were used to evaluate the viscosity at different temperatures where y, is the viscosity and x, is the temperature. Figure 3.13 presents the data of fitted curve equations for all the fluids.

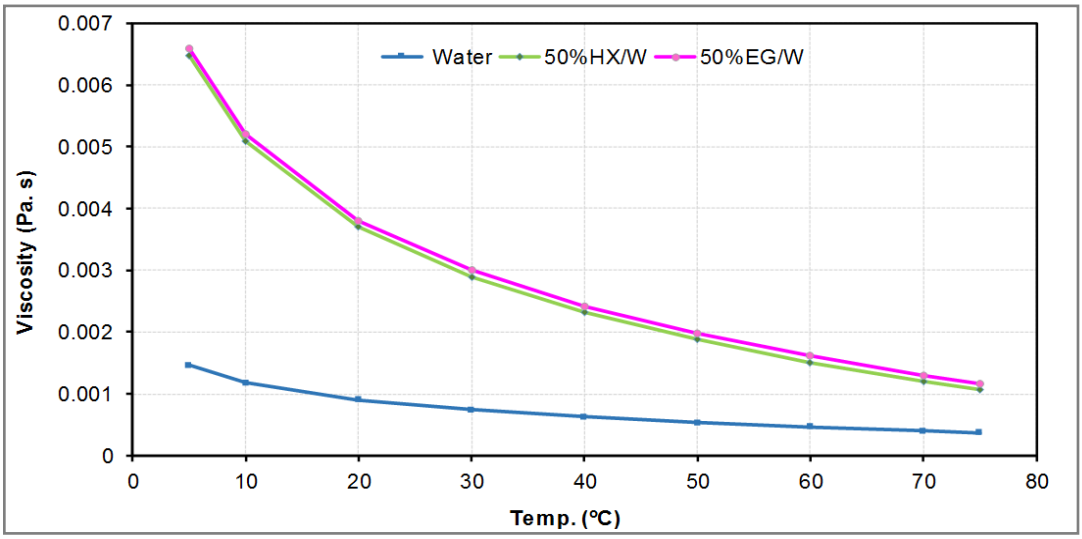

Figure 3.13: Viscosity Results as a Function of Temperature

From Figure 3.13, it can be seen that the 50% HX/W and 50%EG/W are more viscous at low temperatures compared to water and they are less viscous at higher temperatures. The viscosity values that were evaluated by fitted logarithmic curve equations for the HTFs under investigation are shown in Table 3.2. The percentage of standard deviations of using these equations are less than 1%.

Table 3.2: Viscosity Test Results

Tempe. (°C)	Viscosity (Pa. s)			Reduction in viscosity between 50% EG/W and 50%HX/W (%)
	Water	50% HX/W	50% EG/W	
5	0.00146	0.00648	0.00658	1.5
10	0.00118	0.00510	0.00520	1.9
20	0.00090	0.00371	0.00381	2.6
30	0.0007	0.00290	0.00299	3.0
40	0.00062	0.00232	0.00242	4.1
50	0.00054	0.00188	0.00198	5.1
60	0.00046	0.00151	0.00161	6.2
70	0.00040	0.00120	0.00130	7.7
75	0.00037	0.00108	0.00117	7.7

From the above table, it is clear that 50% HX/W mixture is less viscous than 50% EG/W mixture, especially at higher temperatures.

3.3.3 Specific Heat Capacity

Specific heat capacity (C_p) is another thermophysical property; it represents the amount of heat required to increase the temperature of a one-unit mass of the material by one degree Celsius. The C_p was measured for distilled water, 50% HX/W and 50% EG/W using a calorimeter, which consists of an electrical coil, insulated vessel, stirrer and thermometer ranging from 0ºC to 50ºC with 0.1ºC scale as shown in Figure 3.14.

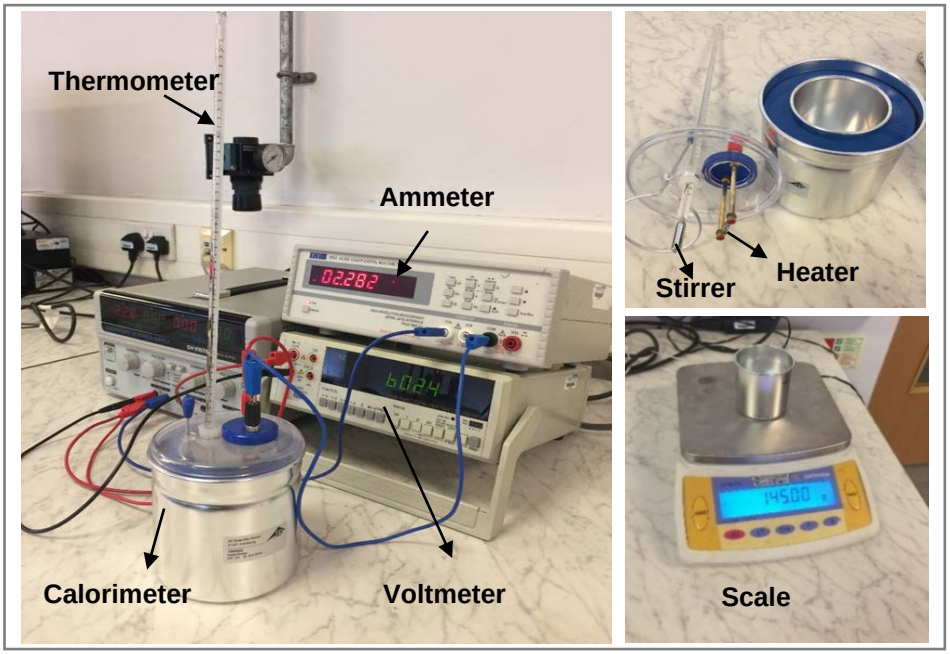

Figure 3.14: Equipment Used for Specific Heat Capacity Measurement

The specific heat capacity test was performed as follows:

- Measured a certain mass of the tested fluid (m) using a digital scale (Sartorius-CP2202S with an accuracy of ±0.02 g)
- Measured the initial temperature (T_o) of the fluid and recorded manually
- Connected the calorimeter's coil to power supply at fixed current (I) and voltage (V).
- Turned the calorimeter's coil 'on' to heat the fluid for a specific time while monitoring and recording the temperature of the fluid at two minutes' interval. Stirring of the fluid inside the calorimeter was maintained throughout the test. The temperature of the fluid was read using a thermometer with 0.1ºC scale. Then, specific heat capacity (C_P) was evaluated as per equation 3.1.

$$C_P = (V * I * (t_i - t_o))/(m * (T_i - T_o)) \quad \textbf{(3.1)}$$

Where (T_i and T_o) are the final and initial temperatures of the fluid and (t_i and t_o) are the final and initial time; the time interval was 120 seconds (2 minutes). The test was performed with distilled water as a calibration process. The test with each fluid was repeated twice, and the average of the temperature and time measurement was considered to evaluate the C_P. The tests were performed for water, 50% HX/W and 50% EG/W mixtures. The recorded fluids temperature versus time is plotted and presented in Figure 3.15.

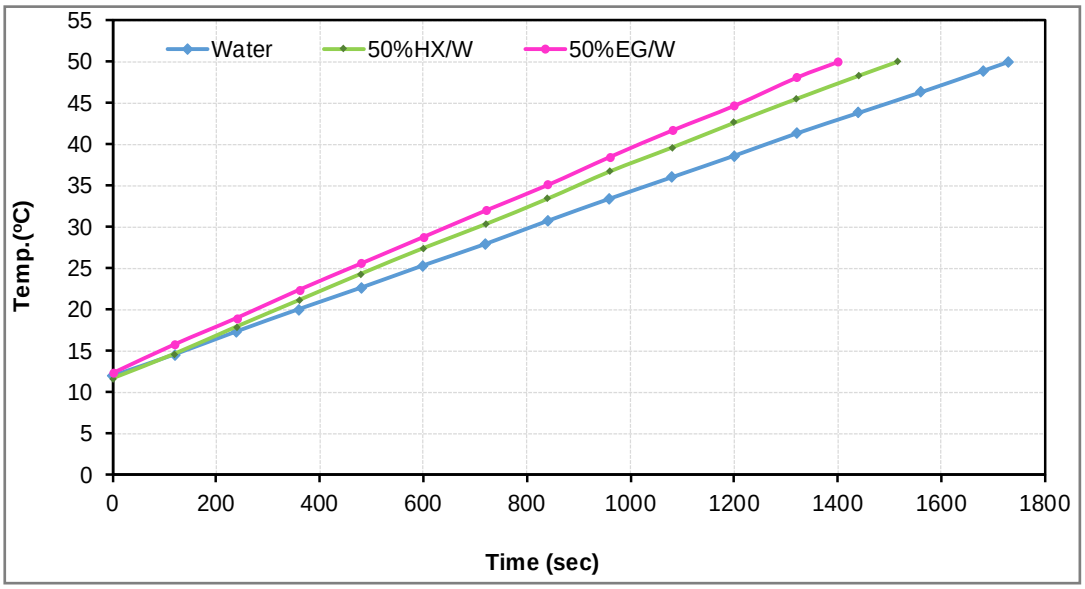

Figure 3.15: Temperature Versus Time for Specific Heat Capacity Tests

The above figure shows that the temperature of the fluid increased linearly with time and the time required to change the temperature (from about 12.5ºC to 50ºC) of the water was more than that required to change the temperature of 50% HX/W and 50% EG/W mixtures. The specific heat capacity was calculated using equation 3.1, considering the following parameters:

- Mass of fluid (145 g),
- Constant voltage (6.024 V)
- Constant current (2.282 Amp).

In order to minimise the errors due to the heat transferred to or from the surroundings, data for two minutes before and after the required data point was considered to evaluate the specific heat capacity. The specific heat capacity results for all fluids are presented in Figure 3.16.

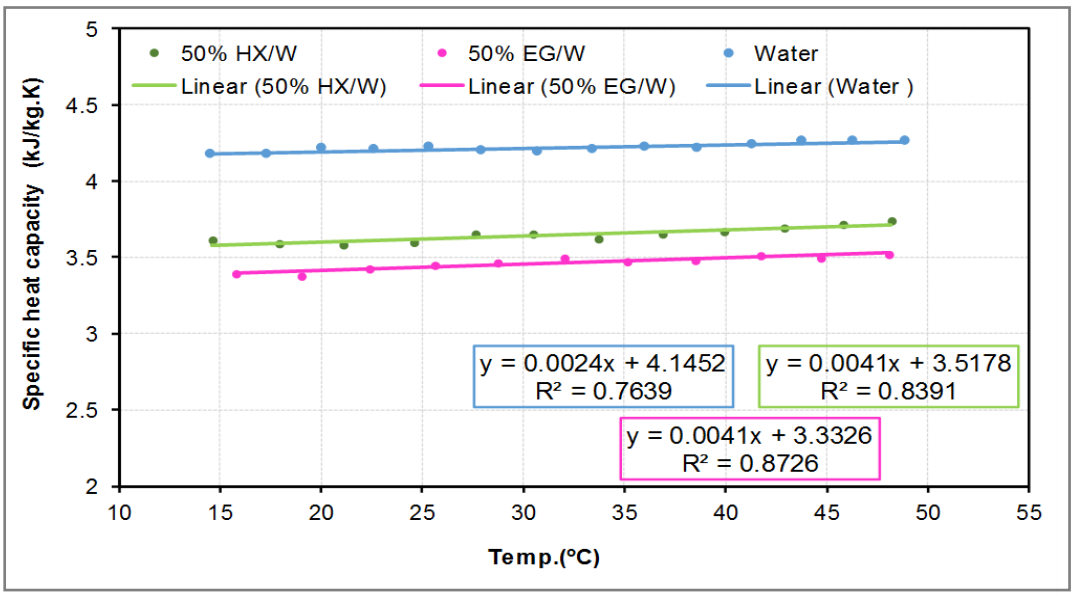

Figure 3.16: Liner Best-Fit Equation for Specific Heat Capacity

It is clear from the above figure that the calculated specific heat capacity (C_p) for water is higher than that of 50% HX/W and 50% EG/W. The specific heat capacity of 50% HX/W is slightly higher than 50% HX/W. In order to verify the procedure of the specific heat capacity test, the results obtained for water were compared and validated against the water specific heat capacity data published in CIBSE guide C [78], as presented in Figure 3.17.

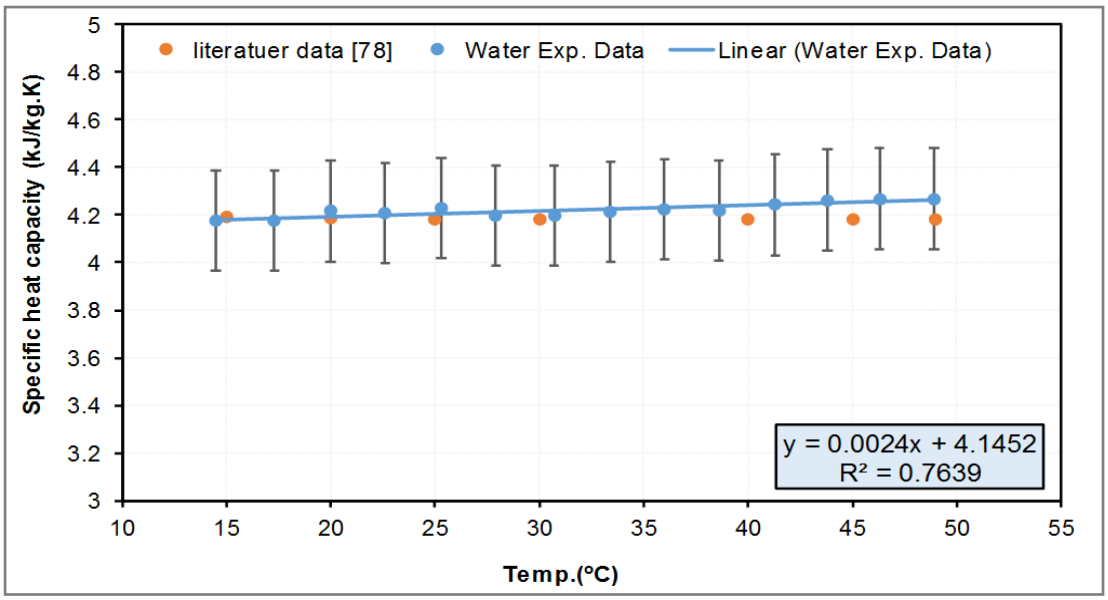

Figure 3.17: Comparison of Water Specific Heat Capacity Results with Literature Data

As could be seen from Figure 3.17, the specific heat capacity results (with the standard error of ±5%) obtained with water correlated well with the data published in CIBSE guide C [78], this confirms the validity of the test procedure and results. Therefore, The linear fitted curve equations (see Figure 3.16) were used to evaluate the C_p of the fluids at different temperatures where (y) is the C_p and x is the temperature. Figure 3.18 presents the data of the linear fitted curve equations for all the fluids.

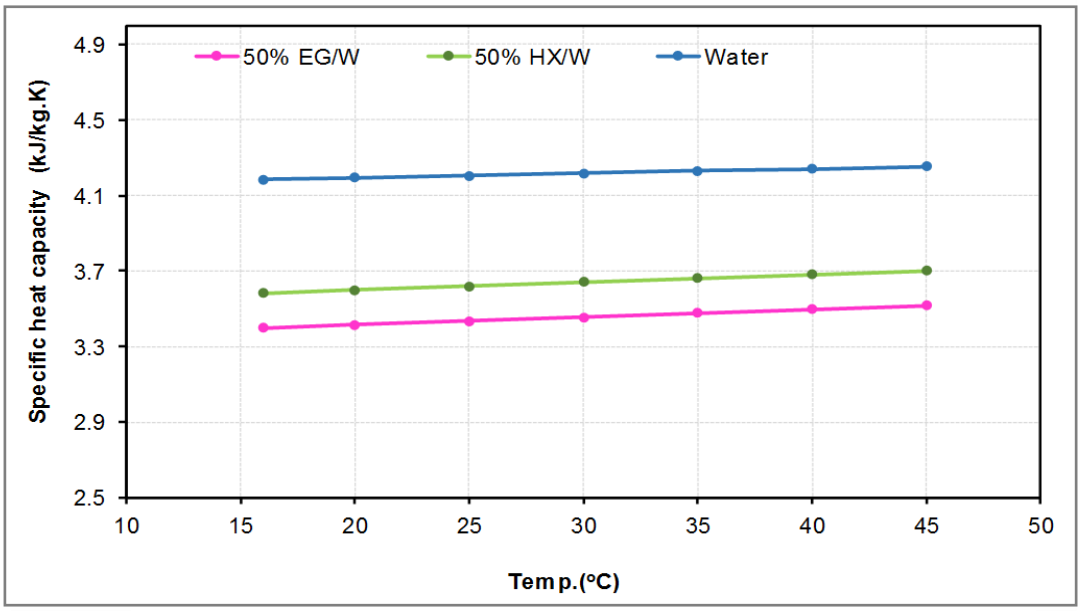

Figure 3.18: Specific Heat Capacity as a Function of Temperature

The above figure shows the specific heat capacity results obtained from the linear fitted curve equations presented in Figure 3.16. The value of specific heat capacity is presented in Table 3.3; the percentage of the standard deviations of using these equations was found to be 4%.

Table 3.3: Specific Heat Capacity at Different Temperatures

Temperature (°C)	Specific heat capacity (C_P) kJ/kg. K		
	Water	50% HX/W	50% EG/W
15	4.181	3.579	3.397
20	4.193	3.599	3.416
25	4.205	3.620	3.436
30	4.217	3.641	3.455
35	4.229	3.661	3.475
40	4.241	3.682	3.494
45	4.253	3.702	3.514

From the above table, it is clear that the 50% HX/W and 50% EG/W have lower specific heat capacity compared to water. Water specific heat capacity is higher by 18% and 13% compared to 50% HX/W and 50% EG/W respectively while the specific heat capacity of 50% HX/W is higher than 50% EG/W by 5%.

3.3.4 Density

The density of the considered fluids was measured at room temperature using a Sartorius-CP2202S digital scale with an accuracy of ±0.02 g and volumetric flask. The procedure was performed by getting a fixed volume of the fluid and measure the weight of that volume. The density was computed by dividing the measured weight over the measured volume. The procedure was repeated three times and the average of three values was considered as the density for the fluids at room temperature. The calibration of the test was the first step, which was carried out by measuring the density of distilled water. The density of the distilled water was found to be aligned well with the literature value (998 kg/m^3) [83]. Table 3.4 presents the density results for the considered fluids.

Table 3.4: Density Results

Trial	Water			50% HX/W			50% EG/W		
	Vol. (ml)	Mass (g)	Density (kg/m^3)	Vol. (ml)	Mass (g)	Density (kg/m^3)	Vol. (ml)	Mass (g)	Density (kg/m^3)
1	250	249.3	997.3	250	266.3	1065.3	250	266.95	1067.8
2	250	249.6	998.2	250	266.2	1064.9	250	266.9	1067.6
3	250	249.6	998.4	250	266.4	1065.6	250	267.3	1069.0
Avg.	997.97 kg/m^3			1065.3 kg/m^3			1068.2 kg/m^3		

The figures in the above table show that the measured density value for water was very similar to the published data in the literature [78&38]. The density of 50% HX/W is very close to 50% EG/W. The density of 50% HX/W and 50% EG/W are higher than the water density by 6%.

3.4 Thermal Properties of the Proposed HTFs in Literature

This section presents a comparison of the measured thermophysical properties of the AHTFs under test against values obtained through the literature search. The thermal properties of 50% HX/W were obtained from data provided by LTPEP [85]. The Tables below show the figures of thermophysical properties (from 20ºC to 80ºC) with the uncertainty of the measurements for all tested fluids, based on the existing literature.

Table 3.5: Thermophysical Properties of 50% HX/W Mixture [85]

Properties	Temperature (ºC)					Uncertainty (u)
	20	40	60	70	80	
Freezing point	-37ºC					/
Boiling point	118 ºC					/
Density (kg/m^3)	1066.6	1054.6	1042.5	1036.3	1030.5	±1%
Viscosity (Pa. s*10 $^{-3}$)	3.313	1.954	1.303	1.124	0.946	±1%
Specific Heat Capacity (kJ/kg. K)	3.418	3.514	3.633	3.613	3.641	± %
Thermal Conductivity (W/m. K)	0.3797	0.397	0.4146	0.423	0.4321	±2%

Table 3.6: Thermophysical Properties of Water [78,83&84]

Properties	Temperature (ºC)					Uncertainty (u)
	20	40	60	70	80	
Freezing point	0°C					/
Boiling point	100°C					/
Density (kg/m^3)	999.8	992.2	983.2	977.8	971.8	± 0.1%
Viscosity (Pa. s*10 $^{-3}$)	1.002	0.651	0.463	0.400	0.351	/
Specific Heat Capacity (kJ/kg. K)	4.183	4.179	4.185	4.191	4.198	±1%
Thermal Conductivity (W/m. K)	0.598	0.629	0.651	0.661	0.667	/

Table 3.7: Thermophysical Properties of 50% EG/W (v/v) Mixture [83]

Properties	Temperature (ºC)					Uncertainty (u)
	20	40	60	70	80	
Freezing point	-36.8°C					/
Boiling point	107.2°C					/
Density (kg/m^3)	1073.4	1063.7	1052.1	1045.5	1038.5	± 0.2%
Viscosity (Pa. s*10 $^{-3}$)	3.941	2.256	1.432	1.1732	0.9759	/
Specific Heat Capacity (kJ/kg. K)	3.280	3.358	3.436	3.474	3.513	±1%
Thermal Conductivity (W/m. K)	0.38	0.394	0.404	0.408	0.411	/

Table 3.8: Thermophysical Properties of 30% EG/W (v/v) Mixture [83]

Properties	Temperature (ºC)					Uncertainty (u)
	20	40	60	70	80	
Freezing point	-13.7°C					/
Boiling point	104.4°C					/
Density (kg/m^3)	1045.2	1036.7	1026.3	1020.4	1013.9	± 0.2%
Viscosity (Pa. s*10 $^{-3}$)	2.195	1.3424	0.9027	0.7598	0.6485	/
Specific Heat Capacity (kJ/kg. K)	3.646	3.703	3.760	3.788	3.817	± 1%
Thermal Conductivity (W/m. K)	0.453	0.473	0.489	0.494	0.499	/

Comparing the thermophysical properties values (Tables 3.5 to 3.8) with the measured values in this research (see Table 3.1, 3.2, 3.3 and 3.4) and bearing in mind the instrumentation uncertainty, it could be concluded that the measured values align well with the literature values for the tested temperatures.

3.5 Summary

This chapter specified the HTFs that were considered to be applied in the HRHS during the course of this research project. Also, it provided detailed information on the supplier of the fluids and preparation of the mixtures that were used as AHTFs in the radiator heating system. Moreover, the methods that were considered to assess the thermophysical properties (thermal conductivity, viscosity, specific heat and density) of all HTFs with the measured results were delivered in this chapter. The importance of this chapter is to verify the thermophysical properties of the tested fluids, especially the new nano-based fluid 50% HX/W.

This chapter expands on the following points:

1- Measurement procedure of the thermophysical properties (thermal conductivity, viscosity, specific heat capacity and density) of the water, 50% HX/W and 50%EG/W.
2- Collect the relevant thermal properties values of the considered fluids from reliable literature to verify the experimental measurement data and to consider them in the required calculation for this project.

Good agreement was found between the measured thermophysical values and the values found in the literature.

CHAPTER 4

Experimental Setup and Testing Methods

4.1 Introduction

This project aims to research and experimentally investigate the performance of a hydronic radiator heating system (HRHS) when using various fluids as an alternative to water under controlled conditions. The effects of using HX as a new alternative heat transfer fluid (AHTF), and also 30% and 50% ethylene glycol/water mixtures were compared to potable water. Achieving controlled conditions, over several months, in real building installations is the main challenge as the weather and operation conditions of any building are uncontrollable. These would influence the heat gain/losses of the building and thus, the amount of heat demand and conditions under which the boiler and radiator operate. This would, in turn, resulted in varied energy consumption and lack of repeatability required for the comparison purposes. Therefore, to carry out the experimental work for this project, a test facility was designed (in liaison with the research sponsor) to be worked under a control condition. The simulate heated zone with HRHS is designed to be monitored and heated to comfort condition under a set winter outdoor condition with the option to repeat the same tests with different heat transfer fluids.

This chapter presents a description of the full tests facility with the concept that was considered to design and develop the test facility and test procedure which would enable experimental testing under controlled conditions. The chapter also includes details of all the instrumentations that were used to collect the data, such as temperature sensors, flow meter, power and energy meter and the thermal imaging camera. The calibration mechanisms of the temperature sensors and flow meter are also discussed. The final

section details the procedure and testing scenarios that were used for this research work.

4.2 Test Facility

The test facility consists of HRHS within a fixed size heated zone (booth) linked to the heating system and full monitoring system. This monitoring system enabled real-time monitoring of the environment inside and outside the booth as well as important system performance indicated, such as power, energy, flow rate and flow and return temperatures. The booth was located inside an environmental chamber which is capable of replicating set external winter conditions (temperature and humidity) for long periods. For each test (with all proposed fluids), the internal environment inside the booth was heated by the radiator by maintaining the same controlled conditions while monitoring the energy consumed by the system and air temperature inside the booth.

As discussed in Chapter 2, the BS EN 442-2 [70] standard was followed for this experimental work. This ensured a consistent test methodology for all the tests, including tests with the base case fluid (water) and the proposed AHTFs under investigation. Figure 4.1 shows a schematic diagram of the test facility with different components.

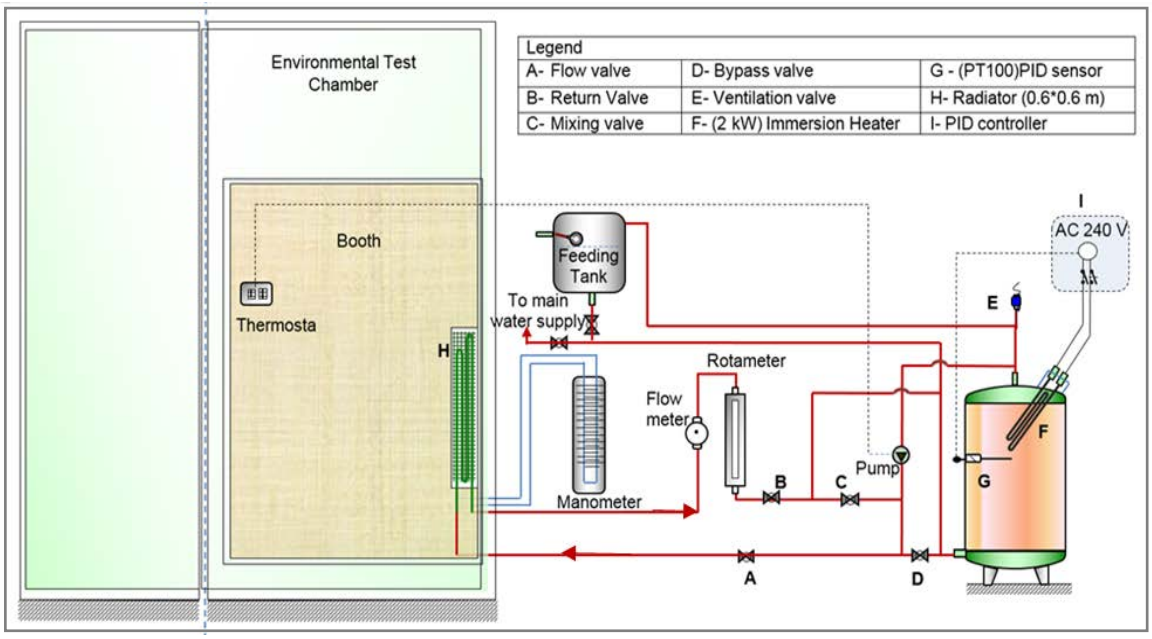

Figure 4.1: Schematic Description of the Test Facility

4.2.1 Design of the Test Facility

The concept design of the test facility is to replicate a real residential heating system working under controlled conditions. The test facility was designed to ensure repeatable conditions for all the tests. It consists of two major parts:

1. Hydronic radiator heating system (HRHS)
2. Test zone (booth) contained within the environmental chamber

The HRHS consisted of the following:

- An insulated hot fluid buffer tank with a 2 kW immersion heater positioned outside the chamber and linked via a set of insulated pipes, control valves and circulation pump.
- A 0.6 m x 0.6 m radiator positioned inside the booth which was located inside the main environmental chamber to ensure that controlled test conditions are applied for all the experiments.

The first step of the design was to determine the system's mass flow rate, which is capable of achieving temperature differences (ΔT) of 10K across the radiator as specified in the BS EN 442-2 [70]. Therefore, The mass flow rate in the system was evaluated based on the design thermal output of the radiator as specified by the manufacturer. The design thermal output ($\dot{Q}_{50}$) of the selected radiator based the manufacturers' catalogues is 0.622 kW, which based on the flow temperature of 75ºC and ΔT across the radiator of 10K. The mass flow rate was evaluated by rearranging equation 2.9 (chapter 2) to be as follows.

$$\dot{m} = \dot{Q}_{50}/(C_p * (FT - RT)) \quad \textbf{(4.1)}$$

Where $\dot{\mathrm{m}}$ is the mass flow rate (kg/s) and $\dot{\mathrm{Q}}_{50}$ is the nominal radiator thermal output and $\mathrm{C_p}$, FT and RT are the water-specific heat capacity, water flow and return temperatures, respectively. The water mass flow rate was found to be 0.0148 (kg/s) then it was converted

to volumetric flow rates based on the density of water (977.8 kg/m^3 at 70ºC), the required volumetric flow rate was found to be 0.054 (m^3/h). The pipes diameters were selected according to CIBSE, Concise Handbook [86] considering the recommended figure for velocity and pressure drop. For pipes diameters 15-50 mm, the recommended velocity between 0.75 m/s to 1.2 m/s and the pressure drop between 100 Pa/m and 400 Pa/m [87]. The pressure drops across the fittings ($\Delta p_{\text{fitting}}$) was calculated using equation 4.2 [78].

$$\Delta p_{fitting} = (\zeta\ \rho\ v^2)\ /\ 2 \qquad \textbf{(4.2)}$$

Where v, is the velocity of the fluid and ζ is the local pressure drops factor which depends on the type of the fittings [88]. The pressure drop of the fittings was evaluated and added to the pressure drop of the pipes to evaluate the total pressure drop in the system (index pressure drop) including static pressure (see Appendix 4.A). The index pressure drop value was used to select a suitable pump for the system.

The selected pump needs to be capable of delivering the required flow rate in the system (0.0148 kg/s) and the bypass flow rate. The bypass valve was kept continuously ‘’on’’ to avoid thermal stratification inside the buffer tank. Moreover, the selected pump need to be capable of overcoming the pressure drop of the system, which was calculated and found to be 16,004.83 (pa), (see Appendix 4.A). Flowmaster CP50 circulation pump was selected for the system. It is suitable for working fluids including water and glycol mixture with a maximum flow rate of 3.5 m^3/h, and operating temperatures ranging from -10ºC to +95ºC was selected.

4.2.2 Heated Zone (Booth)

The booth was designed to be a closed unventilated place comprising of a test space within which the radiator was installed. The only opening part of the booth was the entrance door, which was located at the front wall and opposite to the radiator and is set to be firmly

closed. The booth was made of Medium-Density Fibreboard (MDF- 0.018 m thickness) with internal dimensions of 1.95 m Width x 2.10 m Height x 1.17 m Depth and was located inside the environmental chamber.

Two factors were considered in deciding the booth dimensions:

1. The internal dimensions of the environmental chamber

The environmental chamber has a rectangular shape with internal dimensions of 3.8 m (W), 2.7 m (H), 6.4 m (L). Thus, the booth had to be designed to fit within this space and at the same time, allow enough space around the booth that would enable the chamber to maintain uniform temperature and humidity around the booth.

2. Inside booth dimensions

To accommodate a standard radiator with enough space around the radiator to allow air movement and place of monitoring instruments. Single panels are perfect for space-saving as small rooms require less energy to heat. Therefore, the reduced output of a slimline radiator is ideal. For the test setup, the 0.6 x 0.6 m single panel radiator was the smallest standard residential, office, and commercial wet radiator found on the market.

The radiator under investigation was fixed symmetrically inside the booth (on the rear wall). It was positioned, according to the recommendations of BS EN 442-2 [70], at 0.11 m above the floor of the booth and the gap between the radiator, and the walls were 0.05 m. The walls of the booth were painted white colour (with an emissivity of 0.9).

To control the air temperature inside the booth Drayton analogue thermostat for a range of temperature 10ºC to 30ºC was installed. Small circulation fan (see Appendix 4.B) placed inside the booth at high level served as a mechanism to prevent thermal stratification inside the booth. Figure 4.2 presents a photograph of the booth with the radiator inside the environmental chamber.

Figure 4.2: Booth with Tested Radiator

4.2.3 Environmental Chamber

The environmental chamber was utilised for this project to provide a controlled testing condition. The internal dimensions of the chamber are 3.8 m (W), 2.7 m (H) and 6.4 m (L). The range of temperatures and humidity for the chamber are 5ºC to 45ºC (±1.0K) and 20% to 90% (±3%) respectively. For this experimental work, the environmental chamber was set to provide a temperature of 9ºC and relative humidity (RH) of around 45%- 50% due to the best operation of the environmental chamber. Figure 4.3 shows a photograph of the frontal view of the test chamber with the external part of the HRHS.

.

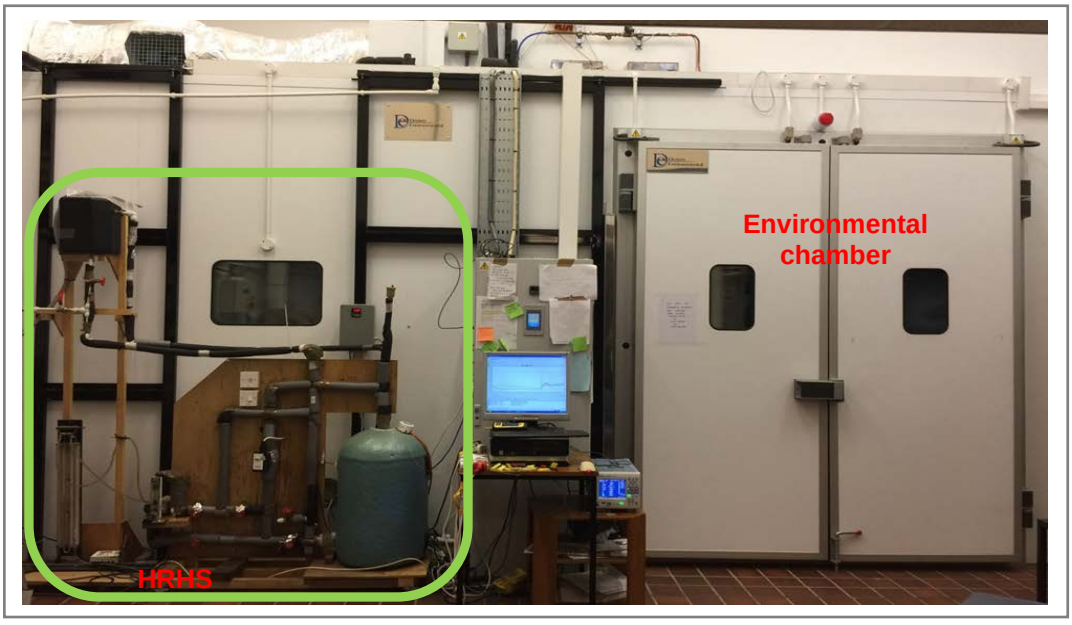

Figure 4.3: Environmental Chamber with the Simulated Heating System Test Rig

4.2.4 Components of the Test Facility

All the components of the test facility with detailed specification and dimensions are summarised in Table 4.1.

Table 4.1: Test Facility Components

No.	Components	Descriptions
1	Booth (test room)	MDF wooden box (1.95 m (W) x1.17 m (L)x 2.10 m (H))
2	Radiator	Single panel radiator (0.6 m x 0.6 m), nominal heat output 0.622 kW
3	Pump	Flowmaster (CP50), circulation pump
4	Buffer tank	Cylinder tank (0.75 m (L) x 0.4 m (diameter)) (94 L)
5	Immersion heater	2 kW (Heatrod element heater)
6	PID controller	INKBIRO PID with PT100 sensor (accuracy of ± 0.2%)
7	Feeding tank	Plastic tank (0.5 m (L) x 0.25 m (H) x0.33 m (W))
8	Valves	0.015 m globe valves to regulate fluid flow
9	Pipes	0.016 m plastic piping with foam lagging
10	Sontex Superstatic 449 meter	Digital flow meter to measure the fluids flow rate with an accuracy of ± 2%
11	Rotameter	To adjust and control the flow rate
12	Drayton Thermostat	Analogue thermostat for a range of temperature 10 - 30ºC
13	Fan	A small fan placed on top of the booth to circulate the air inside the booth to avoid thermal air stratification

4.3 Instrumentations

This section illustrates and describes the instruments used to monitor and record the temperatures, flow rates, power and energy of the system and booth.

4.3.1 Temperature Sensors

Different types of temperature sensor were used to measure the temperature of the fluid, air and radiator surfaces. Platinum resistance temperature sensors PT100 (0.05 m length and 0.005 m diameter Probes) installed inside the flow and return pipes were used to measure the fluid flow and return temperatures. The air inside the booth and radiator wall surfaces temperatures were recorded using welded tip Type-T thermocouples (with a

range of temperature between 0ºC to 200ºC). The sensors were located as detailed below.

1. **Air temperatures**

The thermocouples were positioned at three heights in the centre of the booth; 0.05 m and 0.75 m from the base of the booth and 0.05 m from the ceiling, according to BS EN 442-2 [70]. Another four thermocouples were arranged (0.1 m) above the radiator edge to monitor the air temperature above the radiator (the four thermocouples were spaced equally above the radiator; two above the radiator edges and two placed equally apart above the middle part of the radiator.

2. **Temperatures of the surfaces**

Four thermocouples were positioned on the front surface of the radiator. Two of the thermocouples were positioned on the upper face surface of the radiator. At the same time, the third one was placed on the middle of the radiator and the last one placed on the lower middle part of the radiator surface. Two thermocouples were situated at the flow and return pipes of the radiator as an extra check for the flow and return temperatures as could be seen in Figure 4.4. The thin aluminium tape was used to fix the thermocouples' tips on the surface to ensure that the thermocouples have good contact with the surface and do not get affected by the surrounding environment and radiation.

3. **Globe temperature**

It was measured using a globe bulb which consists of a hollow copper sphere (0.15 m in diameter) painted with a black colour to absorb radiant heat, with a thermocouple at its inside (positioned at the centre of the globe). It was fitted in front of the radiator in the middle of the booth. This was deliberately set to measure the combined effects of radiation and convection on air temperature. The globe temperature was utilised to ascertain whether the implementing of different HTFs in the system have any enhancement on the radiant heat.

4. **Environmental Chamber Temperature**

The temperature of the environment inside the chamber was set to 9ºC and was monitored using installed temperature probes located inside the chamber at mid and return points of

the chamber. These were linked to the chamber control dashboard. An additional thermocouple was also fixed inside the environmental chamber to record the internal air temperatures of the environmental chamber during the whole duration of each test. Figure 4.4 shows some position of the temperature sensors inside the booth and on the radiator.

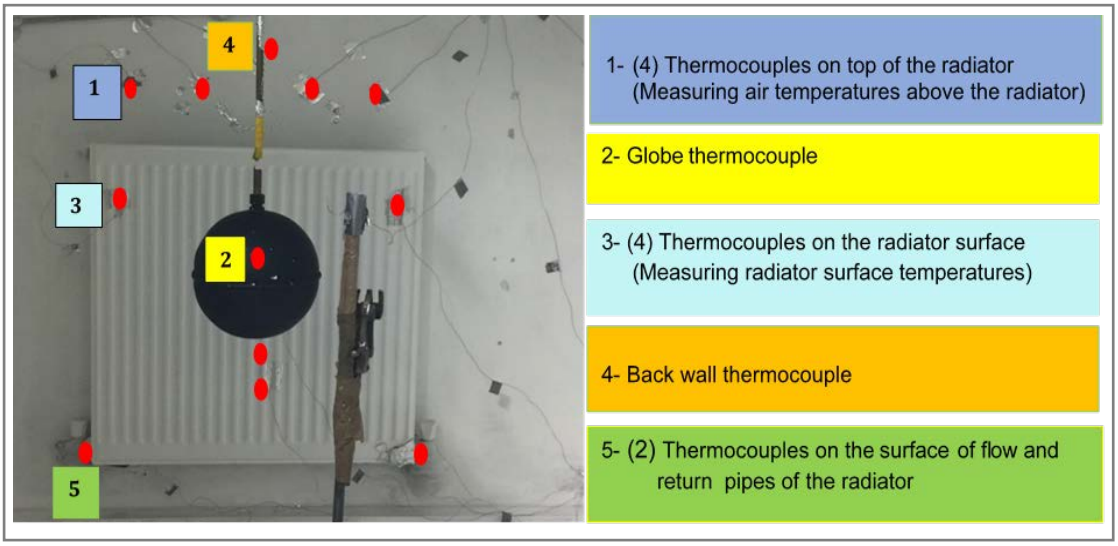

Figure 4.4 : Position of Some Temperature Sensors Inside the Booth

4.3.2 Flow Meter

A digital Sontex Superstatic 449 flow meter with an accuracy of ± 2% was installed on the return side of the radiator to measure the fluids volumetric flow rate through the system. The readings from the digital flow meter were monitored and recorded via the data logger at 5 seconds intervals. In addition, a Platon flow meter (rotameter) was installed after the digital flow meter as an extra check and control point.

4.3.3 Data Logging System

The temperature sensors were connected to a Datataker- DT 500 data logger with an accuracy of 0.25% [89]. This was linked to a computer desktop with data capture software to form the complete data monitoring system. The data were recorded at 5-second intervals. The full data monitoring system with the thermocouples was calibrated using the

water calibration bath before fixing on the test setup. Figure 4.5 shows a photograph of the Data Taker- DT 500 and the related software.

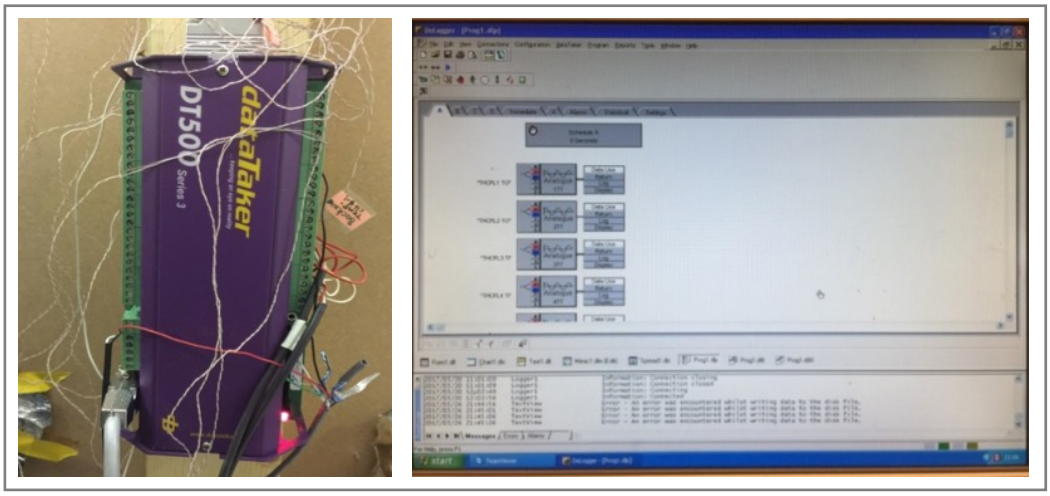

Figure 4.5 : Data Tracker Logger (DT 500)

4.3.4 Power and Energy Meter

Power in kW and accumulated energy in kWh consumed by the system were monitored and recorded using a Yokogawa WT500 power meter with power accuracy of 0.1%. The power and energy readings were stored automatically at 5-second intervals and transferred at the end of each experiment, using a USB, to the temperature data files. It is worth mentioning that the power recorded by the power meter represents all power consumed by the system, including pump power, heater power, actual heat from the radiator and heat loss. Figure 4.6 shows a photograph of the power meter.

Figure 4.6: Yokogawa WT500 Power Meter

4.3.5 Infrared Thermal Imaging Camera

Thermal imaging camera (FLUKE TiS10), with an accuracy of ±2% and measurement temperatures range -20ºC to +250ºC, was used to capture thermal images of the radiator surface and to evaluate the temperature distribution over the radiator surface. The thermal images were analysed using SmartView software, which allows an analysis of the images by defining the temperatures distribution on the radiator. Figure 4.7 shows the thermal imaging camera with related software.

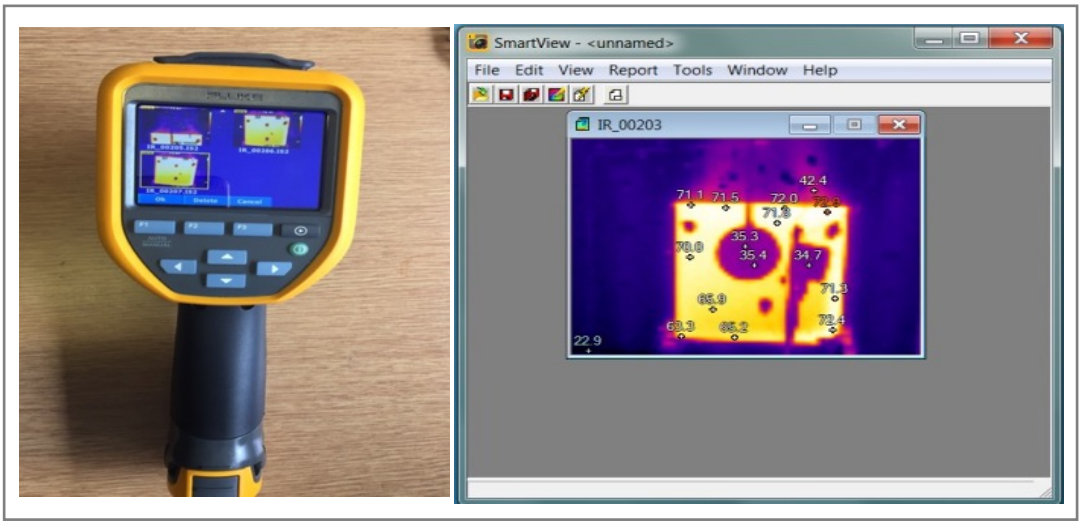

Figure 4.7 : Thermal Imaging Camera and Software-Related

4.3.6 Proportional, Integral, and Derivative (PID) Controller

An Inkbird SSR-40 DA PID controller with an accuracy of ± 0.2%, linked to the immersion heater inside the buffer tank, was used to regulate the power input to the immersion heater and thus ensuring constant flow temperature (FT) from the tank during all the tests. This fluid flow temperature was monitored using a PT100 temperature sensor with a 0.2 m probes, which was fixed inside the buffer tank to detect the fluid temperature. The position of the PID sensor was chosen to be inside the buffer tank to detect the fluid temperature near the heating element to avoid overheating and prevent the heating element from getting damaged. Figure 4.8 shows a schematic diagram of the PID controller and its sensor positions.

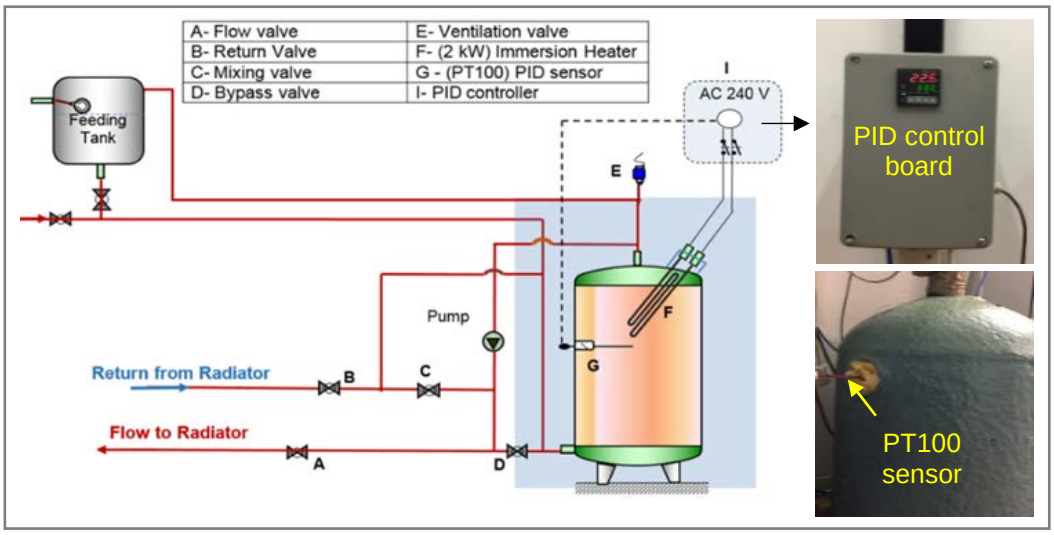

Figure 4.8 : Schematic Diagram of the PID Controller and Sensor Positions

4.4 Calibration of Measuring Instruments

The temperature sensors and flow meter were calibrated to evaluate the accuracy of their measurement.

4.4.1 Temperature Sensors Calibration

The calibration of the temperature sensors was performed using a temperature-controlled stirred water bath (Grant W28 with temperature stability of ±0.004ºC) with a built-in electrical heater, refrigeration unit and temperature controller. The calibration was done for a range of temperature between 12.5ºC to 80ºC.

The calibration process started by adjusting the thermostat of the water bath to a specific temperature, then it was left until it reached a steady state temperature. In addition to that, two pre-calibrated NPL mercury thermometers covering the range 0ºC -100ºC (with 0.1 scales) were used in the calibration process as a temperature reference. All the temperature sensors described in Table 4.2 were immersed in the calibration bath to the same level as the two-reference thermometers to avoid local temperature variation.

Table 4.2: Temperature Sensors Title and Description

No.	Sensor Name	Type	Location
1	TO-1	Type T	At 0.1m above the left flow side of the radiator
2	TO-2		At 0.1m above the right flow side of the radiator
3	Ti-1		At 0.1m above the middle of the radiator
4	Ti-2		At 0.1m above the middle of the radiator
5	CW		Centre wall behind the radiator
6	RT		The surface of the return pipe of the radiator
7	Low Rad T		The lower middle part of the radiator surface
8	Rad Temp F		Upper face surface of the radiator
9	FT		The surface of the flow pipe of the radiator
10	PT100 FT	PT100	Inside the flow pipe of the radiator
11	PT100 RT		Inside the return pipe of the radiator
12	Globe Temp	Type T	Inside the Globe bulb
13	Rad Temp R		On the top radiator surface
14	Mid Rad T		Middle of the radiator surface
15	ECT		At 2 m height inside the chamber
16	Mid box Temp		In the middle of the booth at 0.05 m from the floor of the booth
17	Box Top		In the top of the booth at 0.05 m from the ceiling of the booth
18	Box Bot		In the bottom of the booth at 0.75 m from the floor of the booth
19	Side-wall T		On the surface of the mid-side wall of the booth

The calibration was conducted on the temperature sensors and the full data logging system, including the Data Logger and PC. The temperature readings were compared to reference two mercury thermometers. So, in this case, the complete temperature monitoring system was calibrated. The calibration procedure was carried out as follows:

1. Temperature sensors reading were calibrated for the range of temperature between 12.5ºC, 20ºC, 30ºC, 40ºC, 50ºC, 60ºC and 80ºC.
2. The water bath was set to the required temperature and allowed to reach steady state temperature after that data recording started at 5-second intervals and lasted for 15 minutes. The water bath thermostat was then set to another temperature, and the procedure was repeated.
3. The readings of the temperature sensors were compared to the actual temperature

read from the two mercury thermometers. Then the best-fit equation was generated for each temperature sensor for the full calibration range in the form of Tactual = (A* Treading) ±B, where A is the gradient of the trend and B is a constant. The calibration equations of the temperature sensors were rechecked before being incorporated into an Excel spreadsheet which used to enter the collected data.

Figure 4.9 shows the calibration results of one sensor (PT100FT) versus the NPL thermometer reading, which reflects the water bath setpoint reading. The linear best-fit calibration equation and R^2 of 0.9999 are presented within the graph. The calibration results for the remaining temperature sensors used in experimental work are presented in Appendix 4.C.

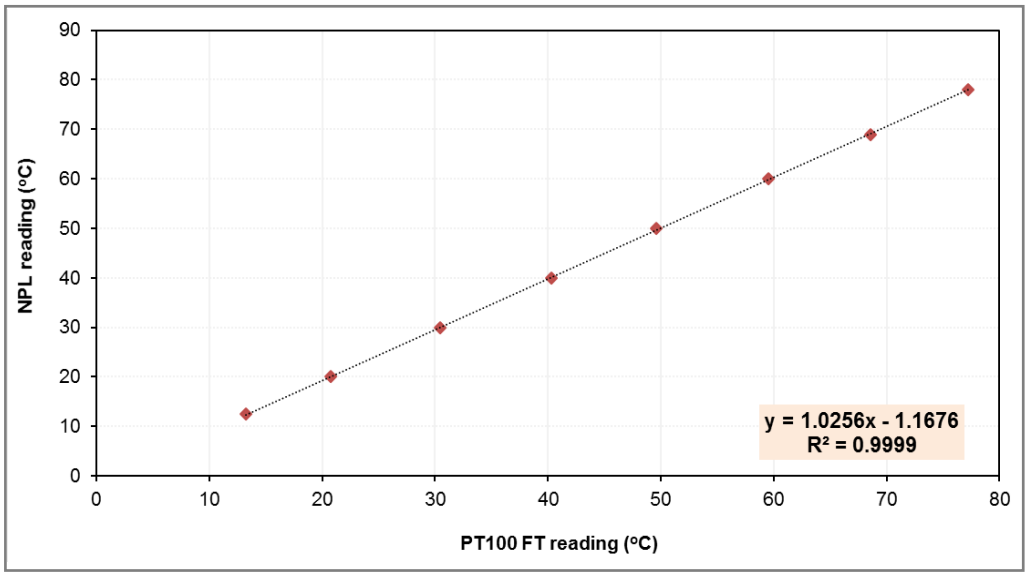

Figure 4.9: Liner Best-Fit Calibration Equation for PT100 FT Sensor

The linear best-fit calibration equation and R^2 value for each thermocouple are presented in Table 4.3 below.

Table 4.3: Calibration Equations of the Temperature Sensors

No.	Sensor Name	Sensor Type	Calibration Equation	R^2
1	TO-1	Type T	$T_{actual} = (1.0201 * T_{reading}) -0.4519$	0.9999
2	TO-2		$T_{actual} = (1.0212 * T_{reading}) - 0.2192$	0.9999
3	Ti-1		$T_{actual} = (1.0226 * T_{reading}) - 0.105$	0.9999
4	Ti-2		$T_{actual} = (1.0278* T_{reading}) + 0.1945$	0.9999
5	CW		$T_{actual} = (1.028* T_{reading}) + 0.1070$	0.9999

6	RT		$T_{actual} = (1.0277* T_{reading}) + 0.1934$	0.9999
7	Low Rad T		$T_{actual} = (1.0185 * T_{reading}) + 0.1823$	0.9999
8	Rad Temp F		$T_{actual} = (1.0185 * T_{reading}) - 0.0546$	0.9999
9	FT		$T_{actual} = (1.033 * T_{reading}) - 0.7762$	0.9998
10	PT100 FT	PT100	$T_{actual} = (1.0256* T_{reading}) - 1.1676$	0.9999
11	PT100 RT		$T_{actual} = (1.0246 * T_{reading}) - 1.5550$	0.9999
12	Globe Temp	Type T	$T_{actual} = (1.0432* T_{reading}) + 1.6891$	1
13	Rad Temp R		$T_{actual} = (1.018* T_{reading}) + 0.1233$	0.9999
14	Mid Rad T		$T_{actual} = (1.022* T_{reading}) + 0.2781$	1
15	ECT		$T_{actual} = (1.0204* T_{reading}) + 0.0995$	1
16	Mid box Temp		$T_{actual} = (1.0001* T_{reading}) - 1.2016$	1
17	Box Top		$T_{actual} = (0.9999* T_{reading}) - 0.0064$	1
18	Box Bot		$T_{actual} = (0.9999* T_{reading}) - 0.5976$	0.9999
19	Side-wall T		$T_{actual} = (0.9985* T_{reading}) - 1.0678$	1

4.5 Uncertainty Analysis of Temperature Sensors

The validation of the best-fit equations for all temperature sensors incorporated into the Excel spreadsheet at different temperature range was performed. This validation was carried out by comparing five calibrated reading from each setting with the NPL reading and the uncertainty analysis for each sensor was evaluated based on the validation results as presented in Appendix 4.D. Uncertainty Analysis is the prediction of the uncertainty interval, which associate with the experimental measurements.

The total uncertainty (u_{tot}) of the measurement contains systemic (bias) (u_{Sys}) and random (Precision) (u_{Random}) errors. The u_{Sys}, is the uncertainty or fixed errors which tend to move all measurements systematically, so their mean value is displaced. It represents the difference between the mean value of the data and the actual value. The u_{Random} is the errors which fluctuate from one measurement to the next. They produce results distributed about some mean value and they can occur for a variety of reasons [90&91]. Calculation of the total uncertainty (u_{tot}) depend on the three-following information:

- The bias error u_{Sys}

- The standard deviation of the mean ($\overline{\sigma_S}$) of the set of N data (five readings)
- The number of degrees of freedom (N – 1), where N is the number of data

The u_{Random} was calculated based on the standard deviation (SD) of the mean with a 95% confidence level ($t_{N-1,0.95}$) from equation 4.3:

$$u_{Random} = t_{N-1,0.95} * \overline{\sigma_S} \quad \textbf{(4.3)}$$

Where $\overline{\sigma_S}$ was calculated from equation 4.4.

$$\overline{\sigma_S} = [\frac{1}{N}(\frac{\sum_{i=1}^{N}(T_i - \overline{T}))^2}{N-1}) \,]^{0.5} \quad \textbf{(4.4)}$$

The u_{tot} was evaluated considering Root- Sum- Square model.

$$u_{tot} = \sqrt{{u_{Sys}}^2 + {u_{Random}}^2} \quad \textbf{(4.5)}$$

As an example, the calculation method of uncertainty for the PT100 FT sensor at a temperature of 20ºC are presented in and Table 4.4 below.

Table 4.4: Uncertainty Calculation of PT100 FT Temperature Sensor

No. (N)	NPL reading	PT100 FT reading ($T_{reading}$)	Best-fit equation T_{actual} = (1.0256 * $T_{reading}$) - 1.1676 (T_i)	(T_i - $\overline{T}$)^2
1	20	20.68	20.04	0.0003601
2	20	20.65	20.01	0.000088
3	20	20.65	20.01	0.0000534
4	20	20.66	20.02	0.0000048
5	20	20.66	20.02	0.00000002
Mean ($\overline{T}$)			20.02	∑= 0.00051
Degree of freedom (N-1)				4
The standard deviation (σ_s)				0.01
The standard deviation of the mean ($\overline{\sigma_S}$)				0.00534
Student distribution coefficient for N-1 degree of freedom ($t_{(95\%, N-1)}$)				2.78
u_{Random}		0.015	u_{tot}	± 0.02K

The uncertainty result for each temperature sensor was evaluated for rang of the temperature of 12.50ºC to 80ºC and are presented in Table 4.D-1 in Appendix 4.D.

4.6 Calibration of the Flow Meter

The fluids flow rate was measured and recorded using Digital Sontex Superstatic 449 flow meter and Platon NGX glass standard rotameter were connected in series. The digital flow meter was calibrated for both water and ethylene glycol mixtures by the manufacturer. The calibration certificate gives an accuracy of ± 2%. Furthermore, to achieve confidence with the flow rate measurements, the flow meter reading was rechecked locally for each HTF test at a constant flow rate and temperature (at the return temperature of the radiator, which was about 65ºC). A stopwatch and Labelled standard laboratory contained were used to perform the flow meter reading check. The measurement process was repeated three times and the average of these measurements was considered to check with the reading of the digital flow meter. Table 4.5 shows the measured flow rate data and the flow rate reading from the digital flow meter (water test).

Table 4.5: Calibration of the Digital Flow Meter

Trial	Digital flow meter reading (m^3/h)	Manual measured flow rate data		
		Collected volume (ml)	Time (s)	Flow rate (m^3/h)
1	0.052	400	28.5	0.050526
2	0.051	395	27.78	0.051188
3	0.0518	400	28.68	0.050210
Average flow rate (m^3/h)	0.0516	/		0.050641
SD	0.053%	/		0.050%
Diff % = $\frac{\text{Digital flow rate} - \text{measured flow rate}}{\text{Digital flow rate}}$ = 1.86%				

From the above table, a small difference (1.86%) can be noted between the digital flow meter reading and the manually measured flow rate for the water test. The same technique was followed with the AHTFs and the differences between the digital flow rate reading and manual measurements were found to be 1.9%, 1.87% and 1.95% for 50% HX/W, 50% EG/W and 30% EG/W respectively. The variation between the digital flow meter reading and the manually measured flow rate is within the acceptable range of the manufacturing accuracy (±2%).

4.7 Experimental Outline

This section gives a detailed explanation of the experimental procedure and scenarios that were designed and developed to test the alternative fluids in the test rig. The testing technique was designed to provide comparative results among the examined fluids.

4.7.1 Test Procedure

A consistent test procedure was developed to investigate the performance of the radiator heating system using different heat transfer fluids (water, 50%HX/W, 50% EG/W and 30% EG/W) under controlled environmental conditions. The test procedure as follows:

1. Prepare the alternative heat transfer fluids as described in section 3.2 (Chapter 3)
2. The system was filled with the examined fluid through the feed pipe from feeding and expansion tank
3. Remove the trapped air within the system, using the bleeding valve available on the radiator. Then the pump was turned on to circulate the fluid through the entire system while the bleeding valve was left open until the fluid started to flow out; thus, ensuring that the whole system is filled with the tested fluid.
4. The environmental chamber was turned on and maintained at 9ºC, with a relative humidity of 50% before starting the tests and maintain the same setting for the full duration of the tests to replicated outside cold conditions.
5. The lower chamber temperature was used to cool down the environment inside the booth and also the bulk of fluid in the buffer tank, the bulk of fluid in the buffer tank was cooled down to 21ºC ±1.5ºC. This enabled the start of all experiments from the same initial temperatures.
6. Adjust the flow rate in the system manually using the rotameter valve and the bypass globe valve to get the required temperature differences between the flow and return fluid temperatures across the radiator. The bypass valve was also left slightly open

during the test duration to control the flow rate and maintain the circulation of the fluid in the buffer tank and thus avoid fluid thermal stratification inside that tank.

7. Once the bulk fluid cooled down to the desired temperature, the valve between the radiator and buffer tank (flow valve) was closed and the immersion heater switched on. The PID controller automatically regulated the immersion heater.
8. The PID setpoint was fixed to provide a flow temperature of 75ºC to the radiator.
9. Once the PID setpoint temperature reached, the door of the booth inside the chamber was closed to start the test. The test was initiated by opening the flow valve between the buffer tank and the radiator to circulate the hot fluid in the system while monitoring and recording

   the temperatures, flow rate and energy consumption for the whole test duration.
10. The Datalogger and power meter were set to log data at 5 seconds intervals.
11. Once the required tests with each fluid were completed, the system was emptied and flushed three times before the system was recharged with the new fluid.
12. Repeat the test twice with each fluid to achieve repeatability and confidence in the results.

The volumetric flow rate in the system with each heat transfer fluid was monitored and recorded using the digital flow meter. Then the volumetric flow rate was converted into a mass flow rate by considering the density of the fluid at the return temperature, which the fluid temperature of where the flow meter was located. Therefore, the density-dependent temperature function for each fluid was developed based on the data presented in Tables 3.5 to 3.8 (Chapter 3). The density-dependent temperature functions (see Appendix 4.E) were used to convert the volumetric flow rate into the mass flow rate base on the temperature of the fluid. The test setup was calibrated and validated with water as a HTF, so the testing parameters such as the flow and return temperatures with the flow rate was selected to comply with BS EN 442-2 [70]. Therefore, the flow temperature set to be about 75ºC and the flow rate regular to provide 10K across the radiator resultant 65ºC as return temperature.

4.7.2 Test Techniques

Two different techniques of testing: steady state and thermostat tests were performed using water as a heat transfer fluid, as well as using alternative heat transfer fluids (AHTFs) as follows:

4.7.2.1 Steady State Test

Steady stat test was designed to ascertain the parameters of the test facility once it had reached a stable point and was therefore at a steady state. The test started by cooling the booth down to 9ºC and then heating the booth continuously, using the heating system, until the booth reached steady state condition (heat gain equal to heat loss). For this test, the pump was on continuously and, i.e. no electronic thermostat in place to control the heat input into the booth. Determining the time when steady state condition was based on BS EN 442-2. According to the standard the steady state conditions is only achieved when the standard deviation (SD) for at least 12 measurements of the flow rate, fluid and air temperatures taken within 30 minutes do not exceed the limits listed below:

- Water flow temperature, ± 0.05K
- Air temperature, ± 0.05K
- Flow rate, ± 0.05 %

Thus, there was a need for careful continuous monitoring of the temperatures, flow rate during all the experiments. The system was kept running at steady state for about 9 hours to get reliable, steady state data for various parameters (flow, return temperatures and booth air temperature (IBT)) for all tests.

4.7.2.2 Thermostat Test

This type of tests was designed to replicate real-life conditions of a heating system, with the air thermostat being used to control the indoor temperature at a certain setpoint. The air thermostat used to control hot water flow into the radiator as the booth required to heat-

up to maintain the internal environment at the set temperature. The internal booth temperature (IBT) was chosen to be within a range that would duplicate a comfortable temperature for a living room (20ºC–23ºC) [92] so, the air thermostat was set at 22ºC. Air thermostat (Drayton analogue thermostat) linked to the circulation pump was used to control the IBT. When the temperature inside the booth reached the thermostat setpoint, the thermostat sent a signal to stop the pump until the IBT drops below the set level the pump started working again. For these tests, the flow rate, system and booth temperatures, as well as the energy consumption, were monitored and recorded continuously. Then, they were compared to evaluate the system performance with all tested fluids.

4.7.3 Scenarios of Testing

Two separate and independent scenarios for testing were considered in order to fully understand how the HRHS's performance is affected by the tested fluids. The test scenarios are presented in the following sections.

4.7.3.1 Drop-In Scenario

The drop-in scenario was designed to replicate a situation where the alternative fluids are charged into a heating system without changing the system settings (flow rate and/or temperatures settings). The alternative fluids (50% HX/W, 50% EG/W and 30% EG/W) dropped in as a replacement for water in the test rig by keeping the same settings of the pump, valves and the PID controller as that used for the water tests. The same test procedure was followed and the parameters such as; flow rate, energy consumption and IBT were recorded and monitored to observe the effect of the tested alternative fluids on the hydronic radiator heating system behaviour.

4.7.3.2 Optimised Scenario

This scenario was designed to optimise the parameters that could influence the performance of the radiator when the alternative heat transfer fluids were used as a working fluid in the HRHS. For this scenario, the mass flow rate through the system was adjusted with each AHTF according to the base-case (water test) data as per the following two cases:

Case 1: Adjust the mass flow rate through the system to be at the same level to the mass flow rate of the base case.

Case 2: Adjust the temperature difference across the radiator (ΔT) to be at the same level to that for the base case (water test), (ΔT of 10K).

The internal booth temperature and energy consumption were monitored, measured and compared to observe the effect of the AHTFs on the hydronic heating system performance.

4.8 Summary

This chapter outlined the steps of design and development of the bespoke experimental test facility, which simulates a real HRHS working under a controlled environment. The test facility was built and developed to investigate the effect of AHTFs on the performance of the hydronic radiator heating system under controlled test conditions. The controlled testing conditions were achieved through utilising the environmental chamber as an independent room to provide a controlled condition around the testing zone (booth). Detailed description of components and data acquisition system and measuring instruments were presented. Calibrations of the measuring instruments and uncertainty analysis were also highlighted in this chapter. Besides, this chapter covered the design and plan for test method, types and techniques that were adapted to perform the experimental work of this project.

CHAPTER 5

Radiator Thermal Performance - Energy Balance Approach

5.1 Introduction

This chapter presents the principles and standards that are used to evaluate the heat output from the radiator. Also, this chapter provides the details of a new approach that was developed based on the energy balance principle to determine the heat output from the radiator working with the AHTFs. The new approach enables to determine the heat output from the radiator to the air-side, without being bound by the need to measure the dynamic changes in the thermal properties of the working fluid at different temperatures.

5.2 Radiators Heat Output Based on BS EN 442-2 Standard

The heat output from the radiators is evaluated experimentally in specific testing conditions, and many standards have been developed to specify the testing conditions. For example, ISO 3146, 3150, 3147, DIN 4722 and BS 3528 were used for testing radiators and evaluating the heat output. Based on these standards, radiators were tested for a fixed flow and returned temperatures of 90ºC and 70ºC, respectively, with an indoor air temperature of 20ºC [93]. In 1997 the BS EN 442-2 [70] standard was introduced to cover some additional essential aspects that previous standards did not address, and also to cover some existing aspects more accurately. The BS EN 442-2 standard describes an experimental procedure to test radiators and analyse the heat output. The model used by the BS EN 442-2 standard to assess the radiators heat output on the air-side at steady state conditions is expressed by equation 5.1.

$$\dot{Q}_{50} = K_m \, (\Delta T_{\dot{e}})^n \qquad \textbf{(5.1)}$$

Where $\dot{Q}_{50}$ is the design heat output from the radiator (nominal heat output), K_m and n are the characteristic coefficients of the radiators. These coefficients are established using regression analysis from experimental measurements taken by manufacturers during their testings for the radiators working with water or steam at temperatures below 120ºC. The $\Delta T_{\dot{e}}$ is the radiator excess temperature which represents the design temperature difference between the mean radiators temperature (T_{mean}) and the indoor air temperature (T_{air}). Figure 5.1 shows the temperature points that are considered to assess the excess temperature ($\Delta T_{\dot{e}}$).

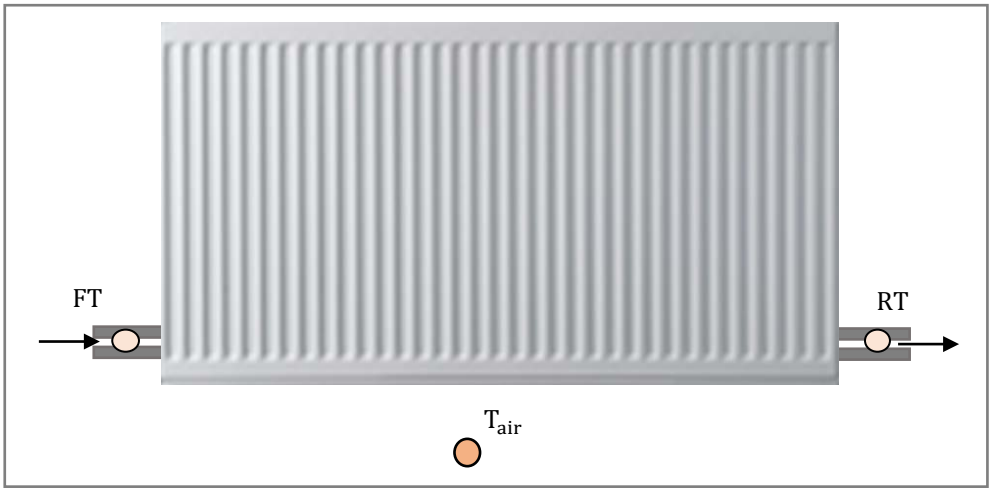

Figure 5.1: Temperature Points for Radiator Excess Temperature Calculation

The radiator access temperature ($\Delta T_{\dot{e}}$) can be determined in two ways based on the T_{mean} (the mean of the flow and return temperatures) evaluation as follows:

- Arithmetic mean radiator temperature (AMRT)

$$\Delta T_{\dot{e}} = ((FT + RT)/2) - T_{air} \quad \textbf{(5.2)}$$

Where T_{air}, FT and RT are the indoor air temperature, flow and return temperatures of the radiator respectively.

- Logarithmic mean radiator temperature (LMRT)

$$\Delta T_{\dot{e}} = (FT - RT)/\ln((FT - T_{air})/(RT - T_{air})) \quad \textbf{(5.3)}$$

To determine whether to use AMRT or LMRT to evaluate the T_{mean}, the following condition

need to be followed when $((\mathrm{FT}-\mathrm{T_{air}})/(\mathrm{RT}-\mathrm{T_{air}}))$ ≥ 0.7, then the AMRT is used; otherwise, LMRT is used [73]. According to the BS EN 442-2, the thermal output from a radiator is defined for a reference air temperature of 20ºC, with the flow and return temperatures of 75ºC and 65ºC respectively. This means that the design thermal output evaluated based on the excess temperature ($\Delta \mathrm{T_{\dot{e}}}$) of 50ºC, (see equation 5.1). For any different excess temperature ($\Delta \mathrm{T_{\dot{e}}}$), the radiator heat output could be determined as follows:

$$\dot{Q}_s = \dot{Q}_{50}\,((((FT+RT)/2)-T_{air})/50)^n \qquad \textbf{(5.4)}$$

The BS EN 442-2 [70], specifies the technical requirements of the test chamber and states the test procedure to evaluate the design heat output of the water radiators under a specific operating condition (ideal condition). These conditions include constant radiative and convective heat transfer between the water radiators and the test chamber environment. These ideal conditions are hard to achieve in real applications, as many factors influence the radiators' heat output. Some of these factors are:

- The actual working conditions
- Variations in flow rate
- Flow and return temperatures
- The hydraulic connections (flow and return pipe connections)

The possible effect of these factors can result in the variation of the characteristic coefficients ($\mathrm{K_m}$ and n) of the radiator and that could affect the heat output from the radiator under actual operating conditions.

5.3 Radiators Heat Output - Energy Balance Approach

This section gives an extensive look into the development of a unique approach which is based on the energy balance inside the heated space to determine the heat output from the radiator to the air-side. This approach is important because of the following benefits:

1. The BS EN 442-2 standard heat output model is only applicable for radiators working with water or steam. Therefore, this approach was developed to assess the heat output from the radiator working with the AHTFs.
2. The unique approach allows the evaluation of the heat output from the radiator during both steady state and transient conditions. It also enables to evaluate the radiator heat output during the 'off' heating period (when there is no flow coming to the radiator).
3. It provides a mechanism of excluding the thermal properties of the HTFs (density and specific heat capacity) when evaluating the radiator heat output.

The energy balance approach has been developed based on the fundamentals of heat transfer in heated space. The heat is transferred from the hot surface of the radiator to the air and the booth's walls by convection and radiation and through the booth's walls by conduction. There is also a transfer of heat by radiation between the environmental chamber's walls and booth's walls. Therefore, the net resultant effect of the total heat transfer is changing in the air temperature inside the booth space (IBT). The instantaneous change in the IBT is the main parameter that was used for developing the energy balance approach. This approach allows the heat output from the radiator to be evaluated during transient conditions, which gradually converges to steady state values when all transient conditions disappeared.

5.3.1 List of Assumptions

The following assumptions were considered for evaluating the radiator heat output:

1. Temperature is distributed uniformly inside the booth space (indoor air)
2. The temperature of the internal booth's walls is equal to the internal air temperature
3. The temperature of the external booth's walls is equal to 9^{o}C, which is the environmental chamber temperature (ECT)
4. Thermal properties (density and specific heat capacity) of the materials that used to

construct the booth and the radiator are known

5. The only source used to heat the booth is the radiator
6. Change in stored heat in the air and booth's walls is due to change in the dry bulb temperature of the indoor space of the booth
7. Conduction is the only means of heat transfer through the booth's walls
8. Neglect infiltration effect inside the booth, as the booth was well-sealed

5.3.2 Theory of the Energy Balance Approach

The energy in the form of heat comes from the fluid flowing through the radiator. That heat is transferred to the wet heating surface (inner surface) of the radiator by convection and the wet heating surface conducts heat to dry surface (outer surface) of the radiator by conduction. Then heat is emitted by the dry heating surface of the radiator to the air and booth walls by convection and radiation. This means the fluid flowing through the radiator loses heat. That heat is picked up by the radiator walls and then transferred to the surrounding by convection and radiation. Figure 5.2 shows the heat balance diagram of a panel radiator.

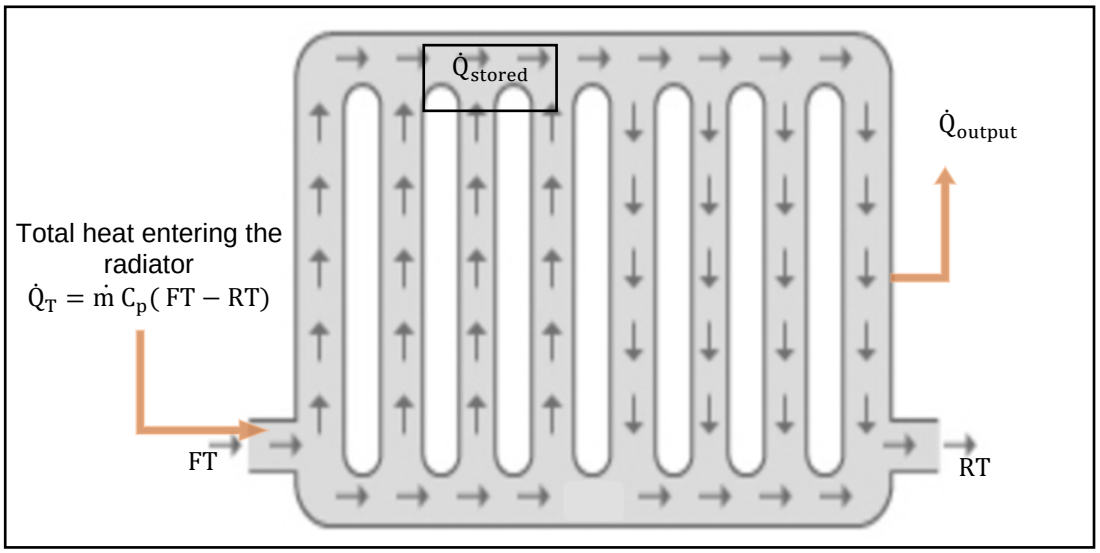

Figure 5.2: Heat Balance Diagram of the Radiator

The transient energy balance equation of the panel radiator can be expressed as follows.

$$\dot{Q}_T = \dot{Q}_{stored} + \dot{Q}_{output} \quad \textbf{(5.5)}$$

The $\dot{Q}_{stored}$ represent the heat stored in the body of the radiator (metal mass) and the fluid trapped inside the radiator. The $\dot{Q}_{stored}$ can be evaluated as follows:

$$\dot{Q}_{stored} = \left(m * C_p\right)_{Radiator} * \frac{dT_s}{dt} + \left(m * C_p\right)_{Water} * \frac{dT_m}{dt} \quad \textbf{(5.6)}$$

Where $\left(\mathrm{m} * \mathrm{C_p}\right)_{\mathrm{Radiator}}$, $\left(\mathrm{m} * \mathrm{C_p}\right)_{\mathrm{water}}$ are the mass and specific heat capacity of the radiator and fluid inside the radiator. $\mathrm{dT_s/dt}$ and $\mathrm{dT_m/dt}$ are the rate of the radiator surface temperature change and the rate of the mean radiator temperature change. Radiator heat output ($\dot{Q}_{output}$) is the heat transferred from the dry heating surface of the radiator to the indoor air and booth's walls by convection and radiation, as stated in Chapter 2,(see equation 2.8). Based on the first law of thermodynamics (at steady state heat flow), all the energy put into a system must come out again [81]. In order for the first law of thermodynamics to be satisfied, the energy enter to the radiator must be equal to the energy coming out at the steady state condition. Therefore, the heat balance of the radiator at the steady state heat flow can be written as per equation 5.7.

$$\dot{Q}_T = \dot{Q}_{output} \quad \textbf{(5.7)}$$

The output heat from the radiator to the air-side leads to raising the temperature of the heated space (air and the booth's walls), as the environmental chamber was controlled at a fixed temperature (ECT) of 9ºC. The change in the IBT leads to creating the following three heat flow components inside the heated space (booth):

- Sensible heat accumulated in the air ($\dot{Q}_{(sen)air}$)
- Sensible heat accumulated in the Booth's walls ($\dot{Q}_{(sen)B,walls}$)
- Heat loss from the booth's structure ($\dot{Q}_{loss}$)

The radiator heat output was evaluated based on the heat balance for the three-heat flow components ($\dot{Q}_{(sen)air}$, $\dot{Q}_{(sen)B,walls}$ and $\dot{Q}_{loss}$) inside the booth as described in the following sections.

5.3.2.1 Energy Balance of the Heated Space (Booth)

The internal space of the booth was designed to be unventilated space and it is heated by a localised point source, i.e. radiator, under controlled outside condition (environmental chamber). When the radiator starts working, the indoor air temperature is at the initial temperature, of approximately 9ºC (same as ECT).

The heat output from the radiator raises the air and the booth's walls temperatures and as a result, balances the heat loss by the booth structure. In this process, the temperature of any mass inside the booth is also raised with time until it reaches a fixed temperature at steady state heat flow. In order to evaluate the heat balance within the heated space, the system boundaries are considered around the outer surface of the booth and the radiator to map the heat flow, as seen in Figure 5.3 below.

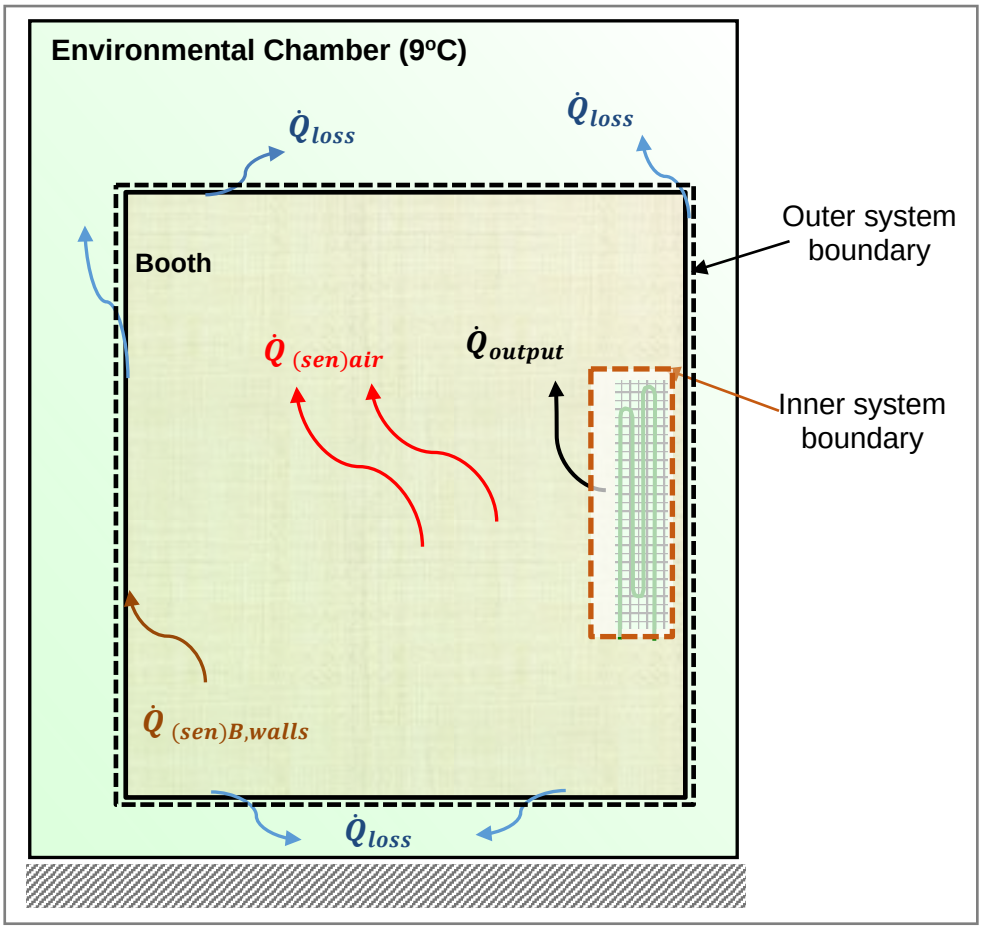

Figure 5.3: Schematic Diagram of the Booth Heat Flow Map

Figure 5.3 shows a vertical mid-section of the test facility with the heat flow map. The hot fluid enters the radiator and causes the radiator surfaces to heat-up. Thus, a temperature difference is created between the indoor air and the radiator. This temperature difference drives the heat transfer from the radiator $\dot{Q}_{output}$ across the (inner system boundary) to the booth space.

The $\dot{Q}_{output}$ is the heat transferred to the surrounding in the form of sensible heat to the air ($\dot{Q}_{(sen)air}$) and to the booth's walls ($\dot{Q}_{(sen)B,walls}$). While the remaining heat crosses the outer boundary of the system as a heat loss ($\dot{Q}_{loss}$) to the environmental chamber due to the temperature differences. As illustrated in Figure 5.3, the heat transfer flow and energy balance to evaluate the $\dot{Q}_{output}$ within the system's boundaries can be divided into three modes, as presented in Figure 5.4.

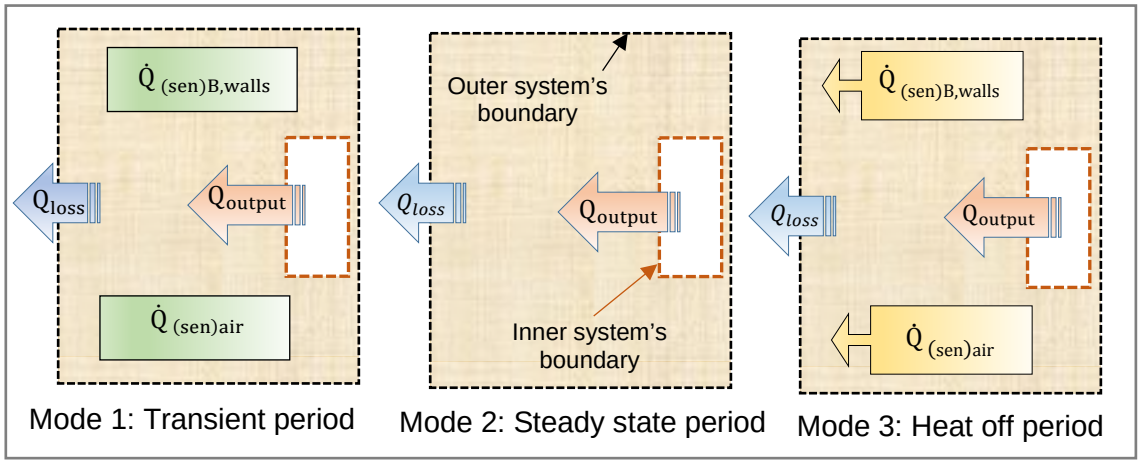

Figure 5.4: Three Different Modes of the Heat Flow Balance

- **Mode 1: During booth heat- up period (transient conditions)**

Heat output from the radiator ($\dot{Q}_{output}$), which is the heat crossing the inner system boundary). Part of this heat will be stored as accumulated sensible heat inside the booth (air and booths' walls sensible heat ($\dot{Q}_{(sen)\,air}$ and $\dot{Q}_{(sen)\,B,walls}$)) and the remaining heat will leave the booth space as a heat loss ($\dot{Q}_{loss}$) through the outer system boundary. The heat balance can be expressed as follows:

$$\sum \text{Heat output} + \sum \text{Heat gain} = \sum \text{Heat loss} + \sum \text{Heat accumulated}$$

$$\dot{Q}_{\text{output}} + 0 = \dot{Q}_{\text{loss}} + \dot{Q}_{(\text{sen})\ \text{air}} + \dot{Q}_{(\text{sen})\ \text{B,walls}}$$

The $\dot{Q}_{\text{output}}$ can be calculated as follows:

$$\dot{Q}_{output} = \dot{Q}_{loss} + \dot{Q}_{(sen)\ air} + \dot{Q}_{(sen)\ B,walls} \quad \textbf{(5.8)}$$

Mode 2: During booth steady state period

As time passes, the transient conditions disappeared; as a result, the booth reaches steady state condition. Therefore, the accumulated sensible heat inside the booth (air and walls sensible heat ($\dot{Q}_{(\text{sen})\text{air}}$ and $\dot{Q}_{(\text{sen})\text{B,wall}}$) reach saturation and air temperature will not change (reaches steady state temperature). At this stage, the heat output from the radiator becomes equal to the heat loss from the booth. The heat balance equation can be expressed as:

$$\sum \text{Heat output} + \sum \text{Heat gain} = \sum \text{Heat loss} + \sum \text{Heat accumulated}$$

$$\dot{Q}_{\text{output}} + 0 = \dot{Q}_{\text{loss}} + 0$$

The ($\dot{Q}_{\text{output}}$) can be calculated as follows:

$$\dot{Q}_{output} = \dot{Q}_{loss} \quad \textbf{(5.9)}$$

Mode 3: During heat off period

During the heating off period when there is no fluid flowing through the radiator, the heat output from the radiator starts to drop, as the heat output during the off period is only the heat that released from the body of the radiator and the fluid trapped inside the radiator. Thus the IBT started to drop as well. Therefore, the accumulated sensible heat in the indoor air and booth's walls turn to be as a heat gain within the heated space. The heat balance equation can be expressed as follows:

$$\sum \text{Heat output} + \sum \text{Heat gain} = \sum \text{Heat loss} + \sum \text{Heat accumulated}$$

$$\dot{Q}_{output} + \dot{Q}_{(sen)\ air} + \dot{Q}_{(sen)\ B,walls} = \dot{Q}_{loss} + 0$$

The ($\mathrm{Q_{output}}$) can be calculated as follows:

$$\dot{Q}_{output} = \dot{Q}_{loss} - \dot{Q}_{(sen)air} - \dot{Q}_{(sen)\ B,walls} \quad \textbf{(5.10)}$$

Excel spreadsheet-based calculator was developed to determine the heat output from the radiator based on the heat balance of $\dot{\mathrm{Q}}_{\mathrm{(sen)air}}$, $\dot{\mathrm{Q}}_{\mathrm{(sen)B,walls}}$ and $\dot{\mathrm{Q}}_{\mathrm{loss}}$ and the combination of the above modes. During heating system operation, the experimental parameters, including IBT and outdoor temperature (ECT), were recorded for the whole test duration and they were considered as main parameters to evaluate the three components of heat. The calculation procedure of the sensible heats and heat loss due to the IBT changes with time are described further in the following sections.

5.3.2.1.1 Analysis of Air Sensible Heat

The sensible heat within the air mass ($\dot{\mathrm{Q}}_{\mathrm{(sen)air}}$) inside the booth is computed by equation 5.11.

$$\dot{Q}_{(sen)air} = V_{air} * \rho_{air} * C_{p\,air} * \left(\frac{dT_{IB}}{dt}\right) \quad \textbf{(5.11)}$$

Where ρ_{air} ,$\mathrm{C_{p\,air}}$ are the density and specific heat capacity of the air, and $\mathrm{dT_{IB}/dt}$ represents the change in the IBT with respect to time. The mass of the indoor air is a combination of dry air and water vapour; the amount of water vapour in the indoor air depends on the relative humidity (RH) and temperature.

The water vapour mass in the indoor air is assessed based on the relative humidity of 45% - 50% at 9ºC (booth initial condition same as environmental chamber condition, see section 4.2.3 of Chapter 4). The mass of water vapour in the indoor air was determined by using a psychometric chart (see Appendix 5.A) and it was found to be 0.0039 kg/ (kg of dry air). The amount of the indoor air was evaluated based on air volume (volume of the internal space of the booth) and the air density of 1.24 kg/m^3 [78], and it was found to be 5.74 kg. The total amount of water vapour in the indoor air is 0.00224 kg, which is too small

compared to the total indoor air mass. Therefore, the effect of the water vapour on the accumulated heat in the indoor air can be neglected and not considered in the calculations. The density and the specific heat capacity of the air are affected by the air temperature. Therefore, density and specific heat capacity were correlated as functions of temperature using data from CIBSE Guide C [78], (see Appendix 5.B), the density and specific heat correlations were then used in equation 5.11.

5.3.2.1.2 Analysis of Booth Wall Sensible Heat

Heat is transferred through the booth walls by conduction due to the temperature differences between indoor and outdoor. The internal booth surfaces temperature is being affected by the indoor air temperature. As a result, the heat will flow through the booth walls; some of this heat is accumulated in the booth's walls and some are lost to the outside until the booth internal conditions reach steady state conditions.

The sensible heat accumulated in the booth walls ($\dot{Q}_{(sen)B,walls}$) can be calculated using equation 5.12.

$$\dot{Q}_{(sen)B,walls} = (A_{B,w} * L * \rho_{B,w} * C_{p\,B,w}) \frac{dT_w}{dt} \quad \textbf{(5.12)}$$

Where $A_{B,w}$, L, $\rho_{B,w}$ and $C_{p\,B,w}$ are the surface area of the booth walls, the thickness of the walls, the density and specific heat capacity of the booth material respectively. The (dT_w/dt) is the changing in the wall temperature with respect to the time. The temperature gradient across the wall's thickness is different at various points until the steady-state condition is reached. The change in the booth's wall temperature was evaluated based on the outer and inner wall surfaces temperature. Initially, the inner and outer booth's walls temperatures were maintained at a fixed temperature of 9ºC, which is the environmental chamber temperature (ECT). When the heating process started the temperature of inner

surfaces (T_i) is raised to a higher value and the outer surface is maintained at the ECT. Therefore, the temperature profile through the wall thickness will change gradually [94].

The temperature of the booth's wall before the heating process began is (T_o), and the inner surface temperature (T_i) increases when the heating starts. The temperature variation within the wall is shown in Figure 5.5 for a condition in which $T_i > T_o$.

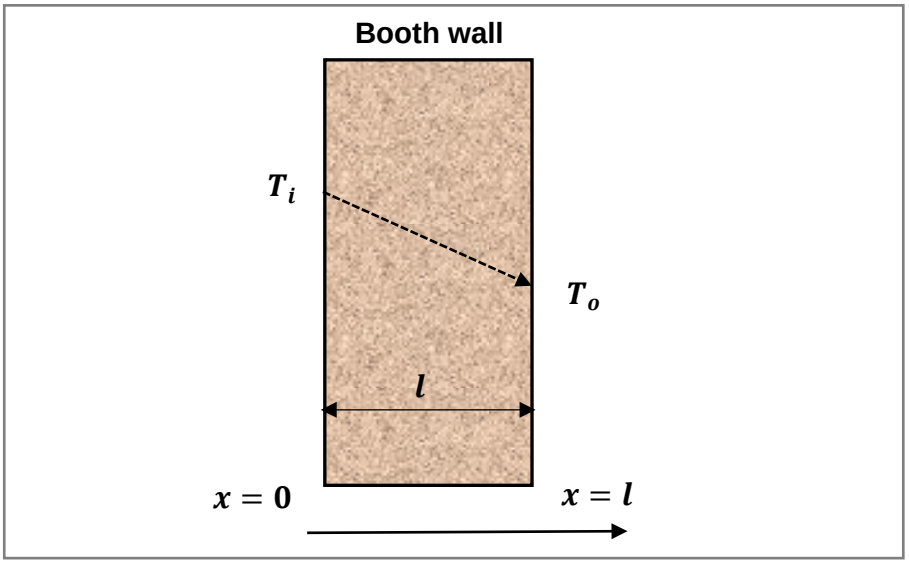

Figure 5.5: Temperature Distribution Through Booth Wall

The instantaneous average temperature of the booth wall is based on the inner and outer surface temperatures and can be calculated as follows:

$$T_w(x) = T_i + ((T_o - T_i)/l) * x) \quad \textbf{(5.13)}$$

Where the $T_w(x)$ is the wall temperature at the position (x) and (l) is the wall thickness. The wall temperature considered to perform the calculation is assessed based on $(x = (1/2)l)$. By substituting (x) value in equation 5.14, the wall temperature can be evaluated as per equation 5.14.

$$T_w = ((T_i + T_o)/2) \quad \textbf{(5.14)}$$

5.3.2.1.3 Analysis of Heat loss

Heat loss ($\dot{Q}_{loss}$) is the total amount of heat transferred through the booth walls. The rate of heat loss from booth depends on the temperature differences between the inside and outside environments and the thermal properties of the booth walls.

The effect of ventilation was not considered as the booth was designed to be unventilated space. While the infiltration effect was neglected as the booth was sealed well to prevent any air leakage, this means that the total heat loss from the booth is evaluated based on the heat transfer through the booth walls. The heat transfer through the walls is by conduction. This was evaluated using equation 5.15.

$$\dot{Q}_{loss} = \sum(AU)_B * \Delta\theta \qquad \textbf{(5.15)}$$

Where ($\Delta\theta$) is the temperature difference between indoor (IBT) and outdoor air (ECT). The ($\sum(\mathrm{AU})_{\mathrm{B}}$) is booth fabrication characteristic, which is the summation of the area of the internal surfaces multiplied by the thermal transmittance of the booth wall (U) which is the rate of heat loss through a material.

At steady state condition, the total heat entering the radiator must be equal to the heat loss and the time it takes to reach the steady state condition depends on the ratio of the wall's ability to conduct heat to its ability to store heat [94]. The heat balance at steady state condition can be written as follows:

$$\sum(AU_B) * (IBT - ECT) = \dot{m}\, C_P\, (F_T - R_T) \qquad \textbf{(5.16)}$$

Figure 5.6 shows the flow chart diagram, which presents the steps of the energy balance approach that was developed to evaluate the heat output from the radiator.

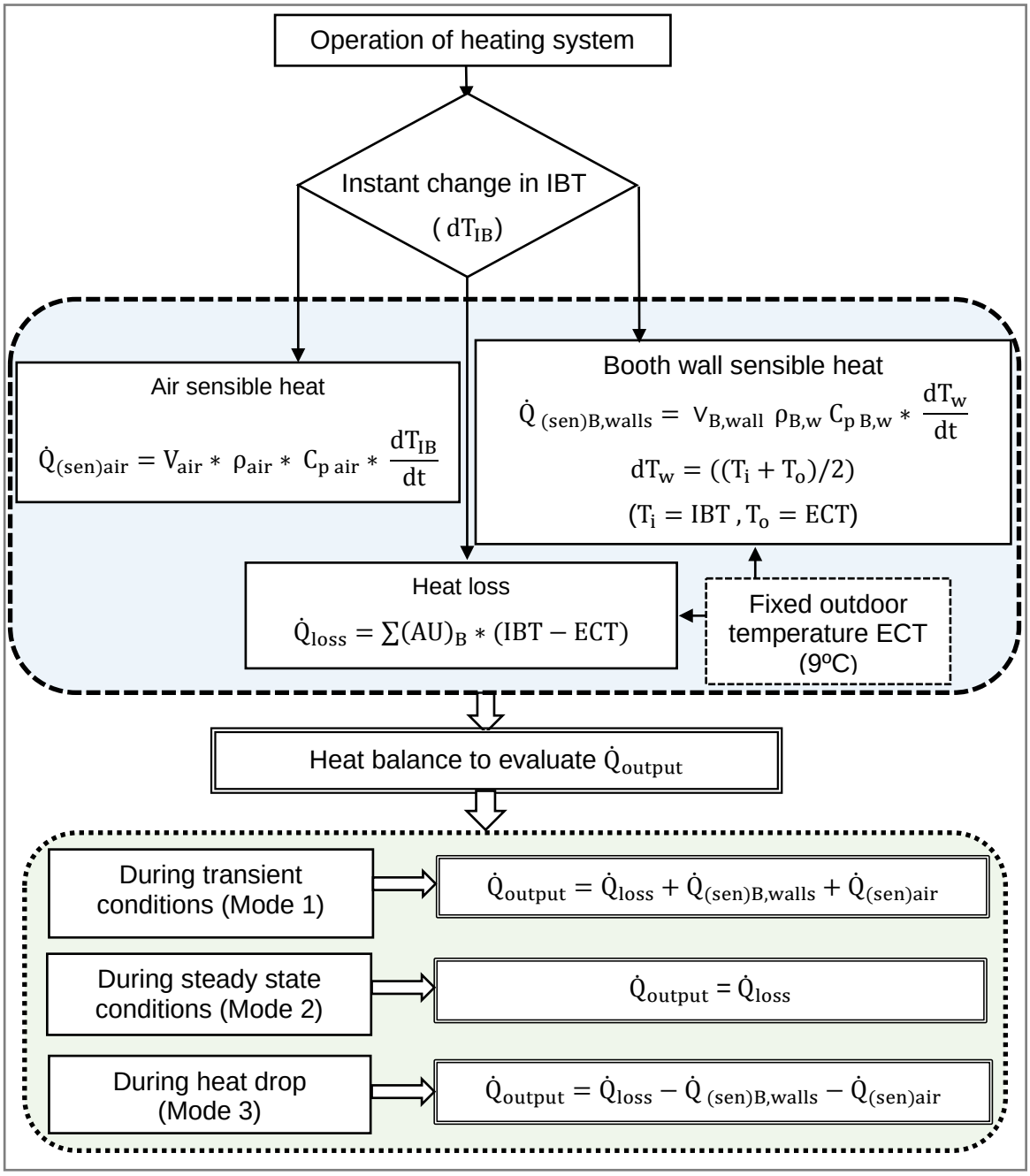

Figure 5.6: Flow Chart Diagram of the Energy Balance Approach

Figure 5.6 outlines the steps for the developed energy balance approach to evaluate the heat output from the radiator. The operating of the heating system resulted in an instantaneous change in the IBT, which leads to changes in the sensible heat in the masses of the indoor air and booth walls. Also, there is a heat loss from indoor space to the outside due to the temperature difference. The radiator heat output could be evaluated based on the heat balance for the three heat components $\dot{Q}_{(sen)air}$, $\dot{Q}_{(sen)B,walls}$ and $\dot{Q}_{loss}$

based on different modes of heat transfer processes. This approach has been applied to evaluate the heat output from the radiator working with AHTFs under test and the results obtained will be presented in chapter 7.

5.4 Summary

This chapter presented the standards used for radiators testing and heat output measurements. It was identified that the current standard (BS EN 442-2) used to evaluate the heat output of radiators, which is only applicable for radiators that utilise water or steam as a HTF and only during steady state conditions. Therefore, due to these limitations, the unique approach based on energy balance principle was developed to include the applications of other HTFs and transient conditions. The energy balance approach was used to evaluate the radiator heat output to the heated space (air-side) and it can be used to overcome the limitations that are associated with the BS EN 442-2 standard.

The concept of the energy balance approach is based on the amount of heat loss and the heat stored or released in all components in the booth (air and walls) due to the change in the IBT. Therefore, this approach allows the heat output from the radiator to be evaluated during steady state and transient conditions and during ‘off’ heating periods (when there is no fluid flow entering the radiator). Also, this approach offers a mechanism of excluding the effect of thermal properties of the heat transfer fluid when evaluating the heat output from the radiator.

CHAPTER 6

Investigating and Interpreting the Experimental Results

6.1 Introduction

The experimental setup outlined in Chapter 4 was designed to investigate and compare the performance of a hydronic radiator heating system (HRHS) when using different heat transfer fluids under controlled test conditions. This chapter presents the investigation and interpretation of the testing results. The initial tests were conducted using potable water as a working fluid in the system and these tests were repeated to establish repeatability and accuracy. After comparing the readings from the water tests and confirming repeatability, the results were validated and used to develop base case temperatures, a base flow rate, and base trends in power and energy consumption. The base results were used as a comparison with various other fluids (50% HX/W, 50% EG/W and 30% EG/W mixtures) examined in this research as alternative heat transfer fluids (AHTFs).

The results for the water test as the base case for testing and the results for the AHTFs tests, under two different test scenarios (drop-in and optimised scenarios), were analysed. All test results (for the AHTFs) were compared with the base case results using the following parameters:

1. Flow and return fluid temperatures (FT and RT)
2. Indoor air temperature: internal booth temperature (IBT) and globe temperature (GT)
3. Amount of energy consumed by the system
4. Temperature distribution across the radiator surface (using a thermal imaging camera)

6.2 Experimental Work with the Simulated HRHS

The experimental work was carried out using the simulated hydronic radiator heating system (HRHS). Tests were performed using different testing scenarios and cases, as outlined in Figure 6.1.

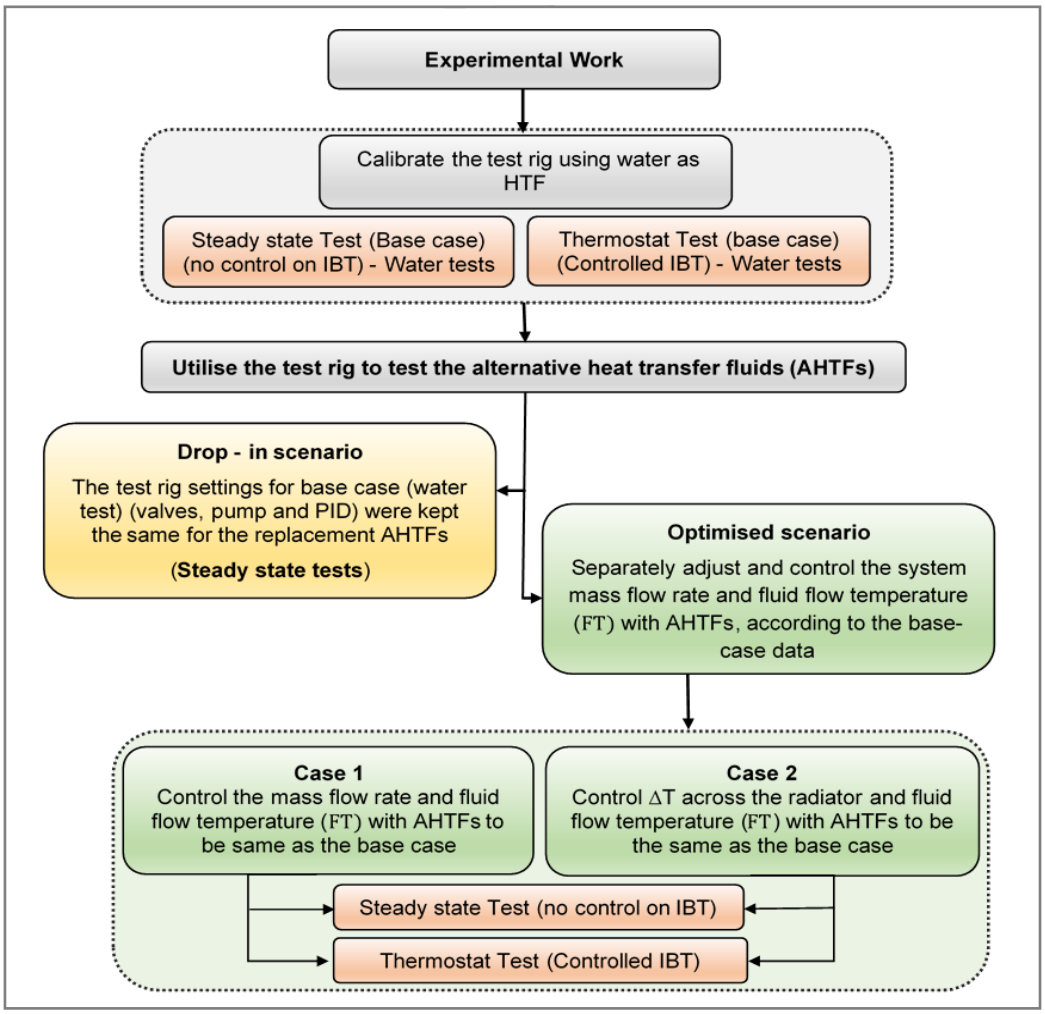

Figure 6.1: Flow Diagram of Experimental Work

Tests with water and with alternative fluids were conducted twice to ensure repeatability and confidence in the testing process. The following parameters were monitored and recorded for each test:

1. The IBT and GT
2. The surface temperature of the front face of the radiator
3. Radiator flow temperature (FT) and return temperature (RT)
4. The flow rate in the system

5. Amount of power and energy consumed by the system

The data from the repeated water tests were analysed and used as a reference point for the AHTFs tests. The results of the base case test and the AHTF tests are demonstrated and discussed in the following sections.

6.3 Base Case (Water Tests) Results

In this section, the data obtained from the water (steady state and thermostat) tests, as described in section 4.7.2 of Chapter 4, are presented and analysed with a focus on temperature and energy.

6.3.1 Steady State Test Results

For the steady state tests, the booth was heated up continuously until it reached a steady state condition. The temperature of the environmental chamber was maintained at 9ºC throughout the tests. The flow temperature (FT) was set to 75ºC and the flow rate was adjusted to provide a temperature difference (ΔT) of 10K across the radiator, making the return temperature (RT) from the radiator 65ºC. Hot water was allowed to circulate through the radiator until steady state conditions were achieved. The duration of the test was 45,000 seconds (12 hours and 30 minutes) and the test was repeated twice to ensure repeatability and accuracy.

The mass flow rate of the water passing through the radiator was adjusted to align with the 0.0148 (kg/s) flow rate calculated using equation 4.1 (Chapter 4). The actual flow rate in the system was monitored and controlled using two separate flow measuring devices: a digital flow meter and a rotameter, both installed in series along the return line. The digital meter presented the flow rate in (m^3/h). This was then converted into a mass flow rate which was dependent on the density of the fluid. Figure 6.2 illustrates the calculated mass flow rates over the duration of the tests.

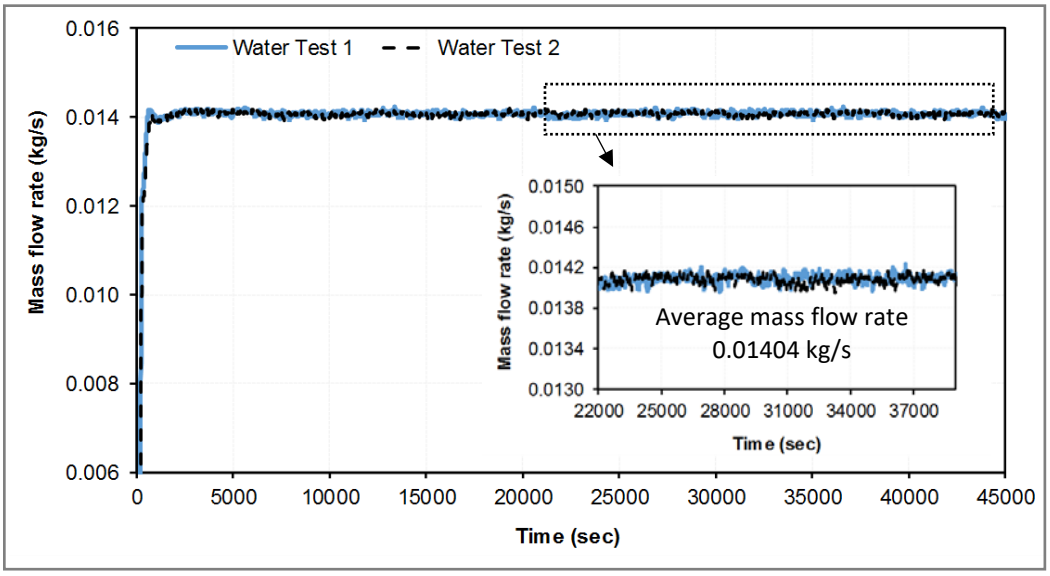

Figure 6.2: Mass Flow Rate for Steady State Water Tests

Figure 6.2 shows that the average mass flow rate of the water in the system (for the two tests) was maintained at approximately 0.01404 (kg/s) for the duration of each test, with a variation of ± 2%. This is the closest value that could be maintained in order to align with the mass flow rate needed to achieve approximately ΔT of 10K across the radiator. The trends of the flow and return temperatures are presented in Figure 6.3.

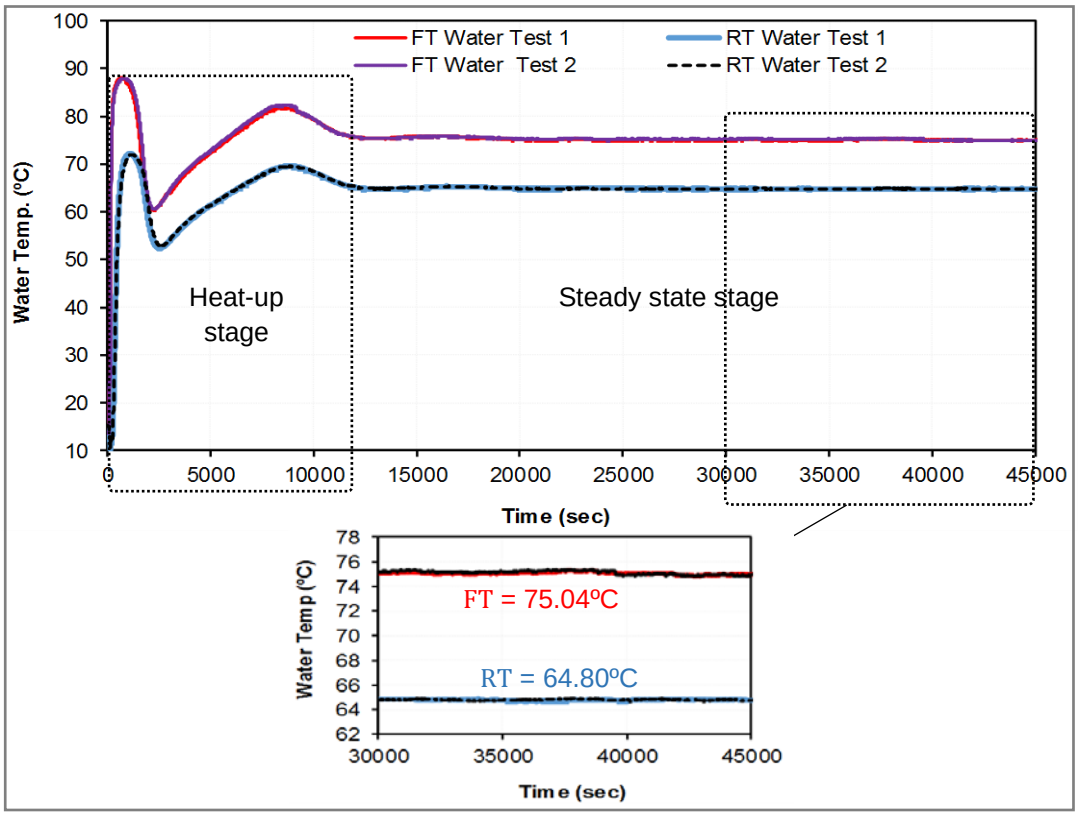

Figure 6.3: Flow and Return Temperatures for Steady State Water Tests

From Figure 6.3, it is clear that flow and return temperatures (FT and RT) of the water fluctuated during the heat-up stage and took approximately 11,000 seconds (3 hours and 4 minutes) to stabilise and reach the PID controller setpoint of 75ºC. The FT and RT during the heat-up stage were influenced by the PID controller overshoot (flow temperature rising above the setpoint, and fluctuating until reaching the PID setpoint). Moreover, the substantial differences between the flow temperature of the hot water, the radiator surface and the booth at the beginning of the experiments (9ºC) caused the temperature of the water to drop rapidly. Therefore, bringing the water temperature back to the PID setpoint took a relatively long time. Once the system had reached a steady state, the recorded data was analysed to validate the steady state conditions of the base case tests; this was conducted in accordance with the BS EN 442-2 standard (see section 4.5.2.1 of Chapter 4). Twelve readings taken within half an hour were used to calculate the most accurate steady state conditions, as shown in Figure 6.4.

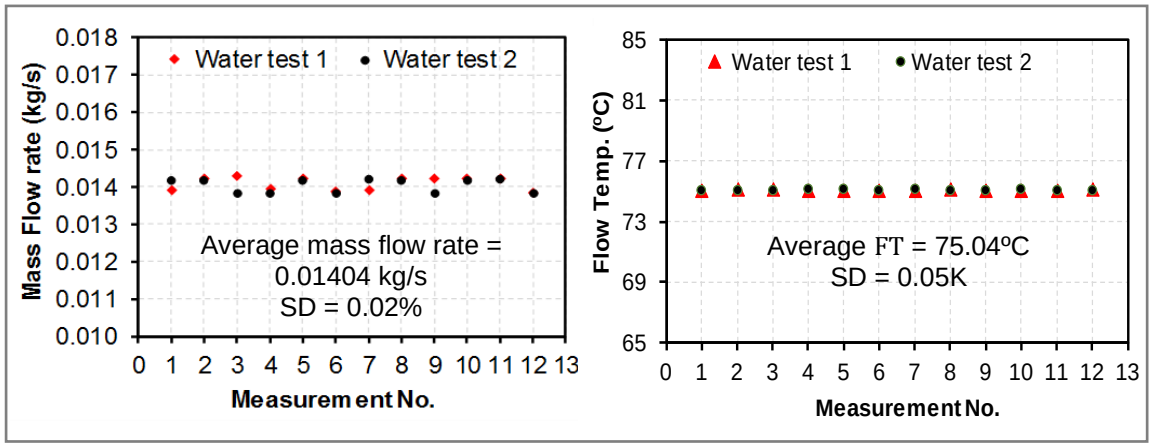

Figure 6.4: Steady State Conditions of Water Tests

Figure 6.4 shows that the flow rate and flow temperature for water tests were complied with the recommended values of the BS EN 442-2 standard, as presented in section 4.7.2.1 of Chapter 4. The IBT and GT were monitored and recorded every 5-seconds, along with the environmental chamber temperature (ECT). Figure 6.5 presents a schematic diagram of the booth, highlighting the positions of the thermocouples and globe used to measure the air and radiant temperatures.

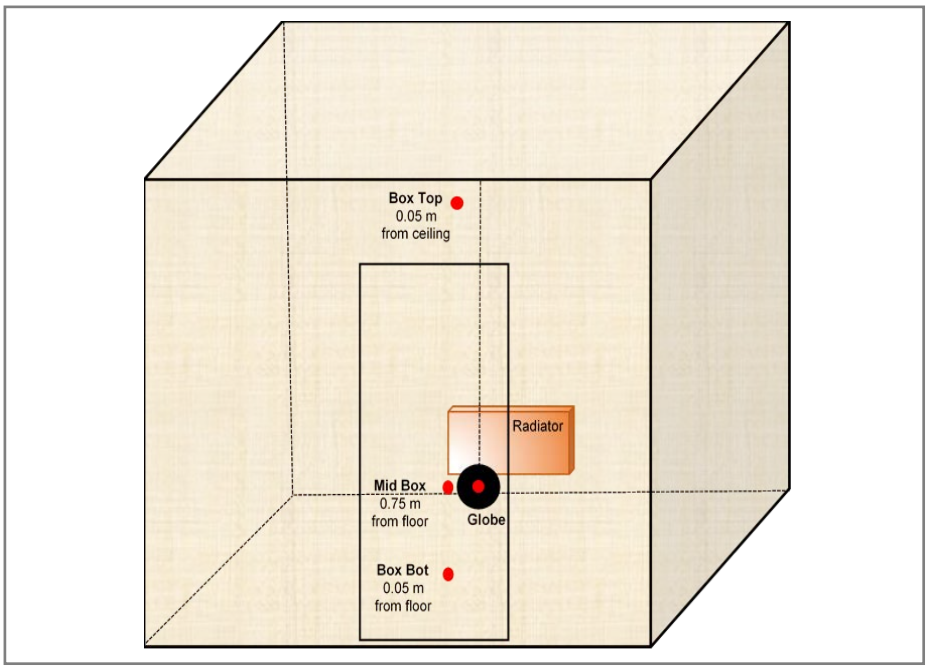

Figure 6.5: Schematic Diagram of Booth with Thermocouples Position

The average IBT was calculated from the readings of the three thermocouples (top, middle and bottom) within the booth, using the following equation.

$$IBT = \left(\Sigma_1^n T/_n\right) \quad \textbf{(6.1)}$$

In this equation, T and n, are the temperature reading and the number of thermocouples used to measure the air temperature inside the booth. Figure 6.6 presents the evaluated IBT and the recorded GT and ECT over the duration of the test.

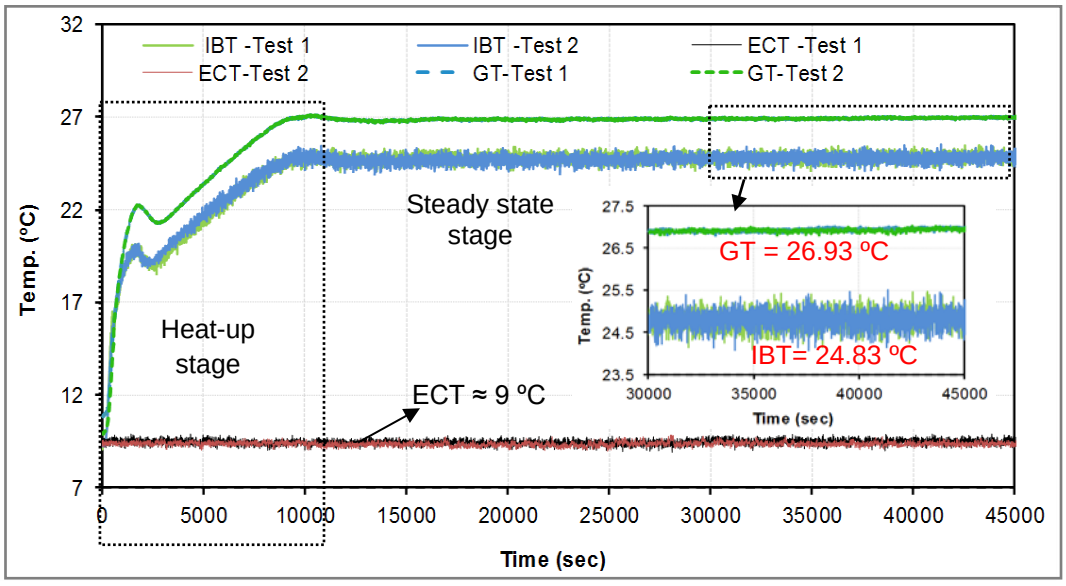

Figure 6.6 : IBT, GT and ECT for Steady State Water Tests

During the heat-up stage, the IBT rose gradually from 9ºC to the steady state temperature of 24.83ºC. The rising trend in IBT is similar to the trends recorded in FT and RT (see Figure 6.3). During the steady state stage, the recorded IBT was 24.83ºC with fluctuation of ± 0.6K, and the recorded GT was 26.93ºC with a variation of ± 0.02K.

For both tests, the ECT was maintained at 9ºC with a variation of ± 0.3K. The difference between the GT and the IBT (2.1K) can be attributed to radiation, as the globe bulb measured the combined effects of radiation and convection on the air temperature (see section 4.3.1, point 3 of Chapter 4). The uncertainty of the IBT was calculated using uncertainty propagation law [95], as seen in the following equation.

$$u(IBT) = (1/n)\left[\sqrt{\sum_1^n (u_T)^2}\right] \quad \textbf{(6.2)}$$

Where u(IBT) is the uncertainty of the IBT in (K), and the u_T is the uncertainty of the individual sensor inside the booth (Top, Mid and Bot) (see Table 4.D-2 of Appendix 4.D). The u(IBT) was found to be ± 0.05K, and the uncertainty of GT was ± 0.09K (see Table 4.D-2 of Appendix 4.D).

On further analysis of the data, a consistent small variation of ± 0.6K was found amongst the IBT results. This was investigated and found to be a result of the circulation fan inside the booth causing air movement over the thermocouples.

The fan served as a low-velocity air movement mechanism to mix the air inside the booth and prevent thermal stratification. Thus, the moving average over every 150 seconds (30 intervals) was calculated and plotted, as shown in the following figure.

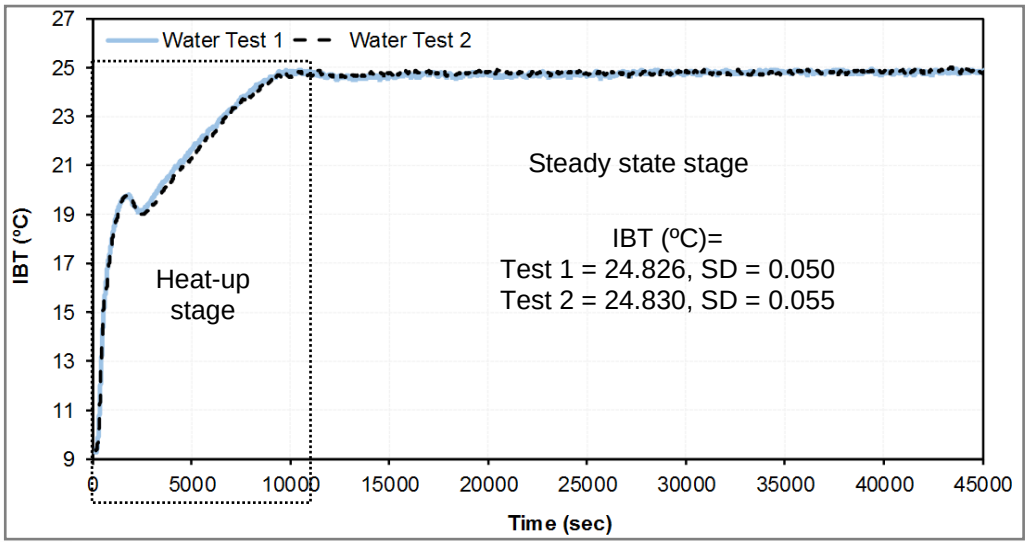

Figure 6.7 : IBT Variation with Steady State Water Tests

Figure 6.7 shows the evaluated IBT during the two water tests. The trends in IBT are similar, confirming experimental repeatability for the duration of the tests. The difference between the mean of the two sets of data is only 0.01K. Once the booth had reached steady state conditions, the differences between the mean and standard deviation for both tests were only 0.004K and 0.01K, respectively. The power and accumulated energy consumption were monitored and recorded for the whole duration of each test using a Yokogawa WT500 power meter with an accuracy of ±0.1%. The measured energy included the total energy consumed by the immersion heater and the pump. Figure 6.8 presents the recorded power and accumulated energy for the duration of the water tests.

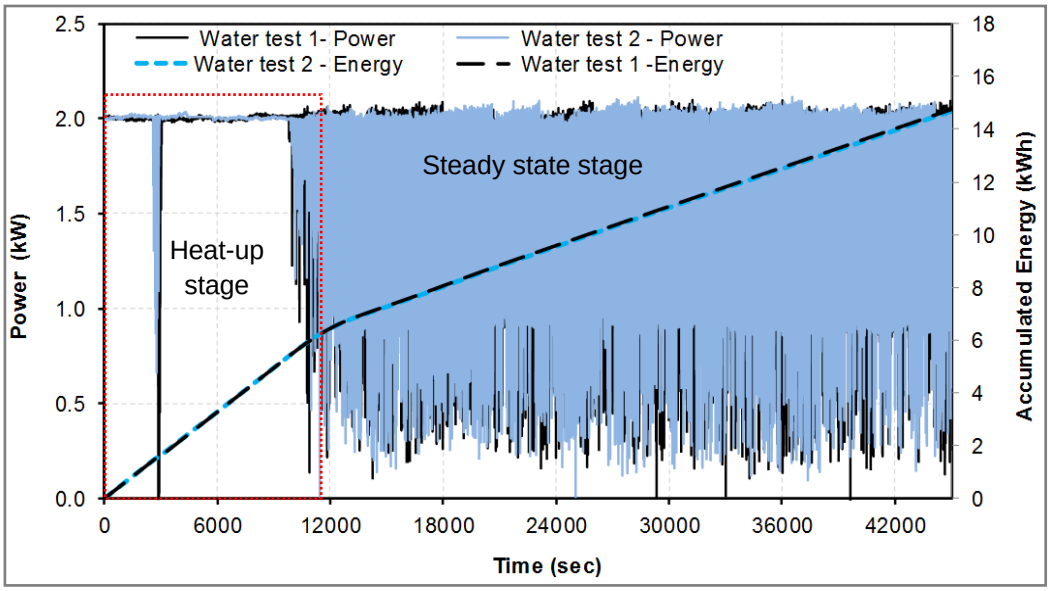

Figure 6.8: Power and Energy Consumption for Steady State Water Tests

The accumulated energy consumption is the total energy used by the system for the duration of the measurement period. This will be compared with the energy consumption recorded during the AHTF tests. During the heat-up stage, the power demand of the system was shown to be constant at approximately 2 kW. This is likely to be due to the demand required to heat the bulk of fluid in the buffer tank, as well as the booth itself. However, once the system had reached a steady state, the power demand ranged between 0.1 and 2 kW. This variation is due to the PID controller modulating the power between the heat required to maintain the IBT and the heat required to overcome the transport losses of the system. As Figure 6.8 shows, the increase in accumulated energy slowed down after the heat-up stage, indicating lower energy consumption once the system had reached a steady state.

In order to set a base energy consumption rate for comparison with the AHTF tests, the average hourly energy consumption ($\mathrm{Avg.hE}$) during each stage was calculated. To determine this, the rise in accumulated energy consumption over time was divided into two stages:

1. Heat-up (Stage 1): energy consumed whilst heating water inside the buffer tank and the booth
2. Steady state (Stage 2): energy consumed when the system reached stability

The $\mathrm{Avg.hE}$ (kWh/h) for each stage was calculated using the following equations.

$$Avg.hE_{\ Stage\ 1} = (E_1/(t_1) \quad \textbf{(6.3)}$$

$$Avg.hE_{\ Stage\ 2} = (E_{total} - E_1)/(t_{total} - t_1) \quad \textbf{(6.4)}$$

Here, $\mathrm{E_1}$ and $\mathrm{t_1}$ are the total accumulated energy consumption during Stage 1 and the total duration of Stage 1 respectively, and $\mathrm{E_{total}}$ and $\mathrm{t_{total}}$ are the total accumulated energy consumption over the entire test and the total duration of the test, respectively. The average amount of energy consumed during each stage is represented in Figure 6.9.

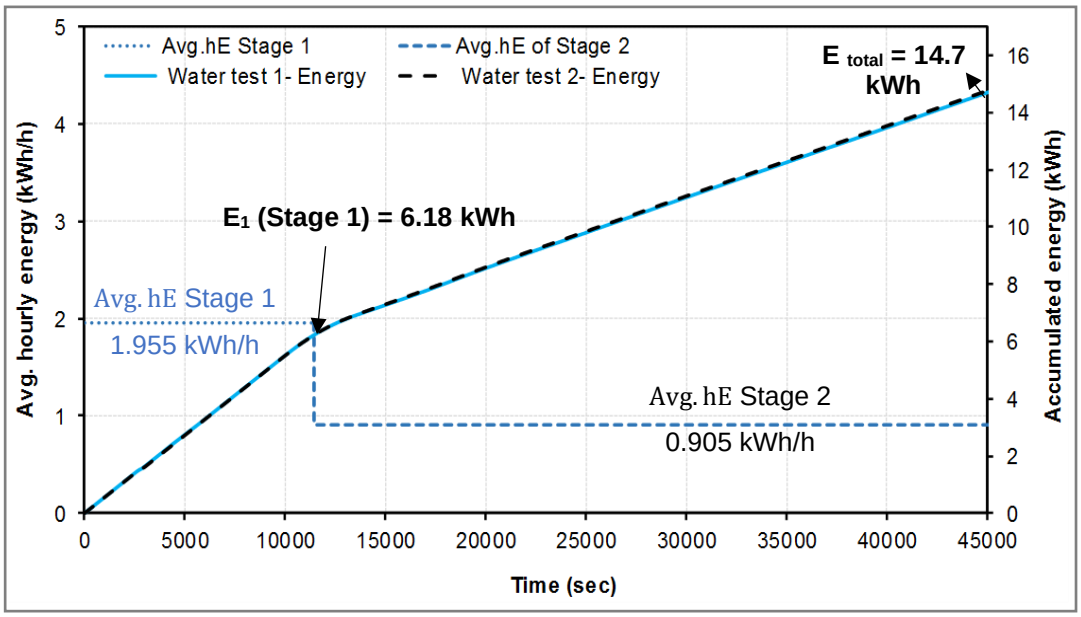

Figure 6.9: Energy and $Avg.hE$ Results for Steady State Water Tests

Figure 6.9 shows the energy consumption recorded with the steady state water tests and the calculated $\mathrm{Avg.\,hE}$. These results represent all the energy consumed by the system, including the energy consumed by the immersion heater and the pump. During stage 1, the $\mathrm{Avg.\,hE}$ was found to be higher than stage 2 by 53.9%. This is due to the high heat required by the bulk fluid to reach the steady state stage. All results are presented in figures (6.2,6.3, 6.6,6.7 and 6.8) show a high degree of consistency between the two steady state tests performed with water as a base case, reflecting the accuracy of the tests and procedure.

6.3.2 Thermostat Test Results

As with the steady state tests, the thermostat tests conducted with water as a heat transfer fluid were repeated twice to ensure reliability and accuracy of results. The tests were conducted using the same test facility and setup (booth and radiator) as the steady state tests. The test parameters (mass flow rate and flow temperature) were constant throughout the tests. However, in these tests, the flow of hot water between the tank and the radiator was controlled by the booth thermostat, which produced an ‘on’ signal when heating was

required and an 'off' signal when the IBT reached the setpoint. The thermostat setpoint was fixed at 22ºC with a 2K differential. This IBT was chosen to be within a range that would replicate a comfortable condition (see section 4.7.2.2 of Chapter 4). The FT, RT and flow rates (FR) recorded with the two tests are illustrated in Figure 6.10.

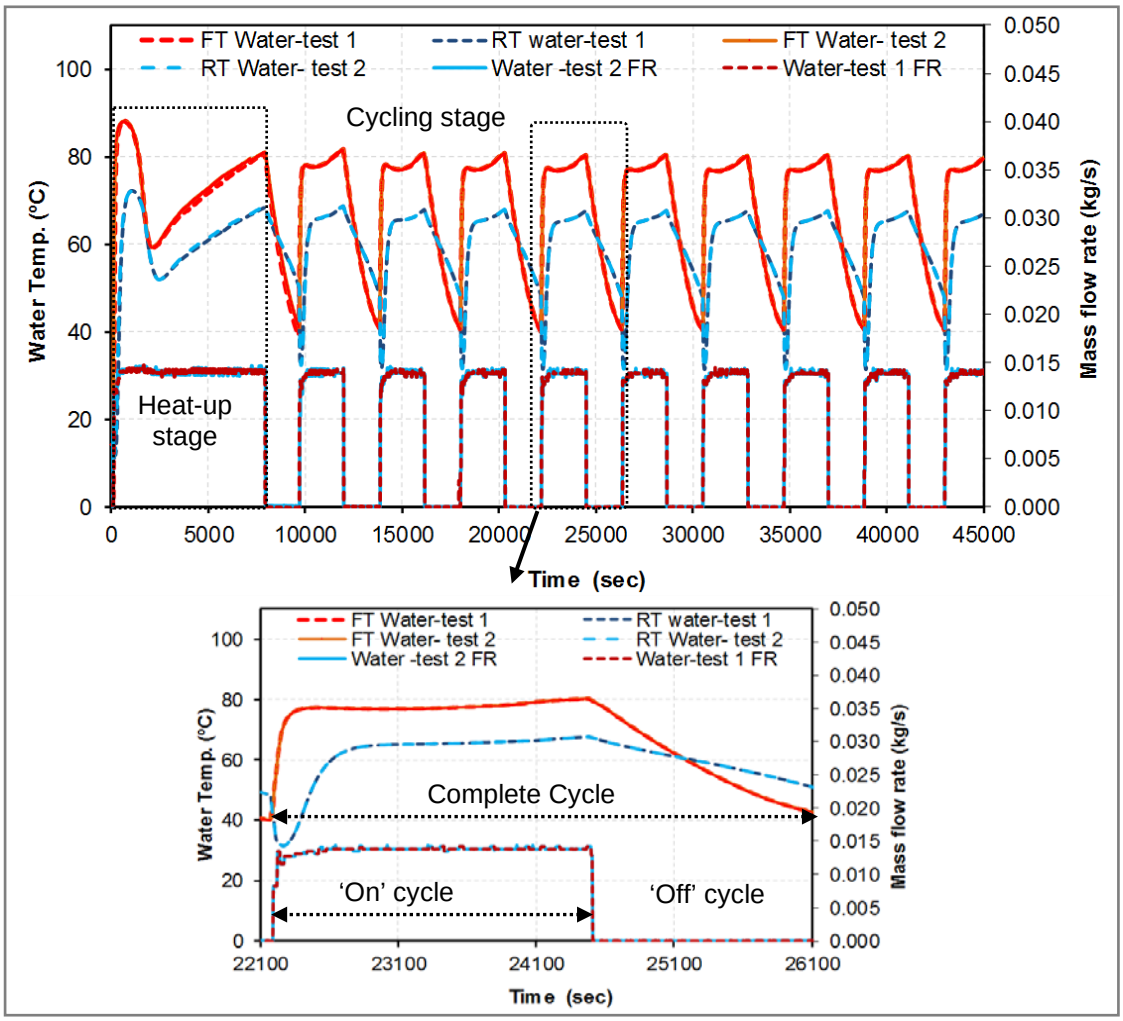

Figure 6.10: Flow Rate, Flow and Return Temperatures for Thermostat Water Tests

Figure 6.10 shows the two stages of the tests: the heat-up stage, which was 8,100 seconds long (2 hours and 15 minutes), and the 'cycling' stage. The flow throughout the system cycled 'on' and 'off' during the cycling stage, based on the heat of the booth, which was controlling the thermostat signal. Each 'on' cycle was 2,304 seconds long (38.4 minutes), and each 'off' cycle was 1,872 seconds long (31.2 minutes), meaning that the complete cycle took 4,176 seconds (1 hour and 9.6 minutes). The IBT, GT and ECT for the thermostat tests were monitored and recorded for the whole duration of the test and

graphically presented in Figure 6.11.

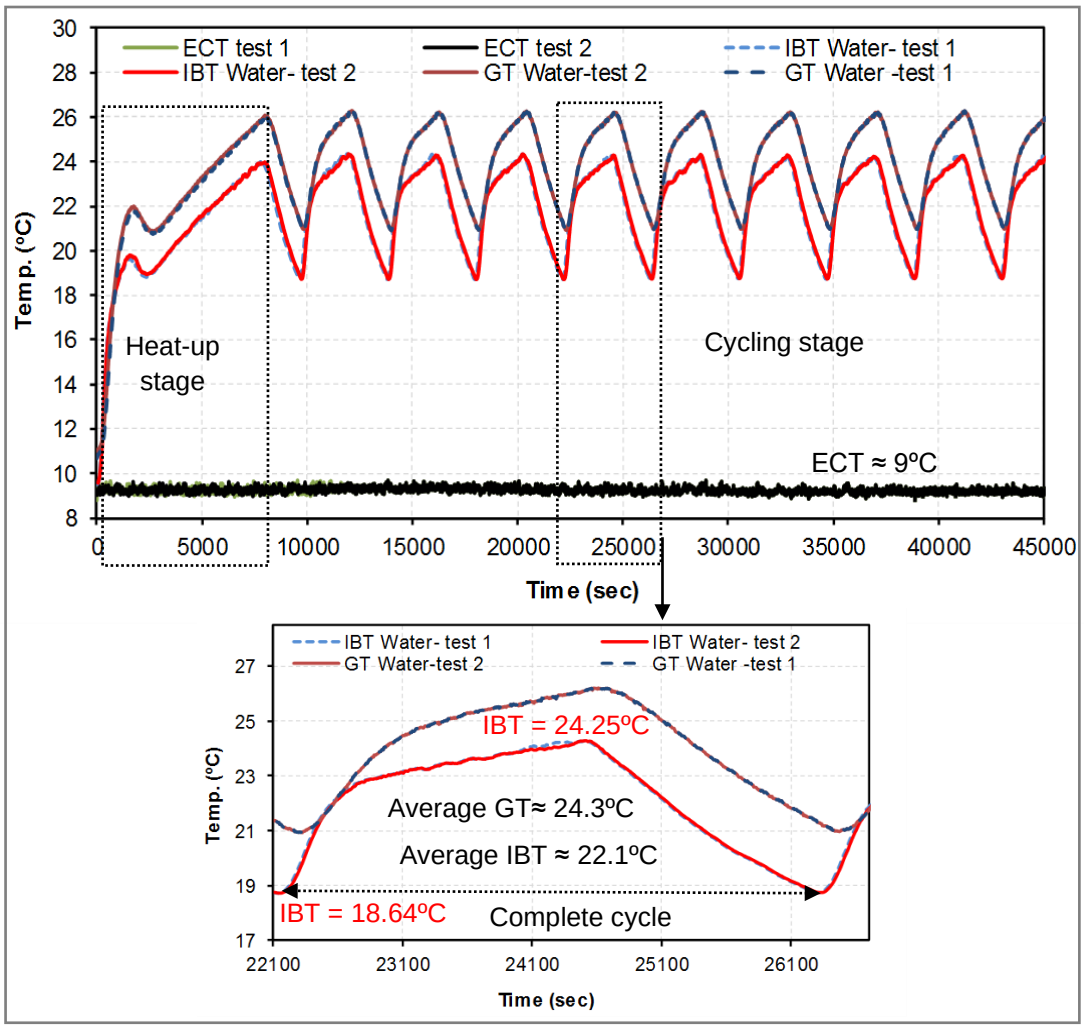

Figure 6.11: IBT, GT and ECT for Thermostat Water Tests

Figure 6.11 shows that the IBT during each heating cycle ranged between approximately 19ºC and 24ºC, giving an average IBT of 22.1ºC for a complete cycle. The GT ranged between 21ºC and 26ºC, giving an average of 24.4ºC for the whole cycle. The GT is likely to be higher than the IBT by 2.3K due to the effects of radiation on the globe bulb thermocouple. The system's 'on' cycle was used to obtain a new parameter denoted here as the duty cycle parameter (DC in %). The duty cycle parameter was calculated based on the ratio of the heating 'on' cycle to the entire cycle, as shown in equation 6.5.

$$DC\ (\%) = (('On'\ cycle\ time)/(Complete\ cycle\ time)) * 100 \qquad \textbf{(6.5)}$$

Duty cycle is expressed in percentage, 100% being fully 'on' while the low duty cycle

corresponds to the power being 'off' for most of the time. During the thermostat water tests, the duty cycle was calculated as 55.2%. This means that the HRHS needed to stay 'on' for 55.2% of each cycle to maintain the required IBT. The power (kW) and accumulated energy (kWh) readings taken throughout the tests are presented in Figure 6.1 2.

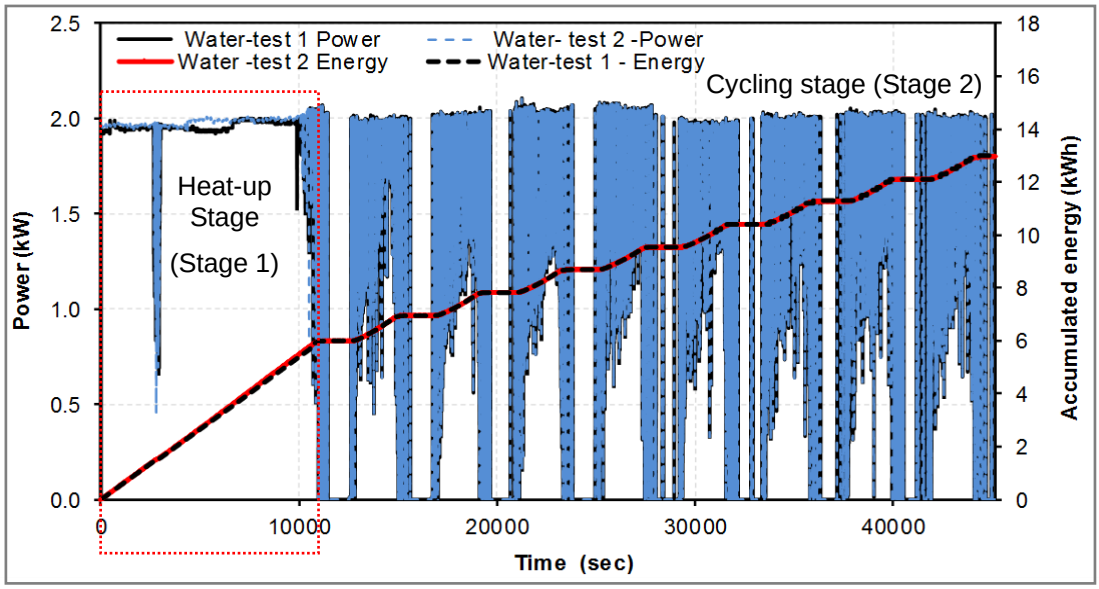

Figure 6.12: Power and Accumulated Energy Consumption for Thermostat Water Tests

The $\mathrm{Avg.hE}$ (kWh/h) during both the heat-up stage (Stage1) and the cycling stage (Stage 2) was calculated using equations 6.3 and 6.4, and the results are shown in Figure 6.13.

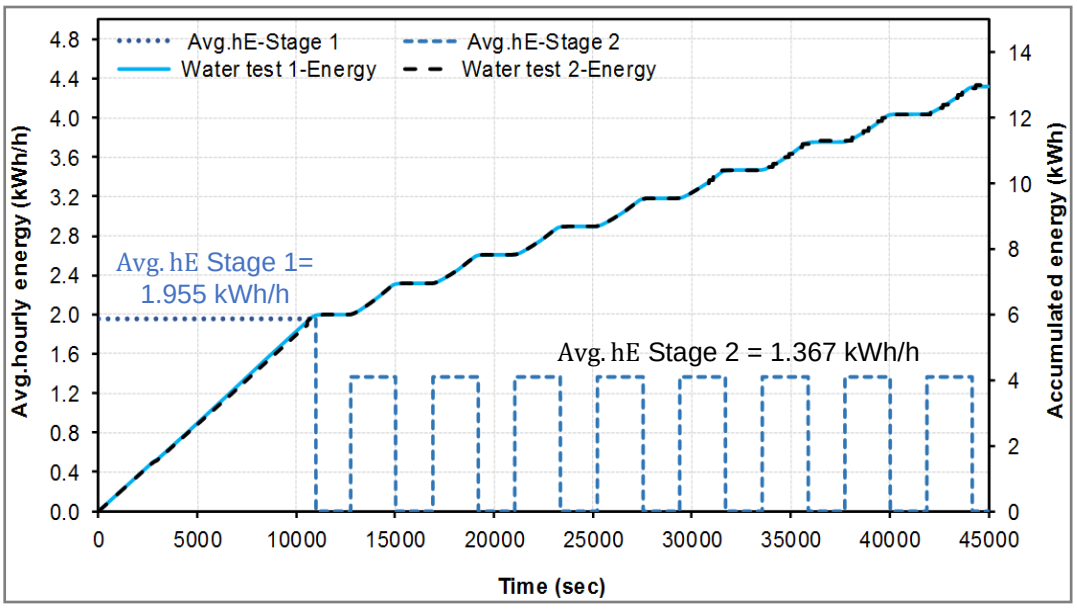

Figure 6.13 : Accumulated Energy and $Avg.hE$ for Water Thermostat Tests

Figure 6.13 reveals that the $\mathrm{Avg.hE}$ during the 'on' period of the cycle stage (Stage2) was

lower than the $\mathrm{Avg.hE}$ during the heat-up stage (Stage1) by 33.4%. This is in-line with expectations as Stage 1 accounts for the heating up of both the fluid and the booth in order to reach steady state conditions. A summary of the base case results for both the steady state and thermostat tests, including measurement uncertainty (u_T), is shown in the following table.

Table 6.1: Summary of Water Test Results- Steady State and Thermostat Tests

Test setting: Mass flow rate =0.01404(kg/s) ± 2% and ΔT across the radiator at steady state =10.24K (± 0.13K)			
Parameters	Steady state tests	Thermostat tests	± (u_T)
FT (ºC)	75.04	78.00	0.10 K
RT (ºC)	64.80	67.00	0.08 K
IBT (ºC)	24.83	22.09	0.05 K
Globe T (ºC)	26.93	24.39	0.09 K
'On' cycle duration (s)	45000	29759	/
'Off' cycle duration (s)	/	15241	/
DC (%)	100	55.2	/
Stage1 energy (kWh)	6.18	5.97	0.1%
Stage 2 energy (kWh)	8.51	8.98	0.1 %

The figures in Table 6.1 form the base case results which will be used for comparison with the AHTFs tests (50% HX/W, 50% EG/W and 30% EG/W mixtures).

6.4 Alternative Heat Transfer Fluid (AHTF) Experiments

Following the completion of the tests using potable water, the HRHS test rig was fully cleaned before beginning the tests using alternative fluids. The monitoring system was also checked to ensure that it was working correctly before experiments were conducted. This meant that all of the temperature sensors and instruments were recorded accurately. Each AHTF was separately tested in two different scenarios as follows:

1. Drop-in tests followed by optimised tests both using 50% EG/W as a heat transfer fluid
2. Drop-in tests followed by optimised tests both using 30% EG/W as a heat transfer fluid
3. Drop-in tests followed by optimised tests both using 50% HX/W as a heat transfer fluid

The following sections present the results obtained from each of the test scenarios.

6.4.1 Drop-In Scenario Test Results

As discussed in Chapter 4 (see section 4.7.3.1), the drop-in scenario is designed to replicate a situation where the alternative fluids are charged into the heating system without changing any of the system settings. The test rig valves, pump and PID settings remained the same as in the base case tests; then the alternative test fluids were dropped in as a replacement for water in the system. As presented in Appendix 6.A, the flow rate was monitored through the rotameter, which was calibrated before and after each test using the labelled standard cylinder and stopwatch (as explained in section 4.4.2 of Chapter 4). The measured flow rate data was converted to the mass flow rate by considering the densities of each fluid. Figure 6.14 illustrates the flow rate results.

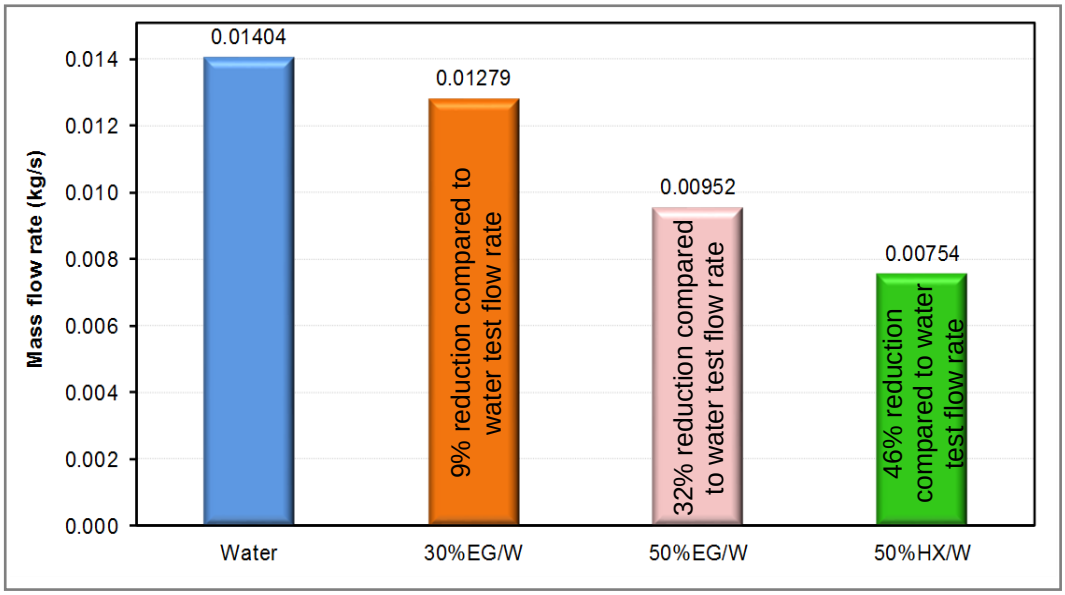

Figure 6.14 : Mass Flow Rates of Tested Fluids in Drop-in Scenario

Figure 6.14 shows that this test scenario resulted in lower flow rates within the system when using the 50% HX/W and 50% EG/W mixtures, in comparison to the base case. The 30% EG/W test also produced a slightly lower flow rate than the water test. The lower flow rate can be attributed to the higher viscosity and density of the alternative fluids. Based on the reduction in flow rate, it is important to understand its resultant effect on the IBT and energy consumption. Thus, the IBT and energy for each test were recorded and compared with the results of the water tests as presented in Figure 6.15 and Figure 6.16.

,

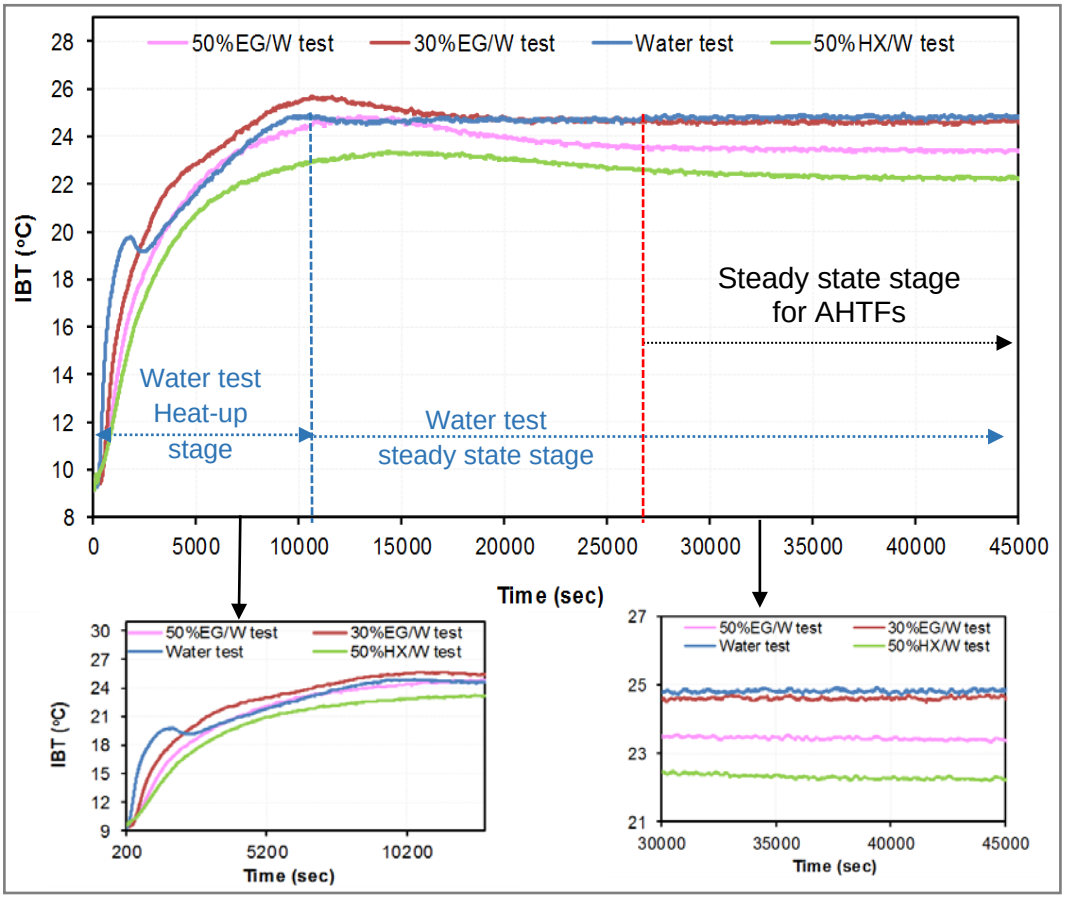

Figure 6.15: IBT for Drop-in Scenario Tests

Figure 6.15 shows the variation in IBT throughout the tests and demonstrates that each fluid had a different effect on the temperature. Notably, the IBT reached a stable point faster when water was used, while the booth's temperature remained unstable when using the AHTFs. The IBT obtained at a steady state condition was lower when using the 30% EG/W, 50% EG/W and 50% HX/W mixtures by around 0.2K, 1.4K and 2.3K respectively.

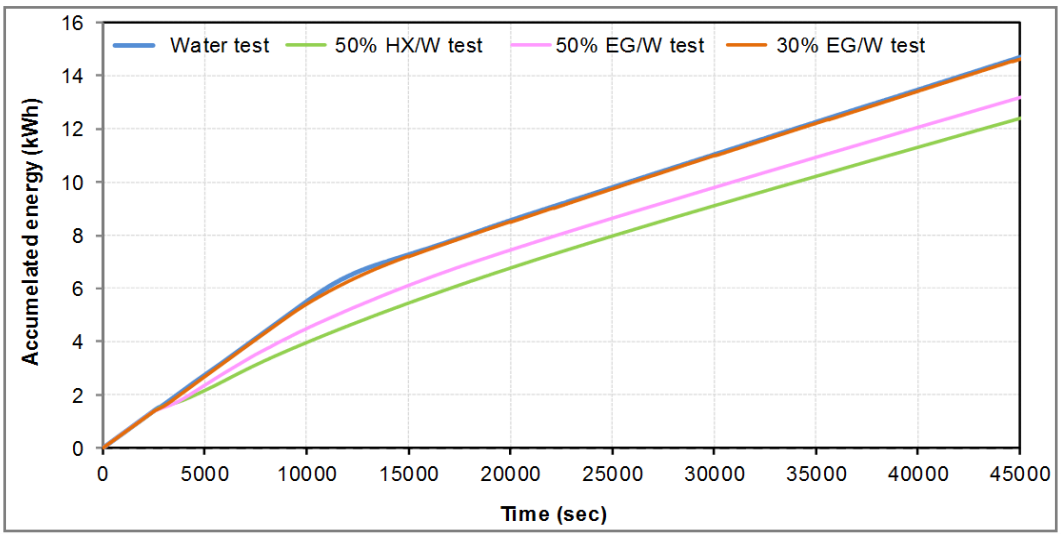

Figure 6.16: Energy Consumption for Drop-in Scenario Tests

Figure 6.16 presents the variation in total energy consumed by the system during each test. As the above figure illustrates, the accumulated energy consumption during the water tests and the test using the 30% EG/W mixture were higher than the total energy consumed when using the 50% EG/W and 50% HX/W mixtures; the smallest amount of energy consumed was recorded during the 50% HX/W test.

Figure 6.17 shows the final IBT and related energy consumption recorded with the drop-in scenario tests for all examined fluids, taking into account varying levels of uncertainty in measurements.

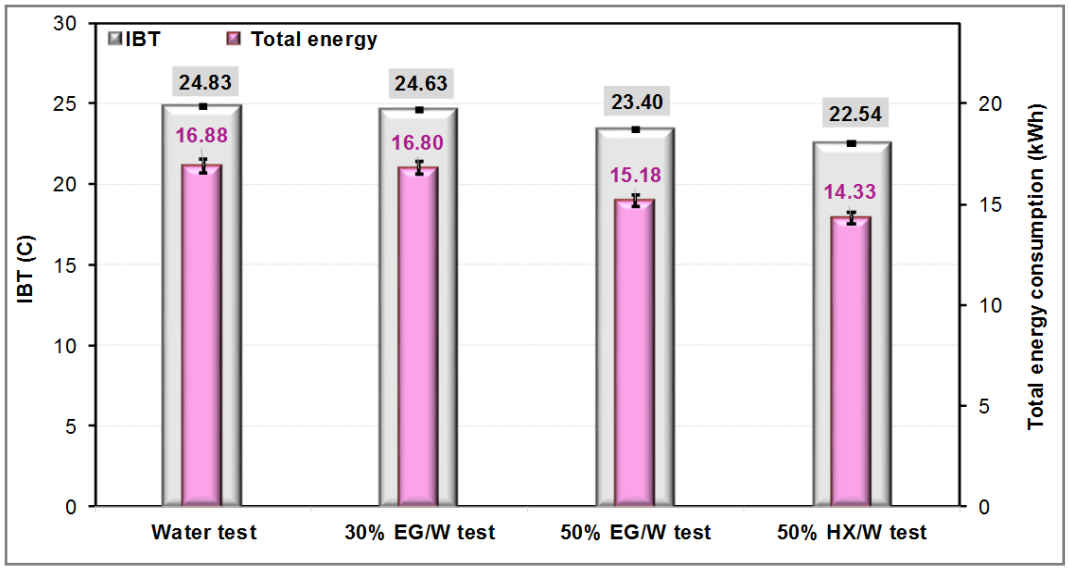

Figure 6.17: Total Energy Consumption and IBT for Drop-in Scenario Tests

Figure 6.17 indicates that the total amount of energy consumed by the system was highest for the water tests (16.88 kWh) and reduced by 10% and 15% with the 50% EG/W and 50% HX/W tests respectively. Likewise, it is clear from Figure 6.17 that the IBT also varied across each of the tests; lower energy consumption resulted in a lower IBT.

The results from the 30% EG/W test are slightly lower than the water test as the reduction in flow rate calculated when using this mixture was only 9%, compared to the water flow rate of 0.01404 (kg/s).

In summary, the results of the drop-in scenario tests reveal that using denser alternative fluids as a straight replacement for water created a reduced flow rate through the system. This, in turn, causes a lower IBT and reduces the amount of energy consumed by the system. When using alternative fluids, the IBT never reached the reference temperature (24.83ºC) achieved when conducting the water tests. This is likely to be due to a lower flow rate as a result of using denser and more viscose fluids such as 50% EG/W and 50% HX/W mixtures, as well as the presence of the synthesise material of the 50% HX/W mixture (see Table 2.1 of Chapter 2). This material may have affected the flow of the 50% HX/W mixture through the system (compared to the base fluid of 50 % EG/W), under the same test rig setting of the water test.

6.4.2 Optimised Scenario Test Results

In the second scenario, the mass flow rate of the fluid passing through the system was adjusted when each AHTF was added, as per the following two cases.

Case 1: Adjust the mass flow rate through the system to be at the same level to the mass flow rate of the base case and maintain the flow temperature (FT) at the same FT of the base case.

Case 2: Adjust the temperature difference across the radiator (ΔT) to be at the same level to that for the base case (water test), (ΔT of 10K) and maintain the flow temperature (FT) at the same FT of the base case.

The following section presents the results obtained from the second test scenario, including both the steady state and thermostat tests.

6.4.2.1 Case 1 Steady State Test Results

In this case, the mass flow rate was set to (0.014 kg/s) (the same mass flow rate obtained with the water test) before each test. The mass flow rate, IBT, energy consumption, and flow and return fluid temperatures were monitored and recorded for the duration of each

test. Test results were collected and compared with the results obtained from the previous water tests. Figure 6.18 presents a comparison of the mass flow rates calculated when using different fluids in the system.

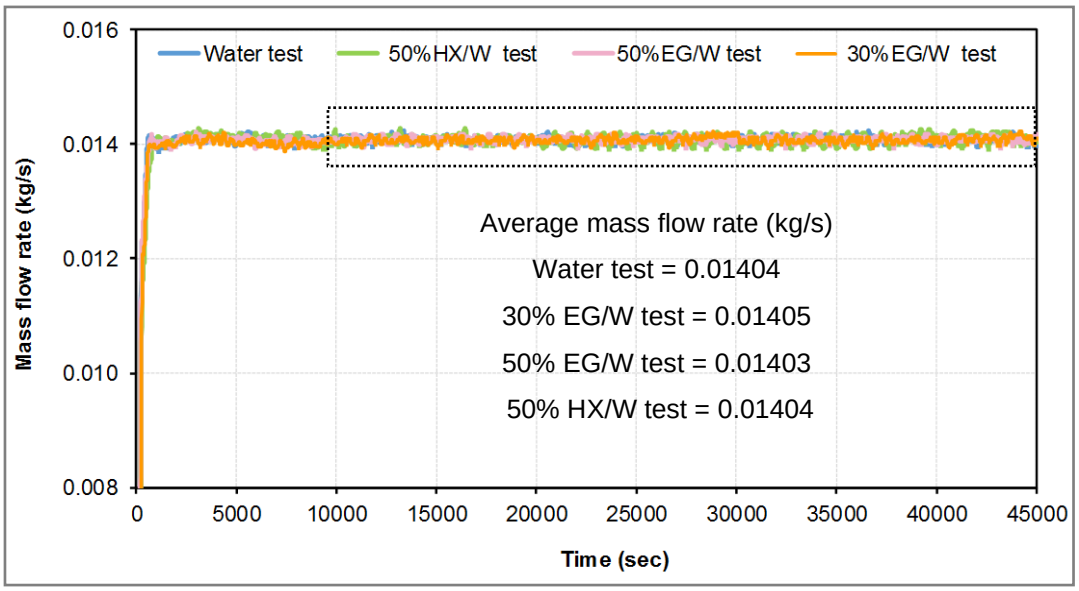

Figure 6.18: Mass Flow Rate Variation for Case 1 Steady State Tests

Figure 6.18 shows the mass flow rate calculated when using different fluids in the system. The mass flow rate calculated when using the AHTFs was very similar to the mass flow rate calculated for the water tests; 0.014 kg/s with a variation of approximately ±0.0002 kg/s.

To achieve similar mass flow rates with the AHTFs to that recorded with the base case, the volumetric flow rates for these fluids had to be lower by 6% and 7% for the 50% EG/W and 50% HX/W tests respectively. This is due to the higher density for these fluids compared to water (see Table 3.5 to 3.7 of Chapter 3). This means that the velocity in the system will also be lower than the base case by the same percentage, as the pipe diameter is fixed. In this particular case, it was important to observe the flow and return temperatures of the fluids. Figure 6.19 provides a comparison of the flow and return temperatures recorded for all tests.

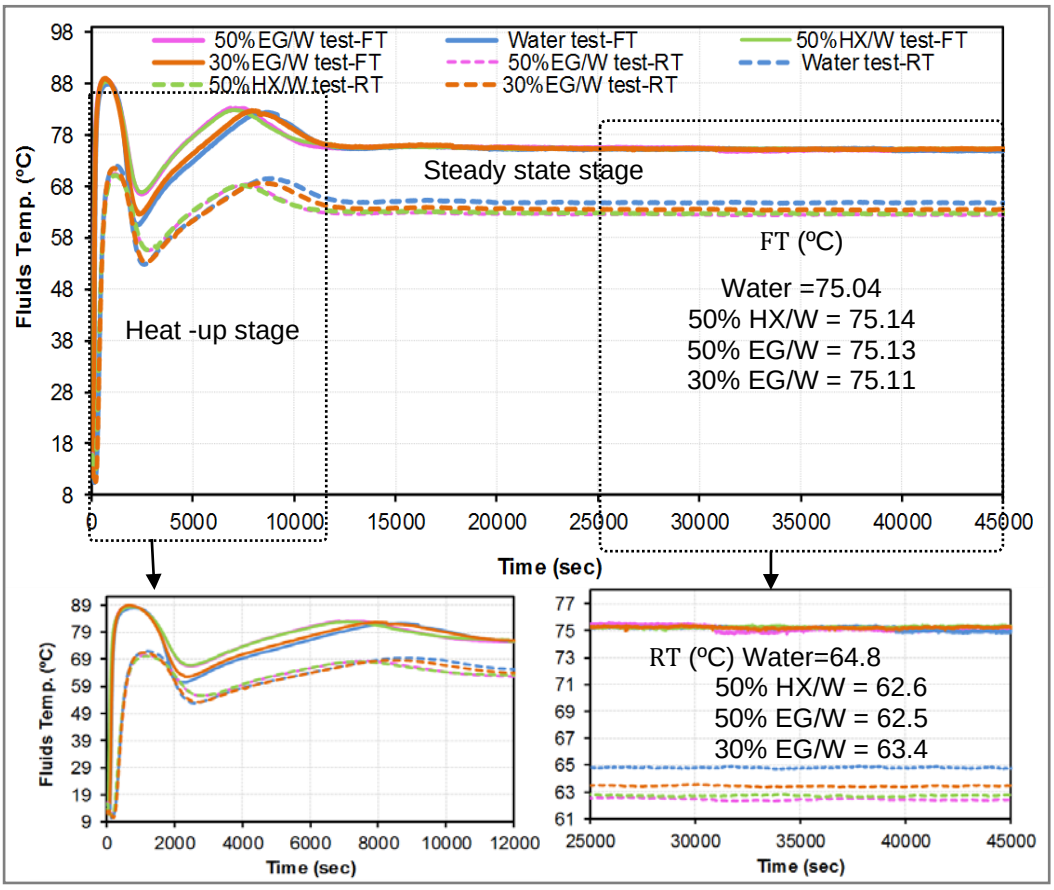

Figure 6.19: Flow and Return Temperatures Variation for Case 1 Steady State Tests

Figure 6.19 shows that the fluid flow and return temperatures fluctuated during the heat-up stage and took time to stabilise and reach the PID controller setpoint (75ºC). As the indoor temperature of the system was significantly lower than the temperature of the hot fluid at the beginning of the experiments, the fluid-cooled down quickly. As a result, it took a long time for the immersion heater to warm up the fluid until the temperature reached the PID controller setpoint. During the heat-up stage, the flow temperature of the 50% EG/W and 50% HX/W mixtures rose noticeably faster than water. The 30% EG/W mixture rose in temperature at a slower rate than the 50% EG/W and 50% HX/W mixtures, but slightly faster than water, indicating that the specific heat capacity (C_p) of each examined fluid had an effect on how quickly their temperature increased. As the 50% EG/W, 50% HX/W and 30% EG/W mixtures have a lower C_p than water (see Tables 3.5 - 3.8 of Chapter 3), they require less heat in order for their temperature to change. During the steady state

stage, the flow temperature of all fluids was very similar to the flow temperature recorded with the base case: 75.04ºC with a variation of ± 0.15K to ± 0.07K. However, the return temperatures recorded for the AHTF tests were lower than that recorded with the water test (64.8 ºC) by 1.4K (30% EG/W), 2.2K (50% HX/W) and 2.3K (50% EG/W), respectively. Having a lower return temperature in real application means heat loss can be reduced from the return pipes [96].

The ΔT values recorded across the radiator with the AHTFs tests were 11.71K, 12.54K, and 12.62K for the 30% EG/W, 50% HX/W and 50% EG/W tests, respectively. The increase in ΔT across the radiator with the AHTF tests can be a result of the fluids' lower heat capacity to maintain heat released from the radiator. The fluctuation in IBT and GT for all tests was also monitored and evaluated. The results are presented in Figure 6.20.

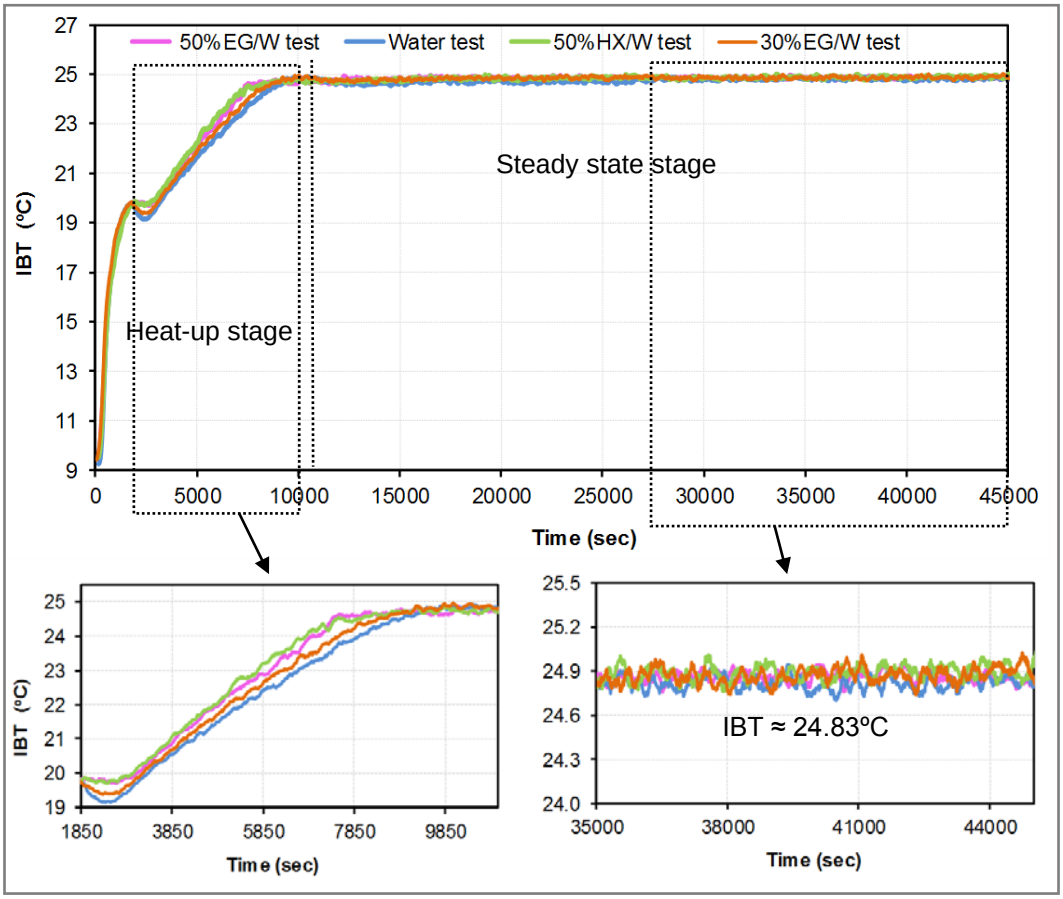

Figure 6.20: IBT Variation for Case 1 Steady State Tests

As Figure 6.20 shows, the IBT increased at a quicker rate during the 50% HX/W and 50% EG/W tests, compared with the water and 30% EG/W tests. The IBT trend lines illustrate that steady state conditions were reached approximately 1,200 seconds (20 minutes) quicker when using the HX/W and 50% EG/W mixtures, in comparison to water. The variation in IBT increase during the heat-up stage reflects each fluid's flow temperature, as the flow temperatures of the 50% HX/W and 50% EG/W mixtures were higher than the water flow temperature (see Figure 6.19). During the steady state stage, the IBT during the AHTF tests was similar to the IBT reached during the water test, with a variation of approximately 0.05K. The GT during all tests was recorded and the results are presented in Figure 6.21.

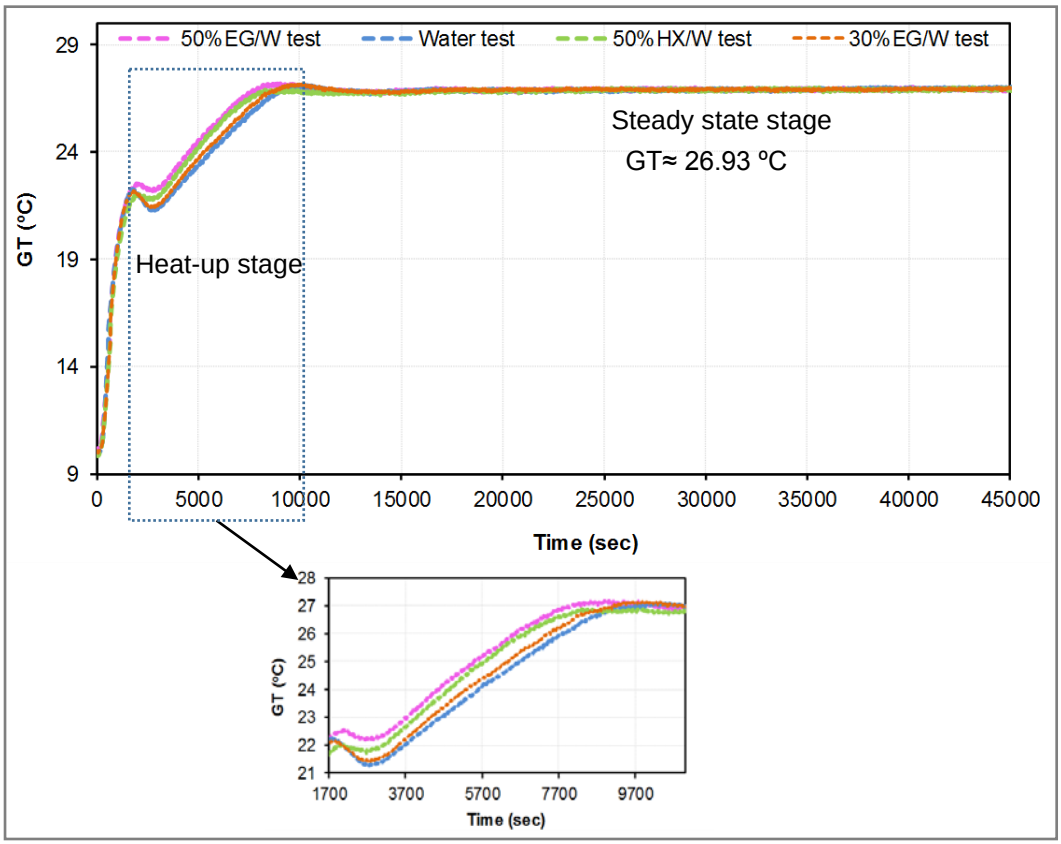

Figure 6.21: GT for Case 1 Steady State Tests

The rising trend in GT seen in Figure 6.21 is similar to the rise in IBT, recording higher values (approximately 2.1K) as a result of the radiation effect occurring during both the heat-up and steady state stages of the experiment. Energy consumption was also recorded for whole the duration of the tests and is presented in Figure 6.22.

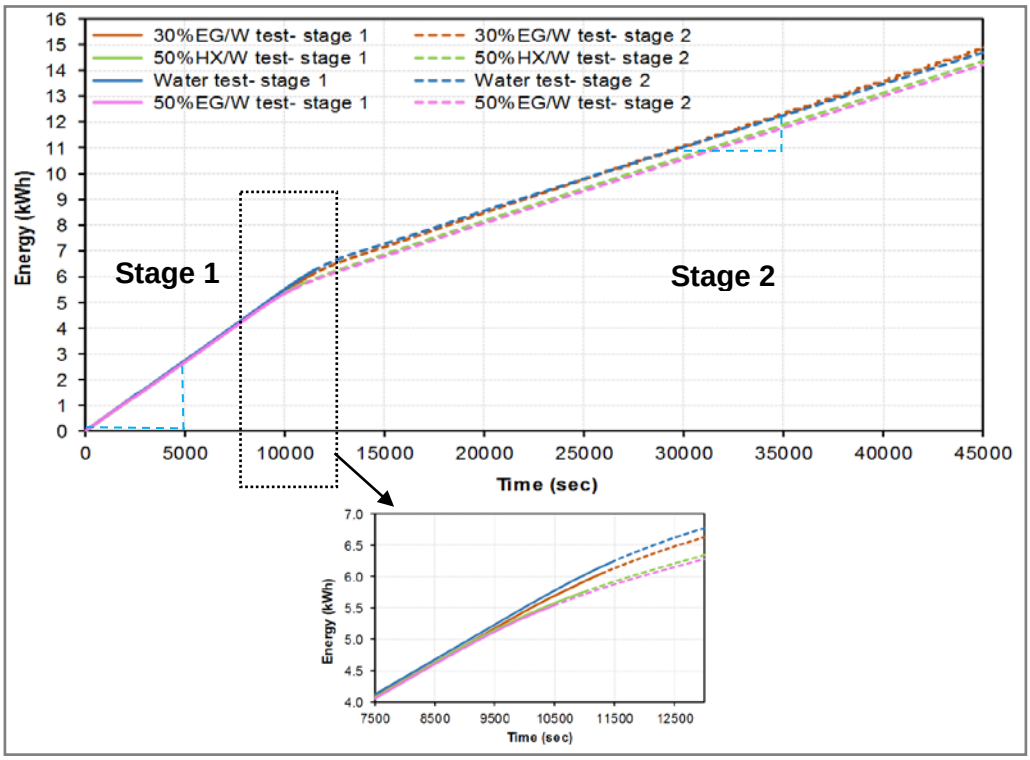

Figure 6.22 : Accumulated Energy Consumption for Case 1 Steady State Tests

Figure 6.22 shows the energy consumption over time, with the gradient of the line reflecting the Avg. hE (kWh/h) consumed by the system during each stage of the AHTF tests. The gradient of the energy line during Stage 1 seems to be higher than in stage 2, which means that the system consumed more energy during the heat-up stage. To visualise the gradient of the energy line throughout both stages, the Avg. hE was calculated using equations 6.3 and 6.4. Figure 6.23 presents the Avg. hE of all tests.

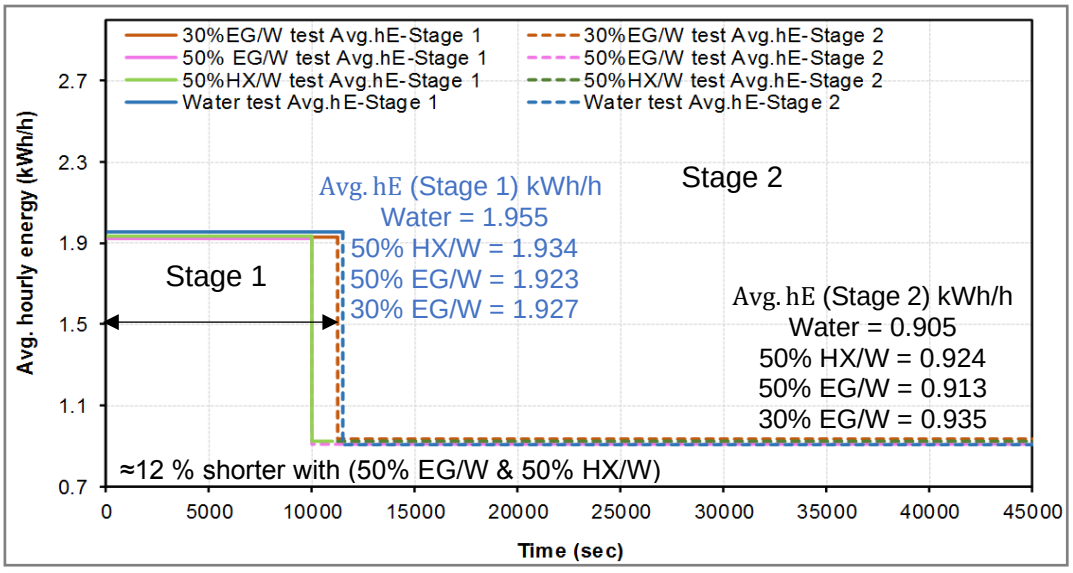

Figure 6.23: Average Hourly Energy for Case 1 Steady State Tests

The above figure indicates that the Avg. hE was higher during Stage 1 than in Stage 2 for all tested fluids. This confirms that the immersion heater operated at full power (with a small amount of variation between fluids) during Stage 1, while in Stage 2, it consumed less energy depending on the demand of the system to maintain a steady temperature. It is also clear that the energy required by the system to reach steady state conditions (stage 2) differs for each fluid used. A shorter Stage 1 period means that the heating system reached stability faster. For example, during the 50% HX/W and 50% EG/W tests, the time it took for the system to reach stage 2 was 12% quicker than when using water. Reaching the desired temperature in a shorter timeframe allowed the system to switch off and therefore reduce its energy consumption. To analyse the comparison between the rise in IBT and accumulated energy consumption during the tests, these have been plotted against each other in Figure 6.24.

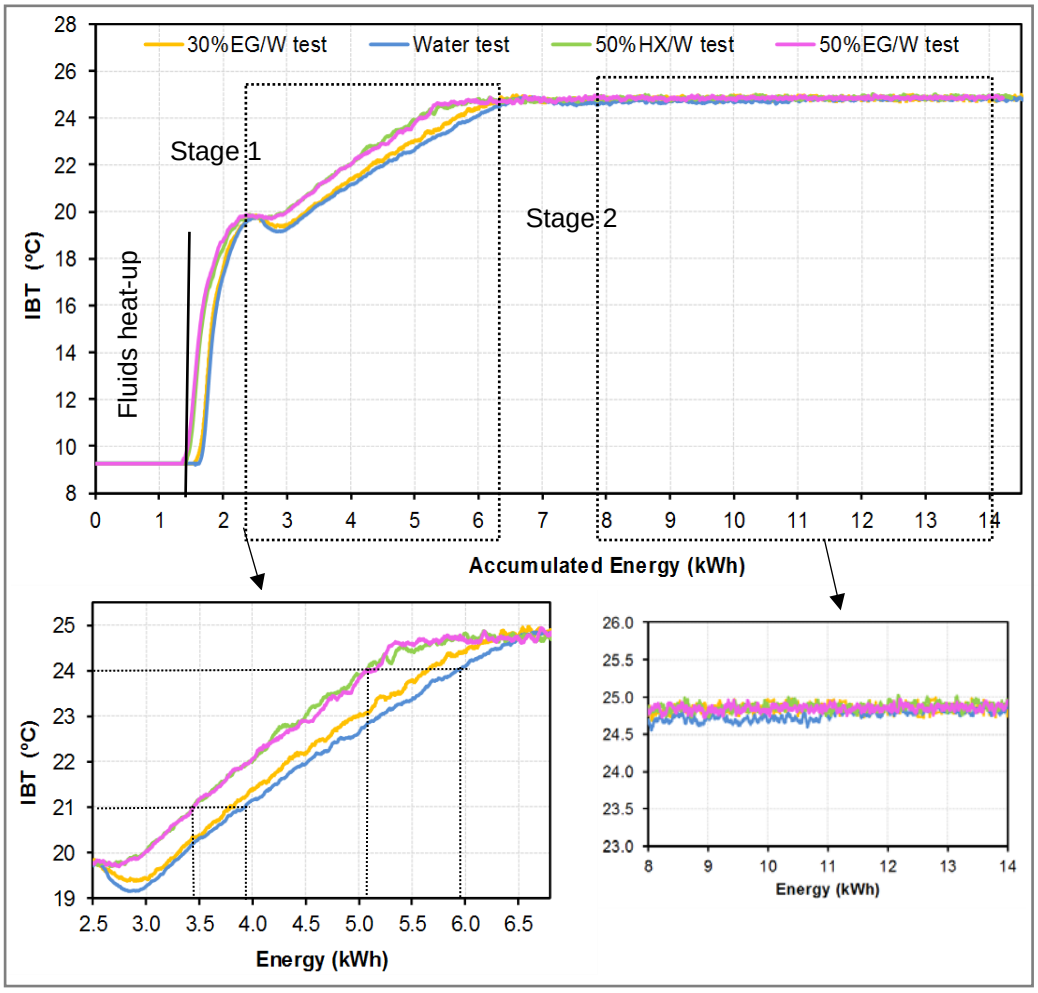

Figure 6.24: IBT Versus Energy Consumption for Case 1 Steady State Tests

As figure 6.24 shows, the same IBT was achieved by using less energy during the 50% HX/W and 50% EG/W tests, in comparison with the base case test. Contrastingly, the results of the 30% EG/W test are very similar to those recorded during the water test. To evaluate the energy saved during Stage 1 across all tests, the energy consumption data was analysed against the IBT readings. The results are shown in Table 6.2; the percentage of energy saved ($ES\ \%$) in comparison with the energy consumed with the water test was calculated using the following equation.

$$ES\ \% = (Energy\ of\ water\ test - Energy\ of\ AHTF\ test)/Energy\ of\ water\ test) \quad \textbf{(6.6)}$$

Table 6.2: IBT Versus Energy for Stage 1 of Case 1 Steady State Tests

IBT ºC	Water test	30% EG/W test		50% HX/W test		50% EG/W test	
	Energy kWh	Energy kWh	ES %	Energy kWh	Saving %	Energy kWh	$ES\ \%$
21	3.93	3.82	3	3.44	12	3.44	12
22	4.52	4.36	4	3.98	12	3.98	12
23	5.21	5.03	3	4.58	12	4.59	12
24	5.93	5.67	4	5.06	15	5.06	15
24.83	6.61	6.61	0	6.15	7	6.15	7
Average saving %			2.8		12		12

As shown in Table 6.2, the percentage of energy saved during the heat-up stage was approximately 12% for the 50% HX/W and 50% EG/W tests, in comparison with the base case tests. However, the percentage of energy saved when using the 30% EG/W mixture was minor. These results reveal that the system required less energy to reach the same IBT when using the 50% HX/W and 50% EG/W mixtures. In order to monitor the influence of different fluids on the temperature of the radiator surface, four thermocouples were attached to the radiator in different positions (Rad Temp R, Mid Rad T, Low Rad T and Rad Temp F), as presented in Table 4.2 of Chapter 4), in order to record the temperatures. The thermocouple readings were then used to calculate the average radiator surface temperature ($\mathrm{Avg.\,R.\,S.\,T}$), as demonstrated by equation 6.7.

$$Avg.R.S.T = (\sum_1^n T)/n \quad \textbf{(6.7)}$$

Where T and n are the thermocouples readings and number of the thermocouples,

Figure 6.25 presents the average radiator surface temperature for all tests.

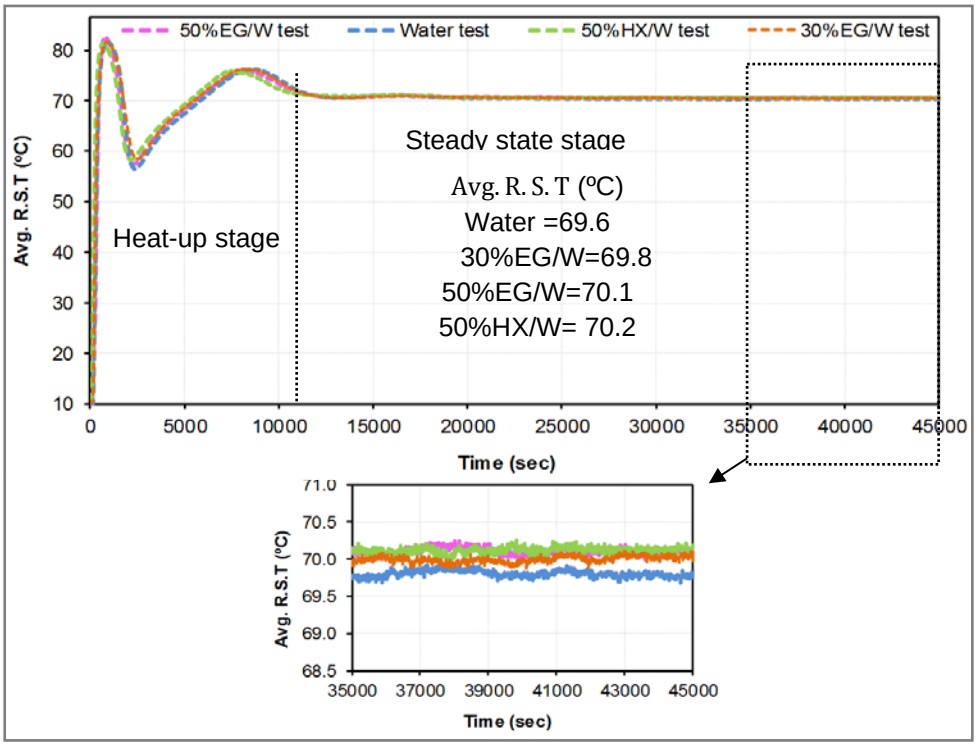

Figure 6.25: Average Radiator Surface Temperature for Case 1 Steady State Tests

As Figure 6.25 shows, that the $\mathrm{Avg.\,R.\,S.\,T}$ during the 50%HX/W and 50%EG/W tests was slightly higher than the $\mathrm{Avg.\,R.\,S.\,T}$ during the water test, while the results from the 30% EG/W test are very similar to the base case results. To further verify the results, the uncertainty of the readings from the four thermocouples were used to calculate the overall uncertainty of the average radiator surface temperature ($u_{\mathrm{Avg.R.S.T}}$) using equations 6.8:

$$u_{Avg.R.S\,T} = (1/n)\sqrt{\sum_1^n (u_T)^2} \qquad \textbf{(6.8)}$$

The u_T represents the uncertainty of an individual sensor that measured the radiator surface temperature (Rad Temp R, Mid Rad T, Low Rad T and Rad Temp F as in Table 4.D-2 of Appendix 4.D). The $u_{\mathrm{Avg.R.S\,T}}$ was calculated as ± 0.05 K. The difference in $\mathrm{Avg.\,R.\,S.\,T}$ between the 50% HX/W, 50% EG/W and the water tests was approximately 0.5K, which is higher than the average uncertainty calculated across all measurements. Additionally, the temperature distribution across the radiator surface was recorded at the end of each test, using the Fluke thermal imaging camera. The thermal images were then

analysed using SmartView software, using a temperature alarm setting for a temperature range of 65ºC to 75ºC (see Appendix 6.B). The thermal images showing the temperature distribution across the radiator surface for all tests are illustrated in Figure 6.26.

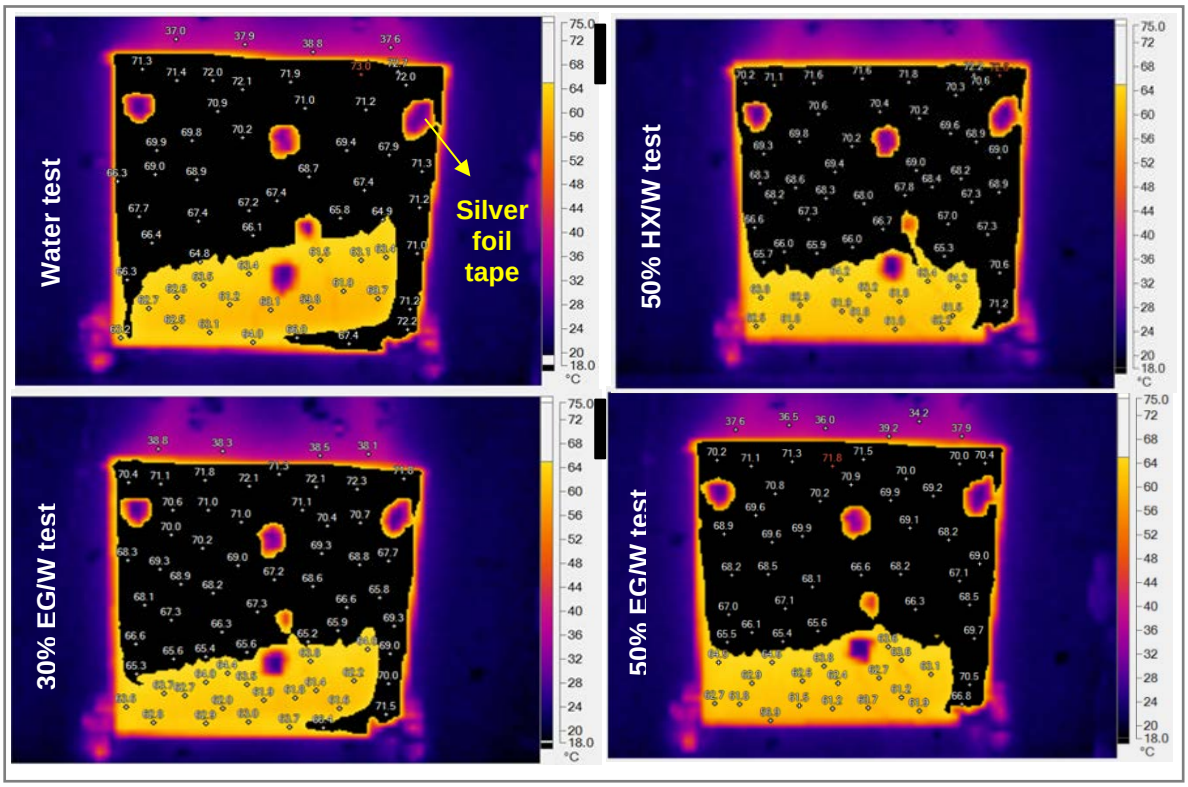

Figure 6.26: Temperature Distribution on the Radiator Surface for Case 1 Steady State Tests

In Figure 6.26, the black areas of the radiator surface represent the distribution of temperatures between 65ºC and 75ºC. The five spots made up of different colours indicate where the thermocouples were positioned on the radiator. The thermocouples were fixed to the radiator using silver aluminium foil tape, which causes the spots on the thermal images as the foil has low emissivity and it works as radiant heat barriers. Wider black areas (within a specified temperature range of 65ºC to 75ºC) can be seen on the images obtained with the AHTF tests. To estimate the percentage increase in radiator surface temperature during the AHTF tests, the black areas in the thermal images were evaluated using Autodesk design review software (see Appendix 6.C). This showed that the black area covered approximately 66% of the total surface area of the radiator (0.36 m^2) during the water test. However, approximately 71%, 70% and 67% of the total surface area of the

radiator appeared black during the 50% HX/W, 50% EG/W and 30% EG/W tests, respectively. When using the 30% EG/W mixture, the percentage of total surface area which appeared black was similar to the percentage shown during the water test. Therefore, the distribution of temperatures across the radiator surface which fell into the specified range between 65ºC and 75ºC was noticeably wider when using the 50% EG/W and 50% HX/W mixtures compared to water. The wider temperature distribution across the radiator surface can be attributed to the lower velocity in the system (by 6% and 7%) with the 50% EG/W and 50% HX/W tests. This increase the contact time between these fluids and the inner surfaces of the radiator. The data analysed in Case 1 shows that the 30% EG/W mixture and water behaved similarly as heat transfer fluids within the HRHS. Consequently, the results of the 30% EG/W test will not be considered for comparative analysis with water as a HTF.

6.4.2.2 Case 1 Thermostat Test Results

After completion of the steady state tests, thermostat tests (see section 4.7.2.2 of Chapter 4) were performed with all examined fluids. Figure 6.27 demonstrates that mass flow rates recorded during the 'on' heating duration; in this case, were similar for all tested fluids. For example, the flow rate was the same during the AHTFs tests and the water test.

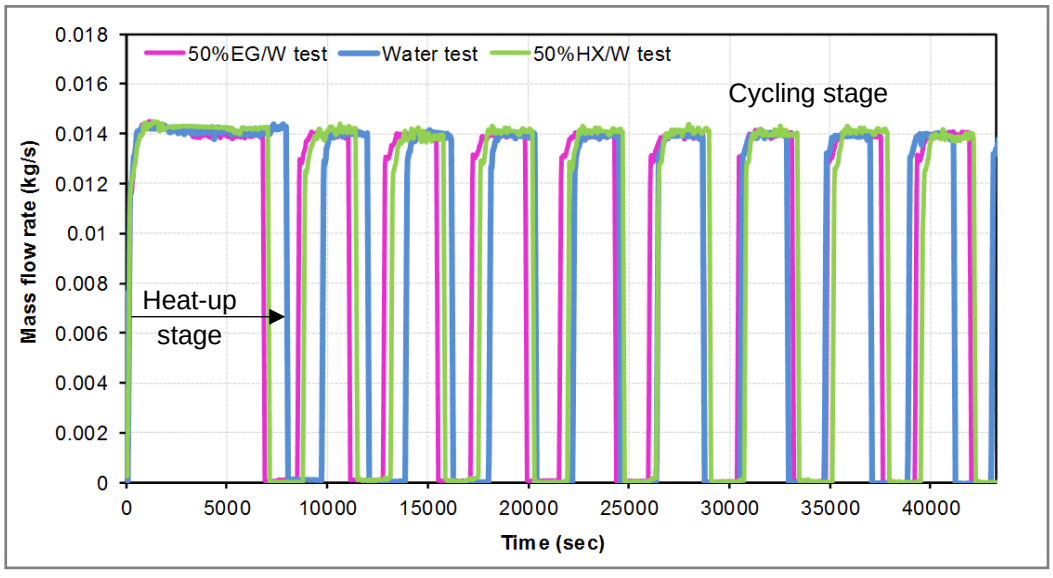

Figure 6.27 : Mass Flow Rate Variation for Case 1 Thermostat Tests

Figure 6.27 demonstrates the consistency of the flow rate throughout the heat-up and cycling stage of the tests. It also shows that the duration of the heat-up stage varied for each different fluid. The heat-up period was shorter when using the AHTFs, and as a result, the cycling 'on' and 'off' of the heat start earlier. The heat-up stage took 7,955 seconds (2 hours and 12 minutes) during the water test, 7,040 seconds (1.96 hours and 58 minutes) during the 50% HX/W test and 6,800 seconds (1 hour and 53 minutes) during the 50% EG/W test. This means that the heat-up stage when using the 50% HX/W and 50% EG/W mixtures, was shorter by about 12% and 15%, respectively. The variation in the starting times of the 'on' and 'off' cycles reduced with time, as the duration of each cycle changed. To assess the total periods of time that the heating cycled 'on' and 'off during each test, the flow rate data was analysed more closely, as shown in Figure 6.28.

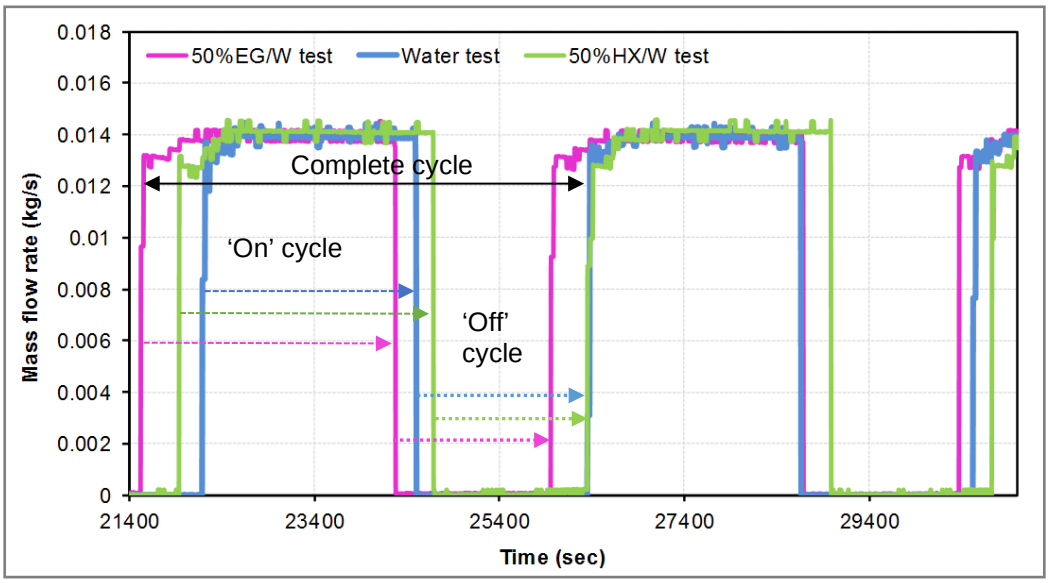

Figure 6.28 : 'On' and 'Off' Heating Cycle for Case 1 Thermostat Tests

Figure 6.28 illustrates that the lengths of each 'on' and 'off' cycle varied across the different tests. The duration of each 'on' and 'off' period for each test are outlined as follows:

Water Test

- Complete cycle duration:4,176 seconds (1 hour and 9.6 minutes)
- 'On' time: 2,304 seconds (38.4 minutes)
- 'Off' time: 1,872 seconds (31.2 minutes)

50% HX/W Test

- Complete cycle duration: 4,427 seconds (1 hour and 13.8 minutes)
- 'On' time: 2,700 seconds (45 minutes)
- 'Off' time: 1,728 seconds (28.8 minutes)

50% EG/W test

- Complete cycle duration: 4,428 seconds (1 hour and 13.8 minutes)
- 'On' time: 2,710 seconds (45.2 minutes)
- 'Off' time: 1,718 seconds (28.6 minutes)

The duty cycle (DC% - equation 6.5) calculated for each test was 61% for the 50% HX/W and 50% EG/W mixtures and 55.2% for water. This indicates that the system must be 'on' for a longer amount of time (during the cycling stage) when using the AHTFs. However, the heat-up stage was shorter by 915 seconds (15 minutes), when using the 50% HX/W mixture and by 1,155 seconds (19 minutes), when using the 50% EG/W mixture, or in other words, its duration was shorter by 12% and 15% respectively. The recorded flow and return temperatures for each test are presented in Figure 6.29.

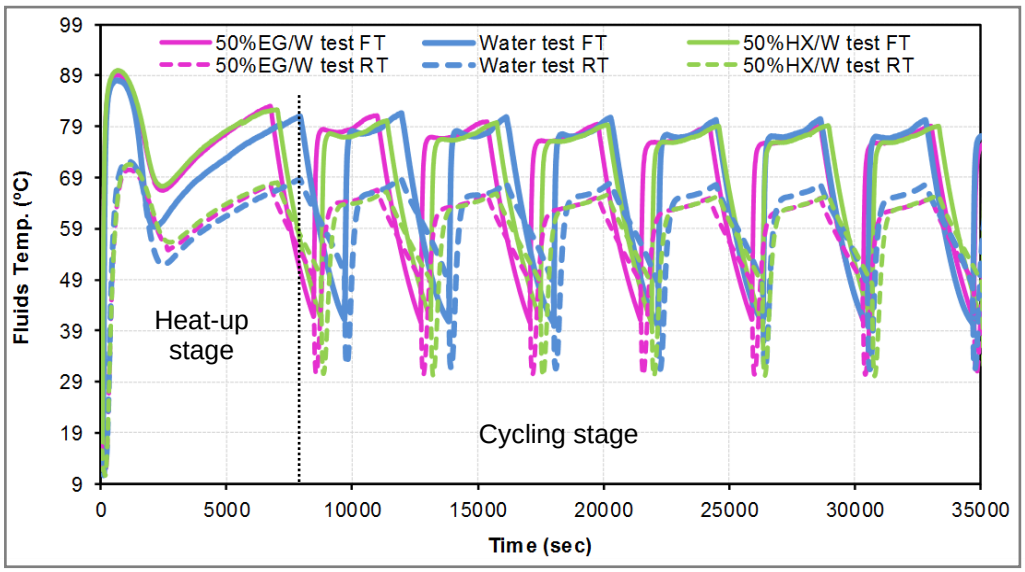

Figure 6.29: Flow and Return Temperatures Variation for Case 1 Thermostat Tests

It is evident from Figure 6.29 that the FT recorded when using the 50% EG/W and 50% HX/W mixtures was very similar to the temperature recorded throughout the water test.

Contrastingly, the RT, when using the AHTFs, was lower by 2.2K. The average IBT was calculated based on the top, middle and bottom temperature readings from the booth, and is illustrated in Figure 6.30.

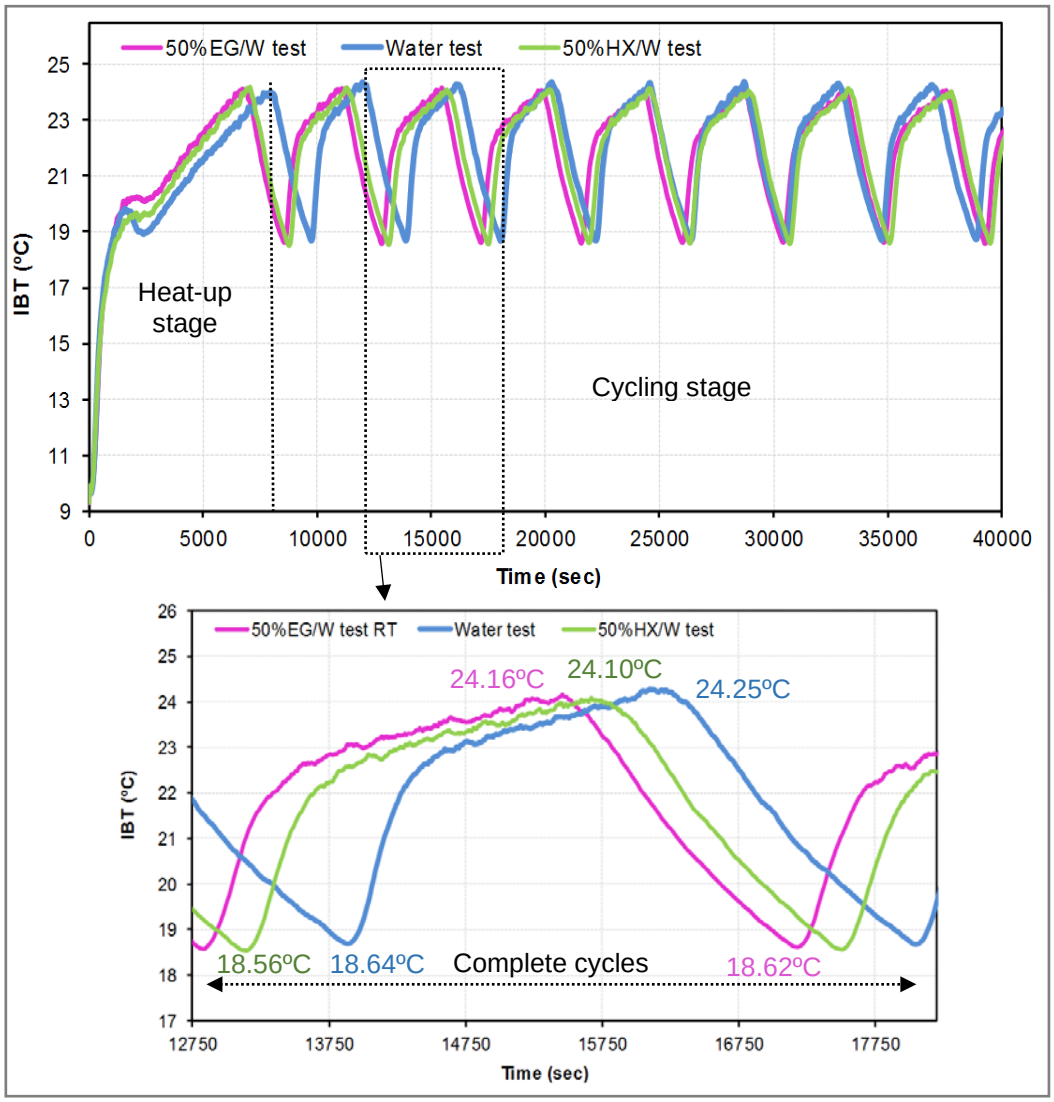

Figure 6.30: IBT Variation for Case 1 Thermostat Tests

Figure 6.30 depicts the rise of the IBT to the thermostat setpoint during all tests. These findings clearly align with the flow temperature readings previously obtained. For example, the duration of the heat-up stage when using the 50% EG/W and 50% HX/W mixtures was shorter than the duration of the heat-up stage when using water. The accumulated energy consumption and Avg.hE, (calculated using equations 6.3 and 6.4) were evaluated for each test, and the results are presented in Figure 6.31.

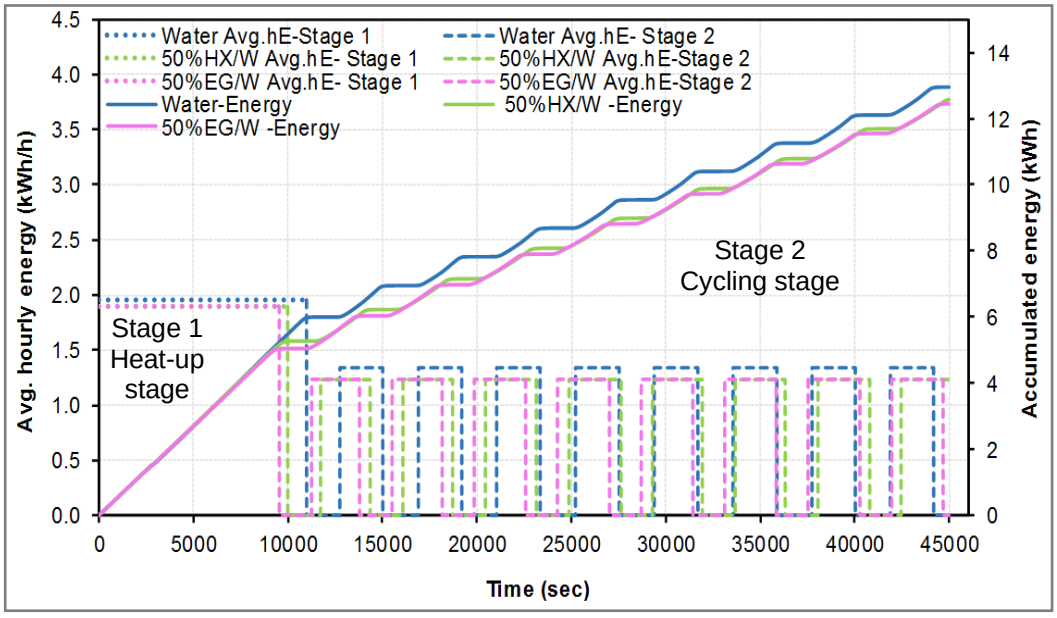

Figure 6.31: Accumulated Energy Consumption and $Avg.hE$ for Case 1 Thermostat Tests

Figure 6.31 shows that the system reached the cycling stage in a shorter time and using less energy when the AHTFs were used as a replacement to water. This is similar to the findings of the steady state tests. During the cycling stage, the 'on' period was slightly longer when using the AHTFs and the 'off' period was shorter than when using water. An analysis of a completed cycle using each test fluid is represented in Figure 6.32

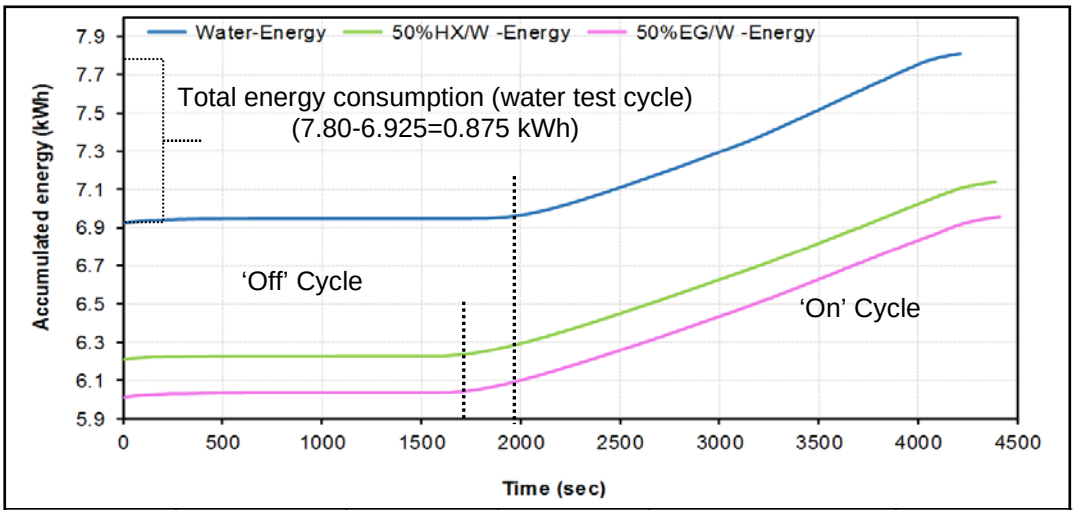

Test	Completed cycle time (sec)	'On' time (sec)	'Off' time (sec)	Total energy for a completed cycle (kWh)	Avg. hE (kWh/ (on time) h)
Water	4176	2304	1872	0.875	1.367
50%HX/W	4428	2700	1728	0.920	1.227
50%EG/W	4428	2710	1718	0.926	1.230

Figure 6.32: Analysis of One Completed Cycle in Case 1 Thermostat Tests

As Figure 6.32 shows, it is clear that the longer ‘on’ cycles seen when using the examined AHTFs reflect the amount of energy consumed during each test. The energy consumed in one completed cycle of the water test was less than the amount consumed during one cycle of the 50% HX/W and 50% EG/W tests. The energy readings were analysed to evaluate the behaviour of the HRHS throughout each test. The duration of each test was 45,000 seconds (12 hours and 30 minutes), and this included both the heat-up stage and the cycling stage. Table 6.3 presents the system’s energy performance (ES% calculated using equation 6.3) during each stage of the experiment.

Table 6.3: Energy Analysis for Case 1 Thermostat Tests

Parameters	Water	50% HX/W	50% EG/W
Stage 1 (Heat-up Stage)			
Heat-up duration (Stage 1) (sec)	11000	10000	9550
Total accumulated energy for Stage 1 (kWh)	5.97	5.27	5.06
ES (%) for Stage 1, [A]	/	12	15
Stage 2 (Cycling Stage)			
Cycling stage duration (Stage 2) (sec), [B]	34000	35000	35450
Duty cycle (DC %) [C]	55.2	61	61
‘On’ time during the cycling stage (sec), [B*C]	18768	21350	21625
Avg. hE for cycling stage (kWh/h)	1.367	1.227	1.230
Total accumulated energy for cycling stage (kWh)	7.127	7.28	7.42
ES (%) for Stage 2, [D]	/	- 2.1	- 4.6
Entire Test Duration (Stage 1 and Stage 2)			
Total accumulated energy for whole test duration (kWh)	13.1	12.57	12.45
Total ‘on’ time for the whole test (sec)	29768	31350	31174
Ratio of Stage 1 energy to the total energy, [E]	/	0.42	0.406
Ratio of Stage 2 energy to the total energy, [F]	/	0.58	0.595
Total ES (%), [(A*E) + (D*F)]	/	4	4

The figures in the above table reveal that the amount of energy consumed by the system during the heat-up stage was 12% and 15% lower when using the 50% HX/W fluid and 50% EG/W fluid respectively, in comparison to the amount of energy consumed when using water. During the cycling stage, the ’on’ period was longer by about 12% to 13% when using the AHTFs, but the total energy consumed was only 2.1% and 4.6% higher

than the total energy consumed using water. Over the duration of the test, the total 'on' time varied for each different fluid, reflecting the total energy consumed. These results confirm that the system worked differently when using the examined AHTFs. In Case 1 of the optimised scenario, the optimum operating time that could achieve 6-7% savings in energy when using the AHTFs was approximately 6 hours (double the duration of the heat-up stage).

The noticeable change in the operating behaviour of the HRHS when using AHTFs is due to the lower specific heat capacity (C_p) of these fluids in comparison to water (see Tables 3.5,3.6 and 3.7, of Chapter 3). During the heat-up stage, 2 kW of power was provided by the immersion heater for all tests. Therefore, the flow temperature of the AHTFs rose to a higher value than the flow temperature recorded with the water test (see Figure and 6.29). As the 50% HX/W and 50% EG/W mixtures have lower specific heat capacity, so they required less heat to raise the temperature. Subsequently, the system reached the cycling stage faster when using AHTFs instead of water. During the cycling stage, the analysis of the result in Table 6.3, revealed that the 'on' time of heating system working with 50% HX/W and 50% EG/W was longer when water was used by about 12 to 13%. The longer on heating cycles is due to the power provided by the immersion heater as this power was modulated by the PID controller based on the demand of the heat required by the system (including the fluid).

A summary of the conclusions that can be drawn from the optimised scenario Case 1 (mass flow rate controlled to replicate the base case), using 50% HX/W and 50% EG/W mixtures as AHTFs in HRHS is outlined as follows:

- Greater ΔT was recorded across the radiator in comparison to the water test, and as a result, the AHTFs had a lower return temperature by around 2K. This helps to reduce the heat loss from the return pipes.

- Greater temperature uniformity across the radiator surface, in comparison to the water test.
- Shorter duration of the heat-up stage meant that the indoor temperature reached the desired level in a shorter time. Consequently, better heat transfer was achieved during this stage when using the AHTFs.
- The IBT reached the reference level during both the steady state and thermostat tests.
- The lower volumetric flow rate was calculated in the system in comparison to water (by 6% and 7%) due to the higher density of the AHTFs. This meant that the smaller-diameter pipes could be used, as the volumetric flow rate is directly proportional to the cross-section area of the pipes.
- Change the operating behaviour of the HRHS during the cycling stage, as a longer duty cycle was calculated when using the AHTFs.

6.4.2.3 Case 2 Steady State Tests Results

In the second test case, the ΔT across the radiator was controlled to remain at around 10K by maintaining the flow temperature at the setpoint used in the base case test. The calculated flow rate during each test is illustrated in Figure 6.33.

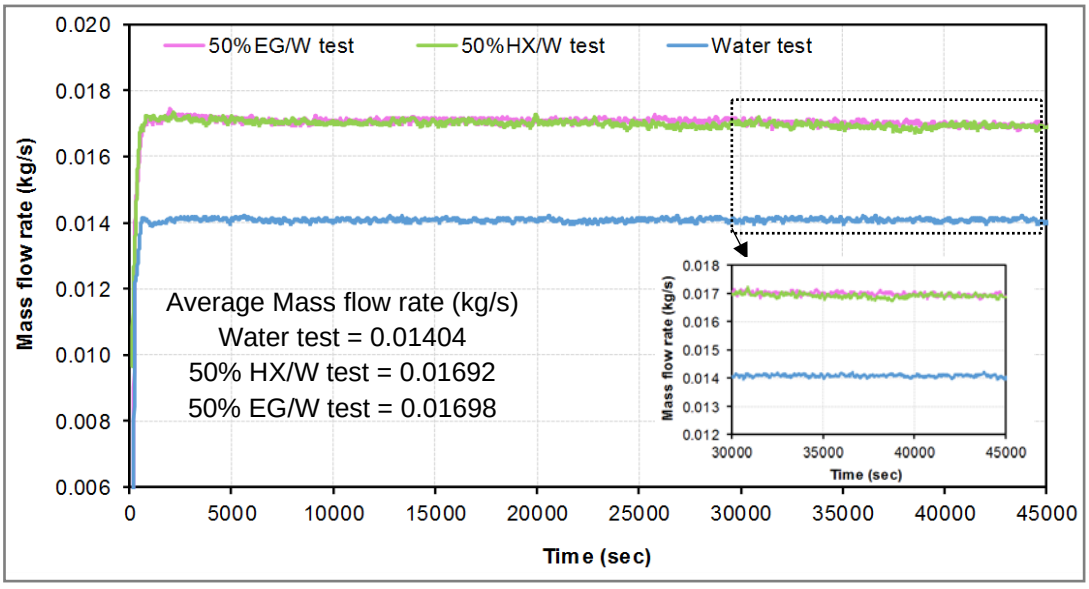

Figure 6.33: Mass Flow Rate for Case 2 Steady State Tests

As figure 6.33 shows, the mass flow rate required to achieve a ΔT of 10K across the radiator surface was higher by about 17% when using the AHTFs compared to the flow rate calculated during the water test. The higher mass flow rate corresponds with the volumetric flow rate and the velocity of the fluids within the system, as their density is higher than water (see Tables 3.5, 3.6 and 3.7 of Chapter 3). The volumetric flow rate in the system increased by 12% when using the AHTFs, while simultaneously, the velocity increased by 12%. A hydronic heating system is specifically designed to use water as a heat transfer fluid, so in order to use AHTFs with a higher velocity, the size of the pipes and pump needs to be taken into consideration. The flow and return temperatures of all fluids were recorded during each test and are presented in Figure 6.34.

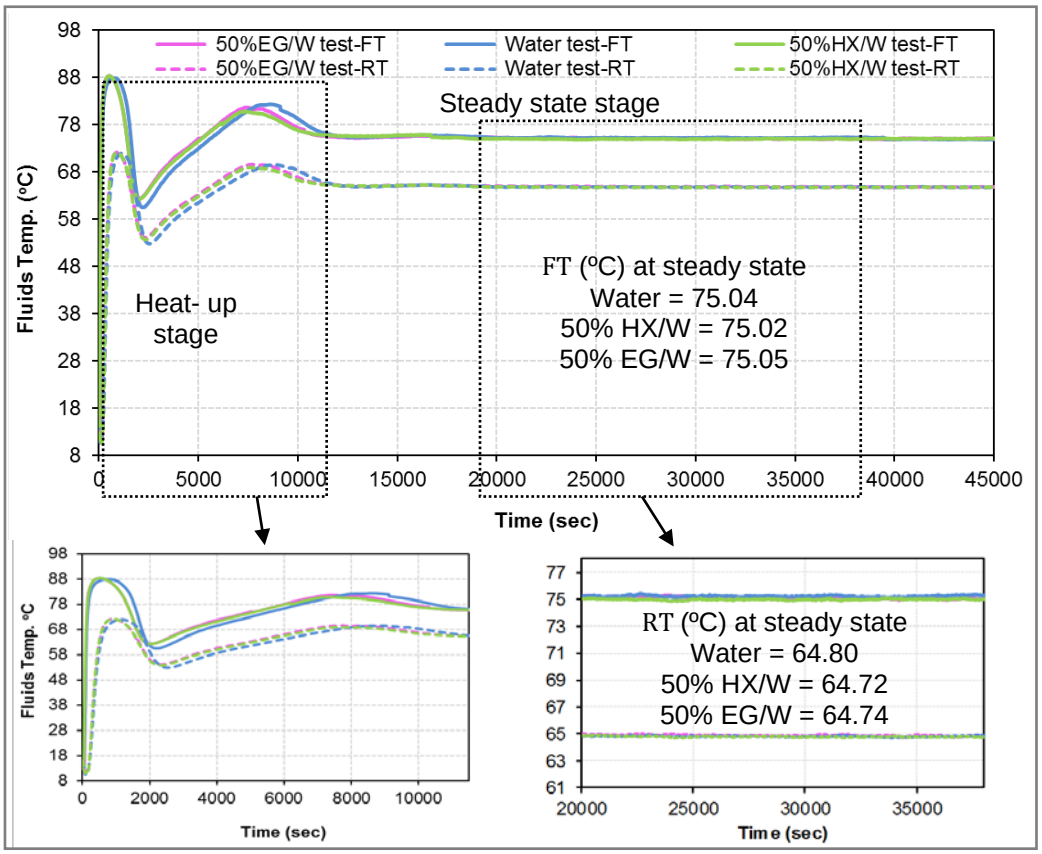

Figure 6.34 : Flow and Return Temperatures for Case 2 Steady State Tests

Figure 6.34 demonstrates that during the heat -up stage, the flow and return temperatures of the fluids fluctuated until the flow temperature stabilised at the PID controller setpoint (75ºC). During the steady state stage, the ΔT across the radiator surface was controlled and set at approximately 10K for the AHTF tests. The flow temperatures at a steady state

for the 50% HX/W and 50% EG/W tests were 75.03ºC and 75.07ºC and the return temperatures were 64.75ºC and 64.76ºC, respectively. The IBT was also recorded during each test and results were compared, as shown in Figure 6.35.

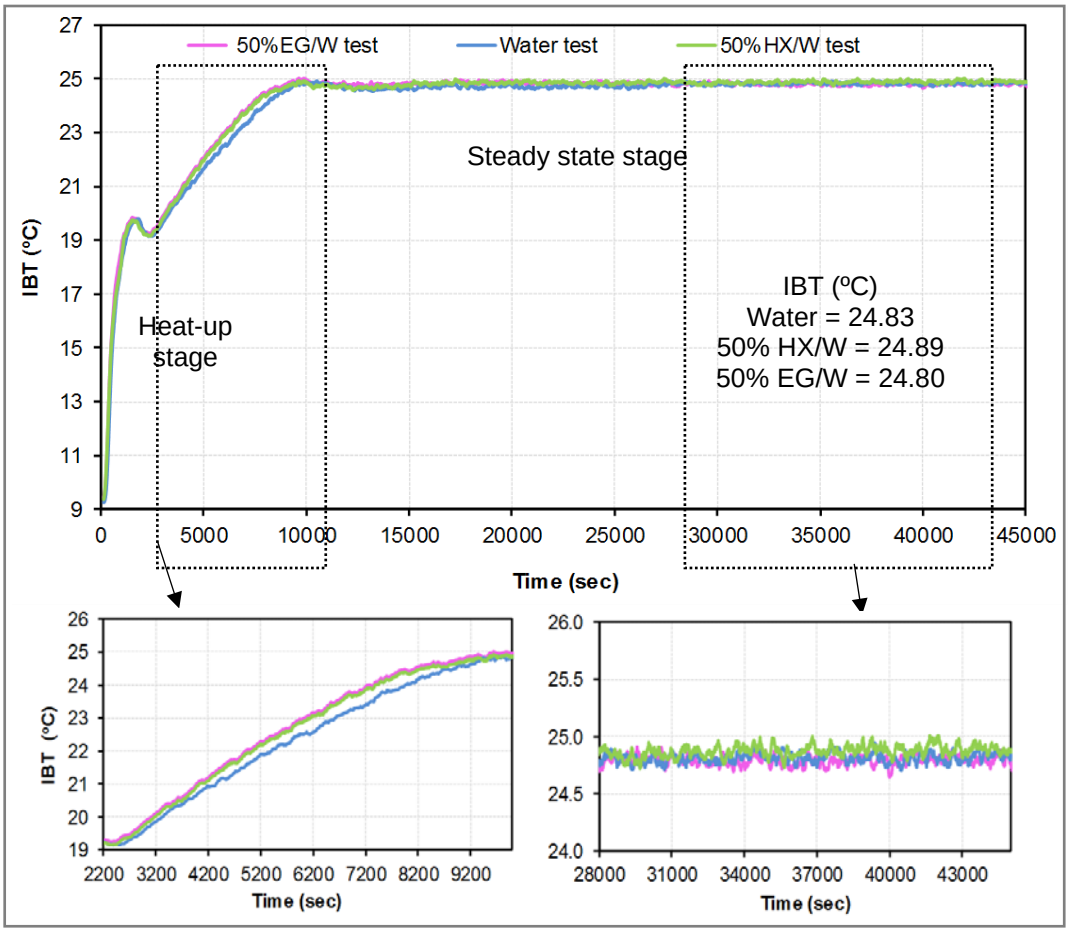

Figure 6.35: IBT Variation for Case 2 Steady State Tests

As Figure 6.35 shows, the IBT increased slightly quicker during the heat-up stage when using the AHTFs as an alternative to water. The rise in IBT during the heat-up stage reflects the flow and return temperature trends of the AHTFs (see Figure 6.34).

During the steady state stage, the IBT recorded was very similar to the temperature recorded in the water test. The amount of energy consumed with each test was also monitored and recorded, then the average hourly energy ($\mathrm{Avg.hE}$) was calculated by using equations 6.3 and 6.4. The results of the accumulated energy and $\mathrm{Avg.hE}$ are presented in Figure 6.36.

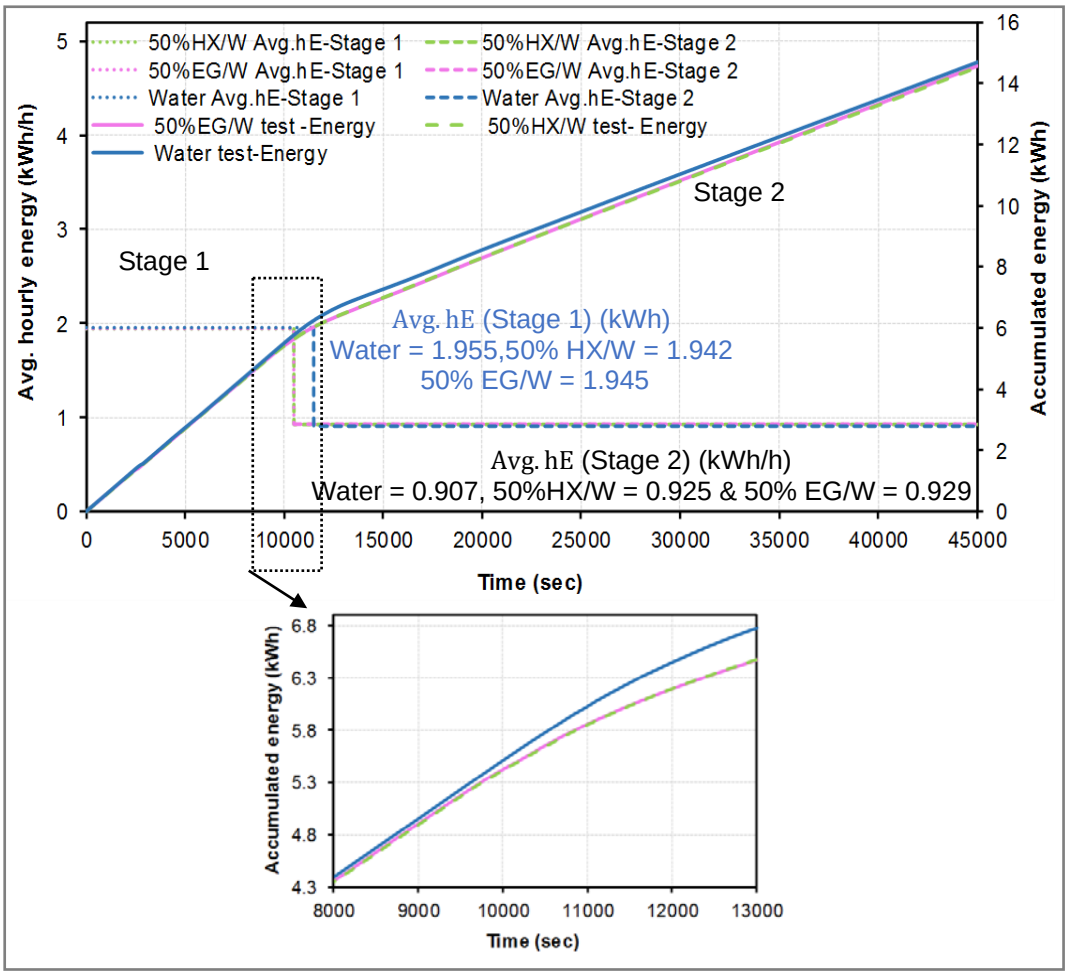

Figure 6.36: Accumulated Energy Consumption and Avg. hE for Case 2 Steady State Tests

As Figure 6.36 shows, the system reached a stable condition (when the increase in accumulated energy line slowed down after stage 1) 7% faster in time with the AHTFs tests in comparison to the water test. The comparison results of Case 2 showed that the performance of the HRHS was similar to that obtained when water used as a heat transfer fluid.

The temperature distribution across the radiator surface was recorded by capturing thermal images of the radiator using the thermal imaging camera (Fluke thermal imaging camera). The thermal images were then analysed using SmartView software, using a temperature alarm setting for a temperature range of 65ºC –75ºC, as shown in Figure 6.37.

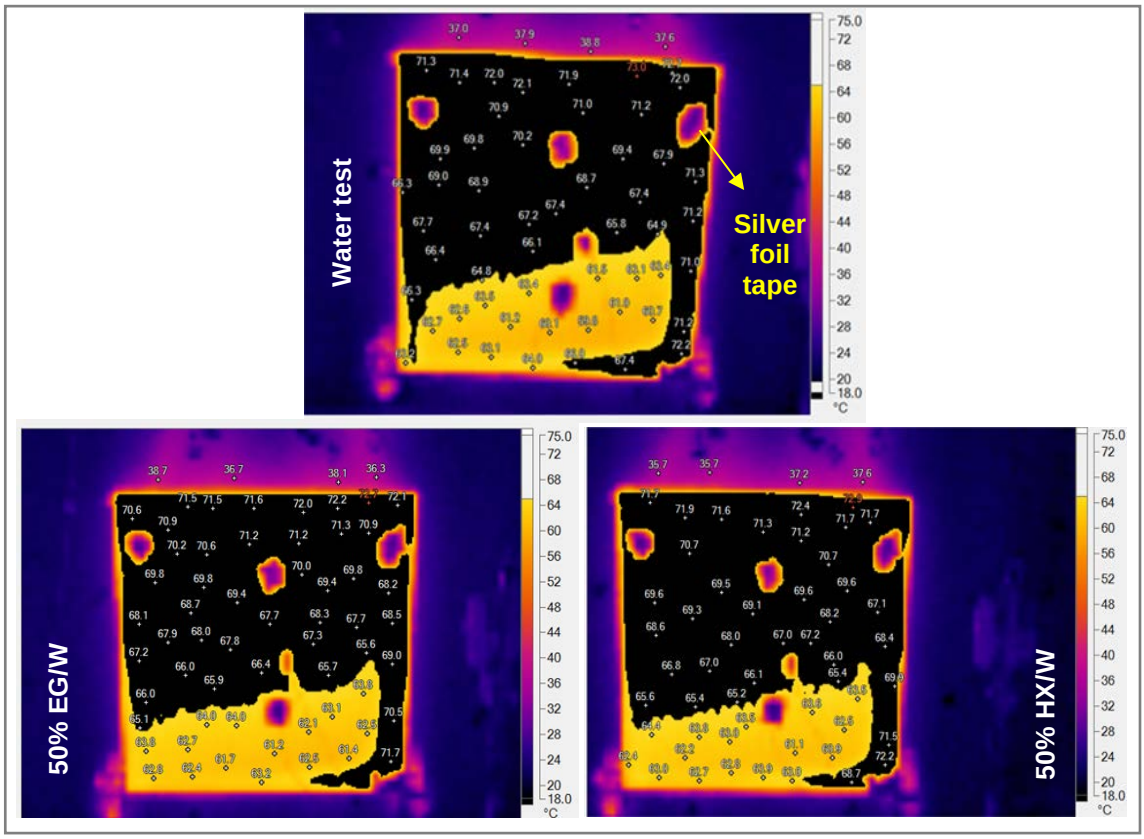

Figure 6.37: Temperature Distribution across Radiator Surface for Case 2 Steady State Tests

Figure 6.37 shows that the temperature distribution across the radiator surface when using the 50% HX/W and 50% EG/W mixtures was similar to the temperature distribution when using water. This can be attributed to a higher flow rate in the system, resulting in higher velocity (by 12% more than the velocity in the system with water) and that reduced the contact time for the 50% HX/W and 50% EG/W mixtures with the inner surface of the radiator.

6.4.3.2 Case 2 Thermostat Test Results

After completion of the steady state tests in Case 2 of the optimised scenario, thermostat tests were conducted using the same fluids. The flow rate was adjusted at the beginning of each test to produce a ΔT of approximately 10K across the radiator surface. Figure 6.38 presents the different flow rates used for each of the tests.

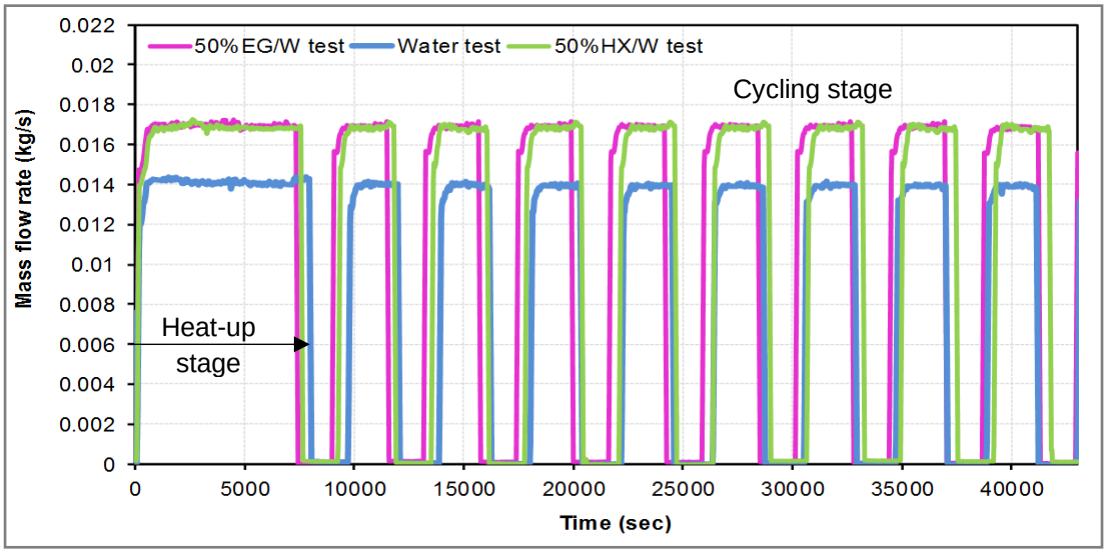

Figure 6.38: Mass Flow Rate Variation for Case 2 Thermostat Test

Figure 6.38 shows that the mass flow rate was higher when using the examined AHTFs in order to achieve a ΔT across the radiator surface of approximately 10K. Figure 6.38 also shows the variation in the time it took for the system to reach the cycling stage when using each fluid. The slightly shorter heat-up stage was seen when using the AHTFs in comparison to water. The duration of the heat-up stage with the 50% EG/W and 50% HX/W tests was 7,570 seconds (2 hours and 6 minutes) and 7,345 seconds (2 hours nd 2 minutes) respectively, while the duration of the heat-up stage with the water test was 7,955 seconds (2 hours and 13 minutes). To assess the duration of the 'on' and 'off' cycles of the cycling stage, the flow rate data were analysed, as shown in Figure 6.39

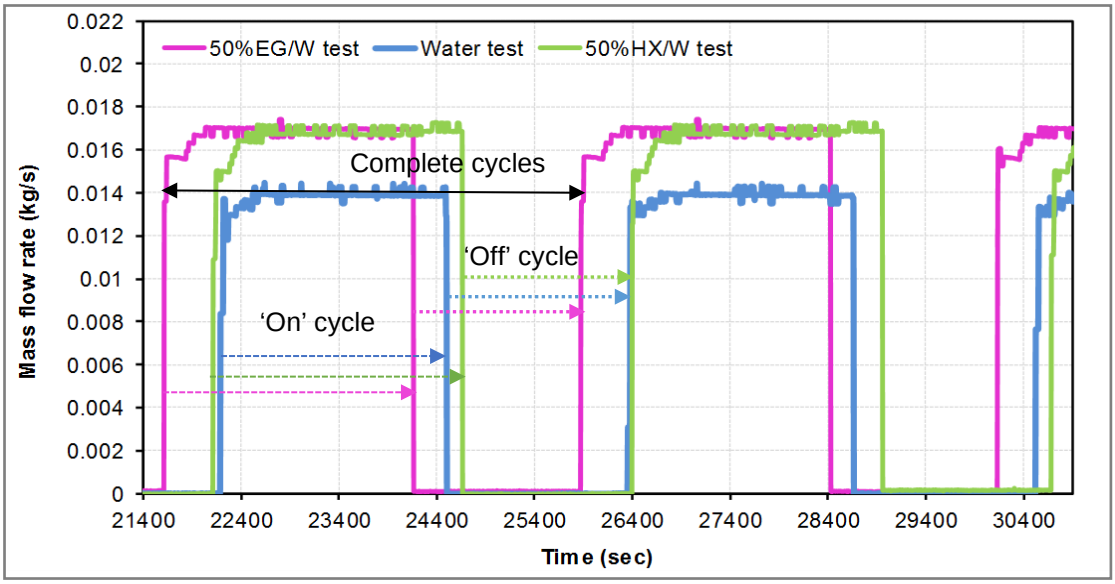

Figure 6.39: Duration of 'On' and 'Off' Heating Cycles in Case 2 Thermostat Tests

Figure 6.39 illustrates that the duration of the ‘on’ and ‘off’ heating cycles during the cycling stage differed for each test. The results from each test are summarised here:

Water test

- Completed cycle duration: 4,176 seconds (1 hour and 9.6 minutes)
- ‘On’ period: 2,304 seconds (38.4 minutes)
- ‘Off’ period: 1,872 seconds (31.2 minutes)

50% HX/W test

- Complete cycle duration: 4,285 seconds (1 hour and 11.4 minutes)
- ‘On’ period: 2,556 seconds (42.6 minutes)
- ‘Off’ period: 1,729 seconds (28.8 minutes)

50% EG/W test

- Complete cycle duration: 4,265 seconds (1 hour and 11.1 minutes)
- ‘On’ period: 2,552 seconds (24.53 minutes)
- ‘Off’ period: 1,713 seconds (28.55 minutes)

The duty cycle (DC%) was calculated using equation 6.5, giving a result of 59.6% and 59.8% for the 50% HX/W and 50% EG/W tests, respectively.

In the water test, DC% was obtained as 55.2%, meaning that the system needed to be ‘on’ for a longer time during the cycling stage when using the 50% HX/W and 50% EG/W mixtures as an AHTFs. However, the duration of the heat-up stage in the 50% HX/W test was 385 seconds (6.4 minutes) shorter than that in the water test, and similarly, it was 610 seconds shorter in the 50% EG/W test. The flow and return temperatures of all tests are presented in Figure 6.40.

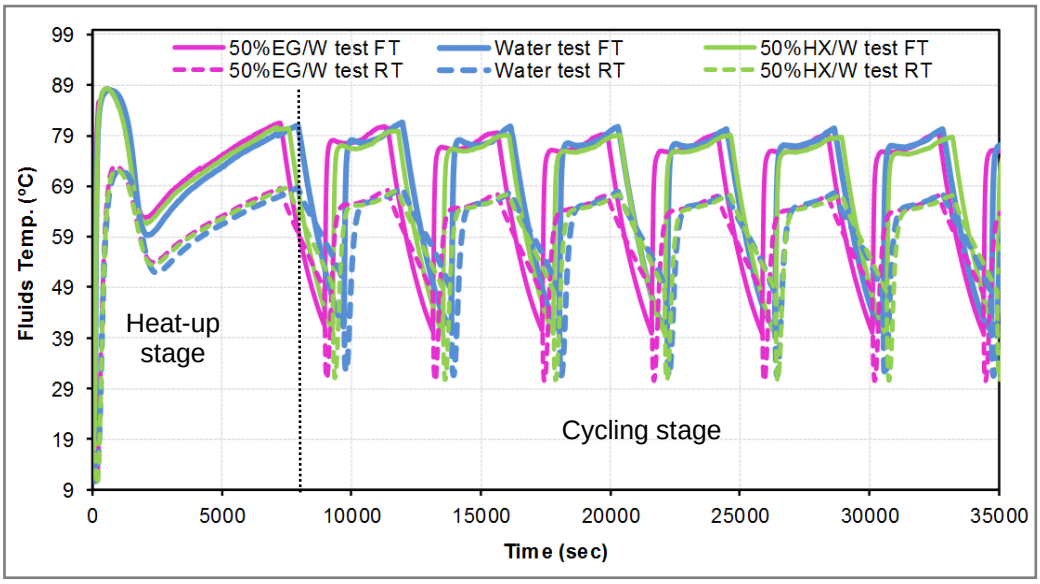

Figure 6.40: Flow and Return Temperatures for Case 2 Thermostat Test

Figure 6.40 shows that the FT and RT of the AHTFs were very similar to the recorded temperatures of the water used in the base case test. A comparison of the IBT across the tests is represented in Figure 6.41.

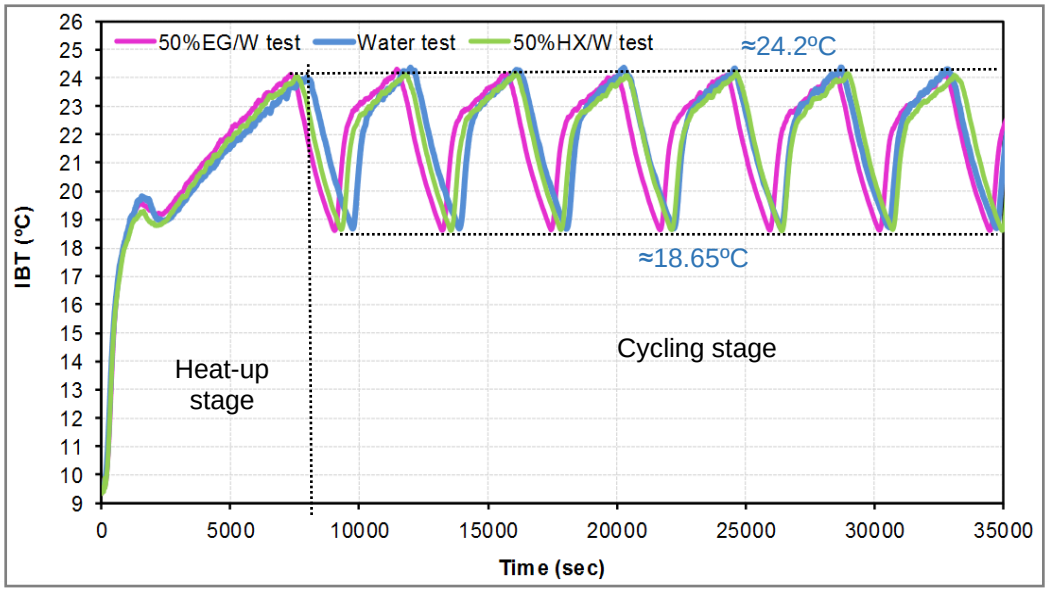

Figure 6.41: IBT Variation for Case 2 Thermostat Test

Figure 6.41 shows that the IBT reacted to the thermostat response and span and the cycling stage start slightly faster (by 5% - 7%) with 50% EG/W and 50% HX/W tests respectively compared to the water test. The accumulated energy consumption for each test was monitored and recorded. Then the Avg. hE was evaluated by using equations 6.3 and 6.4, and the results are shown in Figure 6.42.

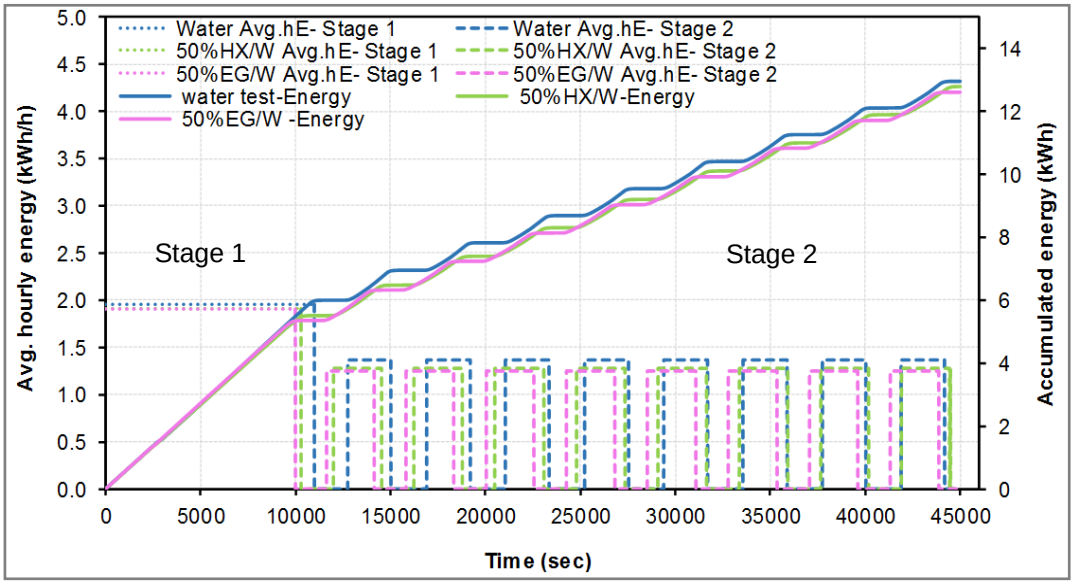

Figure 6.42: Accumulated Energy Consumption and $Avg.hE$ for Case 2 Thermostat Test

Figure 6.42 indicates that the AHTFs reacted quicker during the heat-up stage, but the duration of the 'on' and 'off' cycles varied across the tests. Figure 6.43 shows a closer analysis of one completed cycle of each test.

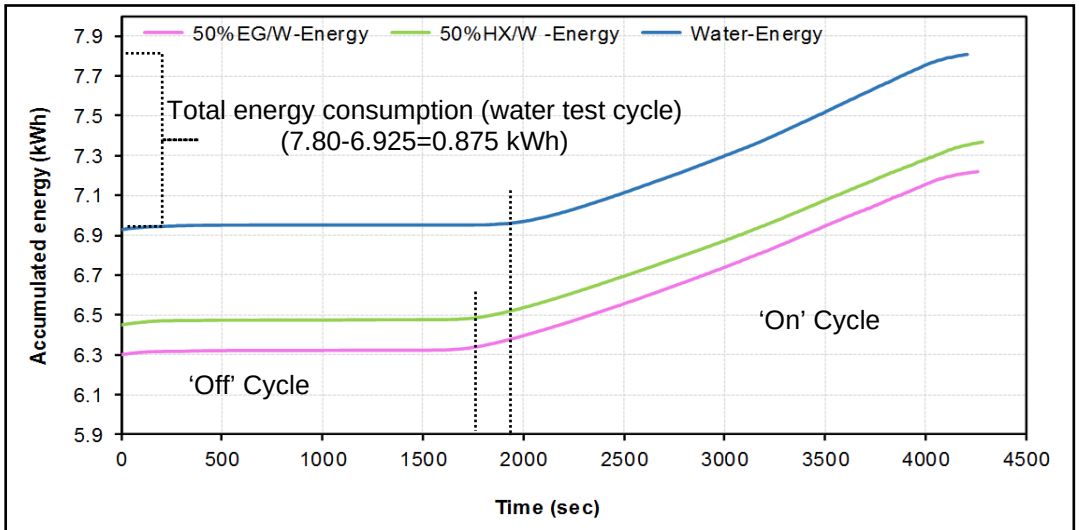

Test	Completed cycle time (sec)	'On' time (sec)	'Off' time (sec)	Total energy for a complete cycle (kWh)	Avg. hE (kWh/ (on time (h))
Water	4176	2304	1872	0.875	1.367
50%HX/W	4285	2556	1729	0.904	1.273
50%EG/W	4265	2552	1713	0.913	1.288

Figure 6.43: Analysis of One Completed Cycle in Case 2 Thermostat Tests

As Figure 6.43 illustrates the total 'off' period was shorter with the AHTFs tests than in the base case, and contrastingly the 'on' period was longer, this means that the amount of

energy consumed over a complete cycle was higher in comparison to the base case. This data was then used to analyse the behaviour of the system during each stage of the test, as well as over the whole test's duration. The results are presented in Table 6.4.

Table 6.4: Energy Analysis for Case 2 Thermostat Tests

Parameters	Water	50% HX/W	50% EG/W
Stage 1 (heat-up stage)			
Heat-up duration (Stage 1) (sec)	11000	10300	10100
Total accumulated energy for Stage 1 (kWh)	5.97	5.47	5.35
ES (%) for Stage 1, [A]	/	8.4	10.4
Stage 2 (Cycling stage)			
Cycling stage duration (Stage 2) (sec), [B]	34000	34700	34900
Duty cycle (DC %) [C]	55.2	59.7	59.8
'On' time during the cycling stage (sec), [B*C]	18768	20716	20870
Avg.hE for cycling stage (kWh/h)	1.367	1.273	1.288
Total accumulated energy for cycling stage (kWh)	7.127	7.325	7.469
ES (%) for Stage 2, [D]	/	-2.8	-4.7
Entire test duration (Stage 1 +Stage 2)			
Total accumulated energy for whole test duration (kWh)	13.1	12.795	12.819
Total 'on' time for the whole test (sec)	29768	31160	31299
Ratio of Stage 1 energy to the total energy, [E]	/	0.43	0.417
Ratio of Stage 2 energy to the total energy, [F]	/	0.57	0.583
Total ES (%), [(A*E) + (D*F)]	/	2	2

As the above table demonstrates, the duration of the heat-up stage was shorter when using the AHTFs in comparison to water, which resulted in a lower percentage of total energy consumed in this stage: approximately 8% to 10% less energy was consumed with the AHTF tests. During the cycling stage, the duration of the 'on' and 'off' periods varied across the water, 50% HX/W and 50% EG/W tests. The longer 'on' period with the AHTF tests meant that more energy was consumed during the cycling stage, almost balancing out the energy savings that were achieved in the heat- up stage. The specific heat capacity (C_p) of both the 50% HX/W and 50% EG/W mixtures, had an influence on the behaviour of heating system. Due to the lower C_p of the examined AHTFs compared to water, the

flow temperature of these fluids rose to a higher value compared to the water flow temperature during the heat-up stage (see Figure 6.40). As the immersion heater work with full power (2 kW). Thus, the heat-up stage was shorter with the 50% HX/W and 50% EG/W. However, during the cycling stage, the power provided by the immersion heater is controlled by the PID controller, which means the heater supply the demanding heat only and yielding longer 'on' heating cycles with the examined AHTFs.

A summary of the conclusions that can be drawn from the optimised scenario Case 2 tests (ΔT across radiator surface controlled to be 10K) using 50% HX/W and 50% EG/W mixtures as AHTFs is outlined in the following section.

- These fluids produced a higher mass flow rate (by 17%) than water. This resulted in a higher volumetric flow rate in the system (by 12%) as well as a higher velocity. If these mixtures are to be used as alternative heat transfer fluids within a HRHS, the size of the system's components needs to be considered, as a higher velocity will impact the size of the pipes and the pump.
- The heat-up stage was slightly shorter in comparison to the base case test, as the indoor temperature reached the desired level at a slightly quicker rate than for the water test, which resulted in less energy being consumed during this stage.
- The IBT reached the reference level in both steady state and thermostat tests.
- Changing the operating behaviour of the HRHS in the thermostat tests resulted in a shorter heat-up period and longer duty cycle during the cycling stage without reflecting on the energy consumption by the system.

6.5 Pump Power

The pump's electrical power was evaluated by conducting a separate extra experiment in which the system was allowed to run with only the pump power monitored and recorded using the power meter. The pump power was recorded with Case 2 tests, as the flow rate

calculated was higher in comparison to the Case 1 tests. Figure 6.44 shows that the pump's power ranged between 0.11 and 0.14kW, aligning with the pump curve values [97]. The measurement of the pump's power equates to less than 1% of the immersion heater's power, which is 2 kW.

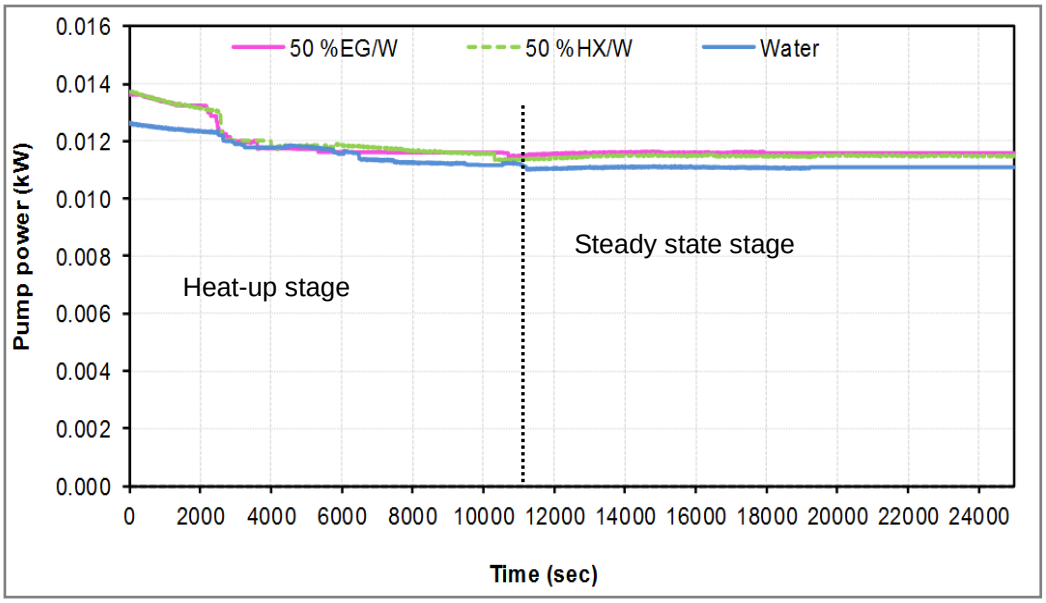

Figure 6.44 : The Pump's Power for Steady State Tests

In Figure 6.44, the higher power readings recorded during the early stage of all tests are caused by the varying temperatures of the fluids during the heat-up stage. The main conclusion that can be drawn from Figure 6.44 is that, during the heat-up stage, the pump power was 7% higher when using the AHTFs in comparison to water. Once the system had reached a steady state, the pump power recorded with the AHTF tests was also higher (by approximately 5%) than when using water. This increase in the power of the pump can be attributed to a higher flow rate in the system obtained with Case 2 tests, as well as the higher density and viscosity of the AHTFs.

6.6 Summary

This chapter collated and analysed the data obtained from the experiments carried out during this project. The experimental results obtained when the HRHS operated with water as a heat transfer fluid were compared to the results obtained when the HRHS operated

with 50% HX/W, 50% EG/W, and 30% EG/W mixtures as alternative heat transfer fluids. The levels of energy consumed and the indoor temperatures of the test zone (the booth) were recorded and compared across all tests. This experiment included various scenarios for testing how the alternative mixtures worked as alternative heat transfer fluids in order to account for different conditions that could affect the behaviour of the HRHS (see Figure 6.1).

The performance of the HRHS was investigated by analysing the IBT, the GT, the radiator surface temperature, the flow and return fluid temperatures and the levels of energy consumption over the duration of the tests. Based on the results obtained, the following conclusions can be made:

1. The 50% HX/W and 50% EG/W mixtures produced similar results, while the 30% EG/W mixture reacted in a similar way to water within the HRHS.

2. The drop-in scenario demonstrated that the type of heat transfer fluid used has a significant effect on the flow rate within the system; the flow rate reduces when using denser and more viscous fluids. When using the 50% HX/W and 50% EG/W mixtures, a lower IBT was recorded, as it failed to reach the comparison point (IBT recorded with the base case: 24.82ºC). The amount of energy consumed by the system with the 50% EG/W and 50% HX/W tests was lower compared to the water test, by 10% and 15% respectively. When using the 30% EG/W mixture, the recorded IBT and amount of energy consumed were very similar to the results obtained from the water test.

3. The optimised scenario involved two parameters being adjusted in the system: the mass flow rate and the temperature difference across the radiator.

4. The mass flow rate was controlled so that it remained at a similar level to the mass flow rate recorded with the water test (Case 1). This resulted in:

- A lower volumetric flow rate within the system due to the different densities of the fluids. Using the 50% HX/W and 50% EG/W mixtures resulted in a reduction in the volumetric flow rate by 6% and 7% respectively.
- Greater ΔT across the radiator surface resulted in lower return temperature by about 2K, and this helps to reduce heat loss from the pipes in real-life application.
- Less energy required for the IBT to reach a steady state, causing a shorter heat-up period.

- Improved temperature distribution across the radiator surface. The thermal images of the radiator surface showed better uniformity in temperatures across the radiator surface ranging between 75ºC and 65ºC when using the 50% HX/W and 50% EG/W mixtures, in comparison to water as a heat transfer fluid. The better uniformity of temperature that was achieved with the 50% HX/W and 50% EG/W tests can be attributed the lower velocity in the system and higher viscosity for these fluids compared to water. Therefore, these fluids stick to the inner surfaces of the radiator more than water, which revealed better temperature distribution across the radiator.

5. In the second case of optimised scenario (Case 2), the ΔT across the radiator was controlled to remain at approximately 10K with all tests. Therefore, the mass flow rate needed to be 17% higher when using the AHTFs in comparison to water. The results indicated that the system performed in a similar way to its behaviour with the base case (water test), in terms of energy consumption, IBT and temperature uniformity across the surface of the radiator. In real-life applications, the size of the system's components (size of the pipes and pump) would need to be taken into consideration when using these fluids, as the HRHS was initially designed to be used with water only.

6. The optimised scenario thermostat test results showed a correlation between the use of AHTFs and the operating behaviour of the system, notably in the duration of its heat-up stage and duty cycle; the heat-up stage was shorter and the duty cycle was longer when using the 50% HX/W and 50% EG/W mixtures in comparison to water. This influenced the amount of energy consumed during the two different stages of the experiment. The thermal properties of the AHTFs, particularly their specific heat capacity (C_p), affected the operating behaviour of the heating system with the thermostat tests.

CHAPTER 7

Radiator Heat Output Results

7.1 Introduction

This chapter presents the radiator heat output results for the base case (water) tests using the energy balance approach (as described in Chapter 5) and determines how the energy balance approach was verified. The chapter also presents an analysis of the radiator heat output results with the alternative heat transfer fluids (AHTFs) and concludes with a comparison of the results against base case water outputs.

7.2 Radiator Heat Output: Base Case Results

This section presents the calculated heat output ($\dot{Q}_{output}$) for the base case tests, including the results from both the steady state and thermostat tests. An Excel spreadsheet was created and used to calculate the $\dot{Q}_{output}$ over the duration of each test, considering the three modes of heat flow balance within the heated space, as discussed in section 5.3.2.1 of Chapter 5. The change in internal booth temperature (IBT) with a fixed environmental chamber temperature (ECT) 9ºC, the thermal transmittance (U) of the booth's wall, and the thermal properties of the air, radiator and booth (see Appendix 7.A), represent the parameters that were considered to calculate the $\dot{Q}_{output}$.

7.2.1 Radiator Heat Output- Steady State Water Test

The $\dot{Q}_{output}$ results from the steady state tests are graphically plotted against the duration of the test in Figure 7.1.

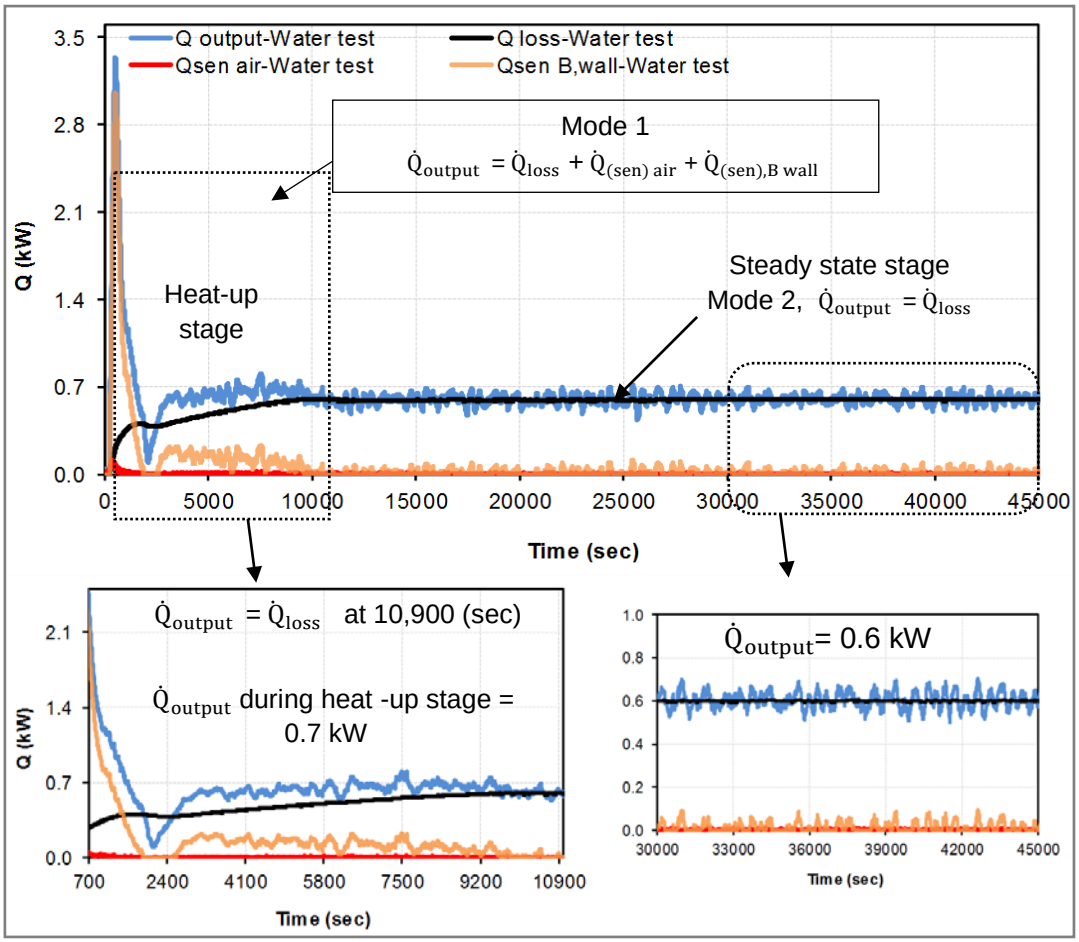

Figure 7.1: Heat Output from the Radiator for Steady State Water Tests

Figure 7.1 shows the calculated heat output ($\dot{Q}_{output}$) over the duration of the tests. During the heat-up stage (0 to 1,0900 seconds (3 hours and 2 minutes)), the $\dot{Q}_{output}$ was calculated using Mode 1 (see equation 5.8 of Chapter 5). During this stage the $\dot{Q}_{output}$ is transferred from the radiator to the surrounding air in the form of sensible heat. The sensible heat within the indoor air and booth's walls (red and orange lines) and heat loss from the booth's walls (black line) to the environmental chamber are shown in Figure 7.1. The heat-up stage led to the steady state stage, where the $\dot{Q}_{output}$ was calculated using Mode 2 (see equation 5.9 of Chapter 5). Figure 7.1 also shows that the sensible heat in the air ($\dot{Q}_{(sen)\,air}$) is lower in comparison with the sensible heat in the booth's walls ($\dot{Q}_{(sen)\,wall}$), and this is due to the difference in mass between the air and booth walls (see Appendix 7.A). The average $\dot{Q}_{output}$ calculated during the heat-up stage was 0.70 kW, and

once the system had reached a steady state, it was calculated at 0.60 kW with a variation of ± 0.04kW around the mean value. The evaluated uncertainty in the heat output value was found to be 3.3% (see Appendix 7.B). To validate the energy balance approach results, the $\dot{Q}_{output}$ at a steady state condition was compared to the radiator's nominal heat output ($\dot{Q}_{50}$), which is the value provided by the manufacturer (0.622kW) [98]. The difference (%) between the $\dot{Q}_{output}$ and $\dot{Q}_{50}$ was calculated using Equation 7.1.

$$Difference\% = |\dot{Q}_{50} - \dot{Q}_{output}|/\dot{Q}_{50} \quad \textbf{(7.1)}$$

The calculated difference was 4%, which is in-line with expectations, as the supply and return pipes of the radiator were fitted to the bottom of the radiator on opposite ends (BBOE) as this is the most comment connection type used in the UK [73]. This type of connection can affect the performance of the radiator. Additionally, the heat output based on the BS EN 442-2 standard ($\dot{Q}_s$) (see equation 5.4 of Chapter 5) was calculated as 0.54 kW. The following parameters were considered when calculating the $\dot{Q}_s$:

- The actual excess temperature ($\Delta T_{\dot{e}}$) = 45.09ºC (as the IBT = 24.83ºC, FT = 75.04ºC and RT = 64.8ºC)
- n = 1.3 [98]

The difference between the $\dot{Q}_s$ and the $\dot{Q}_{50}$ (calculated using Equation 7.1) was 13%, confirming the effect of the actual operating conditions on the characteristic coefficients (K_m and n) of the radiator (as described in section 5.2 of Chapter 5). This proves the effectiveness of the energy balance approach in evaluating the heat output from the radiator under actual operating conditions. The difference between the $\dot{Q}_{50}$ and the $\dot{Q}_{output}$ was less than the difference (%) between the $\dot{Q}_{50}$ and the $\dot{Q}_s$.

7.2.2 Radiator Heat Output -Thermostat Water Test

The energy balance approach was also considered when examining the heat output from the radiator with the thermostat test and the results are presented in Figure 7.2.

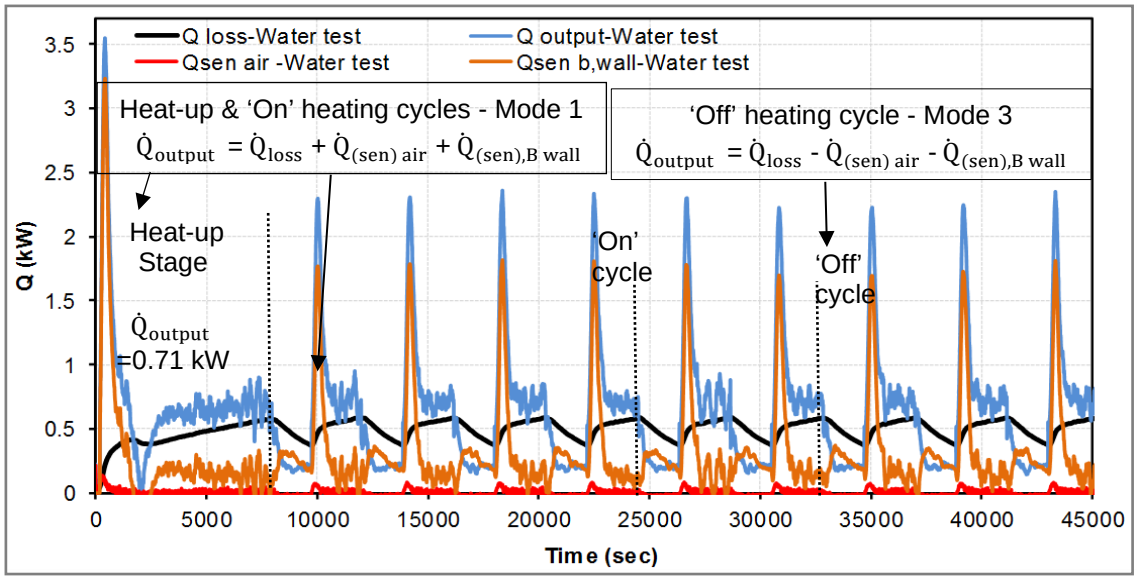

Figure 7.2 : Heat Output from Radiator for Thermostat Water Test

Figure 7.2 shows that the heat output from the radiator was calculated throughout all stages of the test (heat- up stage, cycling heating 'on' and cycling heating 'off'). During the heat-up stage and 'on' heating cycles, the $\dot{Q}_{output}$ was computed considering Mode 1, (see equation 5.8 of Chapter 5). During the 'off'' heating cycles, the $\dot{Q}_{output}$ was evaluated based on the differences between the heat loss and heat released from the booth walls and indoor air (Mode 3, equation 5.10, Chapter 5). The overshoot of the $\dot{Q}_{output}$ during the early stage of the heat-up stage and 'on' heating cycles reflects the fluid flow temperature behaviour, which was affected by the overshoot of the PID controller. The average value of $\dot{Q}_{output}$ during the heat-up stage was found to be 0.71 kW and during 'on' heating cycles was 0.70 kW with a variation of ±0.07 kW. The average value of $\dot{Q}_{output}$ during the 'off' heating cycles (when no hot water was flowing inside the radiator) was found to be 0.24 kW with a variation of ± 0.04 kW.

7.3 Verification of the Energy Balance Approach

Before proceeding to evaluate the $\dot{Q}_{output}$ from the radiator whilst operating with the examined AHTFs, it was necessary to verify the energy balance approach using the base

case (water) tests. Therefore, the results obtained when using the energy balance approach were compared with the total amount of heat entering the radiator ($\dot{Q}_T$), which was calculated using the mass flow rate, water flow and return temperatures, and its specific heat capacity (see equation 2.9 of Chapter 2). The $\dot{Q}_T$ and $\dot{Q}_{output}$ evaluated for the steady state tests are presented in Figure 7.3.

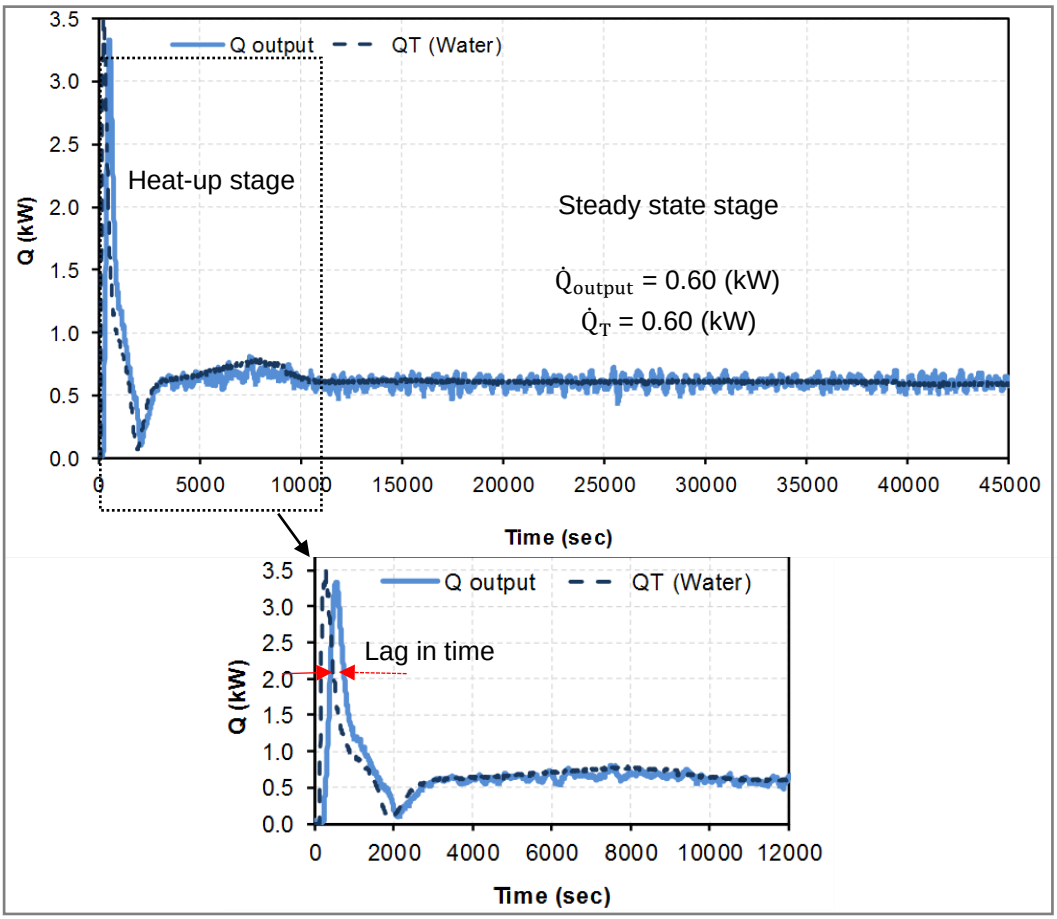

Figure 7.3 : Verification of Energy Balance Approach for Steady State Test

Figure 7.3 shows a strong correlation between the recorded $\dot{Q}_{output}$ and $\dot{Q}_T$, meaning that the heat that entered the radiator, due to the movement of the hot water transferred to that heated space (booth). A lag in time (of approximately 125 seconds, or 2 minutes) can be seen between $\dot{Q}_T$ and $\dot{Q}_{output}$, this shifting in time reflects the delayed response of the air inside the booth to pick up the heat from the radiator. The same evaluation was carried out for the thermostat tests, and the findings are illustrated in Figure 7.4.

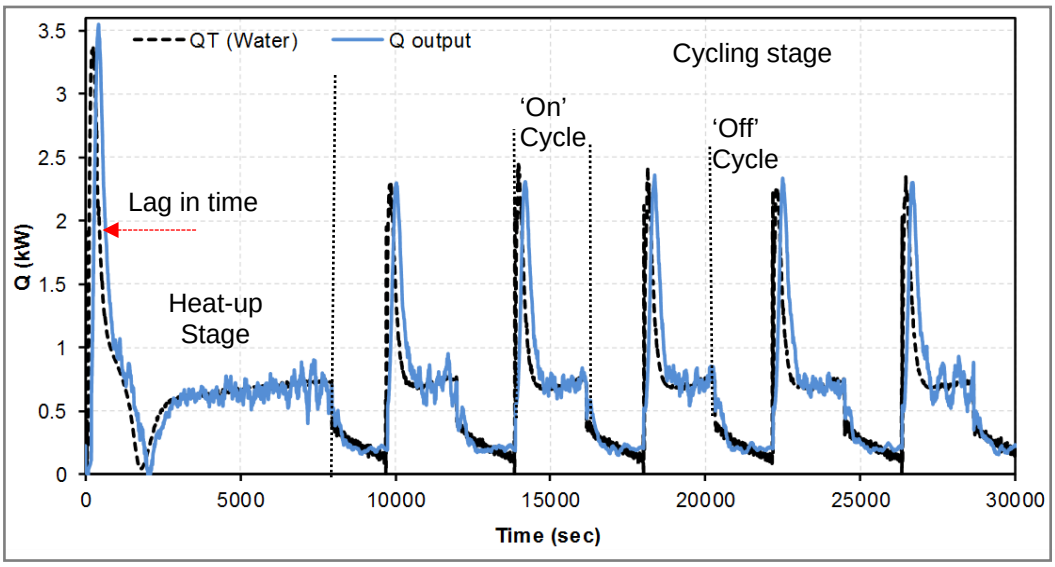

Figure 7.4: Verification of Energy Balance Approach for Thermostat Test

From analysing Figure 7.4, it is evident that the evaluated $\dot{Q}_{output}$ has a similar trend to the $\dot{Q}_T$ over the duration of the test (heat-up stage, 'on' and 'off' heating cycles). The $\dot{Q}_T$ during the 'off' heating cycle was calculated based on the amount of heat stored within the body of the radiator and hot water trapped inside the radiator (see equation 5.6 of Chapter 5). The radiator weighed 10.4 kg and the hot water within it weighed 2 kg [98]. These measurements were used to calculate the $\dot{Q}_T$ during the 'off' heating cycle. The lag in time between the heat output ($\dot{Q}_{output}$) and the heat entering the radiator ($\dot{Q}_T$) was recorded as 130 seconds, which is similar to that recorded throughout the steady state verification (see Figure 7.3). The amount of heat output for both the steady state and thermostat tests correlated with the amount of heat entering the radiator. This confirms that the energy balance approach can be used as a reliable method for evaluating the heat output from the radiator when operating with the 50% HX/W and 50% EG/W mixtures.

7.4 Radiator Heat Output with Alternative Heat Transfer Fluids

The following section presents the evaluated $\dot{Q}_{output}$ for the 50% HX/W and 50% EG/W tests, in both the drop-in and optimised scenarios of the steady state and thermostat tests (Case 1 and Case 2).

7.4.1 Drop-in Scenario Results

This test scenario was designed to replicate the real-life application of 50% HX/W within a hydronic radiator heating system (HRHS). In order to assess the heat output from the radiator when using the 50% HX/W and 50% EG/W mixtures as AHTFs, the energy balance approach was applied. The results are illustrated in Figure 7.5.

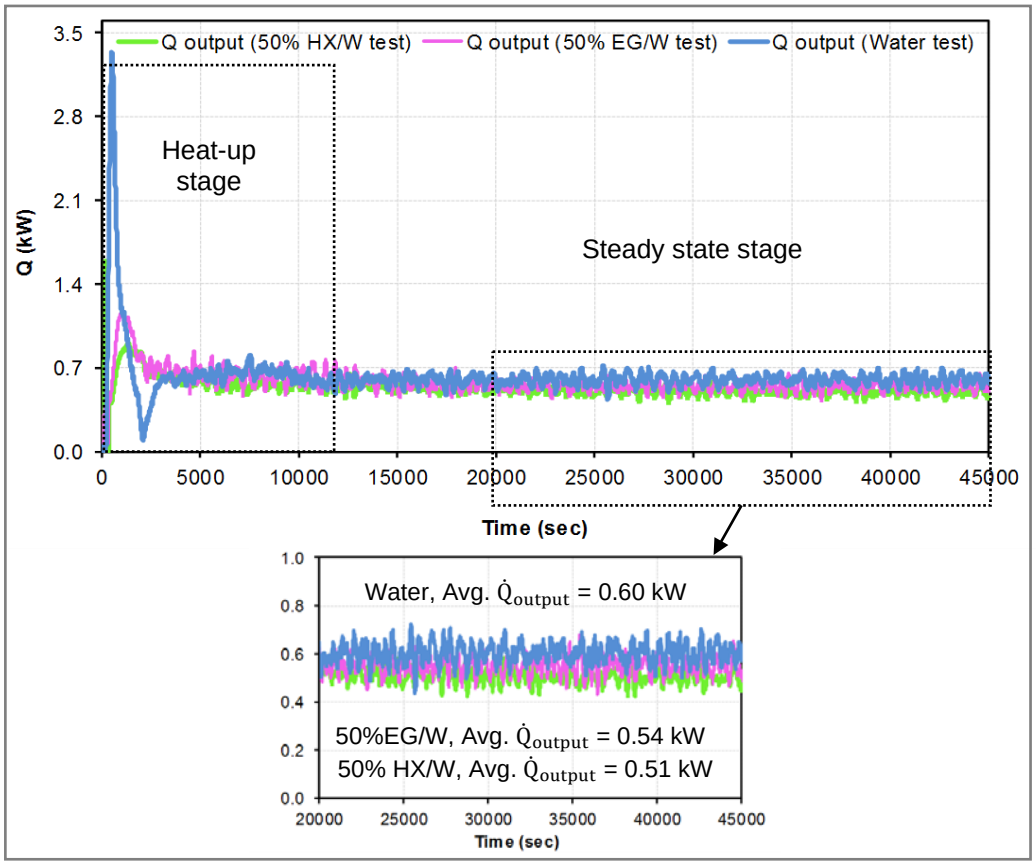

Figure 7.5: Radiator Heat Output for Drop-In Scenario Tests

Figure 7.5 enables a comparison between the $\dot{Q}_{output}$ evaluated throughout the base case tests and the AHTF tests, variation can be seen in the results from the different tests. In this test scenario, the system settings remained the same as in the base case. This resulted in lower mass flow rates with the AHTFs tests (see section 6.4.1 of Chapter 6), which in turn impacted the amount of heat output from the radiator. When the system had reached a steady state, the $\dot{Q}_{output}$ was lower with the AHTF tests (by 15% for 50% HX/W and 10% for 50% EG/W), in comparison to water, due to the variation in mass flow rate

amongst these tests. This reduction in heat output mirrors the reduction in the amount of total energy consumed by the system, which reduced by 15% and 10% for the 50% HX/W and 50% EG/W tests, respectively (see Figure 6.17 of Chapter 6).

7.4.2 Optimised Scenario Results

The heat output from the radiator was calculated using the energy balance approach for Case 1 and Case 2 of the optimised scenario, for both the steady state and thermostat tests. The results are presented in the following section.

7.4.2.1 Radiator Heat Output - Case1 Steady State Results

The heat output ($\dot{Q}_{output}$) evaluated for the steady state tests of optimised scenario Case 1, which involved adapting the mass flow rate to replicate the base case, is presented in Figures 7.6 and 7.7.

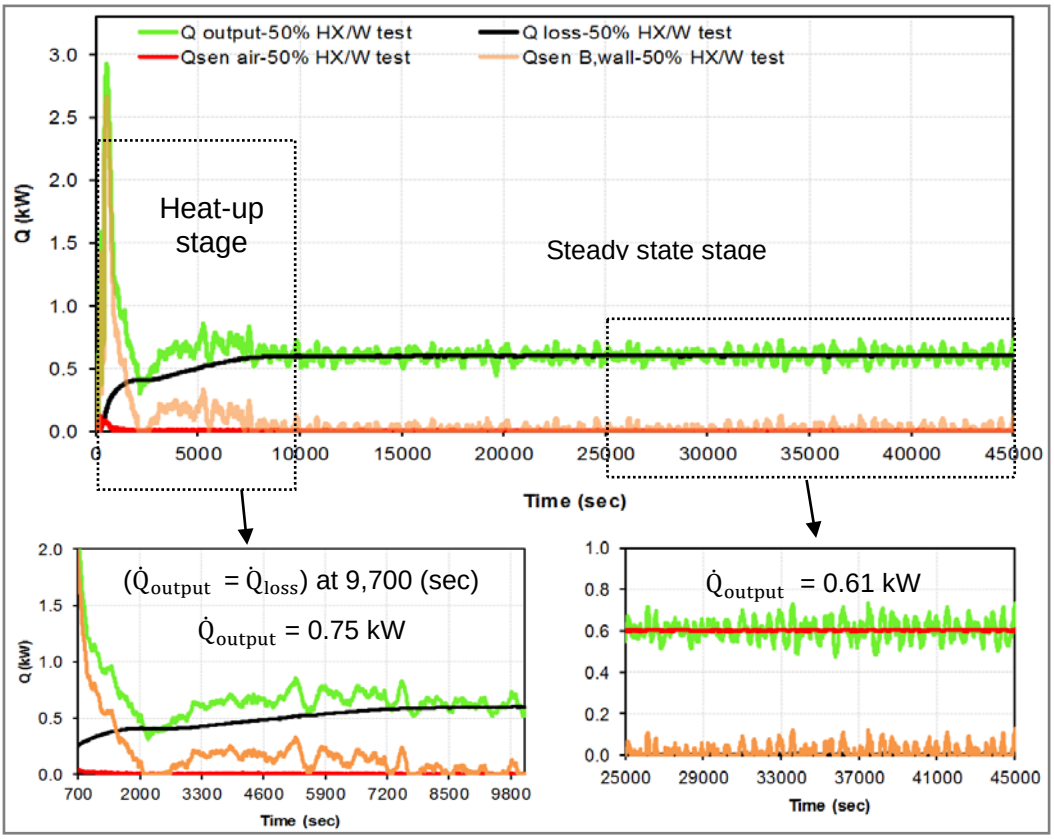

Figure 7.6 : Radiator Heat Output for Case 1 Steady State of 50% HX/W Test

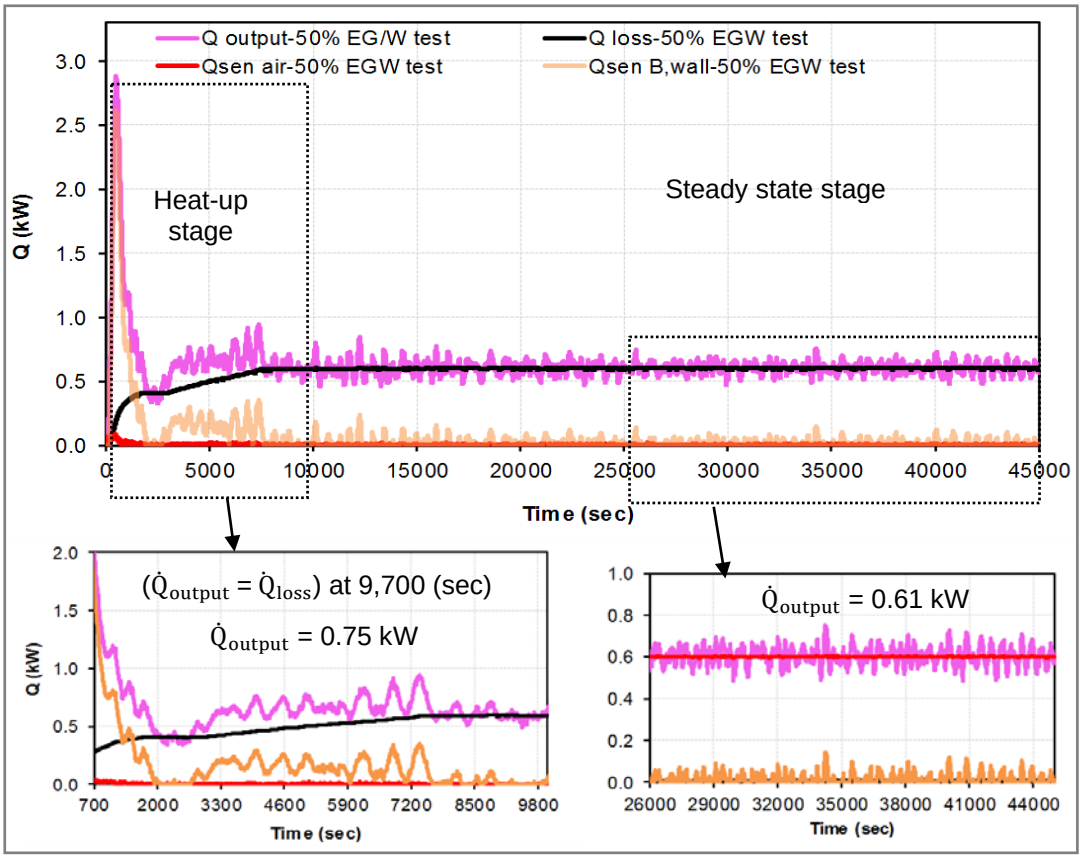

Figure 7.7 : Radiator Heat Output for Case 1 Steady State of 50% EG/W Test

Figures 7.6 and 7.7 show that the average $\dot{Q}_{output}$ obtained during the heat-up stage was 0.75 kW, and the average $\dot{Q}_{output}$ recorded during the steady state stage was 0.61 kW, with a variation of ± 0.05 kW. Using the AHTFs resulted in a higher (7%) heat output during the heat-up stage, in comparison to water. This demonstrates that the required indoor conditions could be achieved in a shorter amount of time, thereby reducing the amount of energy consumed during this stage. Contrastingly, the heat output from the radiator during the steady state stage when using the examined AHTFs was similar to that recorded with the water tests. This means that the thermal performance of the HRHS during the heat-up stage was enhanced when operating with the AHTFs because of their ability to raise their temperature faster than water, for the same amount of heat. The performance of the radiator during the steady state stage of all tests with the AHTFs and water was similar.

7.4.2.2 Radiator Heat Output - Case1 Thermostat Tests

The following two figures represent the evaluated $\dot{Q}_{output}$ for the thermostat tests in Case 1 of the optimised scenario, when using the 50% HX/W and 50% EG/W mixtures.

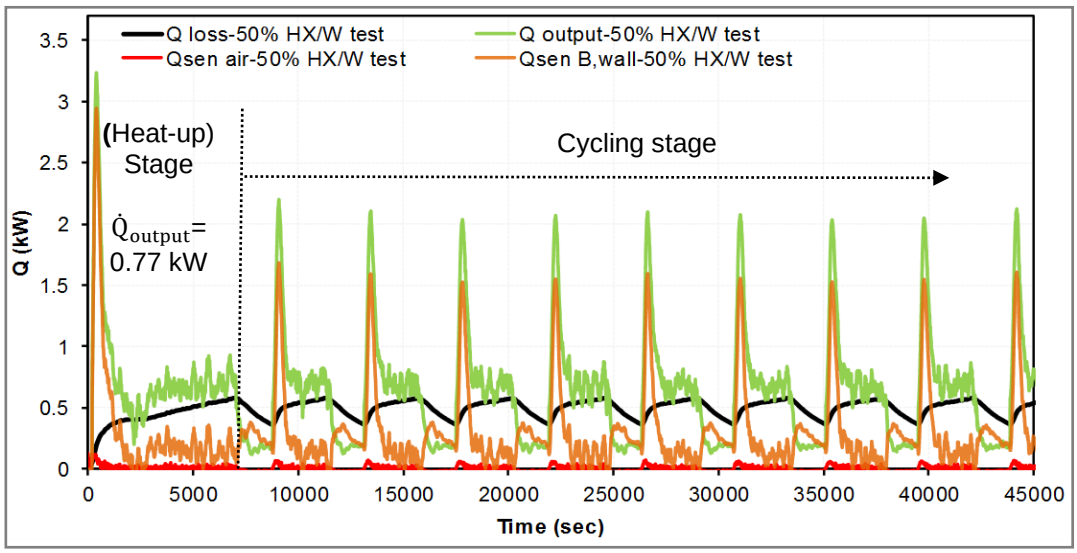

Figure 7.8: Heat Output from Radiator for Case 1 Thermostat of 50% HX/W Test

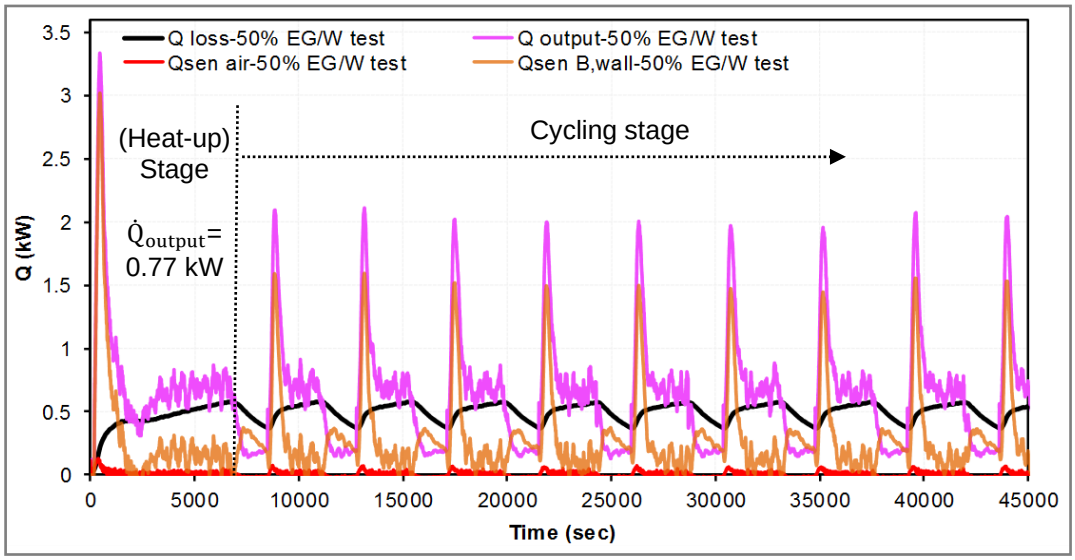

Figure 7.9: Heat Output from Radiator for Case 1 Thermostat of 50% EG/W Test

Figures 7.8 and 7.9 show consistency between the heat output calculated during the 'on' and 'off' heating cycles. The average $\dot{Q}_{output}$ calculated during the heat-up stage was 0.77 kW in both the 50% HX/W and 50% EG/W tests, which is higher than the average recorded with the water test by 8%. The average $\dot{Q}_{output}$ calculated during the 'on' heating

cycles of the 50% HX/W and the 50% EG/W tests was 0.71 kW with a variation of ± 0.08 kW, while the average calculated during the 'off'' heating cycles was 0.25 kW with a variation of ± 0.06 kW. These values are similar to those obtained from the base case (water) tests: 0.70 kW and 0.24 kW for the 'on' and 'off' cycles, respectively. A similar amount of heat was released from the radiator when operating with the 50% HX/W mixture, the 50% EG/W mixture, and water. However, using the AHTFs within the radiator influenced the duration of the heat-up stages and heating 'on' and 'off' cycles. This is due to their low specific heat capacity, which enables them to absorb and release heat faster than water.

7.4.2.3 Radiator Heat Output - Case 2 Steady State Test

The heat output calculated with Case 2 of the optimised scenario tests (ΔT across the radiator surface controlled at 10K) is presented in Figure 7.10.

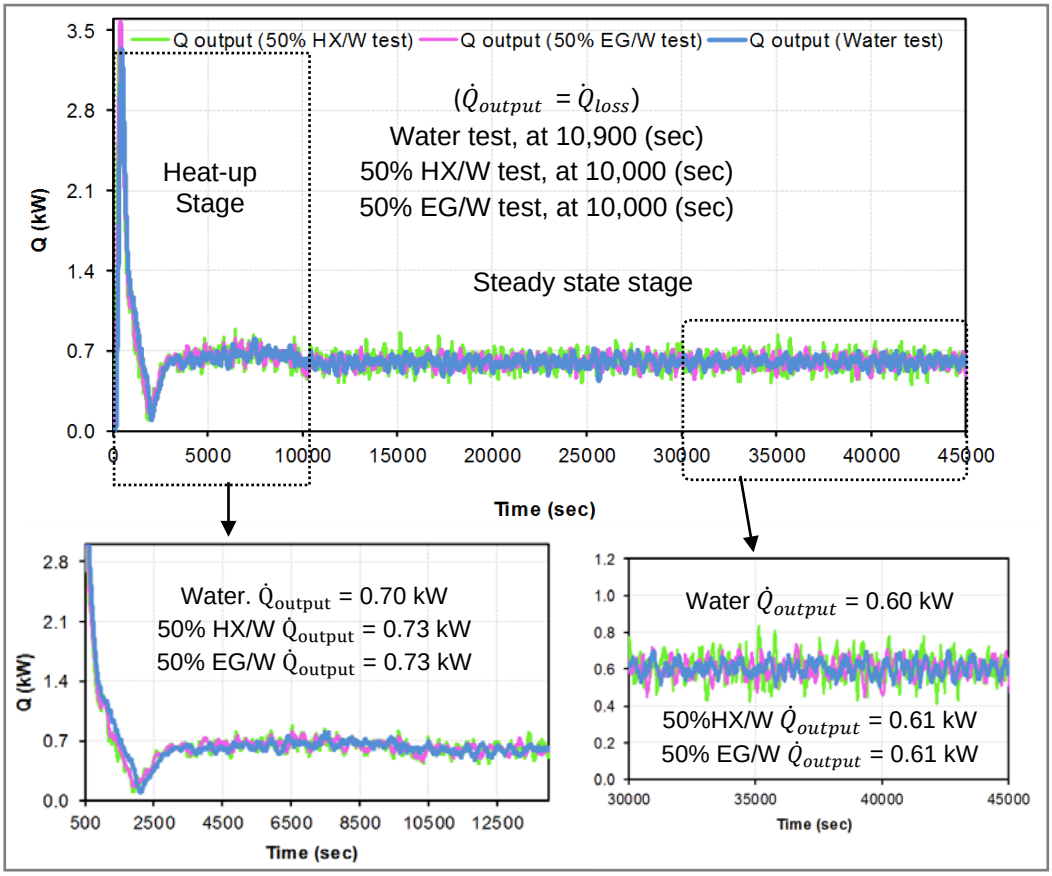

Figure 7.10: Radiator Heat output for Case 2 Steady State Tests

As Figure 7.10 illustrates, the duration of the heat-up stage when using the 50% HX/W and 50% EG/W mixtures was 10,300 seconds (2 hours and 52 minutes), which is 6% shorter than the duration of the heat-up stage when using water, which was 10,900 seconds (3 hours and 2 minutes). The heat output during the heat-up stage was higher (by 4%) when using the 50% HX/W and 50% EG/W mixtures, in comparison to water, while the readings during the steady state stages of each test were similar.

7.4.2.4 Radiator Heat Output - Case 2 Thermostat Test

The heat output calculated with Case 2 of the thermostat tests for all tested fluids is presented in Figure 7.11.

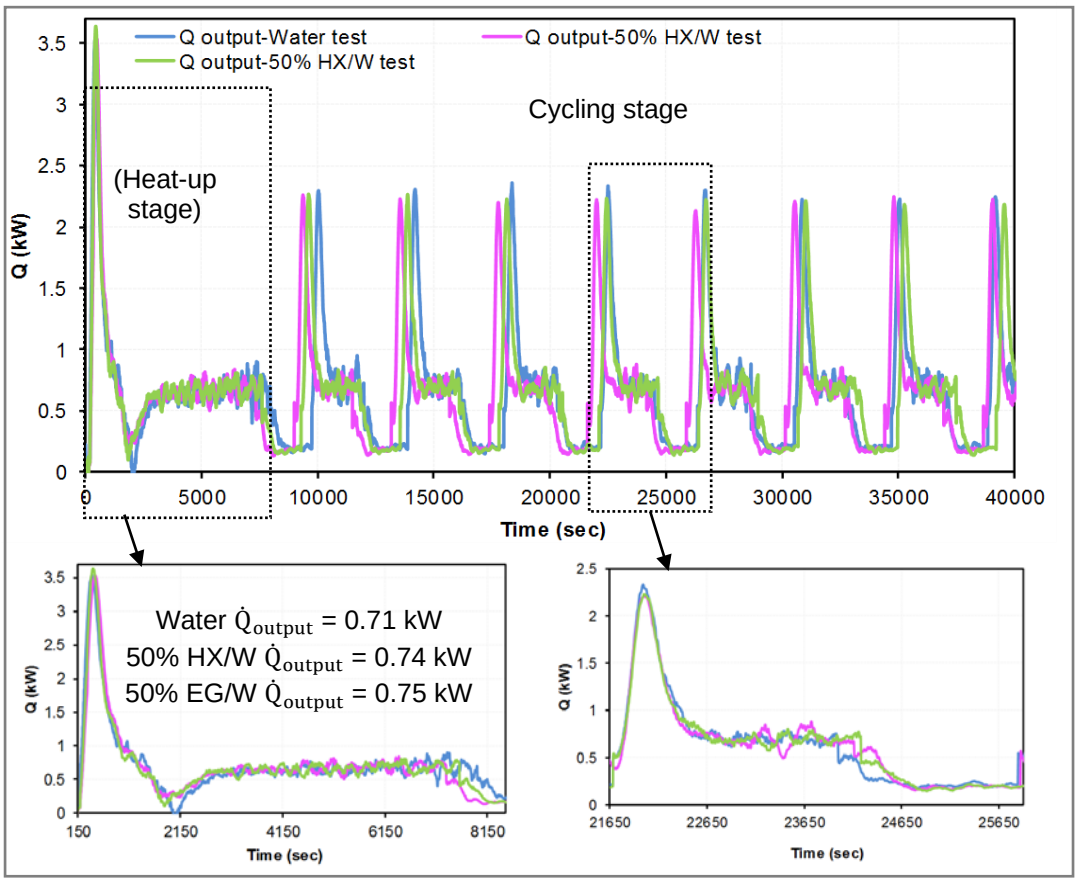

Figure 7.11: Radiator Heat Output for Case 2 Thermostat Tests

Figure 7.11 shows that the duration of the heat-up stage was slightly shorter when using the 50% HX/W and 50% EG/W mixtures within the system, in comparison to water. The

average $\dot{Q}_{output}$ calculated during the heat-up stages of the 50% HX/W and 50% EG/W tests was 0.74 kW and 0.75 kW, respectively. During the second stage of the tests, the average $\dot{Q}_{output}$ evaluated during the 'on' cycle when using the 50% HX/W and 50% EG/W mixtures was approximately 0.70 kW (with a variation of ± 0.06 kW), and during 'off' cycle, approximately 0.24 kW (with a variation of ±0.07 kW). This proves that the HRHS performed in a similar way when the AHTFs and water were used, as the amount of heat released from the radiator to the air-side was similar for all tests.

7.5 Benefits of Using the AHTFs in Heating System

The AHTFs were considered as a way of overcoming the limitations of water as a heat transfer fluid within a heating system. The comparative analysis between the effects of the examined fluids revealed that using the 50% HX/W and 50% EG/W mixtures as AHTFs in the HRHS influenced the operation of the system in the following ways:

- The application of the AHTFs reduced the duration of the heat-up stage, meaning that the heated space reached the desired temperature faster than when using water. This will be useful in real-life applications as the heated space will heat up faster.
- The thermal performance of the radiator was enhanced during the heat-up stage.
- The return temperature from the radiator was lowered (by adapting the radiator mass flow rate), helping to reduce the amount of heat loss from the return pipes.
- Better uniformity was seen for the distribution of temperature across the radiator surface.

Additionally, there are other benefits of using the 50%HX/W and 50% EG/W mixtures as alternatives to water:

- The AHTFs have a lower freezing point compared to water (see Tables 3.5 and 3.7 of Chapter 3). This provides a level of safety against the potential burst pipes and the resulting damage to the systems and buildings that can be caused by harsh weather during the winter.
- The 50% HX/W mixture is an anti-corrosion fluid, meaning that by using the 50% HX/W mixture, the metal components of the HRHS are protected, reducing the system's maintenance cost.

7.6 Summary

This chapter presented the evaluated heat output ($\dot{Q}_{output}$) from the radiator when using the energy balance approach. This approach enables the evaluation of the radiator's heat output, without considering the properties of the working fluids. It also helps overcome the limitations of the BS EN 442-2 standard in applying AHTFs within a heating system. The energy balance approach was first used to evaluate the radiator heat output for the base case (water) tests to ensure that it was validated for further use when examining the behaviour of the AHTFs within the radiator. This approach allowed the heat output from the radiator to be calculated during different stages of the test, including the heat -up and steady state stages. It also enabled the evaluation of the heat output during the 'off' heating cycles (when there is no flow of hot fluid through the radiator). The thermal performance of the radiator when operating with the 50% HX/W and 50% EG/W mixtures was evaluated for each different test scenario (drop-in and optimised scenarios). The results demonstrated that using the AHTFs within the radiator influenced the operating behaviour of the heating system.

For the drop-in scenario, the heat output from the radiator when using the 50% HX/W and 50% EG/W mixtures dropped by 15% and 10% respectively, in comparison with water. This reduction is due to the varying flow rates amongst the examined fluids, as the 50%

HX/W and 50% EG/W mixtures are denser than water, which affects the flow rate within the system. The results from the optimised scenario tests revealed that the thermal performance of the radiator was enhanced during the heat-up stage when operating with the examined AHTFs. This is due to the faster response of these fluids in absorbing heat and therefore raising their temperature (due to their lower specific heat capacity), in comparison with water. Contrastingly, the thermal performance of the radiator was similar throughout the steady state stages of all tests, including the base case test. It was also observed that the operating behaviour of the HRHS working with the 50% HX/W and 50% EG/W mixtures was changed. The shorter heat-up stage recorded when using the AHTFs also had an impact on the ‘on’ and ‘off’ heating cycles in the cycling stage of the test.

CHAPTER 8

Conclusions and Recommendations for Future Research

8.1 Introduction

Heat transfer fluids are essential in all wet heating and cooling systems, water being the predominant heat transfer medium due to its availability, low price and acceptable thermal properties. However, water does have limitations in terms of its heat transfer rate within energy-intense systems and reduced effectiveness as a result of aeration, oxidation and fouling. In addition, water has a high freezing point (0°C) which introduces the risk of pipes freezing and bursting during colder periods or in cooler climates. Alternative heat transfer mediums, including nanofluids, are increasingly being proposed in various industries to overcome the limitations associated with water.

The literature review carried out in this project illustrated that a little work has been conducted into the measurement of radiators' performance at actual operating conditions. Moreover, no work has been done to investigate the effect of alternative heat transfer fluids (AHTFs) on the performance of hydronic radiators. Therefore, this project investigated how different heat transfer mediums can be used as a replacement for water within a hydronic radiator heating system (HRHS), exploring the effects of the AHTFs on the performance of the panel radiator specifically. This chapter presents the conclusions that can be drawn from the research carried out and addresses the objectives of the project that were outlined in Chapter 1. Additionally, it provides recommendations for the direction of future research. The project involved designing and constructing a test facility and method that enabled the examination of the thermal performance of an HRHS under controlled conditions.

The results revealed that the properties of each examined fluid had an impact on the performance and operational behaviour of the system. When using the 50% HX/W mixture and its base fluid of 50%EG/W as AHTFs, the system took a shorter amount of time to heat up, and therefore had a different duty cycle to that produced when using water. The shorter heat-up period resulted in better energy performance; less energy was required for the system to reach the same internal temperature. However, the amount of energy saved decreased gradually over the course of the tests due to the slightly longer duty cycle. Better system performance was achieved when using these fluids when the mass flow rate in the system was fixed at a similar rate to that which was calculated for the water tests. This resulted in greater uniformity in the distribution of temperatures across the radiator surface, and a lower return temperature (by 2K), providing an opportunity to reduce the amount of heat loss from the return pipes in a real-life application.

8.2 Achieving the Project's Objectives

Six objectives were set at the beginning of this project and are outlined in Chapter 1. The following section explains how each objective was met and achieved.

1. **To provide a critical literature review of research on heat transfer fluids in the built environment and current research on alternative nanofluids and their applications in the heat transfer field.**

Chapter 2 provided an analysis of relevant research on heat transfer fluids, including nanofluids and their properties and applications. Besides, investigate the studies related to enhancing the performance of hydronic heating systems were evaluated, which indicated that no work had been conducted to examine the performance of a HRHS while using AHTFs under actual operating conditions.

2. **To understand the thermophysical properties of the proposed heat transfer fluids and compare these properties with the values available in the literature.**

Understanding the thermophysical properties of a heat transfer fluid is key to properly sizing the equipment within a HRHS, such as the pump and pipes. The thermophysical properties of the 50% HX/W mixture were investigated and compared to the 50% EG/W mixture. The results showed that the thermophysical properties of the 50% EG/W mixture were enhanced by approximately 5% in the 50% HX/W mixture. The effective thermal conductivity of the 50% HX/W mixture was also evaluated using two theoretical models. A positive correlation was found between the experimental results and the predicted findings from the theoretical models.

3. **To design and construct a bespoke test facility which can be used to carry out the performance tests, using different heat transfer fluids within a HRHS under controlled conditions.**

Chapter 4 provided a detailed description of the test facility that was built for the purpose of this research. The test facility was designed to replicate a small, residential room that is heated using a standard hydronic heating system with controlled heat loss to the ambient. This was achieved by using specific dimensions for the booth, which had a volume of 1.95 m (W) x 2.10 m (H) x 1.17 m (D). A radiator, air thermostat and other instruments used to monitor, and record data were installed inside the booth.

The booth was placed inside the environmental chamber, which was controlled at a temperature of 9ºC and relative humidity of approximately 50%. The system supplying the heat was a controlled system; the heat was provided using an electrical heater, which was controlled by a PID controller to provide 75ºC flow temperature to the radiator, and the hot fluid was circulated through the system using a pump. The amount of energy consumed by the electrical heater and the pump was recorded using a power meter, which enabled a comparative analysis between the examined fluids. The reasons for choosing

an electrical heating system were its superior control settings and the ability to measure energy, as well as the new legislations surrounding electrical heat.

4. **To develop a test procedure and performance evaluation approach that enables credible comparison between the proposed alternative fluids and water as a base case HTF under the same controlled conditions.**

This objective was addressed in Chapter 4, where it was applied to testing all examined fluids in order to produce comparative results. The challenge of this task was achieving a testing method that could be applied to all heat transfer fluids within the panel radiator whilst continuously monitoring and recording the energy consumption and the indoor air temperature. Therefore, the testing method was developed carefully in order to ensure consistency and repeatability. This meant that all experiments begun under the same conditions, including the same initial temperature of the bulk fluid in the buffer tank. Different scenarios were used for testing the AHTFs in order to cover all the parameters that could potentially affect the performance of the system. The results presented in Chapter 6 demonstrate that this objective was successfully met.

5. **To validate the test facility by conducting base-case experiments using water as a heat transfer fluid.**

This objective was achieved after creating the test facility and developing a reliable testing method. The results of the base case experiments are presented in Chapter 6. A base case was established by using the criteria specified in the BS EN 442-2 standard: ΔT across the radiator of 10K and flow and return temperatures of 75ºC and 65ºC, respectively. The base case test was carried out two times to ensure repeatability and consistency of data. The duration of each test was also considered to ensure consistency between the data recorded and the system's behaviour. Two methods of testing (steady state and thermostat tests) were performed, and the results of these experiments (IBT, energy consumption, ΔT across the radiator and the uniformity of temperature distribution

on radiator surface) were set as benchmarks for comparison with the AHTF tests. The results were also analysed to validate the steady state conditions of each test, in accordance with the BS EN 442-2 standard.

6. **To conduct a range of experiments under controlled conditions to investigate the performance of the HRHS when using the proposed AHTFs, by analysing both the amount of energy consumed and the air temperature inside the booth**

The results presented in Chapter 6 demonstrate how this objective was successfully met by conducting a wide range of tests to obtain reliable and accurate data. Two different test scenarios were considered to enable comparative analysis between the examined fluids:

1. Drop-in scenario

This scenario was designed to replicate a situation where the alternative fluid is charged into the heating system as a replacement for water without changing the system setting.

2. Optimised scenario

This scenario was created to measure the effects of controlling various parameters within the HRHS (mass flow rate and ΔT across the radiator) when using AHTFs as a replacement for water.

Results from all experiments with water and the AHTFs were examined and are represented in various graphs in Chapter 6. Several conclusions can be drawn from analysing the results:

- The drop-in scenario test results revealed that the properties of the different fluids have an impact on the flow rate within the system. The flow rate dropped by 9%, 32% and 46% when the denser and more viscous fluids (30% EG/W, 50% EG/W and 50% HX/W) were used. As a result, the HRHS operated differently, which then affected the system output, and thus the internal booth temperature (IBT) and energy consumption. A lower IBT was recorded when using the 50% EG/W and 50% HX/W mixtures as heat transfer fluid, in comparison to water. At the same time, less energy

was consumed with the AHTF tests, compared to the base case results, as shown in section 6.4.1 of Chapter 6. The IBT recorded when using the 50% EG/W and 50% HX/W mixtures was 23.4ºC and 22.54ºC, respectively, compared to 24.83ºC recorded when using water. Similarly, the amount of energy consumed was lower when using the AHTFs (see Figure 6.17 of Chapter 6). The IBT and energy consumption recorded with the 30% EG/W test were very similar to those recorded with the water tests.

- The results of the optimised scenario tests showed that the type of fluid influenced the working conditions of the radiator, which resulted in a shorter heat-up period. This is due to the lower specific heat capacities of the examined AHTFs, in comparison to water.
- By adapting the mass flow rate within the system to 0.014 kg/s when using the examined AHTFs resulted in greater ΔT across the radiator (by 18%), a lower return temperature (by 2K) and better uniformity in the temperatures recorded across the radiator surface.
- By controlling the ΔT across the radiator at 10K when experimenting with the AHTFs, a higher mass flow rate (by 17%) was calculated, in comparison to the base case water tests. Thus, in real-life application, upgrade of the system's components (pipes and pump) may be required if the HRHS had been designed for water without adequate contingencies.
- The results of the experiments carried out showed that 30% EG/W mixture behaved in a similar way to water within the HRHS. The 50% HX/W mixture (as a nonfluid) and its base fluid, the 50% EG/W mixture, also behaved similarly in the HRHS. This could be due to little enhancement in thermophysical properties between the 50% HX/W mixture and its base fluid.

Another achievement of this project was successfully creating a performance evaluation approach, which is outlined in Chapter 5, and demonstrated in Chapter 7. The approach,

which is based on the energy balance principle, was created to evaluate the heat output from the radiator when using AHTFs, as the current model (EN BS 422-2) is only applicable to radiators operating with water or steam as a heat transfer medium. Developing the energy balance approach was particularly challenging, as the idea was to evaluate the heat output from the radiator without considering the thermal properties of the heat transfer fluids.

The main parameter that was considered when developing the energy balance approach was the instantaneous change in air temperature inside the heated zone (booth). The heat output from the radiator into the booth (air-side) was measured when using the AHTFs. This approach allowed the heat output from the radiator during steady state and transient conditions, as well as during 'off' heating periods (when there is no flow entering the radiator), to be assessed, with an uncertainty of ± 3.3%. The results obtained when applying the energy balance approach prove that using the 50% HX/W and 50% EG/W mixtures within the HRHS enabled a similar amount of heat to be produced by the radiator as that obtained from base case (water test).

8.3 Contribution to the knowledge

This section outlines the original contribution to the knowledge of this research work. This research makes contributions by:

- Designing a bespoke test facility and methodology for conducting repeatable tests which evaluate the performance of a HRHS when using different heat transfer fluids under the same environmental conditions.
- Developing an innovative approach (based on the energy balance principle) to evaluating the heat output from a radiator when operating with AHTFs. This approach allows assessing the heat output during steady state and transient conditions, as well as during the period when the heating system is 'off'. Also, it helps to overcome the

limitations of the BS EN 442-2 model, which is only applicable to radiators that operate with water or steam.

- Providing a better understanding of the performance of radiator heating systems when using alternative fluids in terms of flow, temperature and energy.

8.4 Recommendations for Future Work

Based on the conclusions made in this project, further work is required to investigate the following:

1. Based on the result obtained from this research work, it was noticed the 50% HX/W and 50% EG/W mixtures raising the temperature faster compared to water. Therefore, investigation of using these fluids in solar panels as an absorbing medium need to be considered. Also, these fluids could be investigated in cooling and refrigeration systems.
2. Look into a possibility of modelling the heat and mass transfer for the 50% HX/W and 50% EG/W mixtures in the system. In order to control more parameters that could influence the behaviour the fluids in the system such as, Reynold number and flow temperature.
3. Look into a possibility of investigating different concentrations of the nanoparticles with the nano-based fluid HX, to get optimum concentration which could enable better enhancement in the thermophysical properties of this fluid (HX) compared to its base fluid.
4. Test other types of nanofluids, utilising the test facility that was developed during this project.

REFERENCES

1. Anisimova, N., ‘’The Capability to Reduce Primary Energy Demand in EU Housing’’, Energy and Buildings. Vol. 143, Issue 10, Pp.2747–2751, October 2011. DOI: 10.1016/j.enbuild.2011.06.029

2. Waters L., “Energy Consumption in the UK “Department of Business, Energy and Industrial Strategy, 2016.

3. Waters L. “Energy consumption in the UK “Department of Business, Energy and Industrial Strategy, 2018.

4. Nick K., Paul T.’’ Future Energy Demand in the Domestic Sector’’2012, Available from, http://www.topandtail.org.uk/publications/n.kelly.wp2%201reportfutureenergydemand.pdf

5. ASHRAE Handbook, Fundamentals. Atlanta: American Society of Heating, Refrigerating and Air-Conditioning Engineers, Inc, 2005.

6. Environmental product declaration https://epdturkey.org/wpcontent/uploads/hydromx_iso_14025_epdturkey_en.pdf

7. Chaer, I. ‘’Comparison of the Heat Transfer Through Hydromx with That of Water. Witness Report, London South Bank University, Department of Urban Engineering, 2013.

8. Wet Central Heating Systems: Treatment of Heat Transfer Modifiers, Inhibitors, Flushing Techniques and Inline Cleaners In the National Calculation Methodology for Energy Rating of Dwellings’’ June 2014. Available from: Https://www.ncmpcdb.org.uk/sap/filelibrary/pdf/principle%20papers/sap-principle-paper-treatment-of-heat-transfer-modifiers-inhibitors-flushing-techniques-and-inline-cleaners-v1.2.pdf

9. Andrej L., Youngsuk N., Evelyn W. ‘’ Solar Thermal, Heat Transfer Fluids’’ Annual Review of Heat Transfer 15, 2012. Available from: https://www.researchgate.net/publication/271198334

10. Ennis T. ‘’ Safety in Design of Thermal Fluid Heat Transfer Systems’’ Cheshire: Haztech Consultants Ltd (2009).

11. Srivastava U., Malhotra R. and Kaushik S. “Recent Developments in Heat Transfer Fluids Used for Solar Thermal Energy Applications” Fundamental Renewable Energy Application, 2015.

12. PA Press Association Personal Finance Correspondent, PA Money News, Article by Vicky Show, 5 June 2018.

13. Bhatia S.C.'' Advanced Renewable Energy Systems- Solar thermal energy '', 2014. Available From:https://www.sciencedirect.com/topics/engineering/glycol-system

14. Saif E.'' Protecting Glycol-Water Closed Systems'' Technical Bulletin 3-004,2011. Available from:https://www.scribd.com/document/127131604/CATB3-004-2-11

15. Choi, S.U.S and Jeffrey A. E.," Enhancing Thermal Conductivity of Fluids With Nanoparticles" Energy Technology Division and Materials Science Division, Argonne National Laboratory, Argonne, Illinois,1995. Available from: http://www.iaea.org/inis/collection/nclcollectionstore/_public/27/043/27043758.pd

16. Younes, H. Christensen G., Li, D., Hong H., Ghaferi A. "Thermal Conductivity of Nanofluids: Review "Journal of Nanofluids, Vol. 4, Number 2 - Pp. 107-132 (26), 2015.

17. Yimin X. , Qiang L. '' Heat Transfer Enhancement of Nano-Fluids'' School of Power Engineering, Nanjing University of Science and Technology, Nanjing 210094, 1999. Available from: http://www.sciencedirect.com/science/article/pii/s0142727x99000673

18. Maxwell, J. C. A "Treatise on Electricity And Magnetism" Oxford, NY, UK: Oxford: Clarendon, 1873. Available From: http://www.aproged.pt/biblioteca/maxwellii.pdf

19. Wei Yu. and Huaqing Xie. ''A Review on Nanofluids: Preparation, Stability Mechanisms, and Applications'' Journal of Nanomaterial, Article ID 435873, Hindawi Publishing Corporation 2012.

20. Dongsheng W., Yulong D. "Formulation of Nanofluids for Natural Convective Heat Transfer Applications'2005, International Journal of Heat and Fluid Flow Vol.26, Pp.855–864, 2005.

21. Choi, S., Eastman, J. A., Li, S., Yu W. and Thompson, L.'' Increased Effective Thermal Conductivities of Ethylene Glycol-Based Nanofluids Containing Copper Nanoparticles'' Appl. Phys. Lett., 78(6), Pp. 718-720, 2001.

22. Yanjiao Li A., Jing'en Zhou A., Simon T. "A Review on Development of Nanofluid Preparation and Characterization" Powder Technology 196 – Pp. 89–101, 2009.

23. Sarit K., Stephen U., Choi, S., Yu T. "Nanofluids, Science and Technology", John Wiley & Sons, Inc, 2008.

24. Nader N. 'Engineering Nanofluids for Heat Transfer Applications 'Doctoral Thesis In Materials Chemistry, Stockholm, Sweden 2014. Available from: http://www.diva portal.org/smash/get/diva2:712511/fulltext01.pdf

25. Unilab S. '' What are Nanofluids and Which are Their Applications?'' 2013. Available from:http://www.unilab.eu/wp-ontent/uploads/2013/09/newsletter_9_nanofluid_eng.pdf

26. Lee, S., Choi, S., Li, S., And Eastman, J. A. "Measuring Thermal Conductivity of Fluids Containing Oxide Nanoparticles." Transactions of the ASME. Journal of Heat Transfer, 121(2), Pp. 280-289, 1999.

27. Yu, W., France, D., Routbort, J. and Choi, S. ‘’Review and Comparison of Nanofluid Thermal Conductivity and Heat Transfer Enhancements, ‘’ Heat Transfer Eng., 29(5), Pp. 432-460, 2008.

28. Ibrahim P., Sanjeeva W., Zafira M., Yulong D. ‘’Stability of Glycol Nanofluids – the Consensus Between Theory and Measurement’’ Institute of Particle Science and Engineering, School of Process, Environmental and Materials Engineering, University of Leeds.Uk. Available from: http://ac.els-cdn.com/s0017931011002699/1-s2.0-s0017931011002699-ain.pdf?tid=f5d43f5c-b60b-11e5-89d5-00000aacb361&acdnat=1452259999_21748d1717370ad1da9e14fca0c395f4

29. Kin Y, L. ‘’ The Effect of Surfactant on Stability and Thermal Conductivity of Carbon Nanotube-Based Nanofluids’’ Department of Mechanical Engineering University of Pertahanan Nasional Malaysia. Available from: http://www.doiserbia.nb.rs/img/doi/0354-9836/2014%20online-first/0354-98361400078l.pdf

30. Yimin X., Qiang L., Peng T. ‘’The Effect of Surfactants on Heat Transfer Feature of Nanofluids’’ Experimental Thermal and Fluid Science Journal.2012.

31. Sayantan M., Somjit P. “Preparation and Stability of Nanofluids- a Review “ IOSR Journal of Mechanical and Civil Engineering, E-Issn: 2278-1684, P-ISSN: 2320-334x, Vol. 9, Issue 2, Pp. 63-69, 2013.

32. Hwang Y., Lee J., Lee C., Jung Y., Cheong S., Lee C., Ku B., Jang S. ‘’Stability and Thermal Conductivity Characteristics of Nanofluids’’ Thermochim. ACTA 455, Pp.70–74, 2007.

33. Wei X., Zhu H., Kong T., Wang L. ‘’Synthesis and Thermal Conductivity of Cu_2O Nanofluids’’ International Journal of Heat and Mass Transfer Vol.52 - Pp.4371–4374, 2009.

34. Fovet Y., Gal J., Chemla T. ‘’Influence of PH and Fluoride Concentration on Titanium Passivating Layer: Stability of Titanium Dioxide’’, ATLANTA 53 (5), Pp.1053–1063, 2001.

35. Xian-Ju W. and Xin-Fang, L. “Influence of PH on Nanofluids' Viscosity and Thermal Conductivity,” Chinese Physics Letters, Vol. 26, No. 5, Pp.. 056601, 2009

36. Devadatta P. and Kulkarni “Comparison of Heat Transfer Rates of Different Nanofluids on the Basis of The Mouromtseff ‘ Number” 2007. Available from: http://www.electronicscooling.com/2007/08/comparison-of-heat-transfer-rates-of-different-nanofluids-on-the-basis-of-the-mouromtseff-number

37. Laura F., Laura C., Sergio B., Simona B. and Filippo A. ‘’Experimental Stability Analysis of Different Water Based Nanofluids’’ Springer Open, Nanoscale Research Letters 2011. Available from: Http://www.nanoscalereslett.com/content/6/1/300.

38. Elena V. ‘’Nanofluids for Heat Transfer – Potential and Engineering Strategies, Two-Phase Flow, Phase Change and Numerical Modeling’’, ISBN: 978-953-307-584-6, 2011. Available from: http://www.intechopen.com/books/two-phase-flow-phase-change-and-numericalmodeling/nanofluids-for-heat-transfer-potential-and-engineering-strategies

39. Wang X., Xu X. and Choi S U.S., “ Thermal Conductivity of Nanoparticle–Fluid Mixture” Journal of Thermophysics and Heat Transfer, Vol. 13, No. 4, October–December 1999. Available from: http://web.me.iastate.edu/wang/1999_j.%20thermo.%20and.%20ht_nanofluid.pdf

40. Hamilton R. and Crosser O. “ Thermal Conductivity of Heterogeneous Two-Component Systems”, Industrial & Engineering Chemistry Fundamentals, Vol. 1, No. 3, August 1962.

41. Davis, R. “ The Effective Thermal Conductivity of a Composite Material with Spherical Inclusions” International Journal of Thermo-Physics, Vol. 7, Issue 3, Pp. 609-620, 1986.

42. Bruggeman,D., ‘’Berechnung Verschiedener Physikalischer Konstanten Von Heterogenen Substanzen, I. Dielektrizitatskonstanten Und Leitfahigkeiten Der Mischkorper Aus Isotropen Substanzen’’. Annalen Der Physik, Leipzig, 24, Pp. 636–679, 1935.

43. Khalil K. and Kambiz V. ‘’ A Critical Synthesis of Thermos Physical Characteristics of Nanofluids ‘’ International Journal of Heat and Mass Transfer Vol. 54, Pp.4410–4428, 2011.

44. Jacopo B., David C., Venerus, Et Al.” A Benchmark Study on the Thermal Conductivity of Nanofluids” Published By the AIP Publishing Llc. Journal of Applied Physics. 106, 094312, 2009. Http://Dx.Doi.Org/10.1063/1.3245330

45. Paul G., Chopkar M., Manna I., Das P. ‘’ Techniques for Measuring the Thermal Conductivity of Nanofluids: A Review ” Renewable and Sustainable Energy Reviews, Vol.14, Pp.1913–1924, 2010.

46. Xie H., Wang J., Xi T., Liu Y., Ai F., and Wu Q. " Thermal Conductivity Enhancement of Suspensions Containing Nanosized Alumina Particles " Journal of Applied Physics, Vol. 91, Pp. 4568-4572, 2002.

47. Choi, S., Zhang, Z., Yu, W., Lockwood, F., and Grulke, E. ‘’ Anomalously Thermal Conductivity Enhancement in Nanotube Suspensions’’ Applied Physics Letters, Vol. 79, Pp. 2252-2254, 2001.

48. Han Z., “ Nanofluids with Enhanced Thermal Transport Properties ”, Dissertation Submitted to the Faculty of the Graduate School of the University of Maryland, College Park 2008.

49. Xiang-Qi W. and Arun S. ‘’ A Review on Nanofluids - Part I: Theoretical and Numerical Investigations’’ Brazilian Journal of Chemical Engineering, Vol. 25- No. 04, Pp. 613 - 630, 2008.

50. Nelson I., Banerjee D., Ponnappan R. ‘’ Flow Loop Experiments Using Polyalphaolefin’’ Journal Theosophy’s Heat Transfer Vol. 23, Pp.752–761, 2009.

51. Shin D. and Banerjee D. ‘’ Enhanced Specific Heat of Silica Nanofluid’’ ASME J. Heat Transfer 133, 2011.

52. Saidur R., Leong K., Mohammad H. “ A Review on Applications and Challenges of Nanofluids “ Renewable and Sustainable Energy Reviews, Vol.15, Pp.1646–166, 2011.

53. Golakiya S., Sarvaiya B., Makwana S., Thumar A., Rathwa M.’’ Analysis of Radiator With Different Types of Nanofluids’’ Journal of Engineering Research and Studies, Vol. 6,Issue I,Jan. 2015.

54. Leong K., Saidur R., Kazi S., Mamun A. ‘’ Performance Investigation of an Automotive Car Radiator Operated with Nanofluid Based Coolant (Nanofluid as a Coolant In a Radiator)’’. Appl Therm Eng. 30 (17–18): Pp. 2685–92, 2010.

55. Ramgopal V., Manikantan K., Hadi B., Vasudeva R.,’’ Enhancement of Heat Transfer Coefficient in an Automobile Radiator Using Multi-Walled Carbon Nanotubes (MWCNTS)’’ ASME, International Mechanical Engineering Congress and Exposition, Imece November 14-20, 2014.

56. Kuo K., Risha G., Evans B., Boyer E. “ Potential Usage of Energetic for Nano-Sized Powders for Combustion and Rocket Propulsion. Mater’’ Research Society Proceedings 2004.

57. Kulkarni D., Das D. and Vajjha R. ‘’ Application of Nanofluids in Heating Buildings and Reducing Pollution’’ Applied Energy, Vol. 86, No. 12, Pp. 2566–2573, 2009.

58. Verma V., Kundan L. ‘’ Thermal Performance Evaluation of a Direct Absorption Flat Plate Solar Collector (DASC) Using AL_2O_3-H_2O Based Nanofluids’’ IOSR Journal of Mechanical and Civil Engineering; Vol.6: Pp.29-35, 2013.

59. Mahendran M., Lee G., Sharma K., Shahrani A. and Bakar R. ‘’ Performance of Evacuated Tube Solar Collector Using Water-Based Titanium Oxide Nanofluid’’ Journal of Mechanical Engineering and Sciences (JAMES), Vol. 3, pp. 301-310, 2012.

60. Majgaonkar A. '' Use of Nanoparticles in Refrigeration Systems: A Literature Review Paper'' International Refrigeration and Air Conditioning Conference at Purdue, 2016.

61. Reji Kumar R., Sridhar K., Narasimha M. '' Transfer Enhancement in Domestic Refrigerator Using R600a/Mineral Oil/Nano-Al_2O_3 as Working Fluid'' International Journal of Computational Engineering Research, Vol. 03, Issue, 4, 2013.

62. Haque M., Bakar R., Kadirgama K., Noor M. and Shaka M. '' Performance of a Domestic Refrigerator Using Nanoparticles-Based Polyol Ester Oil Lubricant'' Journal of Mechanical Engineering and Sciences (JAMES), ISSN (Print): 2289-4659; E-Issn: 2231-8380; Vol. 10, Issue 1, Pp. 1778-1791, 2016.

63. Oluseyi O., Ajayi A., Daniel E.,et al.,. '' Investigation of the Effect of R134a/Al_2O_3 – Nanofluid on the Performance of a Domestic Vapour Compression Refrigeration System'' 2nd International Conference on Sustainable Materials Processing and Manufacturing, 2019.

64. Cong Q., Jinding H., Maoni L., Leixin G., Zhonghao R.'' Experimental Study on Thermo-Hydraulic Performances of CPU Cooled By Nanofluids'' Energy Conversion and Management, Vol.153, Pp. 557–565, 2017.

65. Ijam, A., Saidur, R., & Ganesan, P. '' Cooling of Mini-Channel Heat Sink Using Nanofluids' International Communications In Heat and Mass, Vol.39, Pp.1188-1194, 2012.

66. Material Safety Data Sheet (MSDS), Available from http://galaxyens.com/reports-certificates/01.pdf

67. 'What Is Hydromx'', Available from https://www.hydromx.com/our-technology/

68. Chaer I. and Haddowe S.,et al. '' Alternative Heat Transfer Fluid in Heating Systems-Energy Results from a Real Case Site'' 9th International Conference on Thermal Engineering: Theory and Applications, March 24-26 2016.

69. Lawrence G. 'How to Design a Heating System'' The Chartered Institution of Building Services Engineers (CIBSE), London, 2006.

70. BSI Standards Publication "Radiators and Convectors, Part 2: Test Methods and Rating'' BS EN 442-2, 2014.

71. Walters K. and Fine R. '' The Performance of Radiators and Convectors Using Medium Temperature Hot Water Laboratory Report '' Heating and Ventilation Research Association, 1973.

72. American Society of Heating, Refrigerating and Air-Conditioning Engineers Systems and Equipment Handbook (Si) '' Hydronic Heat- Distributing Units and Radiators'', (ASHRAE), 2000.

73. Mcintyre D. A. ‘’ Output of Radiators at Reduced Flow Rate’’ Building Services Engineering Research &Technology, Vol. 7, No. 2, 1986.

74. John S. ‘’Modern Hydronic Heating for Residential and Light Commercial Building’’ Delmar, Cengage Learning, 2012.

75. Fernandez-Seara J., Francisco J., Series J., Campo A. ‘’ A General Review of the Wilson Plot Method and Its Modifications to Determine Convection Coefficients in Heat Exchange Devices’’ Applied Thermal Engineering, Vol.27, ,et al.2745–2757, 2007.

76. Cengel Y. ‘’Heat and Mass Transfer a Practical Approach’’ Mcgraw Hill, CRC Press, 2006.

77. Long C. and Sayma N. ‘’Heat Transfer’’ Bookboon.Com, 2009.

78. CIBSE Guide C ‘’Reference Data’’ Chartered Institution of Building Services Engineers, 2007.

79. Mirmanto M., Sulistyowati E., Okariawan I. ‘’ Effect of Radiator Position and Mass Flux on the Dryer Room Heat Transfer’’ Results in Physics, Vol. 6, Pp. 139–144, 2016.

80. Embaye M. ‘’Enhancement of Panel Radiator Based Hydronic Central Heating System Using Flow Pulsation’’ A PhD Thesis, School of Mechanical Engineering, University of Birmingham, 2016.

81. Beck S., Grinsted S., Blackey S., Worden K.’’ A Novel Design for Panel Radiators’’ Applied Thermal Engineering, Vol 24, 1291-1301, 2005.

82. Labcell specialist instrumentation, Available from: http://www.labcell.com/environmental/thermal-analyser/kd2-pro-supplied-sensors-information

83. Kleiber M., Joh R. ‘’D3, Properties of Pure Fluid Substances, Liquids and Gases’’ VDI Heat Atlas, Pp.301-418,2010.

84. Engineering toolbox ‘’Ethylene glycol heat-transfer fluid.’’ https://www.engineeringtoolbox.com/ethylene-glycol-d_146.html

85. Hydromx Properties Investigation Report, Available from: http://hydromx.us/images/sertifikalar/source/hydromx_properties_investigation_report.pdf

86. Chartered Institution of Building Services Engineers, CIBSE Concise Handbook, London, 2008.

87. American Society of Heating, Refrigerating and Air-Conditioning Engineers ASHRAE ‘handbook fundamentals’’,2009.

88. Neutrium ‘’ Pressure Loss from Fittings – Excess Head (K) Method’’ Available from: https://neutrium.net/fluid_flow/pressure-loss-from-fittings-excess-head-k-method/

89. Getting Started With DT50, DT500 and DT600 Series Data Takes (Introductory Guide), Available from: http://www.datataker.com/downloads/dt500/docs/um0073a0.pdf

90. Moffat, R. "Contributions To the Theory of Single-Sample Uncertainty Analysis "Journal of fluids engineering, Vol. 104, Pp. 250-258, 1982.

91. Stephanie B.’’ A Beginner’s Guide to Uncertainty of Measurement’’ Centre For Basic, Thermal and Length Metrology National Physical Laboratory, Measurement Good Practice Guide No. 11.

92. CIBSE Guide B1, “CIBSE Guide B: Heating,” Institution of Building Services Engineers, Heating, London, 2002.ISSN

93. Ward, I.’’ Domestic Radiators: Performance at Lower Mass Flow Rates and Lower-Temperature Differentials Than Those Specified in Standard Tests’’ Building Serv. Eng. Res. TECHNOL. Vol.12, Pp.84-87,1991.

94. Childs K., Courville G. and Bales E. ‘’ Thermal Mass Assessment, an Explanation of The Mechanisms by Which Building Mass Influences Heating and Cooling Energy Requirements’’ ORNL/CON-97, 1983.

95. Vern L. ‘Uncertainties and Error Propagation Part I of a Manual on Uncertainties’2000. Available from: http://www.geol.lsu.edu/jlorenzo/geophysics/uncertainties/Uncertaintiespart2.html

96. Martin C. ’’ The Perfect Return – Heat Network Return Temperatures’’ 2016. https://www.cibsejournal.com/technical/the-perfect-return-heat-network-return-temperatures/ (accessed4/4/2019)

97. Pump specification https://www.pumpsalesdirect.co.uk/media/wysiwyg/datasheets/cp50.pdf

98. Quinn Radiators ‘Panel Radiator Range, General Specifications’ Available from: https://www.plumbaseindustrial.co.uk/general/sites/PI/quinnpanelradiators.pdf

99. MDF Thermal Properties, Available from: https://www.makeitfrom.com/material-properties/Medium-Density-Fiberboard-MDF

Appendix 2.A: Nanofluids Effective Thermal Conductivity

This appendix demonstrates the most common models that were found in the literature to estimate the effective thermal conductivity of nanofluids.

Remarks &Ref.	Models	symbols	Limitation of the models
Maxwell's model [18]	$K_{eff} = \frac{k_p+(n-1)k_f+(n-1)\phi_p(k_p-k_f)}{k_p+(n-1)k_f-\phi p(k_p-k_f)}$ kf	K_{eff} = the effective thermal conductivity of the solid-liquid mixture k_f = the thermal conductivity of the base fluid, k_p = the thermal conductivity of particles ϕ_p = the particle volume fraction α = thermal conductivity ratio (α = kp/kf) T= temperature	Maxwell model is applicable for a range of volume fraction Φp ≪1 OR | (kp/kf) − 1| ≪ 1 (best results can be obtained @ Ambient temperature).
Hamilton & Crosser model[40]	$\frac{K_{eff}}{k_f} = \frac{3(\alpha-1)\phi_p}{(\alpha+2)-(\alpha-1)\phi_p}\ [\phi_p + f(\alpha)\phi_p{}^2 + O(\phi_p)^3]$		Hamilton &Crosser model is applicable for a thermal conductivity ratio (Kp/Kf) equal or larger than 100 and it represents good results for smaller volume fraction Φp≤ 4%. (best results can be obtained at ambient temperature).
Bruggeman model [42]	$\frac{K_{eff}}{K_f} = \frac{\left[(3\emptyset p-1)\left(\frac{K_p}{K_f}\right)+[3(1-\emptyset_p)-1]+\sqrt{\Delta}\right]}{4}$ $\Delta = \left[(3\emptyset_p-1)\left(\frac{K_p}{K_f}\right)+\{3(1-\emptyset_p)-1\}\right]^2 + 8\ \frac{K_p}{K_f}$		Bruggeman model' is applicable for a large volume fraction of spherical particles. (best results can be obtained @ ambient temperature). For low-volume fractions, the Bruggeman model results reduce to the Maxwell model.
Khanafer&Vafai model [43]	$\frac{K_{eff}}{k_f}$ = 0.9843+0.398 $\emptyset_p{}^{0.7383}$ $\left(\frac{1}{d_p(nm)}\right)^{0.2246}$ $(\frac{\mu_{eff}(T)}{\mu_f(T)})^{0.0235} - 3.9517\ \frac{\emptyset_p}{T}$ +34.034$\frac{\emptyset_p{}^2}{T^3}$ + $32.509\frac{\emptyset_p}{T^2}$		Khanafer&Vafai model is based on nanoparticles diameter, volume fraction, and dynamic viscosity of water (base fluid). It is applicable for 1%≤ Φp≤ 9 %, 13 ≤ d ≤ 131 nm and 20°C ≤ T ≤ 70°C

Appendix 3.A: Effective Thermal Conductivity Calculator

This appendix presents pictures for effective thermal conductivity (k_{eff}) calculator (based on excel spreadsheets) that was developed during this project to predict the k_{eff} for the nanofluids. This calculator was developed based on Hamilton & Crosser [40] and Maxwell [18] models.

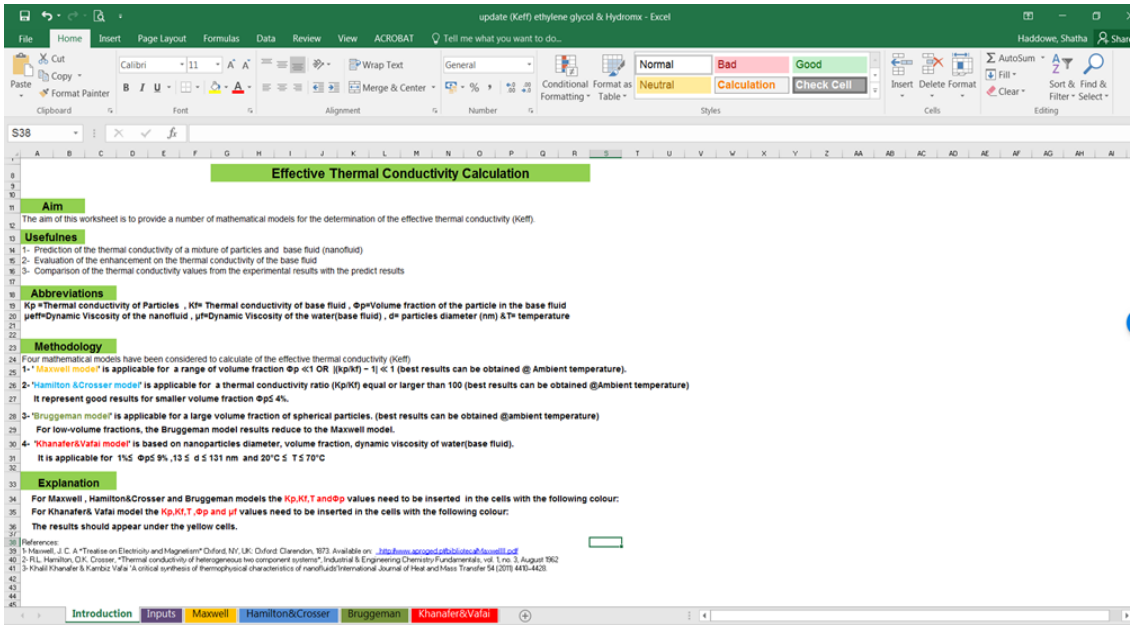

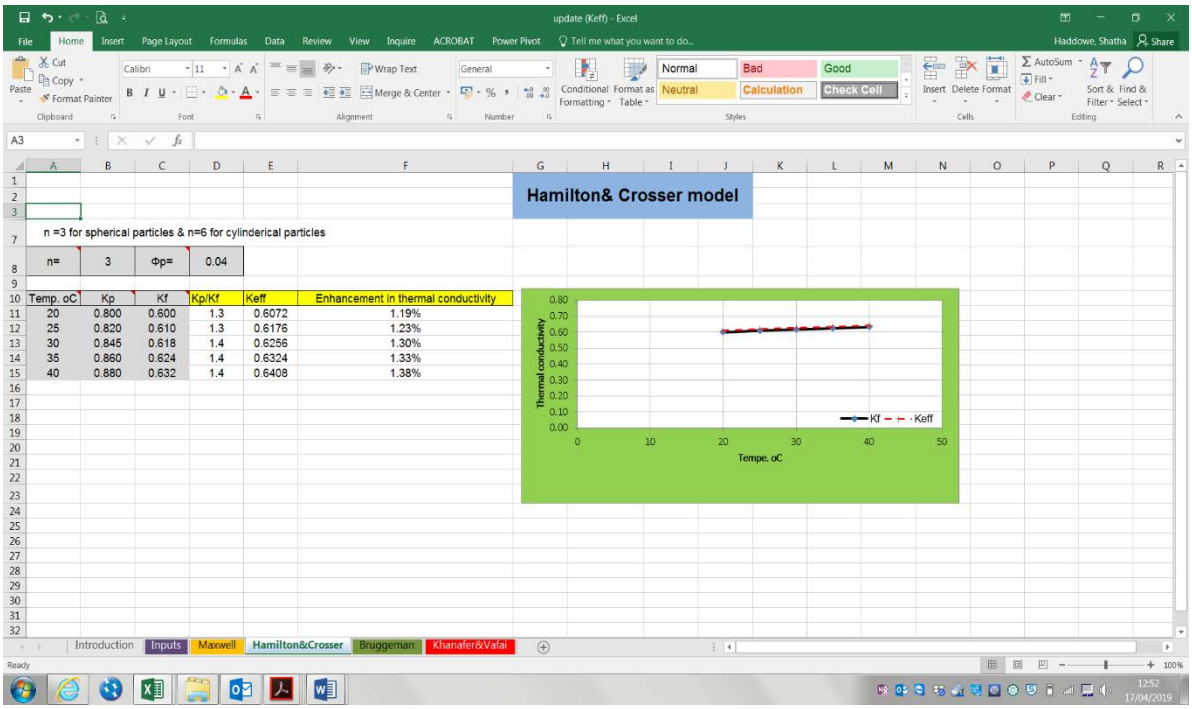

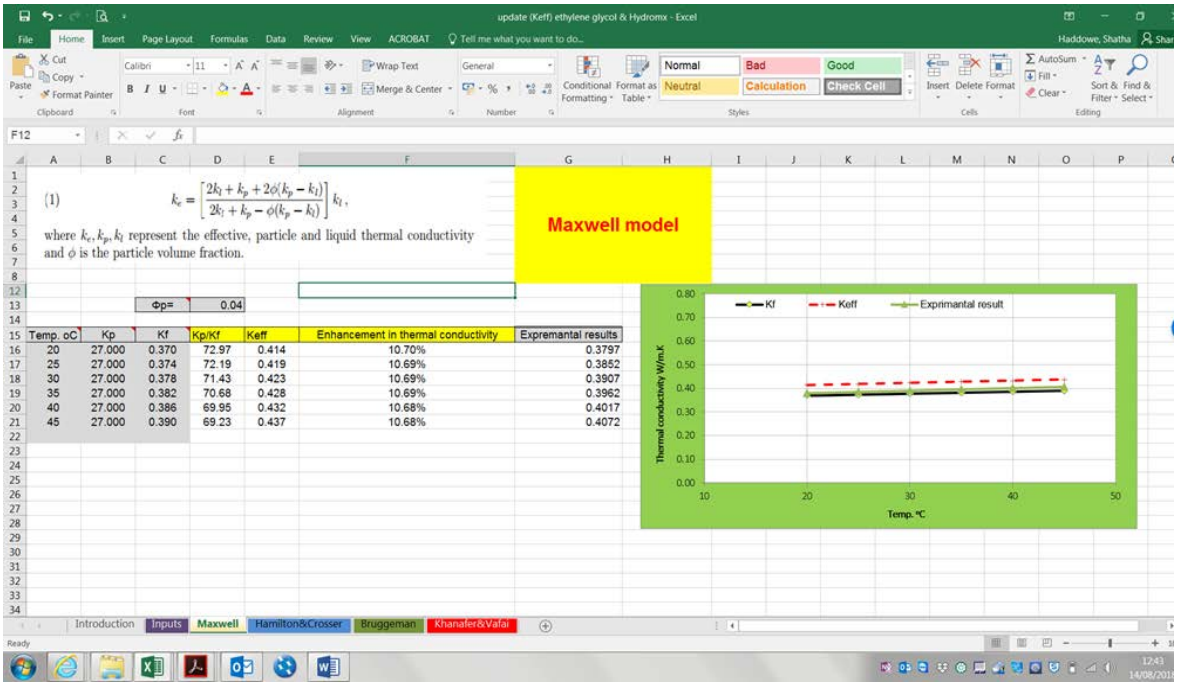

Temp. oC	Kp	Kf	Kp/Kf	Keff	Enhancement in thermal conductivity	Expremantal results
20	27.000	0.370	72.97	0.414	10.70%	0.3797
25	27.000	0.374	72.19	0.419	10.69%	0.3852
30	27.000	0.378	71.43	0.423	10.69%	0.3907
35	27.000	0.382	70.68	0.428	10.69%	0.3962
40	27.000	0.386	69.95	0.432	10.68%	0.4017
45	27.000	0.390	69.23	0.437	10.68%	0.4072

Appendix 4.A: Pipes Sizing of the Test Facility

This appendix shows the pipe sizing for the test facility, based on the pipe sizes recommended in the CIBSE, Concise Handbook [86].

Pipes	load kW	ΔT (K)	Flow rate (kg/s)	Pipe Dia. [86] (mm)	*Available pipe Dia. (mm)	Δp (Pa/m)	Pipe length (m)	Δp Pipe (Pa)	Fittings Type & No.		Δp factor [88] ζ	Δp fitting (Pa)	Total Δp (pa)
Flow pipe	0.622	10	0.0148	16	15	27.50	5.5	151.25	Elbow 90º	6	0.75	14.42	236.17
									Tees	4	1	12.82	
									Valves	3	6	57.68	
Return pipe	0.622	10	0.0148	16	15	27.50	5	137.50	Elbow 90º	6	0.75	14.42	241.65
									Tees	4	1	12.82	
									Valves	4	6	76.91	
Static pressure - (P = H* ρ*g), H = the height from feeding tank to the bottom of the buffer tank													15527.0
Index Δp													16004.83

*Commercially pipes diameter available

Appendix 4.B: Specification of the Fan Inside the Booth

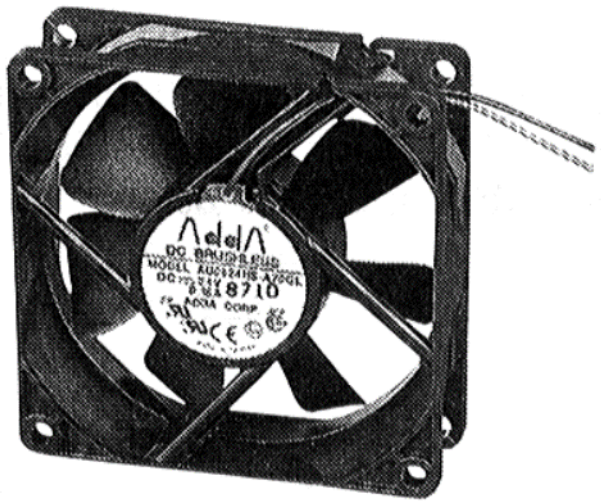

80mm Low Voltage
Axial Fan
Addax – AD0812HS-A70GL
Specifications
Model No.: AD0812HS-A70GL
Dimensions: 80 x 80 x 25mm
Bearing Type: Sleeve, Oil-Impregnated
Rated Voltage: 12.0V DC
Operating Voltage Range: 10.8 to 13.2 V DC
Start-up Voltage: 7.0 V DC Nominal
Rated Current: 0.25 A +10% Max.
Rated Power: 3 Watt
Rated Speed: 3,010 RPM □10%
Air Flow: 38.6 CFM Nominal
Static Air Pressure: 0.160 Inch Water
Noise Level: 34.4 dB Nominal
Motor Protection: By Impedance
Connection Lead Type: Wire, UL1007, AWG #24, Length 300 □10mm (Red +, Black -)
Life Expectancy: 31,000 Hours at 25ºC
Net Weight: 86 Gram.
Insulation Resistance: >10M@500V DC
Dielectric Strength: 1,500V AC for 60 seconds.
Operating Temperature: -10ºC to +70ºC
Storage Temperature: -40ºC to +70ºC
Humidity: 95% RH, 40 ±2ºC

Appendix 4.C: Calibration of Temperature Sensors

This appendix presents the calibration results for all temperature sensors used in experimental work.

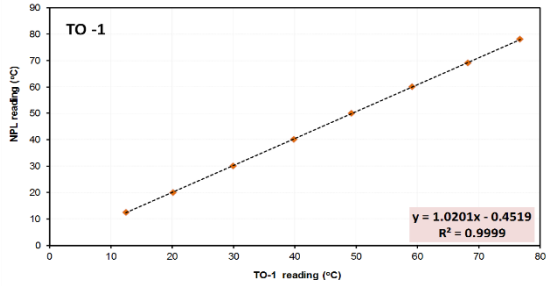

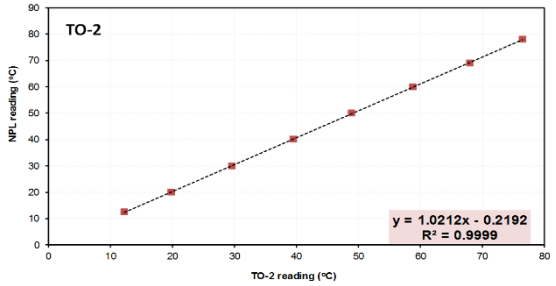

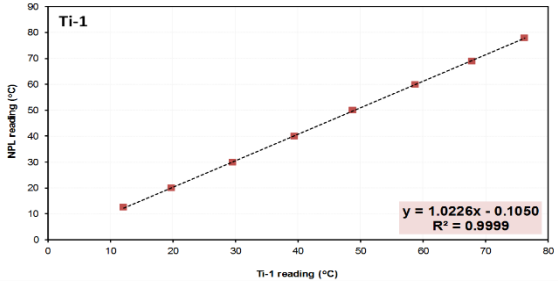

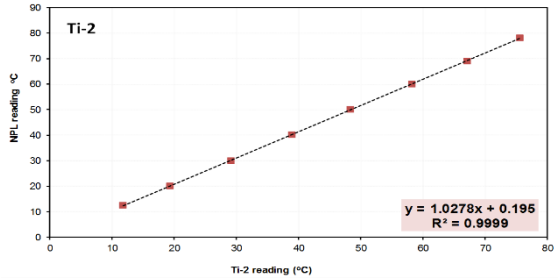

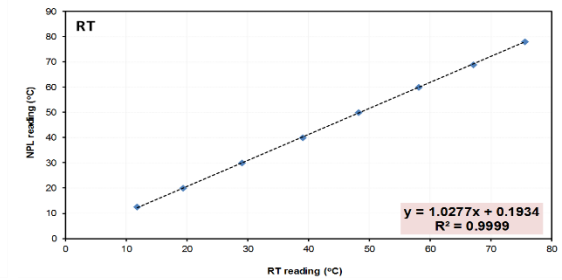

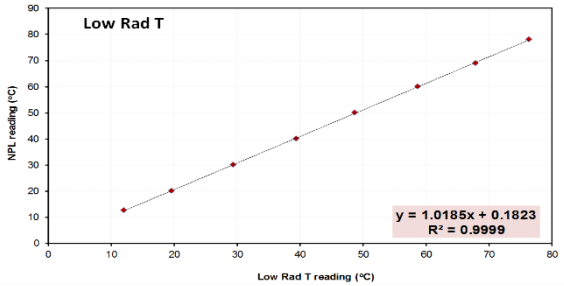

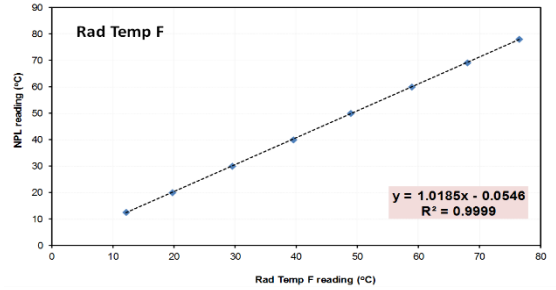

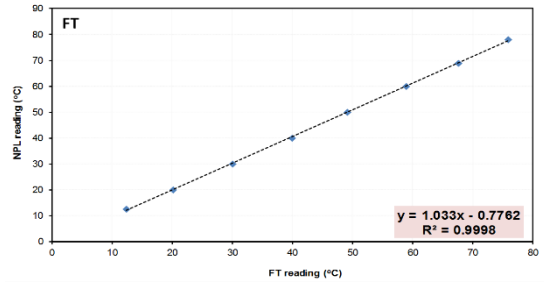

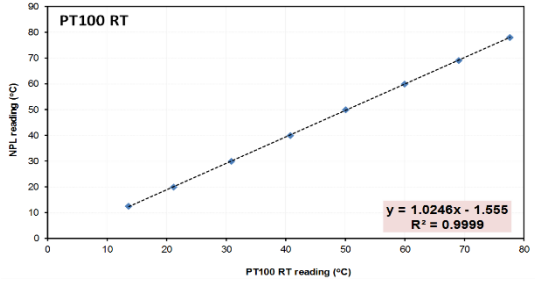

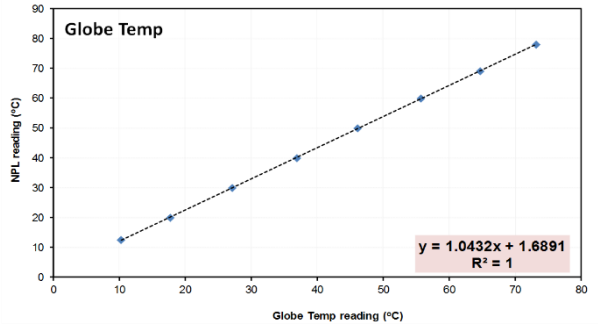
Globe Temp
y = 1.0432x + 1.6891
R² = 1
NPL reading (°C)
Globe Temp reading (°C)

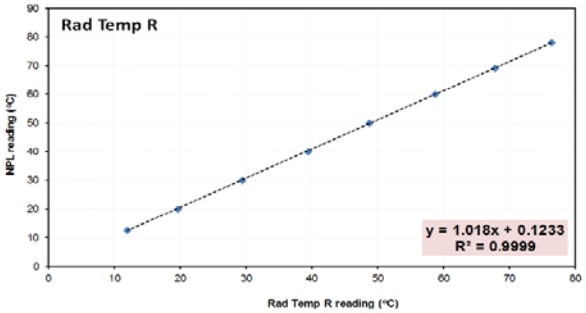
Rad Temp R
y = 1.018x + 0.1233
R² = 0.9999
NPL reading (°C)
Rad Temp R reading (°C)

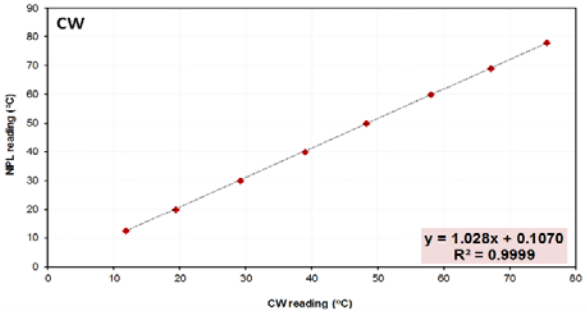
CW
y = 1.028x + 0.1070
R² = 0.9999
NPL reading (°C)
CW reading (°C)

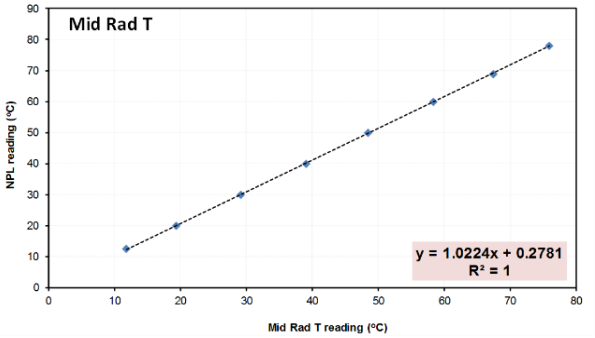
Mid Rad T
y = 1.0224x + 0.2781
R² = 1
NPL reading (°C)
Mid Rad T reading (°C)

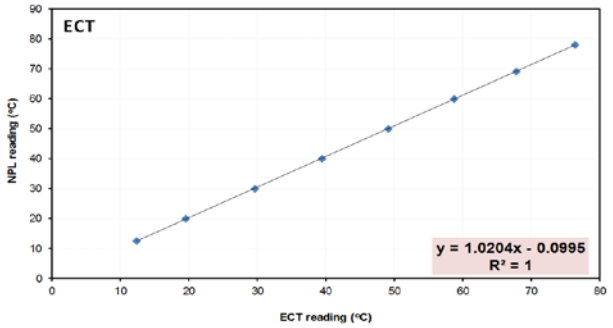
ECT
y = 1.0204x - 0.0995
R² = 1
NPL reading (°C)
ECT reading (°C)

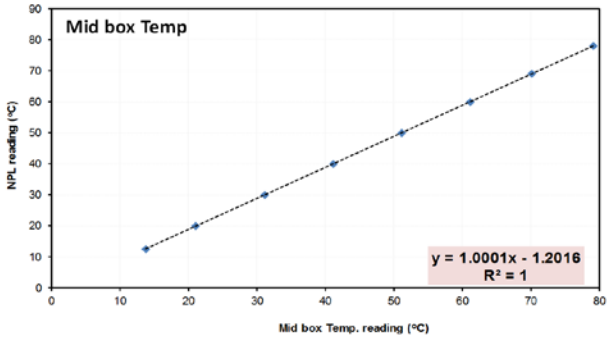
Mid box Temp
y = 1.0001x - 1.2016
R² = 1
NPL reading (°C)
Mid box Temp. reading (°C)

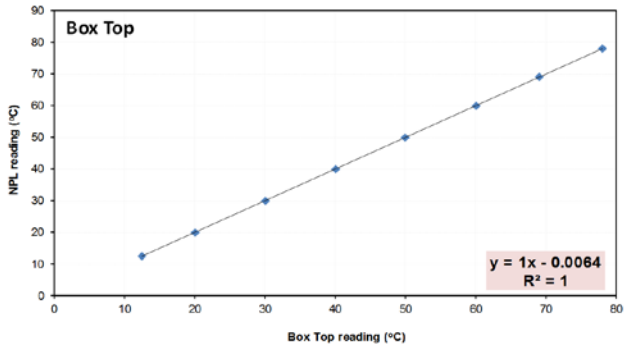
Box Top
y = 1x - 0.0064
R² = 1
NPL reading (°C)
Box Top reading (°C)

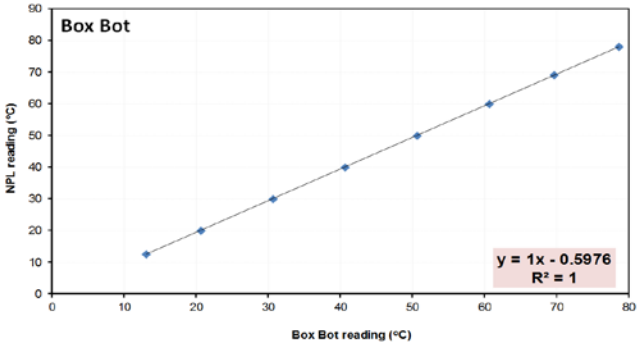
Box Bot
y = 1x - 0.5976
R² = 1
NPL reading (°C)
Box Bot reading (°C)

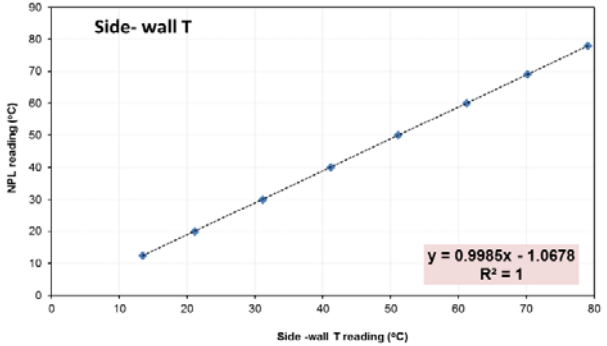
Side- wall T
y = 0.9985x - 1.0678
R² = 1
NPL reading (°C)
Side -wall T reading (°C)

Appendix 4.D: Uncertainty Analysis for All Temperature sensors

Table 4.D-1 gives the uncertainty result for each temperature sensor after calibration.

Table 4.D.1: Uncertainty Results

NPL Reading ºC	Sensor Name	Mean ($\overline{T}$)	σ_s	u_{Random}	u_{tot} (K)
12.5	TO-1	12.50	0.04	0.11	0.12
	TO-2	12.51	0.03	0.10	0.10
	Ti-1	12.49	0.03	0.08	0.09
	Ti-2	12.50	0.03	0.08	0.09
	CW	12.49	0.03	0.07	0.08
	RT	12.48	0.03	0.09	0.09
	Low Rad T	12.51	0.02	0.05	0.05
	Rad Temp F	12.49	0.037	0.102	0.11
	FT	12.51	0.03	0.08	0.09
	PT100 FT	12.49	0.02	0.04	0.04
	PT100 RT	12.51	0.03	0.08	0.09
	Globe Temp	12.51	0.03	0.08	0.09
	Rad Temp R	12.53	0.04	0.10	0.11
	Mid Rad T	12.50	0.03	0.08	0.09
	ECT	12.50	0.03	0.08	0.09
	Mid box Temp	12.51	0.03	0.08	0.09
	Box Top	12.53	0.03	0.08	0.09
	Box Bot	12.51	0.03	0.08	0.09
	Side-wall T	12.45	0.03	0.09	0.09
20	TO-1	19.98	0.04	0.12	0.13
	TO-2	20.01	0.04	0.10	0.11
	Ti-1	19.98	0.03	0.08	0.09
	Ti-2	19.96	0.03	0.08	0.09
	CW	20.02	0.04	0.10	0.11
	RT	19.97	0.03	0.09	0.09
	Low Rad T	20.01	0.02	0.06	0.06
	Rad Temp F	20.02	0.03	0.10	0.10
	FT	19.93	0.04	0.11	0.12
	PT100 FT	20.01	0.01	0.02	0.02
	PT100 RT	20.10	0.01	0.01	0.01
	Globe Temp	20.07	0.03	0.07	0.08
	Rad Temp R	19.96	0.03	0.08	0.09
	Mid Rad T	20.01	0.02	0.07	0.07

	ECT	19.99	0.03	0.08	0.09
	Mid box Temp	20.16	0.03	0.084	0.09
	Box Top	19.99	0.03	0.07	0.08
	Box Bot	20.03	0.02	0.07	0.07
	Side-wall T	20.06	0.03	0.08	0.09
30	TO-1	30.02	0.03	0.08	0.09
	TO-2	30.02	0.05	0.14	0.15
	Ti-1	30.07	0.04	0.10	0.11
	Ti-2	29.99	0.04	0.10	0.11
	CW	30.16	0.03	0.08	0.09
	RT	30.01	0.03	0.07	0.08
	Low Rad T	30.01	0.02	0.06	0.06
	Rad Temp F	30.06	0.03	0.08	0.09
	FT	30.25	0.03	0.08	0.09
	PT100 FT	30.02	0.03	0.02	0.04
	PT100 RT	31.25	0.02	0.06	0.06
	Globe Temp	30.00	0.03	0.09	0.09
	Rad Temp R	30.01	0.03	0.09	0.09
	Mid Rad T	30.05	0.04	0.10	0.11
	ECT	30.01	0.02	0.07	0.07
	Mid box Temp	30.12	0.02	0.06	0.06
	Box Top	30.030	0.029	0.081	0.09
	Box Bot	30.07	0.03	0.08	0.09
	Side-wall T	29.97	0.03	0.08	0.09
40	TO-1	40.03	0.04	0.12	0.13
	TO-2	40.14	0.03	0.09	0.09
	Ti-1	40.00	0.03	0.08	0.09
	Ti-2	40.16	0.04	0.10	0.11
	CW	30.16	0.04	0.11	0.12
	RT	40.18	0.03	0.09	0.09
	Low Rad T	40.22	0.02	0.05	0.05
	Rad Temp F	40.24	0.03	0.10	0.10
	FT	40.39	0.04	0.10	0.11
	PT100 FT	40.16	0.01	0.04	0.04

	PT100 RT	41.37	0.02	0.05	0.05
	Globe Temp	40.15	0.03	0.08	0.09
	Rad Temp R	40.23	0.04	0.11	0.12
	Mid Rad T	40.16	0.03	0.09	0.09
	ECT	40.26	0.03	0.08	0.09
	Mid box Temp	40.17	0.03	0.07	0.08
	Box Top	40.23	0.03	0.08	0.09
	Box Bot	40.13	0.03	0.08	0.09
	Side-wall T	40.05	0.05	0.13	0.14
50	TO-1	49.96	0.05	0.13	0.14
	TO-2	49.66	0.03	0.08	0.09
	Ti-1	49.91	0.03	0.08	0.09
	Ti-2	49.64	0.03	0.08	0.09
	CW	49.84	0.03	0.09	0.09
	RT	49.90	0.03	0.09	0.09
	Low Rad T	49.38	0.02	0.06	0.06
	Rad Temp F	49.75	0.03	0.09	0.09
	FT	49.92	0.03	0.08	0.09
	PT100 FT	49.68	0.02	0.07	0.07
	PT100 RT	49.60	0.01	0.03	0.03
	Globe Temp	49.71	0.03	0.08	0.09
	Rad Temp R	49.97	0.04	0.12	0.13
	Mid Rad T	49.84	0.04	0.11	0.12
	ECT	49.68	0.03	0.08	0.09
	Mid box Temp	49.64	0.03	0.08	0.09
	Box Top	49.67	0.03	0.07	0.08
	Box Bot	49.66	0.03	0.07	0.08
	Side-wall T	49.72	0.03	0.09	0.09
60	TO-1	59.97	0.04	0.10	0.11
	TO-2	59.82	0.04	0.10	0.11
	Ti-1	60.09	0.01	0.09	0.09
	Ti-2	59.85	0.03	0.09	0.09
	CW	59.98	0.03	0.09	0.09
	RT	60.01	0.03	0.07	0.08

	Low Rad T	59.89	0.01	0.04	0.04
	Rad Temp F	59.90	0.03	0.09	0.09
	FT	60.01	0.03	0.09	0.09
	PT100 FT	59.80	0.02	0.06	0.06
	PT100 RT	59.80	0.01	0.03	0.03
	Globe Temp	59.73	0.03	0.08	0.09
	Rad Temp R	59.82	0.04	0.11	0.12
	Mid Rad T	59.81	0.03	0.09	0.09
	ECT	59.82	0.03	0.08	0.09
	Mid box Temp	59.79	0.03	0.08	0.09
	Box Top	59.87	0.03	0.07	0.08
	Box Bot	59.94	0.02	0.06	0.06
	Side-wall T	59.69	0.04	0.11	0.12
70	TO-1	68.97	0.04	0.12	0.13
	TO-2	69.57	0.03	0.09	0.09
	Ti-1	69.53	0.04	0.10	0.11
	Ti-2	69.69	0.04	0.11	0.12
	CW	69.54	0.04	0.10	0.11
	RT	69.87	0.05	0.13	0.14
	Low Rad T	69.68	0.02	0.06	0.06
	Rad Temp F	69.65	0.04	0.10	0.11
	FT	69.57	0.04	0.11	0.12
	PT100 FT	69.57	0.03	0.09	0.09
	PT100 RT	69.58	0.02	0.05	0.05
	Globe Temp	69.53	0.03	0.08	0.09
	Rad Temp R	69.60	0.04	0.11	0.12
	Mid Rad T	69.83	0.04	0.10	0.11
	ECT	69.68	0.03	0.08	0.09
	Mid box Temp	69.574	0.029	0.081	0.09
	Box Top	68.873	0.025	0.070	0.07
	Box Bot	69.498	0.027	0.076	0.08
	Side-wall T	69.13	0.04	0.11	0.12
	TO-1	78.00	0.03	0.09	0.09
	TO-2	77.99	0.04	0.10	0.11

80	Ti-1	78.04	0.03	0.04	0.05
	Ti-2	77.98	0.03	0.07	0.08
	CW	78.03	0.03	0.09	0.09
	RT	78.02	0.03	0.09	0.09
	Low Rad T	77.99	0.01	0.02	0.02
	Rad Temp F	77.98	0.04	0.11	0.12
	FT	77.60	0.02	0.06	0.06
	PT100 FT	77.982	0.029	0.081	0.09
	PT100 RT	77.984	0.021	0.058	0.06
	Globe Temp	78.301	0.028	0.077	0.08
	Rad Temp R	77.98	0.04	0.11	0.12
	Mid Rad T	77.98	0.03	0.09	0.09
	ECT	77.986	0.030	0.083	0.09
	Mid box Temp	78.036	0.029	0.079	0.08
	Box Top	77.318	0.028	0.077	0.08
	Box Bot	78.040	0.024	0.067	0.07
	Side-wall T	78.22	0.03	0.08	0.09

The maximum uncertainty in measurements for each temperature sensor for a range of temperatures of 12.5 ºC to 80 ºC was found and tabulated in Table 4.D-2.

Table 4.D.2: Maximum Uncertainty of Each Temperature Sensor

Sensor Name	Maximum u_{tot} (K)
TO-1	0.14
TO-2	0.15
Ti-1	0.11
Ti-2	0.12
CW	0.12
RT	0.14
Low Rad T	0.06
Rad Temp F	0.12
FT	0.12
PT100 FT	0.09
PT100 RT	0.09
Globe Temp	0.09
Rad Temp R	0.12
Mid Rad T	0.11
ECT	0.09
Mid box Temp	0.09
Box Top	0.09

Box Bot	0.08
Side-wall T	0.14

Uncertainty in the difference between the flow and return temperatures across the radiator ($u\Delta T$) has been evaluated by applying propagation law [95].

$$u\Delta T = \sqrt{(u(F_T))^2 + (u(R_T))^2}$$

Where uF_T and uR_T are the uncertainty in PT100 FT and PT100 RT, respectively.
$u\Delta T$=0.13 K

Appendix 4.E: Fluids Density and Specific Heat Capacity-Dependent Temperature Functions

The density and specific heat capacity-dependent temperature function for each fluid was developed based on the data presented in Tables 3.5 to 3.8 of Chapter 3) for a specified range of temperature (20ºC to 80ºC). The best fit of the data points was considered to get an exact match between the data points and best fit with the maximum coefficient of determination (R^2).

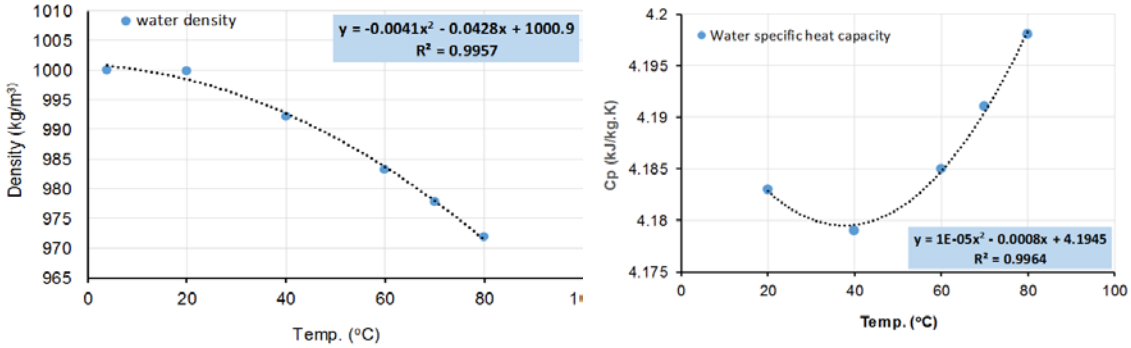

Figure 4.E.1: Density and Specific Heat Capacity Dependent Temperature Functions for Water

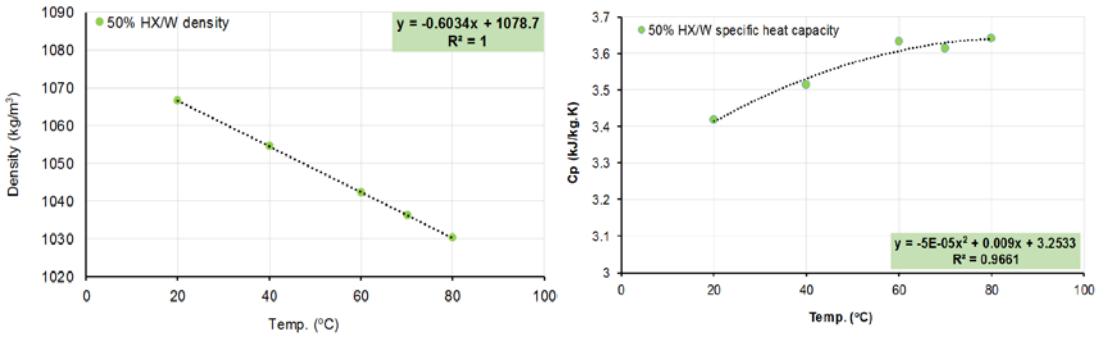

Figure 4.E.2: Density and Specific Heat Capacity Dependent Temperature Functions for 50% HX/W Mixture

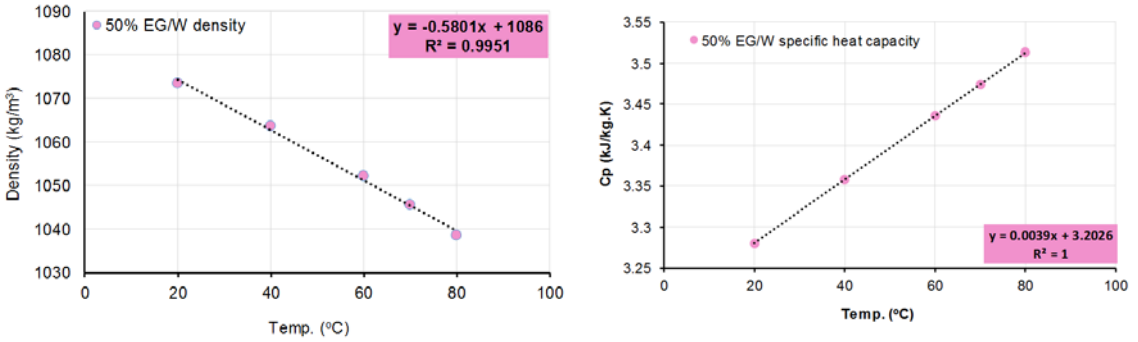

Figure 4.E.3: Density and Specific Heat Capacity Dependent Temperature Functions for 50% EG/W Mixture

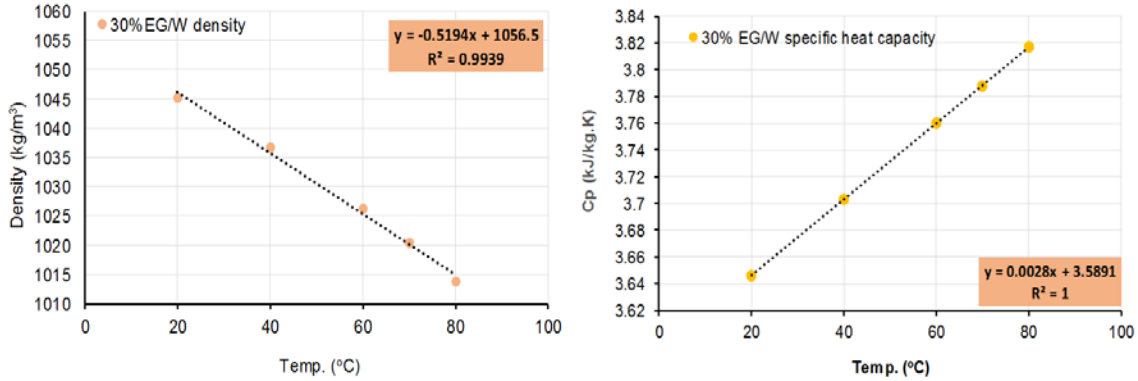

Figure 4.E.4: Density and Specific Heat Capacity Dependent Temperature Functions for 30% EG/W Mixture

Appendix 5.A: Determination of the Mass Water Vapour in Indoor Air

Using the psychometric chart to determine the mass of water vapour in the air inside the booth.

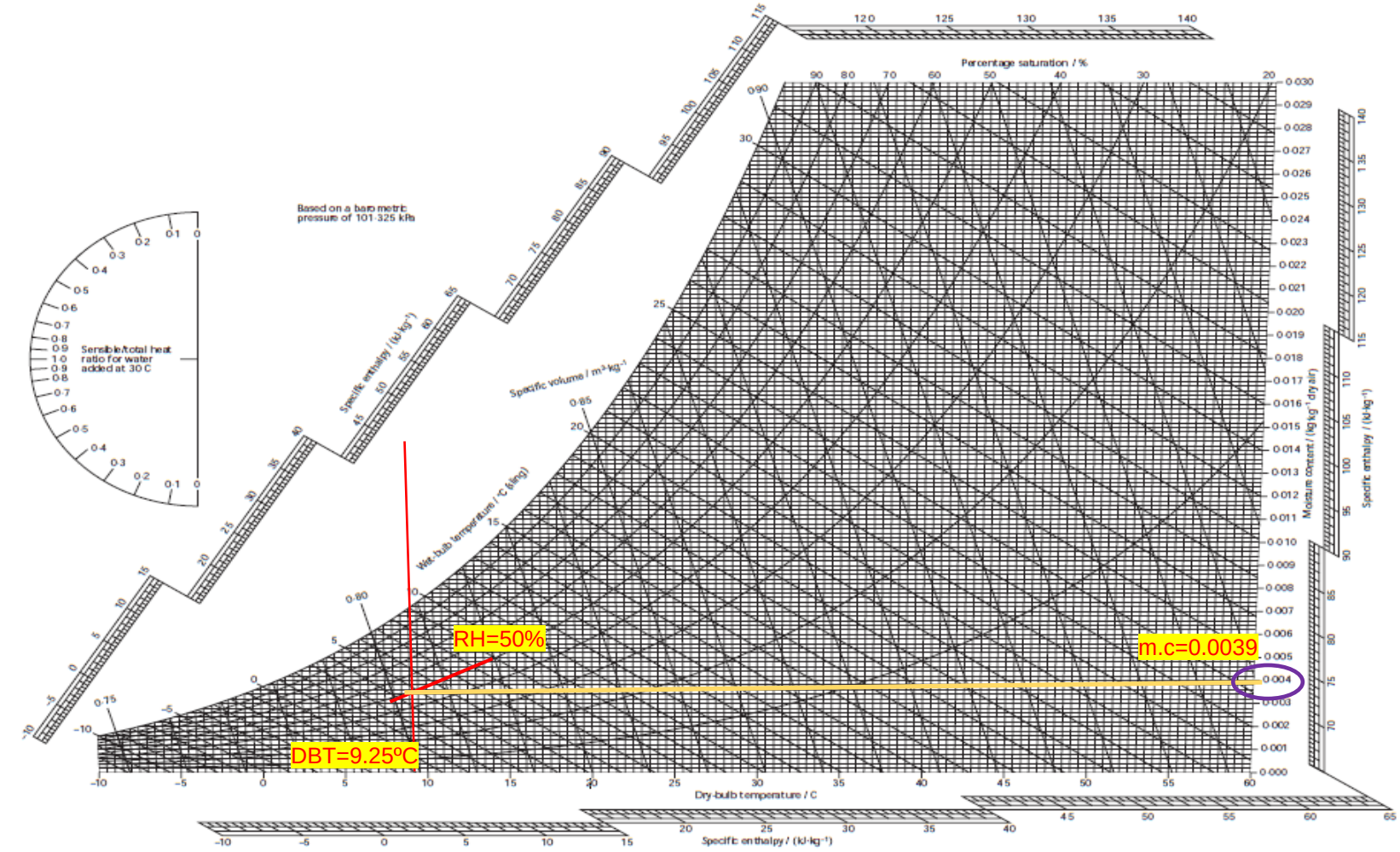

: CIBSE psychrometric chart (–10 to +60 °C)

Appendix 5.B: Air Density and Specific Heat Capacity- Dependent Temperature Functions

The density and specific heat capacity-dependent temperature function for the air was developed based on the published data in CIBSE guide C for a range of temperature of 5ºC to 30ºC. The best fit of the data points was considered to get an exact match between the data points and best fit with the maximum coefficient of determination (R^2).

Air density and specific heat capacity for different temperature [78]

Temperature (ºC)	Density (kg/m^3)	Specific heat capacity (kJ/kg.K)
5	1.27	1.009
10	1.24	1.011
15	1.22	1.014
20	1.2	1.018
25	1.18	1.022
30	1.16	1.03

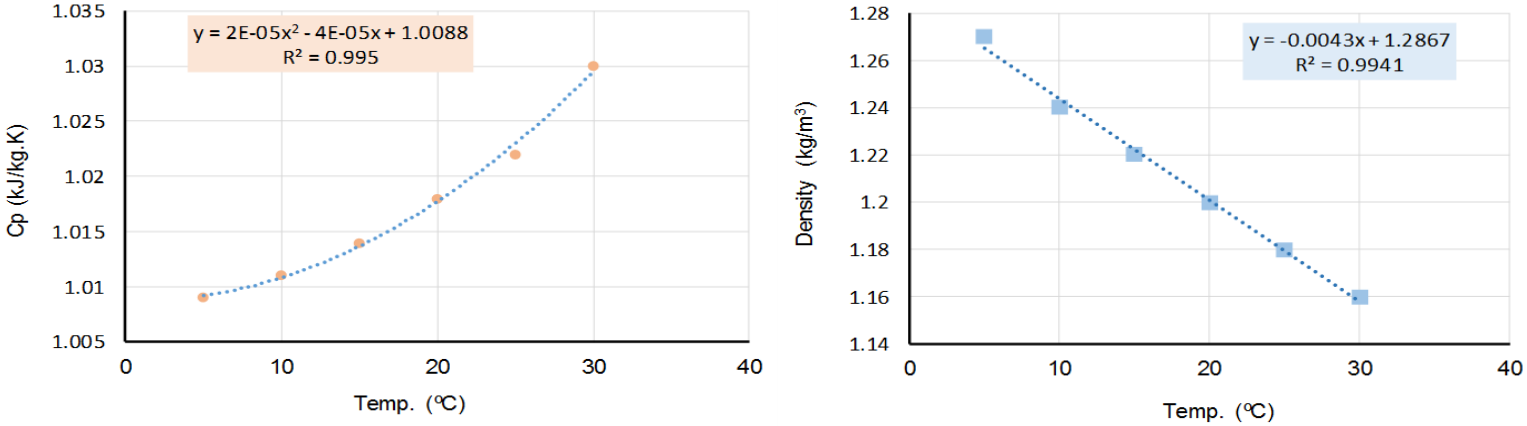

Figure 5.B.1: The Air Density and Specific Heat Capacity Dependent Temperature

Appendix 6.A: Flow Rate - Drop-in Scenario Tests

Figure 6.A.1 presents pictures for the rotameter that used to monitor the flow rate in the system for drop-in scenario tests.

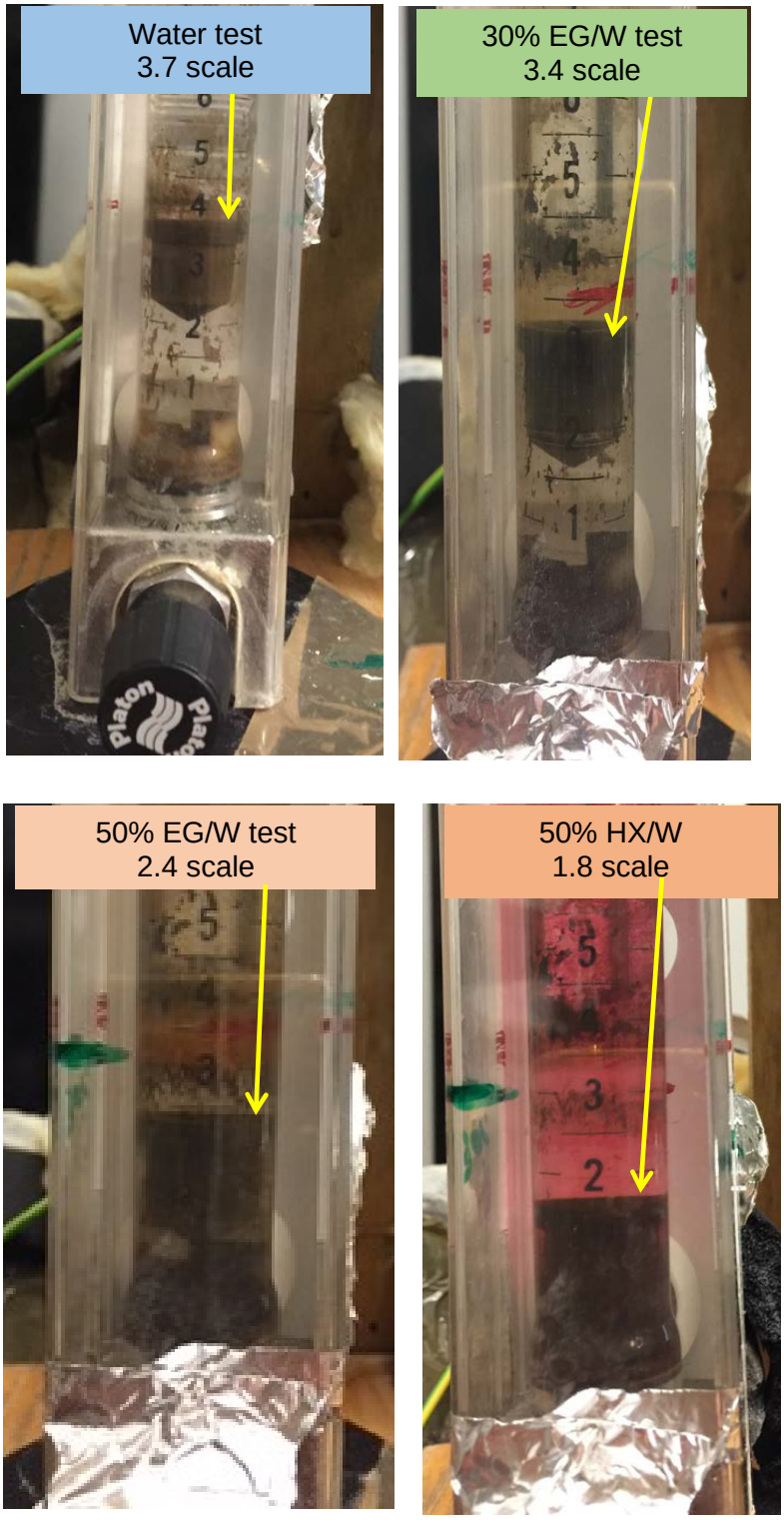

Figure 6.A.1: Rotameter Reading- Drop-In Scenario

Appendix 6.B: Thermal Images of the Radiator Surface

The thermal images for the radiator surface were analysed using SmartView and the temperature distribution area on the radiator measured using Auto desk Design Review Software.

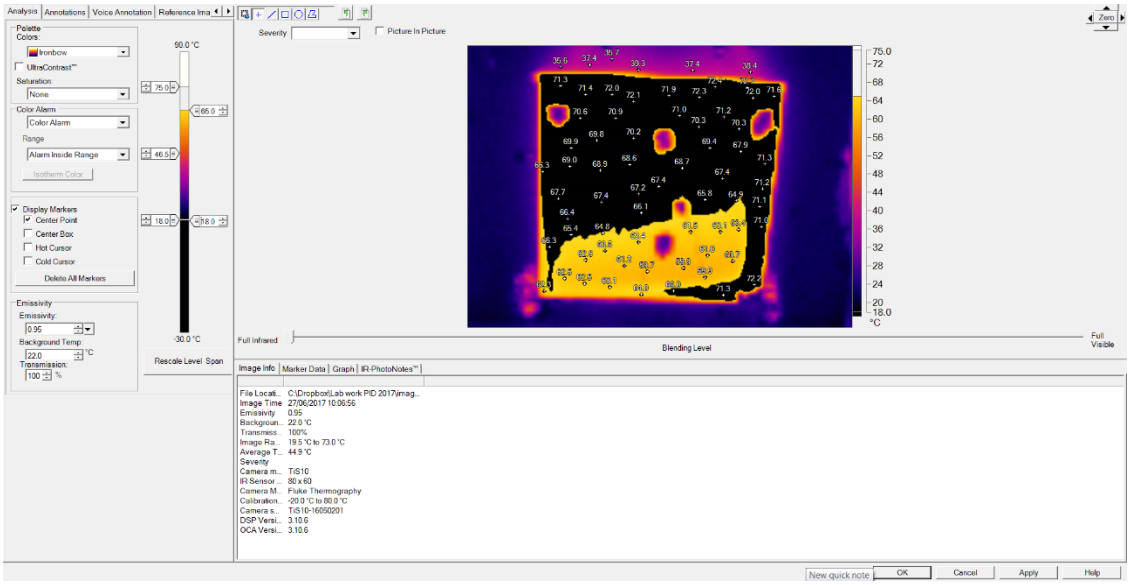

Figure 6.B.1: Analyse The Radiator Thermal Images Using SmartView Software

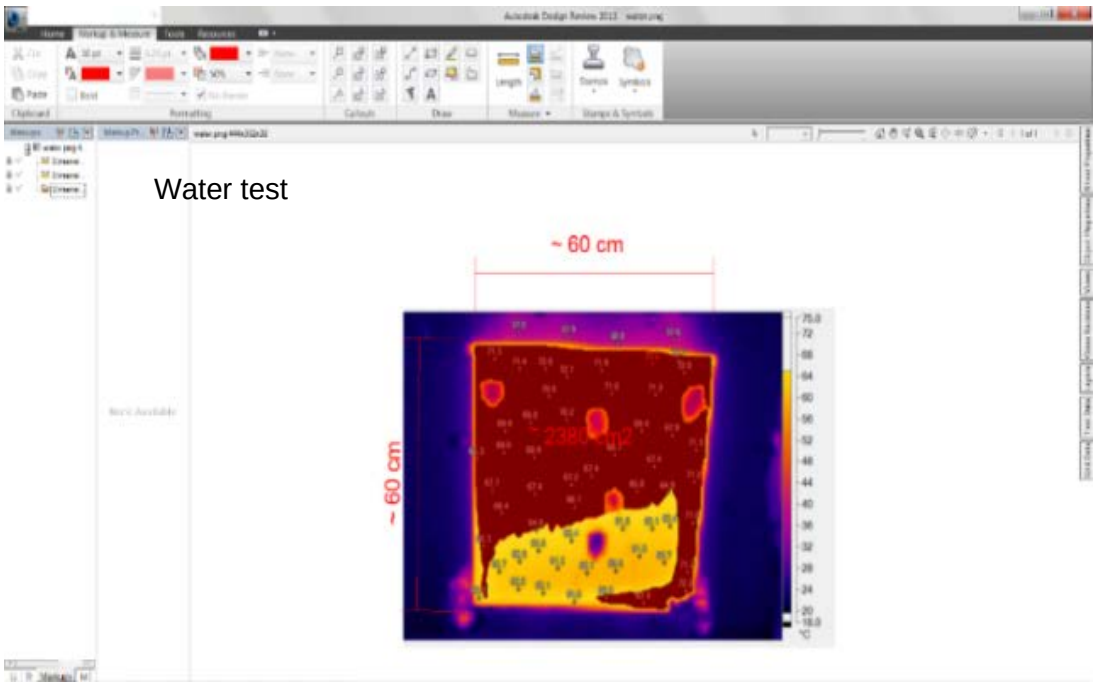

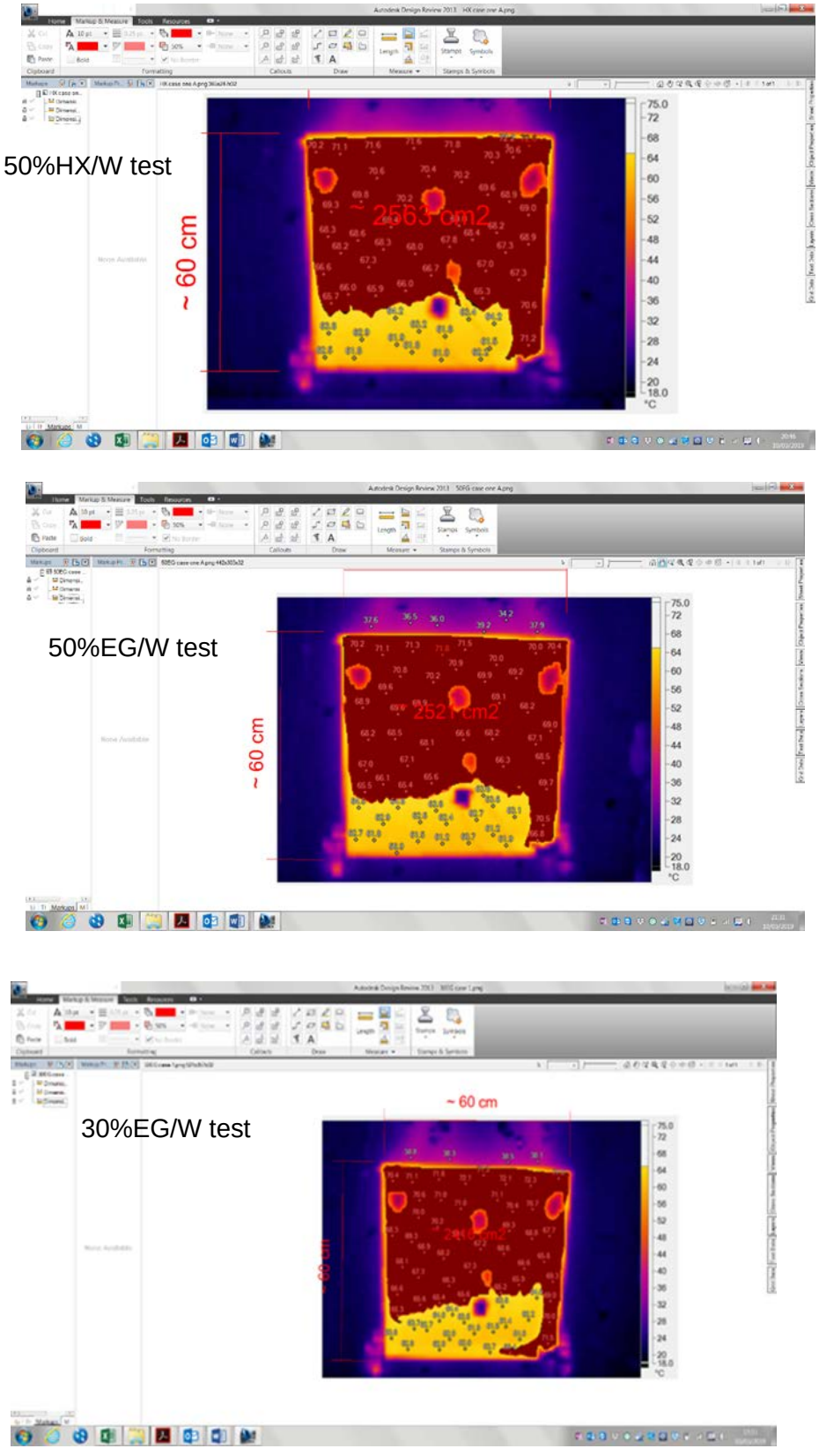

Figure 6.B.2: Measurements of the Black Area on the Thermal Images of the Radiator Surface Using Autodesk Design Review Software

Appendix 7.A: Energy Balanced Approach

This appendix outlines the evaluation procedure for the parameters that were used to calculate the heat output from the radiator based on the energy balance approach.

- Evaluation of Booth Thermal Transmittance (U)

To evaluate the heat loss from the booth, the thermal transmittance of the booth's wall ((U). need to be determined. So, the actual value of the thermal transmittance of the booth's wall was calculated based on operating conditions from the experimental results (steady state water test). At steady state condition, the heat output from the radiator is equal to the heat loss from the booth. Therefore, the heat balance as in equation 5.16, (Chapter 5,) can be rearranged to evaluate $[\sum((\mathrm{AU})_{\mathrm{B}})]$ as follows:

$$[\sum((AU)_B)] = (\dot{m}\, C_p(\, F_{T-}R_T))/(IBT - ECT) \qquad \textbf{(7.A.1)}$$

All the parameters in the above formula *(*$\mathrm{F_T}$, $\mathrm{R_T}$, $\mathrm{\dot{m}}$, $\mathrm{C_{p,}}$ IBT and ECT) are obtained with the water steady state tests results at steady state condition (Table 6.1- Chapter 6), and the ($\sum((\mathrm{AU})_{\mathrm{B}})$ was found to be (38.322 W/K).

Other parameters that were considered to evaluate the radiator heat output based on the energy balance approach are:

- Air properties (density and specific heat capacity) as a function of air temperature (see Appendix 5.B)
- Air volume inside the booth which is equal to the internal booth volume (the radiator's volume extract from that space) and it was found to be 4.784 m^3.
- Booths' walls volume and it was found to be 0.32 m^3.
- Thermal properties of the booth material (the density measured on-site, and it was found to be 600 $kg/m^{3,}$ and the $\mathrm{C_p}$ is 1.7 kJ/kg. K [99])

Appendix 7.B: Uncertainty Evaluation for Heat Output Results

This section outlines the evaluation of the uncertainty associated with the calculated heat output from the radiator ($\dot{Q}_{output}$) and the total heat entering the radiator ($\dot{Q}_T$).

1. Uncertainty in $\dot{Q}_T$

The total heat entering the radiator due to the movement of the hot fluid inside the radiator was evaluated according to equation 2.9 (Chapter 2), ($\dot{Q}_T = \dot{m}\, C_P\, (F_T - R_T)$ or $Q_T = \rho\, \dot{V}\, C_P\, (F_T - R_T)$). The uncertainty in the Q_T data was calculated by applying the uncertainty propagation law [95], as shown in equation 7.B.1.

$$(u\, Q_T)\,\% = \sqrt{(uC_p)^2 + (u\rho)^2 + (u\dot{V})^2 + (\frac{u\Delta T}{\Delta T})^2} \qquad \textbf{(7.B.1)}$$

Where $uC_p, u\rho$ are the percentage of the uncertainty in the specific heat capacity, and density of water (see Table 3.6 of Chapter 3) and ($u\dot{V}$) is the percentage of the uncertainty in the volumetric flow rate measurements (see section 4.4.2, Chapter 4). The ($u\Delta T$) is the uncertainty in the fluid flow and return temperatures across the radiator, which is equivalent to 0.13 K (see Table 4.D-2 of Appendix 4.D). The percentage of uncertainty in the $\dot{Q}_T$ was found to be ± 2.3%.

2. Uncertainty in $\dot{Q}_{output}$

Since the radiator heat output ($\dot{Q}_{output}$) at steady state conditions is equal to the heat loss from the booth. Therefore, the uncertainty in the heat loss ($\dot{Q}_{loss}$) need to be assessed. The uncertainty of the Q_{loss} was evaluated by applying the uncertainty propagation law, as follows.

$$u(\dot{Q}_{loss})\% = \sqrt{(u\sum(AU)_B)^2 + (\frac{u\Delta\theta}{\Delta\theta})^2} \qquad \textbf{(7.B.2)}$$

The $\Delta\theta$ is the difference between the IBT and ECT and the uncertainty in $\Delta\theta$ was evaluated as follows:

$$u\Delta\theta = \sqrt{(u(IBT)^2 + (u(ECT)^2} \qquad \textbf{(7.B.3)}$$

The $u\Delta\theta$ was found to be 0.101K, since the $(\sum \mathrm{AU_B})$ at steady state condition was calculated by considering the following formula:

$$\sum(AU_B) = \dot{Q}_T/(IBT - ECT) \quad \textbf{(7.B.4)}$$

Therefore, the uncertainty in the $\sum(\mathrm{AU_B})$ was evaluated by applying the uncertainty propagation law as follows:

$$u\sum(AU)_B\ \% = \sqrt{(uQ_T)^2 + (\frac{u\Delta\theta}{\Delta\theta})^2} \quad \textbf{(7.B.5)}$$

The uncertainty of the $\sum((\mathrm{AU})_\mathrm{B})$ was found to be 2.4%, this value was substituted in equation (7.B.2) to evaluate the $u(\mathrm{Q}_{loss})$, and it was found to be 3.3%. The percentage of the uncertainty in the heat output $u(Q_{\mathrm{output}})$ was found to be ± 3.3%.